Elucidating the protein interactome of the human ion channel TRPV4

A mutli-pronged approach to reveal the secrets of the fascinating N-terminal TRPV4 protein interactome *in vitro* and *in cellulo*

Dissertation zur Erlangung des Grades

"Doktor der Naturwissenschaften" im Promotionsfach Chemie

am Fachbereich 09 - Chemie, Pharmazie, Geographie

und Geowissenschaften

der Johannes Gutenberg-Universität Mainz

Erika Diehl

née Pfeifer in Krasnoje, Republic of Moldova

May 2021

Dekan:

1. Gutachterin:

2. Gutachterin:

Tag des öffentlichen Promotionskolloquiums: 19.08.2021

D77 (Dissertation Universität Mainz)

Urheberschaftserklärung

Ich, Erika Diehl (née Pfeifer), versichere, dass ich die vorliegende Dissertation mit dem Titel „Elucidating the protein interactome of the human ion channel TRPV4“ selbst verfasst, nicht andere als die in ihr angegebenen Quellen oder Hilfsmittel benutzt, alle vollständig oder singemäß übernommenen Zitate als solche gekennzeichnet sowie die Dissertation in der vorliegenden oder einer ähnlichen Form noch bei keiner anderen in- oder ausländischen Hochschule anlässlich eines Promotionsgesuchs oder zu anderen Prüfungszwecken eingereicht habe.

Für meine Eltern, Familie und Freunde. Danke für Alles.

"*Nature always wins but that doesn't mean we have to bow or grovel to it. That maybe even if we're not always glad to be here, it's our task to immerse ourselves anyway: wade straight through it, right through the cesspool, while keeping eyes and hearts open.*"

- The Goldfinch, Donna Tartt

Abbreviations

4α-PDD	4α-phorbol-12,13-didecanoate	5',6'-EET	5',6'-epoxyeicosatrienoic acid
A			
AA	arachidonic acid	ACN	acteonitrile
Abs	absorbency	AIP4	atropin-1-interacting protein 4 (ITCH)
ATP	adenosine triphosphate	ALS	amyotrophic lateral sclerosis
AT1aR	angiotensin receptor subtype 1a	Avi	avidin tag
ABC	ATP-binding casette		
B			
BSA	bovine serum albumin	BmrA	Bacilus subtilis multidrug resistance ABC transporter ATP-binding Protein
C			
CaM	calmodulin	CD	circular dichroism
cDNA	complementary DNA	CFP	cyan fluorescent protein
CTD	C-terminal domain	CV	column volume(s)
CMT2C	Charcot-Marie-Tooth Type 2C		
D			
ddH_2O	double distilled water	DDX3X	DEAD (Asp-Glu-Ala-Asp) box RNA helicase 3
DNA	desoxyribonulceic acid	DSS	disuccinimidyl suberate
DTT	dithiothreitol	DAG	diacyl glycerol
DMF	dimethylformamide		
E			
E. coli	*Escherichia coli*	EDTA	ethylenediaminetetraacetic acid
EM	electron microscopy	ER	endoplasmatic reticulum
F			
FA	fetal akinesia	F-BAR	Fes/CIP4 homology Bin-Amphiphysin-Rvs
FDAB	Familialr digital arthropathy-brachydaxtyly	FRET	Förster resonance energy transfer
G			
GO	gene ontology	GPCR	G-protein coupled receptor
GFP	green fluorescence protein	ggV4N	*Gallus gallus* TRPV4 N-terminus
H			
HEK293 cells	human embrionic kidney 293 cells	HECT	homologous to E6-AP C-terminus
His_6-tag	hexahistidine-tag	hsV4N	human TRPV4 N-terminus
hsV4N Avi	avidin-tagged human TRPV4 N-terminus	hsV4 ARD	human TRPV4 Ankyrin Repeat Domain
HSQC	heteronuclear single quantum coherence		
I			
IEX	ion exchange chromatography	IMAC	immobilized metal ion chromatography
IMS	ion mobility spectrometry	IP_3	inositol-1,4,5-triphosphate
IPTG	isopropyl β-D-1-thiogalactopyranosid	ITCH	E3 ubiquitin-protein ligase Itchy homolog

IDR	intrinsically disordered region	ITC	isothermal calorimetry
M			
MRW	mean residue weight	MW	molecular weight
MS	mass spectrometry / spectrometer	MD	metatropic dyplasia
N			
NH	amide group	Ni^{2+}-NTA	Divalent nickel-nitrilotriacetic complex
NMR	nuclear magnetic resonance	NTD	N-terminal domain
O			
OD_{600}	optical density at 600 nm		
P			
PACSIN	protein kinase C and casein kinase substrate in neurons	PBD	phosphoinositide binding domain
PCR	polymerase chain reaction	PDB	protein data bank
PI(4,5)P_2	Phosphatidylinositol-4,5-bisphosphate	PLC	Phospholipase C
PKA	Protein kinase A	PM	Plasma membrane
PRR	Proline rich region	PPI	protein-protein interaction
PTM	posttranslational modification		
R			
RNA	ribonucleic acid	dxRNA	duplex ribonucleic acid
RhoA	Ras homolog family member A	RBP	RNA-binding protein
RT	room temperature	RNP granule	ribonucleoprotein granule
S			
SDS-PAGE	sodium dodecyl sulfate-polyacrylamide gel electrophoresis	SH3	Src homology domain 3
		PCC	Pearson correlation coefficient
SEC	size exclusion chromatography	SD	standard deviation
Strep-POD	streptavidin-peroxidase	SG	stress granule
T			
TMD	transmembrane domain	Tris	Tris(hydroxymethyl)aminomethane
TRP	transient receptor potential	Tx100	TritonX-100
TOF	Time-of-flight		
U			
UDMS^E	ultra high-definition mass spectrometry^E		
W			
wt	wild type/ wild typic		
X			
XL-MS	cross-linking mass spectrometry		
Y			
Y2H	yeast-two hybrid		

Summary

Transient receptor potential vanilloid 4 (TRPV4) is an integral membrane protein which functions as a non-selective cation channel. TRPV4 plays a central role in mammalian sensory perceptions like the sense of touch and temperature sensing. Although research steadily increases, our knowledge of TRPV4 as well as other TRP superfamily members and their complex regulation mechanisms still remain poorly understood. TRPV4 is also involved in not well-characterized diseases, including peripheral neuropathies and skeletal dysplasias caused by channel point mutations. Many of these point mutations are located in the human TRPV4 N-terminus (hsV4N). The either solely skeletal or neuronal impact of these mutations led to the assumption that hsV4N may interact with tissue specific proteins and that these protein-protein interactions would then be specifically disturbed in the presence of disease-causing point mutations. To this point, data on the protein interactome of hsV4N are fragmentary and further investigations to shed light on the complex interaction network of TRPV4 are required.

In this work, recombinant hsV4N as well as the TRPV4 ankyrin repeat domain (hsV4 ARD), as a part of hsV4N and notorious hot-spot for disease causing mutations, were investigated with regard to their protein interactome in HEK293 cells using ultra high-definition mass spectrometry (UDMS^{E}) in cooperation with the RG [redacted] (University Medicine Mainz, JGU Mainz). The interactome results revealed ribonucleotide binding proteins as a new potential class of TRPV4 interacting proteins and indicate hsV4N as an until now unkown hub in the regulatory mechanism of cytoplasmic ribonucleoprotein granule formation. These findings were underlined by the here shown direct interaction *in vitro* between recombinant hsV4 ARD and the granule nucleating protein DDX3X. Interestingly, this interaction increased in the presence of the neuropathy-causing R232C mutation in hsV4 ARD.

Another hsV4 ARD interacting protein studied in the course of this thesis is the small GTPase RhoA. It was shown via nuclear magnetic resonance spectroscopy (NMR) that recombinantly expressed ^{15}N-RhoA directly interacts with hsV4 ARD and that this interaction significantly decreases in the presence of the neuropathy-causing mutation R269C in hsV4 ARD (hsV4

ARD R269C). In a cooperation with the RG [redacted] (Department of Neurology, Johns Hopkins University School of Medicine) it was shown that this neuropathy mutation-dependent loss-of-interaction leads to aberrant neurite-growth *in cellulo* and *Drosophila melanogaster*. These findings strongly hint at that the disruption of TRPV4-RhoA interaction is one determinant of the tissue-specific toxicity of TRPV4 neuropathy mutations.

An additional determinant for the tissue-specific toxicity of TRPV4 neuropathy mutations could be the loss-of-interaction between neuropathy-causing TRPV4 R269C and the neurospecific protein and known direct TRPV4-binding partner PACSIN1 that was demonstrated in this work. PACSIN1 dampens hypotonicity-induced TRPV4-dependent Ca^{2+}-influx in transiently transfected HEK293 cells. This ability to desensitize TRPV4 to hypotonicity is lost in the presence of the neuropathy-causing mutation TRPV4 R269C, probably due to a loss-of-interaction as shown via co-immunoprecipitation. Strikingly, the PACSIN1-orthologue PACSIN3 retained its TRPV4 interaction and modulation upon hypotonicity. Further comprehensive studies with PACSIN chimeras hint towards different binding mechanisms between TRPV4 and PACSIN1 or TRPV4 and PACSIN3, respectively.

Furthermore, in this thesis the foundation was laid to elucidate the possible role of post-translational modifications in TRPV4s protein-protein interactions. It was shown that hsV4N directly interacts with the E3 ubiquitin ligase ITCH and that lysine residues in close proximity to important regulatory sites within the intrinsically disordered region (IDR), preceding the hsV4 ARD in hsV4N, are ubiquitinated.

Thus this thesis provides a comprehensive study of new potential TRPV4 protein interactors and first explanations for the tissue-specificity of neuropathy-causing TRPV4 mutations.

Zusammenfassung

Transient receptor potential vanilloid 4 (TRPV4) ist ein integrales Membranprotein, das als nichtselektiver Kationenkanal fungiert. TRPV4 spielt eine zentrale Rolle bei Sinneswahrnehmungen von Säugetieren wie dem Tastsinn und der Temperaturwahrnehmung. Obwohl die Forschung über TRP-Kanäle stetig zunimmt, ist unser Wissen über TRPV4 sowie über andere Mitglieder der TRP-Superfamilie und deren komplexe Regulationsmechanismen noch immer wenig verstanden. TRPV4 ist auch an nicht gut charakterisierten Krankheiten beteiligt, darunter periphere Neuropathien und skeletale Dysplasien, die durch Punktmutationen im Kanal verursacht werden. Viele dieser Punktmutationen befinden sich im N-Terminus von humanem TRPV4 (hsV4N). Die entweder ausschließlich skeletale oder neuronale Auswirkung dieser Mutationen führte zu der Annahme, dass hsV4N mit gewebespezifischen Proteinen interagieren könnte und dass diese Protein-Protein-Interaktionen bei Vorhandensein von krankheitsverursachenden Punktmutationen dann spezifisch gestört sein würden. Bis zu diesem Zeitpunkt sind die Daten über das Proteininteraktom von hsV4N lückenhaft und weitere Untersuchungen, die mehr Klarheit über das komplexe Interaktionsnetzwerk von TRPV4 bringen sollen, sind erforderlich.
In dieser Arbeit wurden rekombinantes hsV4N sowie die TRPV4-Ankyrin-Repeat-Domäne (hsV4-ARD), als Teil von hsV4N und notorischer *hot spot* für krankheitsverursachende Mutationen, hinsichtlich ihres Proteininteraktoms in HEK293-Zellen mittels Ultra-High-Definition-Massenspektrometrie (UDMS^{E}) in Kooperation mit der RG [redacted] (Universitätsmedizin Mainz, JGU Mainz) untersucht. Die Interaktom-Ergebnisse enthüllten Ribonukleotid bindende Proteine als eine neue potentielle Klasse von TRPV4-interagierenden Proteinen und weisen darauf hin, dass hsV4N ein bisher unbekannter Knotenpunkt im Regulationsmechanismus von der Bildung von zytoplasmatischen Ribonukleoproteingranula sein könnte. Diese Erkenntnisse wurden durch die hier gezeigte direkte Interaktion *in vitro* zwischen rekombinantem hsV4 ARD und dem Granula nukleierenden Protein DDX3X untermauert. Interessanterweise verstärkte sich die Protein-Protein-Interaktion von DDX3X mit hsV4 ARD in Gegenwart der neuropathieverursachenden R232C-Mutation in hsV4 ARD.

Ein weiteres hsV4 ARD interagierendes Protein, das im Rahmen dieser Arbeit untersucht wurde, ist die kleine GTPase RhoA. Mittels Kernspinresonanzspektroskopie (NMR) wurde gezeigt, dass rekombinant exprimiertes ^{15}N-RhoA direkt mit hsV4 ARD interagiert und dass diese Interaktion in Gegenwart der Neuropathie verursachenden Mutation R269C in hsV4 ARD (hsV4 ARD R269C) signifikant abnimmt. In einer Kooperation mit der RG [redacted] (Department of Neurology, Johns Hopkins University School of Medicine) konnte gezeigt werden, dass dieser mutationsabhängige Interaktionsverlust zu aberrantem Neuriten-Wachstum *in cellulo* und *Drosophila melanogaster* führt. Diese Befunde weisen stark darauf hin, dass die Störung der TRPV4-RhoA-Interaktion eine Determinante für die gewebespezifische Toxizität von TRPV4-Neuropathie-Mutationen ist.

Eine weiterer wichtiger Faktor für die gewebespezifische Toxizität von TRPV4-Neuropathiemutationen könnte der hier gezeigte Verlust der Interaktion zwischen der Neuropathie verursachenden TRPV4 R269C und dem neurospezifischen Protein und bekannten direkten TRPV4-Bindungspartner PACSIN1 sein. PACSIN1 schwächt den Hypotonie induzierten TRPV4-abhängigen Ca^{2+}-Influx in transient transfizierten HEK293-Zellen ab. Diese Fähigkeit, TRPV4 gegenüber Hypotonie zu desensibilisieren, geht in Gegenwart der Neuropathie verursachenden Mutation TRPV4 R269C verloren Dies geschieht wahrscheinlich aufgrund eines Interaktionsverlustes, wie durch Co-Immunopräzipitation gezeigt werden konnte. Auffallend ist, dass das PACSIN1-Ortholog PACSIN3 seine TRPV4-Interaktion und -Modulation bei Hypotonie beibehielt. Weitere umfangreiche Untersuchungen mit PACSIN-Chimären deuten auf unterschiedliche Bindungsmechanismen zwischen TRPV4 und PACSIN1 bzw. TRPV4 und PACSIN3 hin.

Weiterhin wurde in dieser Arbeit der Grundstein gelegt, um die mögliche Rolle von posttranslationalen Modifikationen in den Protein-Protein-Interaktionen von TRPV4 aufzuklären. Es konnte gezeigt werden, dass hsV4N direkt mit der E3-Ubiquitin-Ligase ITCH interagiert und dass Lysinreste in unmittelbarer Nähe zu wichtigen regulatorischen Stellen innerhalb der intrinsisch ungeordneten Region (IDR), die der hsV4-ARD in hsV4N vorgelagert ist, ubiquitiniert sind.

Somit liefert diese Arbeit eine umfassende Studie neuer potentieller TRPV4-Proteininteraktoren und erste Erklärungen für die Gewebespezifität der Neuropathie verursachenden TRPV4-Mutationen.

Contents

1 Introduction

1.1 A little grasp of the TRP channel world

TRP stands for *Transient Receptor Potential* - a term introduced by Cosens *et al.* in a publication with the title "Abnormal Electroretinogram from a *Drosophila* Mutant".[1] In this paper, Cosens *et al.* described transient instead of steady electric activities in *Drosophila melanogaster* retinas upon light stimuli, caused by a spontaneous mutation in these flies. It took another 20 years to identify and characterize the responsible *Drosophila melanogaster trp* gene locus and to show that this gene encodes for an integral membrane protein. In 1992 Baruch Minke and Roger Hardie showed this integral membrane protein to be a Ca^{2+}-gating ion channel.[5] The identification of mammalian TRP channels not just only founded a whole new protein superfamily, consisting of 28 members divided into 6 subfamilies (figure 1.1) - intensive

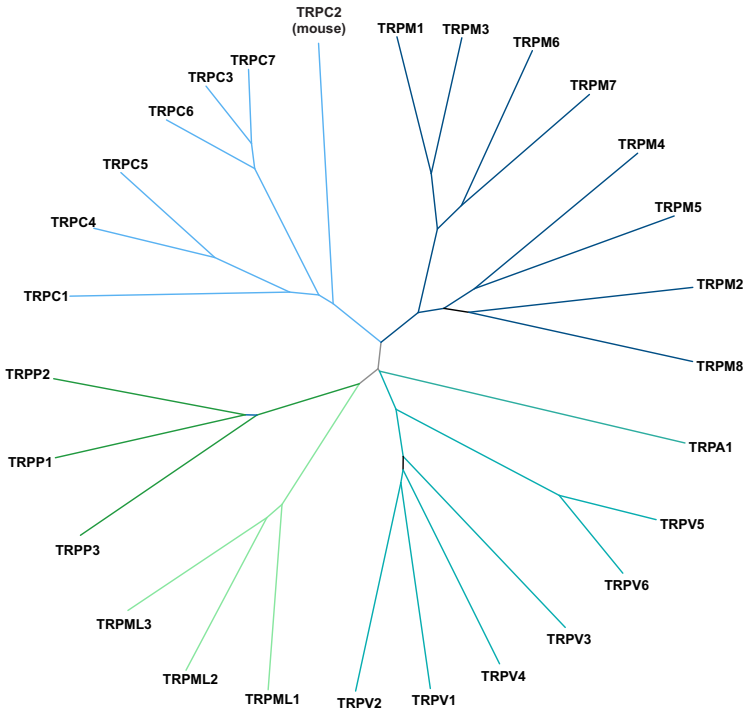

Figure 1.1: **Multiple alignment phylogenetic tree of the mammalian TRP channel superfamily.** The phylogenetic tree shows the relations between the TRP subfamilies based on sequence similarity. TRPP (polycystin), TRPC (canonical), TRPM (melastatin), TRPA (ankyrin), TRPV (vanilloid) and TRPML (mucolipin). Note that TRPC2 is a pseudogene in humans and therefore was substituted with the mouse variant. Multiple sequence alignment and phylogenic tree generation was performed with ClustalW2 at the EMBL-EBI server.[2] Tree Rendering was performed with DrawTree 3.66 via http://www.phylogeny.fr/.[3,4]

investigations also underpinned again a common catch in biochemical nomenclature: the initial name often underestimates the plethora of physiological functions the proteins are covering - and the TRP superfamily is a remarkable example for this.[6]

TRP channels are expressed at the plasma membrane and/or in intracellular organelle membranes of almost every cell and tissue type. With their function as tetrameric cation channels and slight preference for Ca^{2+}, TRP channels play an important role in different physiological processes including muscle contraction, cell proliferation or neurotransmitter release.[6] In addition, since they couple intra- and extracellular signals to flux ions across the membrane, TRP channels are also important mediators between the two membrane sides and are therefore well suited to fulfill their role in somato-, osmo-, thermo- and photosensation as well as nociception, amongst others sensory perceptions.[7–13] *In cellulo* experiments revealed a broad diversity among TRP channel activating/modulating stimuli, including ligand activation by exogenous synthetic and natural chemical compounds or endogenous lipids and purine nucleotides as well as temperature and cell swelling. This polymodality hints towards to a highly complex and diverse regulation of TRP channels, defining their (patho)physiological role by the respective cellular context in terms of the lipid- and proteome, for example. As diverse as the activation stimuli and physiological roles are the pathological outcomes of mutated TRP channels - diseases which can be grouped into so called channelopathies.[14–17] TRP channelopathies span from kidney disorders (e.g. focal segmental glomerusclerosis, TRPC6 OMIM:603965, polycystic kidney disease, TRPP2 OMIM:613095), skeletal dyplasias (e.g. metatropic dyplasia, TRPV4 OMIM:156530), lysosomal storage disorders (e.g. mucolipidosis type 4, TRPML1 OMIM:252650), skin disorders (e.g. erythrokeratodermia veriabilis et progressiva 6, TRPM4 OMIM: 618531) to neurodegenerative disorders (e.g. hereditary motor and sensory neuropathy type IIC, TRPV4 OMIM:606071).

TRP channels share structural motifs among each other, but also exhibit structural diversity - especially between the different TRP subfamilies. Each TRP monomer consists of structurally conserved six transmembrane helices (S1-6) with a so-called reentrant loop between S5 and 6, forming the ion pore in a TRP tetramer (figure 1.2 A). S1-4 form the so-called voltage sensor-like domain (VSLD), which affects channel gating by ligand binding.[18–20] The biggest structural differences between TRP channels are displayed within the intracellular N- and C-termini as well as by large extracellular domains present in some subfamilies. Due to these differences, the mammalian TRP superfamily can be divided into two groups. Group 1 (TRPM, TRPA, TRPV and TRPC, figure 1.2 B) includes the TRP subfamilies with large cytosolic N-termini,

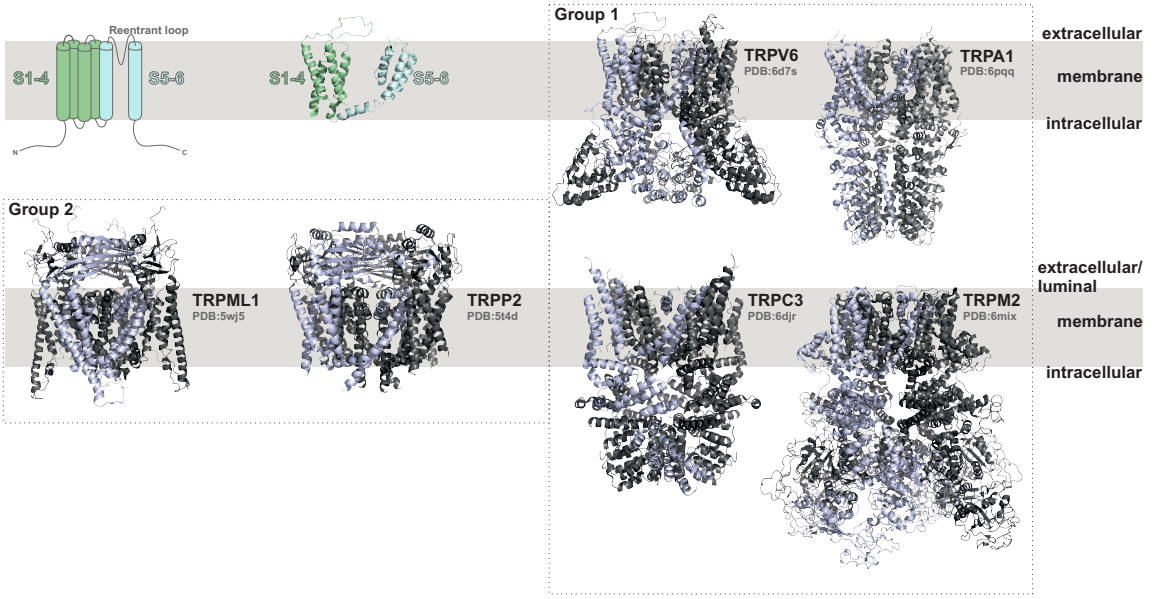

Figure 1.2: **One representative structure of each human TRP subfamily. A** Each TRP monomer consists of a structurally conserved core of six transmembrane helices (S1-6) shown here as ribbon diagram (left) and topolgy model (right). **B** Selected members belonging to group 1 of human TRP subfamilies, including TRPV6, TRPA1, TRPC3 and TRPM2. Monomers are highlighted in violet. For TRPV6, TRPA1 and TRPC3, only the ankyrin repeat domains (which are mostly α-helical structures) of the whole cytosolic N-terminus of respective TRP channel are resolved. The preceding parts are putatively unstructured and therefore not resolved in shown structures. For TRPM2 and the other TRPM channels a large so-called melastatin homology region defines the N-terminus.[21–24] **C** Selected members belonging to group 2 of human TRP subfamilies, including TRPML1 and TRPP2 with their extracelluar/luminal domains spanning from the S1 to S2 transmembrane helix.

harboring pivotal regulatory sites like lipid binding sites or regulatory domains like ankyrin repeat domains (ARDs). ARDs are α-helical motifs which serve as protein interaction platforms and play a role in ion channel assembly.[25–28] Group 2 TRP channels (TRPP amd TRPML, figure 1.2 C) are characteristic for their large domains spanning from S1 to S2, either being called extracellular domain or extraluminal domain in the case of lysosomal localization of TRPML.

While structural investigations of (human) TRP channels immensely advanced in the past 10 years, the elucidation of human TRP channel protein interactomes is still underrepresented.[20] Figure 1.3 shows current protein-protein interaction (PPI) networks deposited in the manually curated TRP channel PPI database TRIP.[29,30] Strikingly, most of the shown PPIs were determined with rodent proteins, whereas only a minority depicts PPIs with human proteins (see also table 6.1). Besides the prominent Ca^{2+}-binding protein Calmodulin and other calcium sensors like ALG-2 and NCS-1, especially cytoskeletal associated (KIF3A, α-actinins, Tropomyosin 1) and scaffolding proteins (AKAP5, NHERF-1, Homer-1) are represented. Furthermore, interactors like Orai1, IP3R3 and RyR underline the role of TRP channels in store operated Ca^{2+} entry. Most of these proteins are part of large protein complexes to achieve physiological func-

tions and tightly regulate each other. As aberrant human TRP channels are the cause of several, also tissue and cell-specific diseases, it is pivotal to determine these protein complexes and ultimately also the regulation mechanisms between distinct PPIs to understand the pathophysiological outcomes of mutated TRP channels. Here, the N- and C-termini of TRP channel are especially interesting, as they harbor important interaction sites like ankyrin repeat domains but also are accessible for a broad range of possible protein interactors due to their cytosolic protrusion (figure 1.2 B). Almost all PPI studies with TRP channels were conducted with full-length channels. Additionally to the need for a more comprehensive knowledge of overall TRP channel PPIs, it is also pivotal to determine the exact interaction sites at the channels. This leads to a better understanding of these PPIs and ultimately provide modulation possibilities of aberrant PPIs due to mutated TRP channels in diseases.

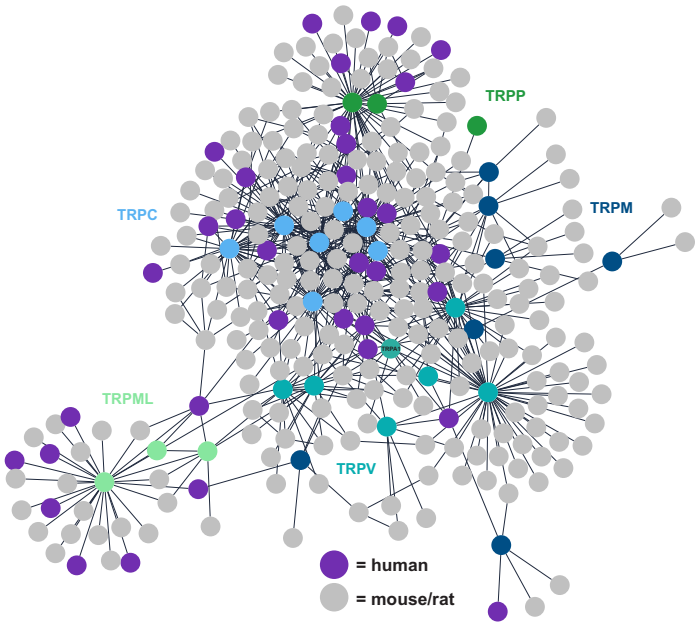

Figure 1.3: **TRP channel PPI network extracted from the TRIP Database.** The majority of the shown PPIs are with rodent proteins (grey nodes), whereas only a minority depicts PPIs with human proteins (purple nodes). Node colors of TRP subfamilies are indicated in the figure. See figure 6.1 for labeled nodes. Network was rendered via with Cytoscape 3.8.0.
29,30

1.2 TRPV4 - the wild child amongst TRPV channels?

In their review "*The puzzle of TRPV4 channelopathies*" published in 2013, Bernd Nilius and Thomas Voets described TRPV4 as follows:

> "*TRPV4 could be compared to Proteus, a God of the sea in Greek mythology, who has characteristics of flexibility, versatility, mutability and adaptability, emerges in many shapes and can appear in frightening forms.*"[31]

This description is still surprisingly accurate, as in the course of this PhD thesis TRPV4 showed another similarity to the sea god. Proteus is able to prophecy the future but is almost unwilling to do so. Only to the ones who are able to capture him with cunning, Proteus will answer their questions. And just as this moody sea god, TRPV4 is unwilling to easily reveal information about its role in physiological and pathological processes. This PhD thesis shows that it took, and it is still going to take, scientific highly versatile and multi-pronged approaches to "capture" TRPV4 to get the desired information.

TRPV4 was first described as an osmoreceptor involved in systemic osmotic pressure in 2000 by Liedtke *et al.*[32] Three years later, two research teams generated *trpv4* null mice and published the outcomes of this deletions in the murinal osmotic regulation.[33,34] Liedtke and Friedmann determined systematic plasma hyperosmolality, diminished drinking and decreased vasopressin plasma levels in these mice. Vasopressin is a peptide hormone synthesized in the hypothalamus and systematically released via the posterior pituitary in response to hyperosmolality, inducing water reabsorbtion in the nephrons and arteriole constriction to increase the peripheral vascular resistance and arterial blood pressure. Therefore, Liedtke and Friedmann suggested that *trpv4* null mice have an impaired osmosensation in the central nervous system (CNS).[33] In contrast, Mizuno *et al.* observed a normal drinking behavior in their *trpv4* null mice and no plasma hyperosmolality. Furthermore, upon a hyperosmolal challenge due to intraperitoneal propylene glycol injection, these mice showed increased vasopressin secretion compared to wild type mice.[34] Taken together, these studies and later conducted *in cellulo* experiments show that TRPV4 is a pivotal key regulator in osmosensation - but how exactly TRPV4 is involved in the vasopression-regulated osmolality homeostasis or even in the smaller cellular context of osmolarity induced cell swelling or shrinkage still remains elusive. These first descriptions of TRPV4 as a osmotically activated channel were then followed by the discoveries of other TRPV4 activation and/or modulating factors such as innocuous temperature,

chemicals like the synthetic phorbol ester 4α-phorbol-12,13-didecanoate (4α-PDD) or the endogenous compound 5',6'-epoxyeicosatrienoic acid (5',6'-EET) as well as plasma membrane embedded phosphoinositides like phosphatidylinositol-4,5-bisphosphate (PI(4,5)P_2).[35–39] Considering the relatively mild phenotypic consequences of *trpv4* null mice, resulting in fertile and viable mice with some impairments like the before mentioned altered osmosensation, impaired osteoclast differentation as well as hearing alteration and compromised vascular endothelial functions, it is striking that mutations in TRPV4 lead to severe diseases in humans.[31,40–45] These autosomal-dominant hereditary TRPV4 channelopathies span from relatively mild outcomes to heavily disabling or even lethal diseases which can be divided in two main groups, namely skeletal dysplasias and peripheral neuropathies.[14,15,31,46]

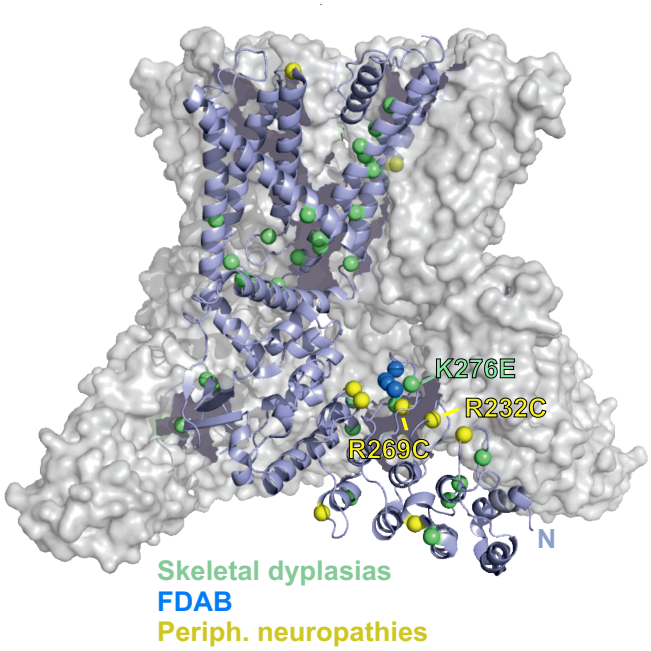

Figure 1.4: **Distribution of TRPV4 channelopathy mutations.** Shown residues of channelopathy-causing TRPV4 mutations are mapped onto the cryo-EM structure of *X. tropicalis* TRPV4 (PDB:6BBJ). Skeletal dysplasia mutants are shown as green spheres, familial digital arthropathy brachydactyly (FDAB) mutations as blue spheres and peripheral neuropathy mutations as yellow spheres. Whereas skeletal dysplasia mutations are distributed over the whole channel, neuropathy-causing mutations are mainly clustered in the cytosolic ankyrin repeat domain (hsV4 ARD). Numbered mutations correspond to the human TRPV4 sequence and were investigated in the course of this thesis. The very N-terminal intrinsically disordered region (IDR, aa 1-149) is not resolved and therefore not shown in the structure. Please note that a human TRPV4 structure, also lacking the IDR, was published by Botte *et al.*, but no structure was deposited in the RSCB Protein Data Bank to date.[18]

To date, five skeletal dysplasias and one other skeletal disease (familial digital arthropathy brachydactyly, FDAB, OMIM: 606835) are known to be caused by TRPV4 mutations (OMIM: 605427). FDAB represents a very mild form of a TRPV4 mutation-induced bone disease, where patients appear normal at birth but develop a deforming and painful osteoarthrithis due to subchondral pathology of the finger- and toe phalanges as well as the metacarpal and -tarsal bones, leading to arthropathy and brachydactyly. The FDAB-causing mutations in TRPV4 which are known to date, were discovered in three unrelated families in the third ankyrin repeat (AR3)

of TRPV4 (G270V, R271P, F273L, see also blue spheres in figure 1.4).[47] Unlike these FDAB-associated mutations, skeletal dysplasia-causing mutations are not as tightly clustered in one specific TRPV4 domain (figure 1.4). However, in sequential proximity, mutations (K276E or I331F) lead to lethal metatropic dysplasia (MD), the severe end of TRPV4 channelopathies.[48,49] Characteristic TRPV4-associated skeletal dysplasia phenotypes are brachydactyly, short trunk and scoliosis.[31] For lethal MD, additionally abnormally thick cartilage and congenital bone deformations were observed like hip dislocation and clubfeet, probably caused by altered endochondral ossification during the fetal development.[49] Recombinant overexpression - either in HEK293T cell lines or *Xenopus tropicalis* oocytes - of skeletal dysplasia-inducing TRPV4 mutations resulted mostly in gain-of-function channels, leading to increased Ca^{2+}-levels in these cells.[50–52] The same observations in terms of elevated basal or activated Ca^{2+}-influx activity were also made with neuropathy-causing TRPV4 mutations.[53,54] TRPV4-associated peripheral neuropathies include two rare forms of spinal muscle arthropies (SMAs), namely congenital distal SMAs (CDSMAs, OMIM:600-175) and scapuloperoneal SMA (SPSMA, OMIM:181405). In most cases (approx. $90\,\%$), the cause of SMA is a mutation in the survival of motorneuron 1 (SMN1) protein, leading to ventral horn motor neuron degeneration and ultimately to progressive muscle wasting of voluntary muscles in the limbs and also respiratory muscles.[55] TRPV4-associated CDSMA and SPSMA primarily affect the muscles of lower limbs and for SPSMA additionally the shoulder blade muscle. While TRPV4-associated CDSMA patients do not have sensory deficits, SPSMA and the third TRPV4-associated neuropathy, Charcot-Marie-Tooth Type 2C (CMT2C, OMIM:606071), share sensory deficits and vocal cord paresis as symptoms. Furthermore, CMT2C patients show, in contrast to the congenital conditions in CDSMA and SPSMA, a progressive and non-congenital muscle weakness and atrophy of distal muscles. Strikingly, mutations causing the before mentioned peripheral neuropathies especially cluster in ankyrin repeats 2 and 4 of the TRPV4 ankyrin repeat domain, whereas skeletal dyplasia causing mutations are spread all over the full-length channel, as shown in figure 1.4.[27,31,49,56]Amongst the TRPV subfamily, only TRPV4 exhibits such a plethora of direct disease-causing mutations. To date, only two other clinical syndromes are known to be caused by TRPV subfamily members. TRPV3 is the until now only known cause of the Olmsted syndrome (mutilating palmoplantar keratoderma with periorificial keratotic plaques, OMIM: 614594), a very rare congenital skin disorder leading to very thick skin on the hand palms and feet soles combined with severe hyperkeratotic plaques around the mouth region. Olmsted syndrome-causing TRPV3 mutations are either located in the loop between transmembrane helices S4 and 5 (G537S and G573C) or in the C-terminus (W629G) and also result, like the disease-causing mutations in TRPV4, in

gain-of-function channels. On the other hand, most of the TRPV6 mutations leading to transient neonatal hyperparathyroidism (OMIM:618188) are loss-of-function mutations spread all over the full-length channel.[57] The impaired placental TRPV6 mediated Ca^{2+} influx induces fetal hypocalcemia, leading to a secondary hyperparathyroidism where too much parathyroid hormone (PTH) is secreted. The consequence is a metabolic bone disease in affected infants, who present prenatal fractures, malformation of long bones and shortened ribs. In contrast to other TRPV channel-associated diseases where treatment is exclusively symptomatic, postnatal recovery was observed after oral Ca^{2+} supplementation.[57] These findings underline the importance of the TRPV ion flux fine tuning in respective tissues. TRPV channels can be divided into two groups: thermosensitive and polymodal TRPVs (TRPV1-4), which show a low basal ion channel activity and comparable low Ca^{2+} ion selectivity in comparison to the second group, consisting of TRPV5 and 6. The latter two are Ca^{2+} selective with a constituent activity and are not ligand-gated. It was shown that calmodulin (CaM) regulates TRPV5 and 6 in a negative, Ca^{2+}-influx dependent feedback loop by blocking the cytosolic side of the ion pore.[58,59] Regarding the disease severity of TRPV4 gain-of-function mutations, TRPV4 seems to be the wild child amongst the TRPV channels. The tissue-specificity of TRPV4-associated diseases hints towards a vulnerability of these tissues due to the higher TRPV4-mediated Ca^{2+}-influx. Systemic antagonism of TRPV4 with the highly selective TRPV4 antagonist HC-067047 in mice lead to no severe side effects regarding parameters like motor coordination, fluid intake, heart rate and thermoregulation.[60] Additionally, the orally available, highly selective TRPV4 antagonist GSK2798745 was recently examined in a phase I clinical trial in healthy subjects and patients with cardiogenic pulmonary edema (NCT02119260). TRPV4 plays a central role in pulmonary capillary endothelium, where the ion channel has a critical role in the development of high pulmonary venous pressure (PVP)-associated lung edema after heart-failures. Pulmonary capillary endothelial TRPV4 gets activated upon high PVP, leading to a reduced alveolar barrier due to endothelial cell detachment in lungs. As a consequence, the pulmonary capillaries show increased fluid (blood plasma) permeability and this leads ultimately to pulmonary edema.[61,62] GSK2798745 was well tolerated by healthy subjects and patients in terms of no detectable changes in vital and clinical laboratory parameters. However, pulmonary edema patients showed shortness of breath and reduced exercise tolerance upon GSK2798745 treatment. Nevertheless, the patients did not show disease worsening. GSK2798745 laid therefore the foundation for a possible, future systemic TRPV4-antagonism in human diseases.[61] As *trpv4* null mice just show mild phenotypes as mentioned above and systemic, pharmaceutically administrated TRPV4 antagonism seems to be well tolerated in mice and humans, it

is hypothesized that TRPV4-mediated Ca^{2+}-influx can be compensated with other ion channels (or in the case of TRPV6-associated neonatal hyperparathyroidism even with nutritional supplementation), but uncontrolled Ca^{2+}-influx leads to pathophysiological consequences in disease-related tissues. Several mechanisms were proposed, coupling TRPV4 mutations with disease pathology, like calcium-induced cell death or altered neuritogenesis.[31] But ultimately, all these hypotheses aim towards either altered gene expression, probably through a Ca^{2+}/CaM-dependent pathway or altered protein-protein interactions between TRPV4 and cell-type specific protein complexes. Especially for the neuropathy-causing mutations, which mainly cluster in the cytosolic TRPV4 N-terminus, altered tissue-specific PPIs could be the reason for the neurospecificity of these mutations.

1.3 Human TRP channels and their protein networks - glimpses of a brave new world

In the last decades, several high-throughput methods to identify protein interactomes emerged and were optimized continuously, such as protein-fragment complementation assay screens (PFCAs) like the yeast two-hybrid assay (Y2H) or mass spectrometry (MS) approaches. PFCAs map binary PPIs in the context of defined libraries of probable interactors, whereas MS approaches can provide qualitative and quantitative information of PPIs in complex protein networks.[63,64] The characterization of ion channel interactomes with MS-based proteomics greatly contributed to a better understanding of these supramolecular complexes, like for the glutamate receptors of the AMPA-type (AMPARs).[65–67] AMPARs are cation channels localized in the central nervous system, where they are involved in signal transmission in glutamatergic synpases. AMPARs are activated by the neurotransmitter glutamate, but also by the synthetic glutamate analog AMPA.[67] Based on classical molecular cloning, AMPARs were assumed to consist of four GluA transmembrane proteins, which are surrounded by up to four auxiliary subunits, which are either the so called transmembrane AMPAR regulatory proteins (TARPs), chornichon homologs or the GSG1-l protein. However, comprehensive MS-based proteomics revealed that AMPARs are more complex supramolecular constructs which assemble from a pool of 34 proteins known to date. From these 34 proteins, 21 were newly identified via MS, underlining the strength of unbiased and hypothesis-free MS-based proteomics.Such MS-based approaches provide roadmaps for further in-depth and structural investigations of the molecular

framework for the highly complex cell physiology of not only AMPARs, but also other ion channels.

Surprisingly, human TRP channel PPIs listed in table 6.1 were either determined via fusion protein-pull down assays with subsequent western blotting or classical Y2H assays. Only for two human TRP channels, namely TRPM4 and TRPV4, MS-based human protein interactome studies are published to date, both conducted in HEK293T cells. For human TRPM4, Caceres *et al.* identified proteins with actin cytoskeleton-related functions as the largest group of putative TRPM4 interactors, whereat McCray *et al.* identified a more diverse range of protein as putative TRPV4 interactors, with the small GTPase RhoA as one of the most significant ones (see also section 4.4 for a more detailed description of this PPI).[68,69] Both approaches were performed with transiently transfected HEK293T cells, expressing the respective full-length channel fused with an affinity tag. This affinity tag enables the purification of the tagged (bait) protein from a cell extract via affinity enrichment, co-purifying putative interactors which are then identified by mass spectrometry.[64] While this approach provides information about the putative interactome of the full-length channels, it is not possible to determine the exact interaction sites of the putative interactors within the channel. The other known (mostly rodent) TRPV4 interactors were mainly determined with non MS-based approaches like Y2H or co-immunoprecipitations (co-IPs) and can be mainly divided into three categories (for a list extracted from the TRIP database see table 6.2). First category compromises cytoskeletal and cytoskeletal associated proteins like α-arrestin 1-2, tubulins, α-actin and PACSIN1-3, indicating TRPV4s role in mechanosensitivity.[70,71] The second category includes interactors which modify TRPV4 post-translationally, like the tyrosin-kinases LYN and FYN or the E3 ubiquitin ligase ITCH. The third category includes transmembrane proteins like other TRP channels or AQP-4, for example. Most of the co-IPs were combined with site-directed mutagenesis to identify the exact TRPV4 interaction site, like for one of the most prominent TRPV4 interactors PACSIN3.[70,71] Whereat approaches like before mentioned co-IPs with site directed mutagenesis of probable interaction sites are able to provide information about direct PPIs, the restriction to binary PPI studies compromises the speed but also an comprehensive overview of putative supramolecular complexes. Overall, little is known about the TRPV4 protein interactome. To get a comprehensive, unbiased overview of a complex proteome or interactome, the highly sophisticated ultra high-definition mass spectrometry^{E} (UDMS^{E}) - first presented by Distler *et al.* - is the method of choice.[72] Shortly described, UDMS^{E} increases drastically the number of identified peptides in a complex mixture by introducing collision-energy dependent traveling wave-based ion-mobility separation (CE-dependent IMS) into liquid-chromatography coupled mass spectrometry (LC-

MS). With this, the precursor ion fragmentation efficiency improves significantly, enhancing the analytical depth of unbiased data-independent data acquisition.[72] With this and by additionally developing a robust and comprehensive in-house software for UDMS^E data analysis ,named ISOQuant, Distler and Kuharev *et al.* increased the numbers of identifiable protein groups compared to other generic MS set-ups significantly.[73,74] With this, UDMS^E is an excellent label-free and quantitative method to elucidate the protein interactome of TRPV4, which is involved in several severe channelopathies, as mentioned above. Due to the accumulation of disease-causing mutations in the cytosolic TRPV4 N-terminus (hsV4N), this domain was chosen as a starting point to elucidate the TRPV4 protein interactome in HEK293 cells. The high sensitivity and in-depth protein coverage of UDMS^E is essential for future TRPV4 interactome investigations in TRPV4 channelopathy-affected tissues, as this method is particularly suitable to identify altered tissue-specific protein-protein interactions as a possible reason for the disease pathology and tissue specificity of respective TRPV4 mutations.[27] Therefore, UDMS^E results serve as an excellent guidance for further in-depth investigations of determined TRPV4 interactome members.

1.4 Aim of this thesis - taming the wild child TRPV4

The TRPV4 N-terminus is a notorious hot-spot of disease-causing mutations, which mostly result in gain-of-function ion channels and dysregulated Ca^{2+}-influx.[49,53,54] Interestingly, especially the N-terminus harbors a significant amount of mutation sites which cause peripheral neuropathies like Charcot-Marie-Tooth Type 2C (CMT2C).[54,56,75] As the TRPV4 N-terminus consists of important protein interaction sites like the ankyrin repeat domain (ARD) or the proline rich region (PRR) and due to its cytosolic protrusion, this thesis elucidates the PPIs of the human (mutated) TRPV4 N-terminus (hsV4N) with a multipronged approach *in vitro* and *in cellulo*. For this, a major focus of this thesis was to elucidate the overall HEK293 cell protein interactome of hsV4N via ultra high-definition mass spectrometry^E (UDMS^E) and to narrow down the interaction sites by conducting identical UDMS^E experiments with the isolated TRPV4 ARD (hsV4 ARD). After data evaluation and protein-protein network analysis via gene ontology enrichment (GO), for example, promising interaction candidates were worked out. Possible direct interactions between hsV4N and respective candidates were then investigated with a versatile spectrum of methods, spanning from *in cellulo* experiments like live Ca^{2+}-imaging, co-immunoprecipitations and fluorescence microscopy to the very detailed elucidation of PPIs with

nuclear magnetic resonance spectroscopy and cross-linking mass spectrometry. Ultimately, this thesis laid the foundation to understand the tissue specific disease outcomes of TRPV4 mutations and for possible future regulations of the pathological Ca^{2+}-influx, which is especially interesting for the progressive motoneuron-degeneration in CMT2C.

2 Materials

2.1 Chemicals

Table 2.1: Chemicals

Chemical	Supplier
Acetic acid 100 % (AcOH)	Roth, Karlsruhe
Acrylamide/Bisacrylamide 37.5 %	Roth, Karlsruhe
Acetonitrile LC-MS grade (ACN)	Roth, Karlsruhe
^{15}N-Ammonium chloride ($^{15}NH_4Cl$)	CIL Inc., Tewksbury (USA)
Ammonium peroxisulfate (APS)	Roth, Karlsruhe
Adenosinediphosphate (ADP)	Roth, Karlsruhe
Adenosinetriphosphate (ATP)	Roth, Karlsruhe
Agar Agar	Roth, Karlsruhe
Agarose	Roth, Karlsruhe
Ampicillin sodium salt (Amp)	Roth, Karlsruhe
L-Ascorbic Acid	Sigma-Aldrich, Munich
D-Biotin	Roth, Karlsruhe
Dynabeads™M-280 Streptavidin	Invitrogen, Darmstadt
Dynabeads™Protein G	Invitrogen, Darmstadt
Bovine serum albumin (BSA)	Roth, Karlsruhe
Benzamidine hydrochlorid	Sigma-Aldrich, Munich
Bromphenol blue sodium salt	Roth, Karlsruhe
3-[(3-Cholamidopropyl)dimethylammonio]-1-propanesulfonate (CHAPS)	Roth, Karlsruhe
Coomassie Brilliant Blue G-250 Dye	Roth, Karlsruhe
Coomassie Brilliant Blue R-250 Dye	Roth, Karlsruhe

Chemical	Supplier
Calcium chloride ($CaCl_2$)	Roth, Karlsruhe
CHS (Cholesteryl hemisuccinate)	Sigma Aldrich, Munich
Digitonin	Roth, Karlsruhe
Dithiothreitol (DTT)	Sigma-Aldrich, Munich
Dimethylsulfoxide (DMSO),	
Headspace Grade or BioScience-Grade	Roth, Karlsruhe
4',6-diamidino-2-phenylindole (DAPI)	Sigma-Aldrich, Munich
Ethanol 99.9 % p.a. (EtOH)	Roth, Karlsruhe
Ethidium bromide 99.9 %	AppliChem, Darmstadt
Formic acid Optima LC/MS (FA)	Thermo Scientific, Waltham (USA)
Fura 2-AM	Invitrogen, Darmstadt
Glycerol	Roth, Karlsruhe
D-Glucose	Roth, Karlsruhe
GSK-1016790A (GSK-101, TRPV4 agonist)	Sigma-Aldrich, Munich
HC-067047 (HC-067, TRPV4 antagonist)	Sigma-Aldrich, Munich
4-(2-hydroxyethyl)-1-piperazineethanesulfonic acid (HEPES)	Sigma-Aldrich, Munich
Hydrochloric acid (HCl)	Roth, Karlsruhe
Isopropyl-β-D-thiogalactopyranoside (IPTG)	Roth, Karlsruhe
Isopropyl alcohol	Roth, Karlsruhe
Imidazol	Roth, Karlsruhe
Kanamycin sulphate	Roth, Karlsruhe
Lipofectamin LTX	Invitrogen, Darmstadt
Methanol 99.9 % p.a. (MeOH)	Roth, Karlsruhe
Magnesium chloride hexahydrate ($MgCl_2 \cdot 6\ H_2O$)	Roth, Karlsruhe
Magnesium sulfate heptahydrate ($MgSO_4 \cdot 7\ H_2O$)	Roth, Karslruhe
Mowiol® 4-88	Sigma-Aldrich, Munich
n-Dodecyl β-D-maltoside (DDM)	Sigma-Aldrich, Munich
β-nicotinamide adenine dinucleotide (NADH)	Sigma-Aldrich, Munich
Nickel nitrilotriacetic acid (Ni^{2+}-NTA) agarose	QIAGEN, Hilden
Paraformaldehyde (PFA)	Sigma-Aldrich, Munich
Pierce™Lysis Buffer	Invitrogen, Darmstadt
CST Protease/Phosphatase Inhibitor Cocktail (100X)	CST, Danvers (USA)

Chemical	Supplier
Precision Plus Protein™ Dual Color Standards	BioRad, Hercules (USA)
Phalloidin-TRITC	Sigma-Aldrich, Munich
Potassium ethylenediaminetetraacetic acid (K-EDTA)	Roth, Karlsruhe
Potassium hydroxide (KOH)	Roth, Karslruhe
Phenylmethylsulfonylfluoride (PMSF)	Sigma-Aldrich, Munich
Phosphoenolpyruvate (PEP)	Sigma-Aldrich, Munich
Potassium chloride (KCl)	Roth, Karlsruhe
PIPES (piperazine-N,N'-bis(2-ethanesulfonic acid))	Roth, Karlsruhe
Roti®-Lumin 1 and 2	Roth, Karlsruhe
SIGMA*FAST* Protease Inhibitor Cocktail Tablet, EDTA-Free	Sigma-Aldrich, Munich
Sodium chloride (NaCl)	Roth, Karlsruhe
Sodiumdodecylsulfate (SDS)	Roth, Karlsruhe
Sodium hydroxide (NaOH)	Roth, Karlsruhe
Sucrose	Roth, Karlsruhe
Tetramethylethylendiamine (TEMED)	Roth, Karlsruhe
Tris(hydroxymethyl)aminomethane (Tris)	Roth, Karlsruhe
Triton X-100	Roth, Karlsruhe
Tween® 20	Roth, Karlsruhe
Water, HPLC gradient grade	Roth, Karlsruhe
Water, LC-MS grade	Roth, Karlsruhe

2.2 Buffer and solutions

Table 2.2: General buffer and solutions

Buffer/solution	Ingredients
10x Running buffer pH = 8.3	20 mM Tris 1.54 M Glycin

Buffer/solution	Ingredients
1x SDS-PAGE-Running buffer pH = 8.3	1x Running buffer
	0.1 % (v/v) SDS
1x SDS-PAGE Wet blot buffer	1x Running buffer
	20 % (v/v) EtOH
4x SDS-PAGE sample buffer	200 mM Tris/HCl pH = 6.8
	400 mM DTT
	8 % (v/v) SDS
	0.4 % (w/v) Bromphenole blue
	40 % (v/v) Glycerol
10x PBS pH = 7.4	2.7 mM KCl
	10 mM Na_2HPO_4
	2 mM KH_2PO_4
	137 mM NaCl
1x PBS/T pH = 7.4	1x PBS
	0.05 % (v/v) Tween® 20
2x HEPES pH = 7.5	12 mM Glucose
	50 mM HEPES
	10 mM KCl
	280 mM NaCl
	1.5 mM $Na_2HPO_4 \cdot 2\ H_2O$
Coomassie staining solution	1 % (w/v) Coomassie blue R250
	40 % (v/v) MeOH
	10 % (v/v) Acetic acid
Coomassie destaining solution	10 % (v/v) Acetic acid
LB-Medium	25 g/L LB-Medium (Luria/Miller Broth) in MP-H_2O
TB-Medium	47.5 g/L TB-Medium (Terrific Broth) in MP-H_2O
Stripping buffer	100 mM NaOH
	2 % (w/v) SDS
	0.5 % (w/v) DTT
Mobile Phase A	0.1 % (v/v) FA
	3 % DMSO
	Ultrapure Water

Buffer/solution	Ingredients
Mobile Phase B	300 mM NaCl
	Ultrapure Water
M9 Medium	15 g/L KH_2PO_4
	33.9 g/L Na_2HPO_4
	0.75 g/L $^{15}NH_4Cl$
	2.5 g/L NaCl
	4 g/L Glucose
	2 mM $MgSO_4$
	10 µM $FeCl_3$
	Trace elements 10 mL/L
	Magic Mix 1 mL/L
Trace Elements	0.2 mg/mL $CaCl_2 \cdot 2H_2O$
	0.2 mg/mL $ZnSO_4 \cdot 7H_2O$
	0.2 mg/mL $MnSO_4 \cdot H_2O$
	5 mg/mL Thiamine
	5 mg/mL Niacin
	0.1 mg/mL Biotin
Magic Mix	1 Centrum Vitamin Tablet in 20 mL H_2O
Artifical CSF (aCSF) buffer	8.185 g/L NaCl
	0.360 g/L KCl
	0.203 g/L $MgCl_2 \cdot 6H_2O$
	0.294 g/L $CaCl_2 \cdot 2H_2O$
	4.320 g/L D-Glucose
	2.350 g/L HEPES pH = 7.4
Hypotonic Artifical CSF (aCSF) buffer	0.360 g/L KCl
	0.203 g/L $MgCl_2 \cdot 6H_2O$
	0.294 g/L $CaCl_2 \cdot 2H_2O$
	4.320 g/L D-Glucose
	2.350 g/L HEPES pH = 7.4
Pulldown lysis buffer	412.0 g/L Sucrose
	12.0 g/L PIPES pH = 6.8
	23.2 g/L NaCl

Buffer/solution	Ingredients
Electrophoresis cathode buffer pH = 8.3	2.6 g/L $MgCl_2 \cdot 6\ H_2O$
	187.5 mg/L Digitonin
	25 mM Tris
	192 mM Glycine
	0.02 % Coomassie-G250

Table 2.3: Buffer and solutions for purification of hsV4N, hsV4NΔ122 and hsV4NΔ132 constructs. hsV4NΔ132 is also referred to as hsV4 ARD, hsV4NΔ122 as hsV4 ARD-PRR.

Buffer/solution	Ingredients
E.coli lysis buffer hsV4N and hsV4NΔ132	20 mM Imidazol pH = 8
	300 mM NaCl
	20 mM Tris-HCl pH = 8
	0.1 % (v/v) Triton X-100
	add fresh:
	1 mM Benzamidine
	1 mM PMSF
	1 SIGMA*FAST* Protease Inhibitor
	RNAse, DNAse, Lysozyme
Wash 1	20 mM Imidazol pH = 8
	300 mM NaCl
	20 mM Tris-HCl pH = 8
Wash 2	50 mM Imidazol pH = 8
	300 mM NaCl
	20 mM Tris-HCl pH = 8
Elution	500 mM Imidazol pH = 8
	300 mM NaCl
	20 mM Tris-HCl pH = 8
SEC buffer	10 mM Tris-HCl pH = 7
	1 mM K-EDTA pH = 7

Buffer/solution	Ingredients
	300 mM NaCl
	1 mM DTT
	1 mM Benzamidine

Table 2.4: Buffer and solutions for purification of hsRhoA

Buffer/solution	Ingredients
E.coli lysis buffer RhoA	200 mM NaCl
	50 mM HEPES pH = 7.5
	0.1 % (v/v) Triton X-100
	10 % (v/v) Glycerol
	add fresh:
	1 mM Benzamidine
	1 mM PMSF
	1 SIGMA*FAST* Protease Inhibitor
	RNAse, DNAse, Lysozyme
IMAC Wash 1	50 mM Imidazol pH = 7.5
	200 mM NaCl
	50 mM HEPES pH = 7.5
	5 % (v/v) Glycerol
IMAC Elution	500 mM Imidazol pH = 7.5
	200 mM NaCl
	50 mM HEPES pH = 7.5
	10 % (v/v) Glycerol
TEV dialysis buffer	200 mM NaCl
	25 mM Tris-HCl pH = 7
	1 mM DTT
	0.5 mM K-EDTA
	TEV: RhoA 1 to 30 molar ratio
Reverse IMAC buffer	10 mM Imidazol pH = 7.5

Buffer/solution	Ingredients
	200 mM NaCl
	50 mM HEPES pH = 7.5
SEC buffer	200 mM NaCl
	50 mM HEPES pH = 7.5
	5 mM $MgCl_2$

Table 2.5: Buffer and solutions for purification of hsDDX3X_aa122-582 (DDX3X)

Buffer/solution	Ingredients
E.coli lysis buffer hsDDX3X	10 mM Imidazol pH = 7.4
	400 mM NaCl
	50 mM NaH_2PO_4 pH = 7.4
	0.1 % (v/v) Triton X-100
	add fresh:
	1 mM Benzamidine
	1 mM PMSF
	1 SIGMA*FAST* Protease Inhibitor
	RNAse, DNAse, Lysozyme
IMAC Wash A buffer	10 mM Imidazol pH = 7.4
	400 mM NaCl
	50 mM NaH_2PO_4 pH = 7.4
IMAC Wash B buffer	20 mM Imidazol pH = 7.4
	400 mM NaCl
	50 mM NaH_2PO_4 pH = 7.4
IMAC High Salt buffer	1 M NaCl
	50 mM NaH_2PO_4 pH = 7.4
IMAC Elution buffer	300 mM Imidazol pH = 7.4
	150 mM NaCl
	50 mM NaH_2PO_4 pH = 7.4
TEV dialysis buffer	300 mM NaCl

Buffer/solution	Ingredients
	25 mM NaH_2PO_4 pH = 7
	1 mM DTT
	TEV: DDX3X 1 : 30 molar ratio
Reverse IMAC buffer	10 mM Imidazol pH = 7.4
	300 mM NaCl
	25 mM NaH_2PO_4 pH = 7.4
SEC buffer	125 mM NaCl
	25 mM HEPES pH = 7.4

Table 2.6: Buffer and solutions for purification of hsITCH

Buffer/solution	Ingredients
E.coli lysis buffer hsITCH	200 mM NaCl
	50 mM Tris-HCl pH = 8
	0.1 % (v/v) Triton X-100
	5 % (v/v) Glycerol
	0.1 % (v/v) DDM
	add fresh:
	1 mM Benzamidine
	1 mM PMSF
	1 SIGMA*FAST* Protease Inhibitor
	RNAse, DNAse, Lysozyme
IMAC Wash 1	25 mM Imidazol pH = 8
	200 mM NaCl
	50 mM Tris-HCl pH = 8
	5 % (v/v) Glycerol
IMAC Elution	500 mM Imidazol pH = 8
	200 mM NaCl
	50 mM Tris-HCl pH = 8
	5 % (v/v) Glycerol

Buffer/solution	Ingredients
TEV dialysis buffer	200 mM NaCl
	50 mM Tris-HCl pH = 8
	1 mM DTT
	TEV: ITCH 1 : 30 molar ratio
Reverse IMAC buffer	10 mM Imidazol pH = 8
	200 mM NaCl
	50 mM Tris-HCl pH = 8
	5 % (v/v) Glycerol
SEC buffer	200 mM NaCl
	50 mM Tris-HCl pH = 8
	1.5 % (v/v) Glycerol

Table 2.7: Buffer and solutions for purification of hsITCH WW domain constructs

Buffer/solution	Ingredients
E.coli lysis buffer hsITCH WW domains	200 mM NaCl
	50 mM Tris-HCl pH = 8
	0.1 % (v/v) Triton X-100
	5 % (v/v) Glycerol
	add fresh:
	1 mM Benzamidine
	1 mM PMSF
	1 SIGMA*FAST* Protease Inhibitor
	RNAse, DNAse, Lysozyme
IMAC Wash 1	25 mM Imidazol pH = 8
	200 mM NaCl
	50 mM Tris-HCl pH = 8
	5 % (v/v) Glycerol
IMAC Elution	500 mM Imidazol pH = 8
	200 mM NaCl

Buffer/solution	Ingredients
	50 mM Tris-HCl pH = 8
	5 % (v/v) Glycerol
TEV dialysis buffer	200 mM NaCl
	50 mM Tris-HCl pH = 8
	1 mM DTT
	TEV: ITCH 1 : 30 molar ratio
Reverse IMAC	10 mM Imidazol pH = 8
	200 mM NaCl
	50 mM Tris-HCl pH = 8
	5 % (v/v) Glycerol
SEC buffer	200 mM NaCl
	50 mM Tris-HCl pH = 8

Table 2.8: Buffer and solutions for purification of TRPC 3, 4 and 6 ARDs

Buffer/solution	Ingredients
E.coli lysis buffer TRPC ARDs	20 mM Imidazol pH = 8
	300 mM NaCl
	20 mM Tris-HCl pH = 8
	0.1 % (v/v) Triton X-100
	add fresh:
	1 mM Benzamidine
	1 mM PMSF
	1 SIGMA*FAST* Protease Inhibitor
	RNAse, DNAse, Lysozyme
IMAC Wash 1	20 mM Imidazol pH = 8
	300 mM NaCl
	20 mM Tris-HCl pH = 8
Wash 2	50 mM Imidazol pH = 8
	300 mM NaCl

Buffer/solution	Ingredients
	20 mM Tris-HCl pH = 8
Elution	500 mM Imidazol pH = 8
	300 mM NaCl
	20 mM Tris-HCl pH = 8
SEC buffer	10 mM Tris-HCl pH = 7
	1 mM K-EDTA pH = 7
	300 mM NaCl
	1 mM DTT
	1 mM Benzamidine

Table 2.9: Buffer and solutions for purification of hsYAP-WW domains

Buffer/solution	Ingredients
E.coli lysis buffer hsYAP WW domains	20 mM Imidazol pH = 7.4
	120 mM NaCl
	30 mM HEPES pH = 7.4
	0.1 % (v/v) Triton X-100
	add fresh:
	1 mM Benzamidine
	1 mM PMSF
	1 SIGMA*FAST* Protease Inhibitor
	RNAse, DNAse, Lysozyme
IMAC Wash 1	20 mM Imidazol pH = 8
	120 mM NaCl
	30 mM HEPES pH = 8
IMAC Wash 2	50 mM Imidazol pH = 8
	120 mM NaCl
	30 mM HEPES pH = 8
IMAC Wash 3	75 mM Imidazol pH = 8
	120 mM NaCl

Buffer/solution	Ingredients
	30 mM HEPES pH = 8
IMAC Elution	500 mM Imidazol pH = 8
	120 mM NaCl
	30 mM HEPES pH = 8
TEV dialysis buffer	300 mM NaCl
	25 mM Tris-HCl pH = 7
	1 mM DTT
	TEV: hsYAP-WW domains 1 : 30 molar ratio
Reverse IMAC buffer	10 mM Imidazol pH = 8
	120 mM NaCl
	30 mM HEPES pH = 8
SEC buffer	120 mM NaCl
	30 mM HEPES pH = 7.4

2.3 Enzymes

Table 2.10: Enzymes

Enzymes	Supplier
Desoxyribonuclease I (DNAse)	Sigma-Aldrich, Munich
DpnI	NewEngland BioLabs, Frankfurt a.M.
HiFi Polymerase	Kapa Biosystems, Wilmington (USA)
Lactate Dehydrogenase (LDH)	Sigma-Aldrich, Munich
Lysozyme	Sigma-Aldrich, Munich
Ribonuclease A (RNAse)	Sigma-Aldrich, Munich
T5 Exonuclease	NewEngland BioLabs, Frankfurt a.M.
Phusion DNA Polymerase	NewEngland BioLabs, Frankfurt a.M.
Pyruvate Kinase (PK)	Sigma-Aldrich, Munich
Taq DNA Ligase	NewEngland BioLabs, Frankfurt a.M.

Enzymes	Supplier
E1 Ubiquitin ligase UBE1	Prof. Sumner, Baltimore (USA)
E2 Ubiquitin ligase Ubc5Hc	Prof. Sumner, Baltimore (USA)

2.4 Antibodies

Table 2.11: Antibodies

Antibody	Supplier
Anti-ANXA2 mouse	Sigma-Aldrich, Munich
Anti-DDX3X rabbit	Sigma Aldrich, Munich
Anti-GFP mouse (3E6)	Invitrogen, Darmstadt
Anti-GFP mouse	Sigma-Aldrich, Munich
Anti-FLAG mouse	CST, Danvers (USA)
Anti-FLAG rabbit	CST, Danvers (USA)
Anti-V5 mouse	CST, Danvers (USA)
Anti-myc mouse	CST, Danvers (USA)
Anti-His_6-HRP	Invitrogen, Darmstadt
Streptavidin-POD (Strep-POD)	Roche, Basel (CH)
Horse anti-mouse HRP-linked IgG	CST, Danvers (USA)
Goat anti-rabbit HRP-linked IgG	CST, Danvers (USA)
Alexa-Fluor-488 goat anti-mouse	Invitrogen, Darmstadt
Alexa-Fluor-555 goat anti-rabbit	Invitrogen, Darmstadt
Alexa Fluor-647 goat anti-mouse	Invitrogen, Darmstadt
Alexa Fluor-647 goat anti-rabbit	Invitrogen, Darmstadt

2.5 Oligonucleotides

The oligonucleotides in tables 2.12 and 2.13 were designed in the course of this work and were obtained from Sigma-Aldrich (Munich). For the estimation of the melting temperatures equation 2.1 was used. The nomenclature of the primers refers to the employed nomenclature at the Hellmich workgroup.

$$T_m = 4 \cdot \#\text{G and C} + 2 \cdot \#\text{A and T} \tag{2.1}$$

Table 2.12: Oligonucleotides for Quickchange PCR

Designation	Sequence ($5^{'}$–$3^{'}$)	Length	T_m [°C]
human TRPV4 S134A_for	GAGAAGCAGCCGCAGGAACCCAAAGCC	27mer	71
human TRPV4 S134A_rev	GTCGGCGTCCTTGGGTTTCGGGGAC	25mer	70
human TRPV4 S134E_for	GAGAAGCAGCCGCAGGAACCCAAAGAA	27mer	67
human TRPV4 S134E_rev	GTCGAAGTCCTTGGGTTTCGGGGAC	25mer	65
human TRPV4 E183K_for	CGCCTAACTGATAAGGAGTTTCGAG	25mer	70
human TRPV4 E183K_rev	GGCTCTCGAAACTCCTTATCAGTTAG	26mer	70
human TRPV4 L199F_for	GCCCAAGGCCTTTCTGAACCTGAGC	25mer	75
human TRPV4 L199F_rev	CATTGCTCAGGTTCAGAAAGGCCTTG	26mer	71
human TRPV4 R232C_for	CATTAACTCGCCCTTCTGTGACATC	25mer	70
human TRPV4 R232C_rev	GATAGTAGATGTCACAGAAGGGCGAG	26mer	72
human TRPV4 R269C_for	GCCCAGGCCTGTGGGCGCTTCTTC	24mer	78
human TRPV4 R269C_rev	GCTGGAAGAAGCGCCCACAGGCCTG	25mer	78
human TRPV4 R271P_rev	CCCGTGGGCCCTTCTTCCAGCC	22mer	75
human TRPV4 R271P_rev	CTTGGGCTGGAAGAAGGGCCCACG	24mer	76
human TRPV4 K276E_for	CGCTTCTTCCAGCCCGAGGATGAG	24mer	75
human TRPV4 K276E_rev	CCCCCTCATCCTCGGGCTGGAAG	23mer	76
human TRPV4 R315W_for	GGCGGACATGTGGCGCCAGGACTC	24mer	78
human TRPV4 R315W_rev	CGCGAGTCCTGGCGCCACATGTC	23mer	77
human TRPV4 R316C_for	GACATGCGGTGCCAGGACTCGCG	23mer	77
human TRPV4 R316C_rev	GCCTCGCGAGTCCTGGCACCGC	22mer	77

Table 2.12: Oligonucleotides for Quickchange PCR

Designation	Sequence ($5'$–$3'$)	Length	T_m [°C]
human TRPV4 I331F_for	CTGGTGGCCTTTGCTGACAACACC	24mer	73
human TRPV4 I331F_rev	GTTGTCAGCAAAGGCCACCAGCGCATG	27mer	77
human TRPV4 D333G_for	CTGGTGGCCATTGCTGGCAACACCCGTG	28mer	80
human TRPV4 D333G_rev	GTTCTCACGGGTGTTGCCAGCAATGGCCAC	30mer	81
human TRPV4 V342F_for	CGTGAGAACACCAAGTTTTTTACCAAGATG	30mer	72
human TRPV4 V342F_rev	GGTCGTACATCTTGGTAAAAAACTTGGTG	29mer	72
human TRPV4 M680K_for	CTGACCATCGGCAAGGGCGAC	21mer	72
human TRPV4 M680K_rev	CGCCCTTGCCGATGGTCAGC	20mer	72

Table 2.13: Oligonucleotides for Gibbson Assembly

Designation	Sequence ($5'$–$3'$)	Length	T_m [°C]
pCAGIG_PACSIN1_V_for	CTCAGATGGTTCCGCAGCACCAGTGGCCC CGGCATG	36mer	64
pCAGIG_PACSIN1_V_rev	CGTCCGTGGTACAGGTCGAGGATGCTACT CCGGAGTGAC	39mer	63
pCAGIG_P1V_P3F_for	CGATGAGGCCTCACTGATGGCTCCAGAA GAGGACGCTG	38mer	62
pCAGIG_P1V_P3F_rev	GCTGCGGAACCATCTGAGATCCTCT TCGTCACTGGCTGCCTC	42mer	63
pCAGIG_P1V_P2F_for	CGATGAGGCCTCACTGGTAGAAGTGTC CAGCGACAGCTTCTG	40mer	63
pCAGIG_P1V_P2F_rev	GCTGCGGAACCATCTGAGGTCCTCCAC TGCATCAGCTGCTCTG	39mer	64
pCAGIG_PACSIN2_V_for	CTGAGGTGGTTCCGAGCCAATCACGGG CCGGGCATG	36mer	65
pCAGIG_PACSIN2_V_rev	TCCAACGGAATCATCATATGTGACAGA CATGGTGCCTGCTTTTTTG	46mer	61

Table 2.13: Oligonucleotides for Gibbson Assembly

Designation	Sequence ($5^{'}$–$3^{'}$)	Length	T_m [°C]
pCAGIG_P2V_P1F_for	CATATGATGATTCCGTTGGAGCGCCAGA GGAGACCACCGAC	41mer	65
pCAGIG_P2V_P1F_rev	CTCGGAACCACCTCAGGTCTTCCTGGGC	37mer	64
pCAGIG_P2V_P3F_for	CATATGATGATTCCGTTGGAATGGCTCC AGAAGAGGACGCTGG	43mer	64
pCAGIG_P2V_P3F_rev	CTCGGAACCACCTCAGATCCTCTTCGTC ACTGGCTGCCTC	40mer	63
pCAGIG_PACSIN3_V_for	CTGCGCTGGTGGCGCAGCACCCACGGGCC AGG	32mer	64
pCAGIG_PACSIN3_V_rev	GGTGGAGCCTGCTTTTTTGTACAAACTTG TGATCAATTCGGTGCTGTC	48mer	62
pCAGIG_P3V_P1F_for	AAAAAAGCAGGCTCCACCGCGCCAGAGGA GACCACCGAC	39mer	65
pCAGIG_P3V_P1F_rev	GCGCCACCAGCGCAGGTCTTCCTGGGCAT CAGCCCCC	37mer	64
pCAGIG_P3V_P2F_for	AAAAAGCAGGCTCCACCGTAGAAGTGTCC AGCGACAGCTTCTGG	39mer	64
pCAGIG_P3V_P2F_rev	GCGCCACCAGCGCAGGTCCTCCACTGCAT CAGCTGCTCTG	40mer	63

Table 2.14: Sequencing oligonucleotides

Designation	Sequence ($5^{'}$–$3^{'}$)	Length
T7_promotor	TAATACGACTCACTATAGGG	20mer
T7_terminator	GCTAGTTATTGCTCAGCGG	19mer
SP6	ATTAGGTGACACTATAG	18mer

2.6 Plasmids and expression constructs

T7_oligonucloetides (table 2.14) were used to determine the DNA sequence of the various modified pET21, pET28a, pET11 and pcDNA3.1 plasmids (table 2.14). For reverse sequencing of pcDNA3.1 the SP6 oligonucleotide was used. mm = *Mus musculus* (mouse), hs = *Homo sapiens* (human), gg = *Gallus gallus* (chicken), rn = *Rattus norvegicus* (rat), d = *Drosophila melanogaster* (fruit fly), dr = *Danio rerio* (zebra fish).

Table 2.15: Expression plasmids generated and used in the course of this work. hsV4NΔ132 is also referred as hsV4 ARD, hsV4NΔ122 as hsV4 ARD-PRR. The nomenclature of the plasmids refers to the employed nomenclature at the Hellmich workgroup.

Plasmid	Construct	Vector	Resistance	Origin
p17	eGFP	pcDNA3.1	Ampicillin	RG[redacted] Mainz
p22	rnTRPV2-cGFP	pcDNA3.1-cGFP	Ampicillin	Prof. [redacted], Cambridge
p24	ggTRPV4-cGFP	pcDNA3.1-cGFP	Ampicillin	Prof. [redacted] Cambridge
p25	dTRPML-cGFP	pcDNA3.1-cGFP	Ampicillin	Prof. [redacted], Cambridge
p34	rnTRPV1-ARD	pET21-cHis$_6$	Ampicillin	Prof. [redacted] Cambridge
p35	drTRPV1-ARD	pET21-cHis$_6$	Ampicillin	Prof. [redacted] Cambridge
p36	ggTRPV1-ARD	pET21-cHis$_6$	Ampicillin	Prof. [redacted] Cambridge
p37	rnTRPV2-ARD	pET21-cHis$_6$	Ampicillin	Prof. [redacted], Cambridge
p41	hsCalmodulin	pET21-cHis$_6$	Ampicillin	Prof. [redacted] Cambridge
p62	Ulp-1	pET28a	Kanamycin	Prof. [redacted], Frankfurt a.M.
p113	hsTRPML-1-nGFP	pEGFP C3	Kanamycin	Prof. [redacted], Cambridge
p114	mmTRPML-2b-c	pcDNA3.1-cYFP	Ampicillin	Prof. [redacted], Santa Barbara
p129	ggV4N-cGFP	pcDNA3.1-cGFP	Ampicillin	[redacted][21], Mainz
p130	ggV4N_aawaa-cGFP	pcDNA3.1-cGFP	Ampicillin	[redacted]¡[21], Mainz
p131	ggV4NΔ53-cGFP	pcDNA3.1-cGFP	Ampicillin	[redacted]¡[21], Mainz
p132	ggV4NΔ53_aawaa-cGFP	pcDNA3.1-cGFP	Ampicillin	[redacted]¡[21], Mainz
p134	hsV4N	pET21-cHis$_6$	Ampicillin	Prof. [redacted], Cambridge (USA)
p138	BirA ligase	pET21-cHis$_6$	Ampicillin	RG [redacted] Mainz
p151	hsV4N Avi2	pET21-cHis$_6$	Ampicillin	B. Sc. E. Diehl, Mainz[76]
p154	hsV4N Avi3	pET21-cHis$_6$	Ampicillin	B. Sc. E. Diehl, Mainz[76]
p155	BirA ligase	pET28a	Kanamycin	B. Sc. E. Diehl , Mainz[76]

Table 2.15: Expression plasmids generated and used in the course of this work. hsV4NΔ132 is also referred as hsV4 ARD, hsV4NΔ122 as hsV4 ARD-PRR. The nomenclature of the plasmids refers to the employed nomenclature at the Hellmich workgroup.

Plasmid	Construct	Vector	Resistance	Origin
p181	ggV4NΔ122-cGFP	pcDNA3.1-cGFP	Ampicillin	M. Sc. [redacted], Mainz
p182	ggV4NΔ132-cGFP	pcDNA3.1-cGFP	Ampicillin	M. Sc. [redacted], Mainz
p222	hsV4NΔ132	pET21-cHis$_6$	Ampicillin	M. Sc. E. Diehl, Mainz[76]
p223	hsV4NΔ122	pET21-cHis$_6$	Ampicillin	M. Sc. E. Diehl, Mainz[76]
p381	hsV4NΔ132 E183K	pET21-cHis$_6$	Ampicillin	[redacted] and M. Sc. E. Diehl, Mainz[77]
p382	hsV4NΔ132 L199F	pET21-cHis$_6$	Ampicillin	[redacted]itt and M. Sc. E. Diehl, Mainz[77]
p383	hsV4NΔ132 R232C	pET21-cHis$_6$	Ampicillin	[redacted] and M. Sc. E. Diehl, Mainz[77]
p384	hsV4NΔ132 R269C	pET21-cHis$_6$	Ampicillin	[redacted] and M. Sc. E. Diehl, Mainz[77]
p385	hsV4NΔ132 R271P	pET21-cHis$_6$	Ampicillin	[redacted] and M. Sc. E. Diehl, Mainz[77]
p386	hsV4NΔ132 K276E	pET21-cHis$_6$	Ampicillin	[redacted] and M. Sc. E. Diehl, Mainz[77]
p387	hsV4NΔ132 R315W	pET21-cHis$_6$	Ampicillin	[redacted] and M. Sc. E. Diehl, Mainz[77]
p388	hsV4NΔ132 R316C	pET21-cHis$_6$	Ampicillin	[redacted] and M. Sc. E. Diehl, Mainz[77]
p389	hsV4NΔ132 V342F	pET21-cHis$_6$	Ampicillin	[redacted] and M. Sc. E. Diehl, Mainz[77]
p390	hsV4NΔ132 Avi2	pET21-cHis$_6$	Ampicillin	[redacted] and M. Sc. E. Diehl[77], Mainz
p793	hsV4NΔ132 E183K Avi2	pET21-cHis$_6$	Ampicillin	[redacted] and M. Sc. E. Diehl, Mainz[77]
p794	hsV4NΔ132 L199F Avi2	pET21-cHis$_6$	Ampicillin	[redacted] and M. Sc. E. Diehl, Mainz[77]
p795	hsV4NΔ132 R232C Avi2	pET21-cHis$_6$	Ampicillin	[redacted] and M. Sc. E. Diehl, Mainz[77]
p796	hsV4NΔ132 R269C Avi2	pET21-cHis$_6$	Ampicillin	[redacted] and M. Sc. E. Diehl, Mainz[77]
p797	hsV4NΔ132 R271P Avi2	pET21-cHis$_6$	Ampicillin	[redacted] and M. Sc. E. Diehl, Mainz[77]
p798	hsV4NΔ132 K276E Avi2	pET21-cHis$_6$	Ampicillin	[redacted] and M. Sc. E. Diehl, Mainz[77]
p799	hsV4NΔ132 R315W Avi2	pET21-cHis$_6$	Ampicillin	[redacted] and M. Sc. E. Diehl, Mainz[77]

Table 2.15: Expression plasmids generated and used in the course of this work. hsV4NΔ132 is also referred as hsV4 ARD, hsV4NΔ122 as hsV4 ARD-PRR. The nomenclature of the plasmids refers to the employed nomenclature at the Hellmich workgroup.

Plasmid	Construct	Vector	Resistance	Origin
p800	hsV4NΔ132 R316C Avi2	pET21-cHis$_6$	Ampicillin	[redacted] and M. Sc. E. Diehl, Mainz[77]
p801	hsV4NΔ132 V342F Avi2	pET21-cHis$_6$	Ampicillin	[redacted] and M. Sc. E. Diehl, Mainz[77]
p412	hsYAP1_WW1 domain	pET11a-nHis$_6$	Ampicillin	obtained from GeneScript, M. Sc. E. Diehl
p413	hsYAP1_WW2 domain	pET11a-nHis$_6$	Ampicillin	obtained from GeneScript, M. Sc. E. Diehl
p414	hsYAP1_WW1+WW2 domains	pET11a-nHis$_6$	Ampicillin	obtained from GeneScript, M. Sc. E. Diehl
p505	hsITCH	pET11a-nHis$_6$	Ampicillin	obtained from GeneScript, M. Sc. E. Diehl
p506	hsITCH_WW1 domain	pET11a-nHis$_6$	Ampicillin	obtained from GeneScript, M. Sc. E. Diehl
p507	hsITCH_WW2 domain	pET11a-nHis$_6$	Ampicillin	obtained from GeneScript, M. Sc. E. Diehl
p508	hsITCH_WW3 domain	pET11a-nHis$_6$	Ampicillin	obtained from GeneScript, M. Sc. E. Diehl
p509	hsITCH_WW4 domain	pET11a-nHis$_6$	Ampicillin	obtained from GeneScript, M. Sc. E. Diehl
p510	hsITCH_WW1+WW2 domains	pET11a-nHis$_6$	Ampicillin	obtained from GeneScript, M. Sc. E. Diehl
p511	hsITCH_WW3+WW4 domains	pET11a-nHis$_6$	Ampicillin	obtained from GeneScript, M. Sc. E. Diehl
p512	hsRhoA	pET11a-nHis$_6$	Ampicillin	obtained from GeneScript, M. Sc. E. Diehl
p513	hsITCH_WW1$-$WW4 domains	pET11a-nHis$_6$	Ampicillin	obtained from GeneScript, M. Sc. E. Diehl
p598	BirA R118A-nP1	pcDNA3.1-cGFP	Ampicillin	[redacted] and M. Sc. E. Diehl, Mainz[78]
p802	hsTRPV4	pcDNA3.1-cGFP	Ampicillin	Prof. [redacted] Baltimore
p803	hsTRPV4 S134E	pcDNA3.1-cGFP	Ampicillin	[redacted] and M. Sc. E. Diehl, Mainz[78]
p804	hsTRPV4 S134A	pcDNA3.1-cGFP	Ampicillin	[redacted] and M. Sc. E. Diehl, Mainz[78]
p805	hsTRPV4 R232C	pcDNA3.1-cGFP	Ampicillin	this work
p806	hsTRPV4 R269C	pcDNA3.1-cGFP	Ampicillin	this work
p807	hsTRPV4 R271P	pcDNA3.1-cGFP	Ampicillin	this work

Table 2.15: Expression plasmids generated and used in the course of this work. hsV4NΔ132 is also referred as hsV4 ARD, hsV4NΔ122 as hsV4 ARD-PRR. The nomenclature of the plasmids refers to the employed nomenclature at the Hellmich workgroup.

Plasmid	Construct	Vector	Resistance	Origin
p808	hsTRPV4 K276E	pcDNA3.1-cGFP	Ampicillin	this work
p809	hsTRPV4 R315W	pcDNA3.1-cGFP	Ampicillin	this work
p810	hsTRPV4 V342F	pcDNA3.1-cGFP	Ampicillin	this work
p811	hsTRPV4 M680K	pcDNA3.1-cGFP	Ampicillin	[redacted] and M. Sc. E. Diehl, Mainz[78]
p812	hsTRPV4	pcDNA3.1-cFLAG	Ampicillin	Prof. [redacted] Baltimore
p813	hsTRPV4 R232C	pcDNA3.1-cFLAG	Ampicillin	[redacted] and M. Sc. E. Diehl, Mainz[77]
p814	hsTRPV4 R269C	pcDNA3.1-cFLAG	Ampicillin	Prof. [redacted], Baltimore
p815	hsV4NΔ132 I331F	pET21-cHis$_6$	Ampicillin	[redacted] and M. Sc. E. Diehl, Mainz[78]
p816	hsV4NΔ132 D333G	pET21-cHis$_6$	Ampicillin	[redacted] and M. Sc. E. Diehl, Mainz[78]
p817	hsDDX3X_aa122-582	pET21-nHis$_6$	Kanamycin	Prof. [redacted] Regensburg
p818	hsDDX3X	pcDNA3.1-nV5	Ampicillin	obtained from GeneScript, M. Sc. E. Diehl, Mainz
p819	mmPACSIN1	pCAGIG-nV5	Ampicillin	Prof. [redacted] Baltimore
p820	mmPACSIN2	pCAGIG-nV5	Ampicillin	Prof. [redacted] Baltimore
p821	mmPACSIN3	pCAGIG-nV5	Ampicillin	Prof. [redacted] Baltimore
p822	hsPACSIN1	pCAGIG-nV5	Ampicillin	Prof. [redacted], Baltimore
p823	hsPACSIN2	pCAGIG-nV5	Ampicillin	Prof. [redacted], Baltimore
p824	hsPACSIN3	pCAGIG-nV5	Ampicillin	Prof. [redacted] Baltimore
p825	hsPACSIN_F1_S2 (hsPACSIN2+1)	pCAGIG-nV5	Ampicillin	this work

Table 2.15: Expression plasmids generated and used in the course of this work. hsV4NΔ132 is also referred as hsV4 ARD, hsV4NΔ122 as hsV4 ARD-PRR. The nomenclature of the plasmids refers to the employed nomenclature at the Hellmich workgroup.

Plasmid	Construct	Vector	Resistance	Origin
p826	hsPACSIN_F1_S3 (hsPACSIN3+1)	pCAGIG-nV5	Ampicillin	this work
p827	hsPACSIN_F2_S1 (hsPACSIN1+2)	pCAGIG-nV5	Ampicillin	this work
p828	hsPACSIN_F2_S3 (hsPACSIN3+2)	pCAGIG-nV5	Ampicillin	this work
p829	hsPACSIN_F3_S1 (hsPACSIN1+3)	pCAGIG-nV5	Ampicillin	this work
p830	hsPACSIN_F3_S2 (hsPACSIN2+3)	pCAGIG-nV5	Ampicillin	this work
p831	mCherry	pcDNA3.1	Ampicillin	Prof. [redacted] Baltimore
p832	hsYAP1	pcDNA3.1-nV5	Ampicillin	Prof. [redacted], Baltimore
p833	hsRUVBL1	pcDNA3.1-nmyc	Ampicillin	Prof. [redacted] Baltimore
p834	Empty Vector (EV)	pcDNA3.1	Ampicillin	Prof. [redacted] Baltimore
p835	hsTRPC3 ARD_aa16-181	pET11a-nHis$_6$	Ampicillin	Prof. [redacted], Cambridge
p836	hsTRPC4 ARD_aa25-185	pET11a-nHis$_6$	Ampicillin	Prof. [redacted] Cambridge
p837	hsTRPC6 ARD_aa87-252	pET11a-nHis$_6$	Ampicillin	Prof. [redacted], Cambridge

2.7 Peptide and protein characteristics

In the following, protein and peptide characteristics of the constructs used in this work are listed. Table 2.16 lists all constructs which were recombinantly expressed in *E. coli* BL21 Gold (DE3) cells and subsequently purified according section 3.7. Characteristics of protein and peptides with no TEV-cleavage site are listed with the His_6-tag, whereas TEV cleavage site containing proteins are listed without His_6-tag.
Table 2.17 lists all protein construct which were recombinantly expressed in HEK293 and/or HEK293T cells (see also sections3.2.1, 3.3, 3.4 and 3.5).

Table 2.16: Physicochemical properties of proteins and peptides recombinantly expressed in *E. coli* BL21 Gold (DE3), purified and used in this thesis. Characteristics were calculated using the Protparam tool (http://web.expasy.org/protparam/). hsV4NΔ132 is also referred to as hsV4 ARD, hsV4NΔ122 as hsV4 ARD-PRR. MW: molecular weight [Da]; AA: number of amino acids; pI: isoelectric point; ϵ 280: extinction coefficient at 280 nm in [L mol^{-1} cm^{-1}]

Peptide/ protein	MW [Da]	AA	pI	ϵ 280
hsDDX3X_aa 122-582	52 057	461	5.61	44 725
BirA ligase	35 312	321	7.76	47 440
hsV4N-cHis_6	44 977	406	8.24	20 650
hsV4N Avi2-cHis_6	46 788	421	7.00	25 900
hsV4NΔ122-cHis_6	30 616	271	9.00	10 680
hsV4NΔ132-cHis_6	29 221	257	8.65	10 680
hsV4NΔ132-cHis_6 R232C	29 221	257	8.65	10 680
hsV4NΔ132-cHis_6 R269C	29 221	257	8.65	10 680
hsV4NΔ132-cHis_6 D333G	29 221	257	8.65	10 680
hsV4NΔ132-Avi2	31 089	273	7.39	16 180
hsV4NΔ132-Avi2 R232C	31 089	273	7.39	16 180
hsV4NΔ132-Avi2 K276E	31 089	273	7.39	16 180
hsV4NΔ132-Avi2 V342F	31 089	273	7.39	16 180
hsTRPC3 ARD_aa16-181-nHis_6	19 887	175	5.49	10 555
hsTRPC4 ARD_aa25-185-nHis_6	18 055	161	5.91	7450
hsTRPC6 ARD_aa87-252-nHis_6	19 923	175	5.55	10 555
hsYAP1_WW1 domain	5184	45	4.89	12 490

Peptide/ protein	MW [Da]	AA	pI	ϵ 280
hsYAP1_WW2 domain	4589	40	4.89	13 980
hsYAP1_WW1+WW2 domains	11 926	105	4.88	26 470
hsITCH	102 859	904	5.94	154 085
hsITCH_WW1 domain	14 112	135	10.34	13 980
hsITCH_WW2 domain	4246	35	8.59	13 980
hsITCH_WW3 domain	3981	34	8.59	12 490
hsITCH_WW4 domain	4923	42	5.58	8480
hsITCH_WW1+WW2 domains	17 926	166	10.48	27 960
hsITCH_WW3+WW4 domains	8772	74	6.94	20 970
hsITCH_WW1-WW4 domains	32 219	286	9.59	57 410
hsRhoA	21 825	194	5.84	18 825

Table 2.17: Physicochemical properties of proteins and peptides recombinantly expressed in HEK293 and/or HEK293T cells in this thesis. Characteristics were calculated using the Protparam tool (http://web.expasy.org/protparam/). MW: molecular weight [Da]; AA: number of amino acids

Protein	MW [Da]	AA
hsTRPV4-cGFP	125 204	1110
hsTRPV4 R232C-cGFP	125 204	1110
hsTRPV4-nFLAG	99 276	879
hsTRPV4 R269C-nFLAG	99 276	879
hsPACSIN-1-nV5	53 776	471
hsPACSIN-2-nV5	58 549	513
hsPACSIN-3-nV5	51 297	451
hsPACSIN-F1-S2-nV5 (hsPACSIN2+1-nV5)	34 879	305
hsPACSIN-F1-S3-nV5 (hsPACSIN3+1-nV5)	40 859	355
hsPACSIN-F2-S1-nV5	53 423	471

Protein	MW [Da]	AA
(hsPACSIN1+2-nV5)		
hsPACSIN-F2-S3-nV5	50 823	444
(hsPACSIN3+2-nV5)		
hsPACSIN-F3-S1-nV5	54 155	479
(hsPACSIN1+3-nV5)		
hsPACSIN-F3-S2-nV5	36 478	318
(hsPACSIN3+2-nV5)		
hsDDX3X-nV5	76 154	690
hsRUVBL1-myc	51 757	470
mCherry	26 722	236

2.8 Kits

Table 2.18: Kits

Designation	Usage	Supplier
E.Z.N.A Plasmid Mini Kit I	Plasmid DNA isolation	Omega Bio-Tek, Norcross (USA)
GenepHlow Gel/PCR Kit	PCR clean up	Geneaid, New Tapei City (TW)
GTPase Glo Assay	Instrinsic GTPase acivity assay	Promega, Walldorf
KAPA HiFi HotStart PCR Kit	PCR ingredients	Kapa Biosystems, Wilmington (USA)
Fluo-4 Direct Calcium Assay	Ca^{2+}-influx assay	Invitrogen, Darmstadt
4 - 15 % Mini-Protean® TGX™ Precast Protein Gels	Blue native (BN) PAGE gels	BioRad, Hercules (USA)

2.9 Media and supplements for cell culture

Table 2.19: Media and supplements for cell culture

Name	Supplier
LB-Medium (Luria Broth)	Roth, Karlsruhe
TB-Medium (Terrific Broth)	Roth, Karlsruhe
Dulbecco's Modified Eagle Medium (DMEM)	Invitrogen, Darmstadt
Fetal calf serum (FCS)	Invitrogen, Darmstadt
10x Trypsin	Invitrogen, Darmstadt
G-418	Sigma-Aldrich, Munich
L-Glutamine	Invitrogen, Darmstadt
Penicillin / Streptomycin (P/S)	Sigma-Aldrich, Munich
Poly-L-lysine	Invitrogen, Darmstadt

2.10 Cells

Cells were obtained from various sources indicated in table 2.20. HEK293-hsV4-cGFP and HEK293-hsTRPML1-nGFP are stably transfected HEK293 cell strains which were obtained in the course of this work (see 3.2.3 for procedure).

Table 2.20: Cells

Name	Source
E. coli strain BL21 (DE3) Gold	Agilent Technologies, Santa Clara (USA)
E. coli strain DH5α	Agilent Technologies, Santa Clara (USA)
HEK293 cells	PD [redacted], Mainz
HEK293T cells	Prof. [redacted], Mainz
	Prof. [redacted] Baltimore (USA)
HEK293-hsV4-cGFP	this work

Table 2.20: Cells

Name	Source
HEK293-hsTRPML1-nGFP	this work

2.11 Laboratory equipment

Table 2.21: Laboratory equipment

Name	Supplier
Acquity UPLC HSS-T3 reverse phase column	Waters Corporation, Milford (USA)
Avanti J-26XP Centrifuge	Beckmann Coulter, Brea (USA)
Bruker AVANCE 600, 700 and 800 MHz spectrometers	Bruker, Karlsruhe
Branson Sonifier 250	Branson, Danbury (USA)
Centrifuge 5810 R	Eppendorf, Hamburg
Centrifuge 5415 R	Eppendorf, Hamburg
Centrifuge rotor JA 25.50	Eppendorf, Hamburg
Centrifuge rotor JLA 8.1000	Eppendorf, Hamburg
Optima MAX XP Ultra-centrifuge	Beckmann Coulter, Brea (USA)
NGC-Quest ÄKTA purifier	BioRad, Hercules (USA)
FlexStation 3 MultiMode Plate Reader	MolecularDevices, San Jose (USA)
FLUOStar Omega Microplate Reader	BMG LabTech, Ortenberg
Frac-920 Fraction collector	BioRad, Hercules (USA)
INCU-line IL 10 Incubator	VWR, Radnor (USA)
J-815 CD Spectrometer	JASCO, Pfungstadt
Lamda DG-4 wavelength switcher	Sutter Instruments, San Francisco (USA)
pH electrode LE409	Mettler-Toledo, Columbus (USA)
Photometer Lambda 25	Perkin Elmer , Waltham (USA)
PowerPac Basic power supply	BioRad, Hercules (USA)
ViewPix700 Scanner	GE Healthcare, Fairfield (USA)

Name	Supplier
Mini-PROTEAN Tetra Cell	BioRad, Hercules (USA)
HiLoad 16/600 Superdex 75 SEC column	GE Healthcare, Fairfield (USA)
HiLoad 16/600 Superdex 200 SEC column	GE Healthcare, Fairfield (USA)
Spectrofluorometric detector RF-20A	Shimadzu, Kyoto (Japan)
STELLA 3200 CCD camera	Raytest GmbH, Straubenhardt
Synapt G2-S HDMS	Waters Corporation, Milford (USA)
Thermomixer comfort	Eppendorf, Hamburg
nanoAcquity UPLC	Waters Corporation, Milford (USA)
NanoDrop 2000c UV-Vis spectrophotometer	Thermo Scientific, Waltham (USA)
Membrane pump MD 4C	Vacuubrand, Wertheim
Thermal cycler Primus 25	MWG Biotech, Ebersberg
Quantum gel documentation	Peqlab, Erlangen
ViewPix 700 Scanner	Biostep, Burkhardtsdorf
Zeiss Axio Observer Z1 Inverted Microscope	Zeiss, Jena
Zeiss LSM800 Confocal Microscope	Zeiss, Jena

2.12 Software

Table 2.22: Software

Name	Source / distributor
Adobe Photoshop CS 5	Adobe Systems GmbH, München
CARA	AG Wüthrich, ETH Zürich (CH)
	`http://cara.nmr.ch/`
CorelDraw 2019	Corel Corporation, Ottawa (CAN)
CytoScape	Cytoscape Consortium
TEXStudio	Free Software Foundation
DrawTree 3.66	LIRMM, Montpellier (FRA)
David Go	Laboratory of Human Retrovirology

Name	
	and Immunoinformatics, Frederick (USA)
BibLaTeX	Free Software Foundation
TeXlive	Free Software Foundation
ProtParam	ExPasy, SIB Swiss Institute of Bioinformatics
TranslateTool	ExPasy, SIB Swiss Institute of Bioinformatics
TOPSPIN 3.5 pl 5	Bruker, Karlsruhe
Clustal Omega	EMBL-EBI, Hinxton (GB)
CAPITO	Fritz Lipmann Institute, Leipzig
OriginLab 7	OriginLab, Northampton (USA)

3 Methods

3.1 General methods

3.1.1 Heat-shock transformation of *E. coli* bacteria

0.5 µL of plasmid DNA were added to 25 µL of competent *E. coli* BL21 (DE33) Gold or DH5α cells and incubated on ice for 30 min. Cells were heat shocked at 42 °C for 45 s and again incubated on ice for 2 min. Afterwards, 300 µL of LB-Medium were added and the cells were grown for 1 h at 37 °C and 225 rpm. Subsequently, the cells were plated onto an antibiotic containing agar plate and incubated over night at 37 °C.

3.1.2 Plasmid DNA preparation from *E. coli*

An over night culture of *E. coli* DH5α cells was cultivated in 5 mL LB medium at 37 °C which contained the suitable amount of antibiotics. After centrifugation at 3900 rpm for 10 min at 4 °C the plasmid DNA was isolated with the E.Z.N.A Plasmid Mini Kit I (protocol I of instruction manual). DNA concentration was determined by absorption measurements at 260 nm with a ThermoScientific NanoDrop 2000c UV-Vis spectrophotometer.

3.1.3 Polymerase chain reaction (PCR)

Modifications and amplifications of DNA fragments were performed via PCR. For this the Kapa HiFi HotStart PCR Kit and a Primus 25 thermo cycler were used. For more details on used oligonucleotides and methods see subsection 3.1.4 and tables 2.13 and 2.12. Prior to further usage, the template DNA was digested with DpnI, which specifically recognizes methylated

DNA. Furthermore the DNA was cleaned up with the GenepHlow Gel/PCR Kit and eluted in 30 µL ddH_2O.

Table 3.1: DpnI digestion reaction mixture

Component	Volume [µL]
10x Cutsmart buffer	5
ddH_2O	22.5
DpnI	1
PCR reaction mixture	22.5

3.1.4 Gibson Assembly

Gibson Assembly is a suitable method to merge linear DNA fragments to obtain, for example, new combinations of insert and vector DNA.[79,80] After generation of linear DNA segments via PCR, annealing of the fragments is performed in a buffer which contains three different enzymes. First, an exonuclease creates single-stranded 3' overhangs for annealing purposes. The occurring gaps in the annealed DNA fragments are filled by a DNA polymerase and a DNA ligase covalently links the fragments. After incubation of the DNA fragments in the isothermal ligation reaction mix (see table 3.2) for 1 h at 50 °C, the DNA was transformed into *E. coli* DH5α cells and isolated as described in sections 3.1.1 and 3.1.2.

Table 3.2: Reaction mixtures for Gibson Assembly

Buffer/solution	Ingredients
5x Isothermal Reaction Mix	0.5 M Tris-HCl pH = 7.5
	0.5 M $MgCl_2$
	1 mM dNTP Mix
	0.25 g/mL PEG-8000
	0.5 M NAD^+
Assembly Master Mix	1x Isothermal Master Mix

Buffer/solution	Ingredients
	0.5 U/µL T5 Exonuclease
	0.3 U/µL Phusion DNA Polymerase
	0.5 U/µL Taq DNA Ligase

3.1.5 Agarose gel electrophoresis

To separate DNA with various sizes agarose gel electrophoresis was performed. 1 or 2 % (w/v) agarose gels were used. Visualization of the different DNA plasmids and fragments was achieved by ethidium bromide staining for at least 20 min and detection with UV-light.

3.1.6 DNA sequencing

To confirm successful cloning of genes, DNA sequencing was performed by *GENterprise* GENOMICS (StarSEQ GmbH, Mainz). The primers from table 2.14 were used. The final sequencing mixture contained 300 - 700 ng plasmid DNA and 1 µL sequencing primer (10 µM stock solution, see also table 2.14) topped up to a total volume of 7 µL with ddH_2O.

3.1.7 SDS polyacrylamide gel electrophoresis (SDS-PAGE)

Proteins were separated according to their molecular weight with SDS-PAGE. For buffer compositions see table 2.2. Amongst other methods (see also section 3.1.8), visualization of the protein bands were accomplished by Coomassie staining. For the compositions of the Coomassie staining and destaining solution also see table 2.2.

Table 3.3: Composition of the stacking and separation gel for SDS-PAGE

Ingredients	separation gel 15 %	separation gel 12 %	stacking gel
ddH_2O	4.6 mL	4.6 mL	4.6 mL
1.5 mM Tris-HCl pH 8.8	5 mL	5 mL	/

Table 3.3: Composition of the stacking and separation gel for SDS-PAGE

Ingredients	separation gel 15 %	separation gel 12 %	stacking gel
1.0 mM Tris-HCl pH 6.8	/	/	0.63 mL
Acrylamid/Bisacrylamid 30 %	10 mL	8 mL	0.83 mL
SDS 10 % (w/v)	0.2 mL	0.2 mL	0.5 mL
APS 10 % (w/v)	0.2 mL	0.2 mL	0.5 mL
TEMED	0.2 mL	0.2 mL	0.5 mL

3.1.8 Western blot and chemiluminescence detection

After SDS-PAGE (see section 3.1.7) separated proteins were transferred onto a PVDF membrane with another electrophoresis step to detect specific proteins and/or their modifications, respectively, with an antibody mediated chemiluminescence reaction. Depending on the used antibodies, the membrane was incubated in different blocking solutions for 1 h at room temperature (see also 3.4). After three wash steps, each for 5 min at room temperature with PBS/T, the membrane was incubated in the particular peroxidase-coupled antibody solution (see also 3.5). Again, three wash steps were performed and chemiluminescence was induced with a 1:1-mixture of Roti®-Lumin reagents 1 and 2 detected either with a STELLA 3200 or GE ImageQuant CCD camera.

Table 3.4: Used primary antibody solutions and blocking solutions

Antibody solution	Blocking solution (% in w/v)
Anti-His_6-HRP 1:5000 in 2 % (w/v) milk powder in PBS/T	5 % (w/v) milk powder in PBS/T
Strep-POD 1:20 000 in 1 % (w/v) BSA in PBS/T	2 % (w/v) BSA in PBS/T
Anti-ANXA2 in 1 % (w/v) milk powder in PBS/T	5 % (w/v) milk powder in PBS/T
Anti-DDX3X 1:1000 in 1 % (w/v) milk powder in PBS/T	5 % (w/v) milk powder in PBS/T
Anti-V5 mouse 1:5000 in 1 % (w/v) milk powder in PBS/T	5 % (w/v) milk powder in PBS/T
Anti-myc mouse 1:1000 in 1 % (w/v) milk powder in PBS/T	5 % (w/v) milk powder in PBS/T
Anti-FLAG rabbit 1:1000 in 1 % (w/v) milk powder in PBS/T	5 % (w/v) milk powder in PBS/T
Anti-FLAG mouse 1:1000 in 1 % (w/v) milk powder in PBS/T	5 % (w/v) milk powder in PBS/T

Table 3.5: Used secondary antibody solutions

Antibody solution
Horse anti-mouse HRP-linked IgG 1:1000 in PBS/T
Goat anti-rabbit HRP-linked IgG 1:1000 in PBS/T

3.1.9 Protein quantification

To determine the protein concentrations various methods were used.

Bradford assay

With the Bradford Assay it is possible to obtain the concentration of protein in a sample via the quantitative assessment of the absorbance shift of Coomassie G-250 based on interactions between dye and proteins. As standards, increasing concentrations of BSA solutions were used (0 to 200 µg/µL).

Absorption measurements

Another method to assess the protein concentration of a sample is to measure the absorption at 280 nm with a ThermoScientific NanoDrop 2000c UV-Vis spectrophotometer due to the absorption of aromatic amino acids (tyrosine, tryptophan, phenylalanine). Because the number of these aromatic amino acids are varying in each protein, the specific molar extinction coefficients at 280 nm were computed using the ExPasy-ProtParam tool (`http://web.expasy.org/protparam/`).

3.1.10 Size exclusion chromatography

Proteins were purified according to their size via size exclusion chromatography (SEC). Depending on the sample volume and protein size, various columns were used (see table 3.6)

Table 3.6: Used SEC columns, manufactured by GE Healthcare

Column name	column volume	sample volume	separation range
HiLoad 16/600 Superdex 200	120 mL	$\leq$ 5 mL	70 000 - 3000 Da
HiLoad 16/600 Superdex 75	120 mL	$\leq$ 5 mL	600 000 - 10 000 Da
Superose™ 6 10/300 GL	24 mL	$\leq$ 500 µL	5 000 000 - 5000 Da

Columns were stored at 4 °C in 20 % (v/v) ethanol. SEC runs for each protein were also carried out at 4 °C and the columns were equilibrated in the appropriate SEC buffer before every protein purification. Chosen protein samples were adjusted to the desired sample volume with a centrifugal concentrator. Potential aggregates were removed by centrifugation at 3900 rpm and 4 °C for 10 min before loading it onto the SEC column. The sample was loaded onto a suitable loop and injected onto the column with a flow rate of 0.5 mL/min. Elution was performed isocratically for 1.1 CV. The flow rates during elution as well as the collected fraction size were adjusted to the individual proteins (see 3.7). The absorbence at 280 nm was detected and the purity of collected fractions verified via SDS-PAGE with subsequent Coomassie staining.

3.2 Cell culture of eukaryotic cells

3.2.1 Cultivation

HEK293 cell strains (see table 2.20) were cultivated in 10 cm dishes at 37 °C, 5 % CO_2 atmosphere and 95 % humidity with DMEM containing 10 % (v/v) FCS, 1 % (v/v) P/S and 1 % (v/v) L-Glutamine. HEK293-hsV4-cGFP were additionally treated with 0.500 µg/mL G-418 and 200 nM

TRPV4 inhibitor HC-067, HEK293-hsTRPML1-nGFP cells with 0.375 µg/mL G-418. Twice a week the cells were splitted in a ratio of 1:8. For splitting, the expended medium was aspirated and the cells were washed with 5 mL PBS. Afterwards, the cells were trypsinized with 1.5 mL trypsin/EDTA in 1.5 mL PBS and diluted to the desired ratio with fresh medium. The cells were then plated on fresh dishes. All media were warmed up to 37 °C in a water bath before use.

3.2.2 Transient transfection of HEK293T cells

For transient transfection of HEK293T cells, 575 000 cells were seeded into 6-well plates per well 24 h before transfection. Cells were transfected according the Lipofectamin® LTX reagent protocol. For fluorescence microscopy (see section 3.3) and live calcium imaging (see 3.5) poly-L-lysinated cover slips were provided in the 6-well dish. Used plasmid DNAs are listed in table 2.15 and used plasmid DNA amounts for transfections in table 3.7. If not otherwise indicated, cells were incubated with the DNA/lipid complex for 24 h.

Table 3.7: Used plasmid DNA amounts for transfections of HEK293T cells with Lipofectamine ® LTX

Expressed construct	Vector	Plasmid DNA amount [ng/well]
ggV4N-cGFP	pcDNA3.1-cGFP	2000
ggV4N_aawaa-cGFP	pcDNA3.1-cGFP	2000
ggV4NΔ53-cGFP	pcDNA3.1-cGFP	2000
ggV4NΔ53_aawaa-CGFP	pcDNA3.1-cGFP	2000
hsTRPV4-cGFP	pcDNA3.1-cGFP	500
hsTRPV4 S134E-cGFP	pcDNA3.1-cGFP	500
hsTRPV4 S134A-cGFP	pcDNA3.1-cGFP	500
hsTRPV4 R232C-cGFP	pcDNA3.1-cGFP	500
hsTRPV4 R269C-cGFP	pcDNA3.1-cGFP	500
hsTRPV4 K276E-cGFP	pcDNA3.1-cGFP	500
hsTRPV4 R315W-cGFP	pcDNA3.1-cGFP	500
hsTRPV4 V342F-cGFP	pcDNA3.1-cGFP	500
hsTRPV4 M680K-cGFP	pcDNA3.1-cGFP	500
hsTRPV4-nFLAG	pcDNA3.1-nFLAG	500

Expresssed construct	Vector	Plasmid DNA amount [ng/well]
hsTRPV4-R269C-nFLAG	pcDNA3.1-nFLAG	500
hsDDX3X-nV5	pcDNA3.1-nV5	1000
mmPACSIN1-nV5	pCAGIG-nV5	1000
mmPACSIN2-nV5	pCAGIG-nV5	1000
mmPACSIN3-nV5	pCAGIG-nV5	1000
hsPACSIN1-nV5	pCAGIG-nV5	500
hsPACSIN2-nV5	pCAGIG-nV5	500
hsPACSIN3-nV5	pCAGIG-nV5	500
hsPACSIN_F1_S2-nV5	pCAGIG-nV5	1000, 48 h
hsPACSIN_F1_S3-nV5	pCAGIG-nV5	1000, 48 h
hsPACSIN_F2_S1-nV5	pCAGIG-nV5	1000, 48 h
hsPACSIN_F2_S3-nV5	pCAGIG-nV5	1000, 48 h
hsPACSIN_F3_S1-nV5	pCAGIG-nV5	1000, 48 h
hsPACSIN_F3_S2-nV5	pCAGIG-nV5	1000, 48 h
mCherry	pcDNA3.1	500
hsYAP1-nV5	pcDNA3.1-nV5	500
hsRUVBL1-myc	pcDNA3.1-nmyc	500

3.2.3 Stable transfection of HEK293 cells

To generate stable HEK293 cell lines stably expressing either hsTRPV4-cGFP or hsTRPML1-nGFP, HEK293 cells were transfected as previoulsy described (see 3.2.2). For used plasmid DNA amounts, see table 3.8. Furthermore, after transfection, HEK293 cells expressing hsTRPV4-cGFP (HEK293-hsV4-cGFP), if not otherwise indicated, were always treated with 200 nM of the TRPV4 antagonist HC-067.

Table 3.8: Used plasmid amounts for stable transfections of HEK293 cells with Lipofectamine ® LTX

Expressed construct	Vector	Plasmid DNA amount [ng/well]	G-418 amount [µg/µL]
hsTRPV4-cGFP	pcDNA3.1-cGFP	500	0.500
hsTRPML1-nGFP	pEGFP C3	2000	0.375

After 24 h incubation with the DNA/lipid complex, cells were examined for GFP-signals on a widefield Zeiss Axio Observer Z1 Inverted Microscope. If GFP-positive, cells were passaged for 2 weeks and selected with G-418 (see table 3.8), with G-418-containing media changes after every 48 h. Large, healthy and GFP-positive colonies were isolated with sterile toothpicks and cultured for another 3 weeks in G-418 medium with media changes after every 48 h. With this, stably expressing, polyclonal cell lines were obtained. Proper protein expression, function and localization were confirmed with Western Blots with subsequent chemiluminescence detection, fluorescence microscopy and Ca^{2+}-influx assays. Generation of monoclonal cell lines failed, as the single cell transfer into 96-well plates resulted multiple times in cell death.

3.3 Immunostaining and fluorescence microscopy

HEK293T or HEK293 cells were stably or transiently transfected with plasmid DNA encoding for the desired protein (see sections 3.2.2 and 3.2.3). To obtain insights in protein localization and protein-protein co-localization in cells, immunostaining was performed on the cells. Cells were washed three times with PBS containing 0.2 % (v/v) Tween®-20 (PBS/T), followed by an incubation step with 50 mM NH_4Cl in PBS for 10 min due to formaldehyde quenching. To permeabilize the cell membranes towards the staining antibodies or reagents, the cells were incubated in PBS containing 0.3 % (v/v) Triton-X for 15 min at RT and washed with PBS for 3 times. After discarding, the cells were incubated in 1 % (w/v) BSA in PBS/T for 30 min and washed with PBS/T for three times. If needed, primary antibodies diluted in 1 % (w/v) BSA in PBS/T (see table 3.9) were applied to the cells and incubated at 4 °C over night. After washing with PBS/T for three times, respective secondary antibodies in PBS/T were applied and incubated for 1 h

at RT. Again three washing steps with PBS/T were performed. For F-actin staining, cells were incubated for 1 h with Phalloidin-TRITC at RT and after 3 PBS/T washing steps, nuclei were stained with DAPI for 30 min at RT. The cells were washed again for three times with PBS/T and finally with pure PBS. The cell bearing cover slips were mounted on microscopic slides with Mowiol® 4-88 and kept in the dark until further usage.

Table 3.9: Antibodies used for cell immunostainings

Antibody	Amount [µg/mL]
Anti-ANXA2 mouse	2
Anti-DDX3X rabbit	2
Anti-FLAG rabbit	2
Anti-V5 mouse	2.5
Anti-myc mouse	2
Alexa-Fluor-488 goat anti-mouse	4
Alexa-Fluor-555 goat anti-rabbit	4
Alexa Fluor-647 goat anti-mouse	5
Alexa Fluor-647 goat anti-rabbit	5
Phalloidin-TRITC	50

Fluorescence microscopic images were obtained with a wide field Zeiss Axio Observer Z1 Inverted Microscope, kindly provided by Prof. Gerald Gimpl (Department of Chemistry, Biochemistry Section, Johannes Gutenberg University, Mainz), or a Zeiss LSM800 Confocal Microscope (Microscopy Core Facility, JHU School of Medicine). The obtained pictures were extracted and processed with the biological-image analysis program Fiji.[81]

3.4 Co-Immunoprecipitation in eukaryotic cells

Co-Immunoprecipitation (co-IP) is a straight-forward technique to evaluate protein complexes under physiological conditions. In this work, an antibody-based co-IP protocol with protein G-coated magnetic beads was performed. Transfected cells (see sections 3.2.2 and 3.2.3) were

washed three times with ice-cold PBS and then harvested with 1 mL/well of a 6-well plate. Cells were lysed with Pierce™Lysis Buffer supplemented with CST Protease/Phosphatase-Inhibitor. After two centrifugation steps at 4600 rpm and 13 900 rpm, respectively, for 15 min at 4 °C, the supernatant was transferred in a fresh, pre-chilled tube. The Protein G-coupled beads were coated with respective antibody for 15 min at RT and then were washed one time with PBS/T. After this, the antibody-coated beads were incubated with the supernatant for 2 h at 4 °C under mild rotation. Beads were then washed three times with PBS/T and finally, proteins were eluted from the beads with 1x SDS-PAGE sample buffer (see table 2.2) at 70 °C for 10 min. Samples then were subjected to SDS-PAGE and western blotting with subsequent chemiluminescence detection (see sections 3.1.7 and 3.1.8).

3.5 Live Ca^{2+} imaging

Live calcium imaging (Ca^{2+} imaging) was performed on a Zeiss Axio Observer Z1 inverted microscope equipped with a Lambda DG-4 wavelength switcher. 24 h prior treatment, 6.8x10^5 cells/well were seeded int a 6-well plate, provided with Poly-L-coated cover slips in each well. 1 h prior treatment and Ca^{2+} imaging, cells were loaded with 2.5 µM Fura2 AM for 60 min at 37 °C. For hypotonic treatment, three volumes of hypotonic aCSF (see 2.2) was added to one volume of aCSF (see table 2.2 for buffer composition). For GSK-101 treatment, GSK-101 was added directly to the aCSF buffer. Cells were imaged every 10 seconds for 1 min prior to stimulation with hypotonic saline or GSK-101, then imaged every 10 seconds for an additional 8 min. Calcium levels at each time point were computed by determining the ratio of Fura-2 AM emission at 380 nm divided by the emission at 340 nm. Data are respresenting raw the Fura ratio.

3.6 Ca^{2+} influx assay

To assure the functionality of stably transfected human TRPV4-cGFP (see also section 3.2.3), fluorescence-based Ca^{2+} influx assays were performed with the Fluo-4 Direct Calcium Assay on a FlexStation 3 MultiMode Plate Reader. Poly-L-lysinated 96-well plates were seeded with 40 000 cells/well and after 24 h, cells were loaded with Fluo-4 Direct™calcium reagent loading

solution according to the manufacturers protocol. After incubation for 1 h at RT, 5 % CO_2 atmosphere and 95 % humidity, cells were treated with 30 nM GSK-101 end concentration. Resulting fluorescence signals were measured every 3 s for 3 min at RT with an excitation wavelength at 494 nm, an emission wavelength 516 nm and a bandwidth of 1 nm.

3.7 Recombinant expression and purification of constructs

3.7.1 Recombinant expression of human N-terminal TRPV4 (hsV4N) constructs

E. coli BL21 (DE3) Gold cells were heat-shock transformed (see section 3.1.1) with the respective plasmid (see table 2.15). In an over night incubation at 37 °C and 225 rpm a preculture in 50 mL LB medium containing 100 µg/mL ampicillin was set up. Subsequently, 1 L TB medium with 0.2 % (v/v) glucose or LB medium were supplemented with 100 µg/mL ampicillin and inoculated with 2 % (v/v) of preculture. The cells were then grown at 37 °C and 225 rpm to an OD_{600} of 0.6. Used IPTG concentrations and conditions for protein expression are listed in table 3.10. The cells were harvested by centrifugation at 5000 rpm and 4 °C for 10 min. After disposing the supernatant, the cell pellet was frozen with liquid nitrogen and stored at −20 °C until further use.

Table 3.10: Expression conditions of human N-terminal TRPV4 (hsV4N) constructs. hsV4NΔ132 is also referred to as hsV4 ARD, hsV4NΔ122 as hsV4 ARD-PRR. Avi2 = c-terminal avidin-tag followed by a His_6-tag. IPTG conc. = IPTG concentration, Temp. = Temperature

Construct	Medium	IPTG conc. [µM]	Duration [h]	Temp. [°C]
hsV4N-His_6	TB	150	16	20
hsV4N R232C-His_6	LB	150	16	20
hsV4N-Avi2	TB	150	16	20
hsV4NΔ122-His_6	LB	75	16	20
hsV4NΔ132-His_6	LB	75	18	20
hsV4NΔ132 R232C-His_6	LB	75	18	20
hsV4NΔ132 R269C-His_6	LB	75	18	20
hsV4NΔ132 D333G-His_6	LB	75	18	20
hsV4NΔ132-Avi2	LB	75	16	20

Construct	Medium	IPTG conc. [µM]	Duration [h]	Temp. [°C]
hsV4NΔ132 R232C-Avi2	LB	75	18	20
hsV4NΔ132 K276E-Avi2	LB	75	18	20
hsV4NΔ132 V342F-Avi2	LB	75	18	20

The below mentioned purifications were all carried out at 4 °C.

3.7.2 Purification of hsV4N constructs

The cell pellet of a 1 L *E. coli* cell culture was suspendend in 100 mL *E. coli* lysis buffer (for all buffer compositions see 2.2). Sonification was performed on ice with a Branson Sonifier 250 using a duty cycle of 5 for 50 s. The cell lysate was cleared via centrifugation at 20 000 rpm and 4 °C for 40 min. The obtained supernatant was loaded onto 1 mL Ni^{2+}-NTA agarose provided in a column which was equilibrated with 2 CV Ni^{2+}-NTA buffer 20 beforehand. The flow through was discarded and the Ni^{2+}-NTA agarose then washed with 20 CV Ni^{2+}-NTA buffer 20, followed by a second and a third wash step with 1 CV Ni^{2+}-NTA buffer 50 and 1 CV Ni^{2+}-NTA buffer 75, respectively. The His_6-tagged protein was eluted with 9 CV Ni^{2+}-NTA buffer 500 and collected in 1 mL fractions, to which 1 mM DTT and 1 mM EDTA were added. Protein purity was analyzed via SDS-PAGE using a 12 % gel. The protein was further subjected to size exclusion chromatography with a HiLoad 16/600 Superdex 200 SEC column, whereas elution was performed over 1.1 CV with SEC buffer hsV4N and collected in 0.5 mL fractions. If necessary, a second SEC with the before purified fractions was performed with SEC buffer hsV4N containing 750 mM NaCl. Purity was analyzed via SDS-PAGE and Coomassie staining.

3.7.3 Purification of hsV4△N122 and hsV4△N132 constructs

hsV4NΔ132 is also referred to as hsV4 ARD, hsV4NΔ122 as hsV4 ARD-PRR. The same purification protocol as described in subsection 3.7.2 above was used. The last wash step (W3) was left out, also 10 elution steps with Ni^{2+}-NTA buffer 500 were performed. For human RhoA interaction studies via NMR with ^{15}N-labeled human RhoA (see section 4.4), the SEC of hsV4NΔ132 R232C-His_6 was performed with the SEC buffer of RhoA (see table 2.4).

3.7.4 Biotinylation and purification of hsV4N constructs

With the insertion of the 15 amino acids containing (GLNDIFEAQKIEWHE) avidin tag (Avi) in the protein of interest it is possible to achieve a specific biotinylation of the desired protein *in vivo* with the *E. coli* biotin ligase BirA. BirA covalently attaches a single biotin to the lysine residue of the avidin tag. The femtomolar affinity constant between biotin and streptavidin can be exploited for further purposes, purification attempts example.[82] In previous works of the research group Hellmich, an avidin tag was inserted on two different positions in hsV4N and hsV4N ΔN132: either before the C-terminal His_6-tag (hsV4N Avi2) or after the C-terminal His_6-tag (hsV4N Avi3).[76] For biotinylation of the avidin tagged proteins, *E. coli* BL21 (DE3) Gold cells were heat-shock co-transformed with the respective plasmids, one expressing the BirA ligase (p155) and the other the respective TRPV4 N-terminal construct. Cell cultivation and protein expression were similar as described in section 3.7.1. Additionally, 40 µM biotin were added to the growth medium to ensure sufficient biotinylation of the target protein.[82]

Purification of biotinylated human N-terminal TRPV4 constructs

The same purification protocol as described in subsection 3.7.2 above was used with minor deviations. The last wash step (W3) was left out, furthermore 6 elution steps with Ni^{2+}-NTA buffer 500 were performed. SEC were executed with a ENrich™ SEC 70 column. Purity was analyzed via SDS-PAGE and Coomassie staining. Successful biotinylation was determined during the purification via dot-blot with a streptavidin-POD (Strep-POD) antibody and also a western blot with the same Strep-POD antibody was performed to verify the correct molecular weight as described previously.[76,77]

3.7.5 Recombinant expression and purification of human RhoA

The same expression protocol as described in section 3.7.1 was used. Protein expression was induced at an OD_{600} of 0.8. Table 3.11 lists the further expression conditions used for human RhoA in this work.

Table 3.11: Expression conditions of human RhoA. IPTG conc. = IPTG concentration, Temp. = Temperature

Construct	Medium	IPTG conc. [µM]	Duration [h]	Temp. [°C]
human RhoA-His_6	LB	250	18	16

The same purification protocol as in subsection 3.7.2 was used with buffer conditions suited to human RhoA (see also table 2.4). Furthermore, if needed, a TEV-cleavage was performed over night to remove the n-terminal His_6-tag (see also table 2.4 for buffer conditions) with subsequent reverse IMAC. Reverse IMAC washing steps were performed until the OD_{280} dropped below 0.4. Concentrated protein containing fractions were then subjected to SEC.

3.7.6 Recombinant expression and purification of human DDX3X_aa122-582 (DDX3X)

The same expression protocol as described in section 3.7.1 was used, but here the used antibiotic was Kanamycin with end concentrations of $50\,\mu g/mL$. Protein expression was induced at an OD_{600} of 0.8. Table 3.12 lists the further expression conditions used for hsDDX3X in this work.

Table 3.12: Expression conditions of hsDDX3X. IPTG conc. = IPTG concentration, Temp. = Temperature

Construct	Medium	IPTG conc. [µM]	Duration [h]	Temp. [°C]
human DDX3X_aa122-582-His_6	LB	1000	18	25

The same purification protocol as in subsection 3.7.2 was used with buffer conditions suited to hsDDX3X (see also table 2.5). Furthermore, the IMAC was differently performed as described

in the following. The obtained supernatant after cell lysis and centrifguation of 1 L *E. coli* cell culture was loaded onto 3 mL Ni-$^{2+}$-NTA agarose provided in a column which was beforehand equilibrated with 2 CV IMAC Wash A buffer. After discarding the flow-through the Ni-$^{2+}$-NTA agarose was washed with 15 mL IMAC wash buffer A, followed by 10 mL IMAC High salt buffer and 10 mL IMAC Wash B buffer. Elution steps were performed with IMAC Elution buffer until the OD_{280} dropped below 0.3. Furthermore, if needed, a TEV-cleavage was performed over night to remove the n-terminal His_6-tag (see also table 2.5 for buffer conditions) with subsequent reverse IMAC. Reverse IMAC washing steps were performed until the OD_{280} dropped below 0.2. Concentrated protein containing fractions were then subjected to SEC.

3.7.7 Recombinant expression and purification of human ITCH

The same expression protocol as described in section 3.7.1 was used. Protein expression in the cells were induced at an OD_{600} of 0.8. Table 3.13 lists the further expression conditions used for human ITCH in this work.

Table 3.13: Expression conditions of human ITCH. IPTG conc. = IPTG concentration, Temp. = Temperature

Construct	Medium	IPTG conc. [µM]	Duration [h]	Temp. [°C]
human ITCH-nHis_6	LB	250	18	16

The same purification protocol as in subsection 3.7.2 was used with buffer conditions suited to human ITCH (see also table 2.6) with the minor deviaton during the IMAC, where three times twice the CV was eluted. Furthermore, if needed, a TEV-cleavage was performed over night to remove the n-terminal His_6-tag (see also table 2.6 for buffer conditions) with subsequent reverse IMAC. Reverse IMAC washing steps were performed until the OD_{280} dropped below 0.4. Concentrated protein containing fractions were then subjected to SEC.

3.7.8 Recombinant expression and purification of human ITCH WW domains

The same expression protocol as described in section 3.7.1 was used. Protein expression in the cells were induced at an OD_{600} of 0.8. Table 3.14 lists the further expression conditions used for human ITCH WW domains in this work.

Table 3.14: Expression conditions of human ITCH WW domains. IPTG conc. = IPTG concentration, Temp. = Temperature

Construct	Medium	IPTG conc. [µM]	Duration [h]	Temp. [°C]
hsITCH_WW1 domain-His_6	LB	250	20	16
hsITCH_WW2 domain-His_6	LB	250	20	16
hsITCH_WW3 domain-His_6	LB	250	20	16
hsITCH_WW4 domain-His_6	LB	250	20	16
hsITCH_WW1+WW2 domains-His_6	LB	250	20	16
hsITCH_WW3+WW4 domains-His_6	LB	250	20	16

The same purification protocol as in subsection 3.7.2 was used with buffer conditions suited to human ITCH WW domains (see also table 2.7), with just three elution steps during the IMAC. Furthermore, if needed, a TEV-cleavage was performed over night to remove the n-terminal His_6-tag (see also table 2.6 for buffer conditions) with subsequent reverse IMAC. Reverse IMAC washing steps were performed until the OD_{280} dropped below 0.2. Concentrated protein containing fractions were then subjected to SEC.

3.7.9 Recombinant expression and purification of human YAP-WW domains

The same expression protocol as described in section 3.7.1 was used. Protein expression in the cells were induced at an OD_{600} of 0.8. Table 3.15 lists the further expression conditions used for human YAP WW domains in this work.

Table 3.15: Expression conditions of human YAP WW domains. IPTG conc. = IPTG concentration, Temp. = Temperature

Construct	Medium	IPTG conc. [µM]	Duration [h]	Temp. [°C]
hsYAP1_WW1 domain-His_6	LB	250	16	20
hsYAP1_WW2 domain-His_6	LB	250	16	20
hsYAP1_WW1+WW2 domains-His_6	LB	250	16	20

The same purification protocol as in subsection 3.7.2 was used with buffer conditions suited to human YAP WW domains (see also table 2.9), with just three elution steps during the IMAC. Furthermore, if needed, a TEV-cleavage was performed over night to remove the n-terminal His_6-tag (see also table 2.6 for buffer conditions) with subsequent reverse IMAC. Reverse IMAC washing steps were performed until the OD_{280} dropped below 0.2. Concentrated protein containing fractions were then subjected to SEC.

3.8 Pulldown assay of biotinylated hsV4N constructs

All steps of the below mentioned pulldown assay were carried out at 4 °C. HEK293 cells of a 10 cm dish were cultivated until 90 % confluency. After discarding the supernatant, cells were washed once with 5 mL ice-cold PBS and incubated for 10 min in pulldown lysis buffer (see table 2.2) under mild agitation. Due to the short incubation in the digitonin-containing pulldown lysis buffer, the plasma membrane of the HEK293 cells permeabilizes, allowing cytosolic proteins to diffuse into the supernatant of the cells without destroying other cell compartments.[83] The supernatant of the still adherent cells was then transferred into a fresh tube and centrifuged for 10 min at 400 rpm. The supernatant again was transferred into a fresh tube and centrifuged for 30 sec at 12 000 rpm. The supernatant was transferred into a fresh tube and the protein concentration was determined via a Bradford Assay (see also sec 3.1.9). 20 µL streptavidin-coated magnetic beads were pre-incubated with 500 ng the respective non- or biotinylated N-terminal TRPV4 protein for 30 min at 4 °C under mild rotation. After three washing steps with PBS, the pre-loaded beads were incubated in 250 µg of the digitonin-extracted HEK293 cytosolic fraction.

To mimic an activation of the TRPV4 cation channel function, some samples were supplemented with 2 mM $CaCl_2$. After an incubation for 30 min at 4 °C under mild rotation, beads were washed again three times with PBS and flash-frozen in liquid N_2 until further use.

3.9 Mass spectrometry

Mass spectrometry based proteomics became an indispensable tool for the analysis of proteins and their interaction partners. Several methods have been developed to investigate the complex networks of cell proteomes. In cooperation with Dr. Ute Distler (AG Tenzer, FZI Core Facility for Mass Spectrometry, Mainz) it was possible to approach towards an investigation of the human TRPV4 N-terminus interactome via ultra high-definition mass spectrometry^{E} (UDMS^{E}). There are several methods to prepare samples for mass spectrometry. In this work, samples were obtained either after in-gel digestion (see subsection 3.9.1) or in-solution digestion (see subsection 3.9.2) after pulldown experiments with magnetic streptavidin beads (see section 3.8). Digestions (see sections 3.9.1 and 3.9.2) were kindly performed by Ruben Spohrer (AG Tenzer, FZI Core Facility for Mass Spectrometry, Mainz), MS measurements and data processing by Dr. Ute Distler (AG Tenzer, FZI Core Facility for Mass Spectrometry, Mainz).

3.9.1 In gel digestion

After SDS-PAGE and Coomassie staining, the protein lanes of interest were cut out of the gel and added to 200 µL 50 mM NH_4HCO_3 buffer in 50 % acetonitrile (ACN), followed by incubation in an ultrasonic bath for 5 min. The supernatant was discarded and the foregoing step was repeated. 200 µL 100 % ACN were added to the left gel pieces and again incubated in an ultrasonic bath for 5 min. The supernatant was discarded again and 100 µL 1 mM DTT solution were added to the gel pieces, followed by an incubation for 60 min at 56 °C. After cooling down the sample to RT, 100 µL iodoacteamide (IAA,c= 10 mg/mL) were applied and incubated for 45 min under light exclusion, followed by another addition of 100 µL 50 mM NH_4HCO_3 buffer in 50 % acetonitrile (ACN) and incubation in an ultrasonic bath for 5 min. After discarding the supernatant the last step was repeated. Afterwards, the gel pieces were incubated in 100 µL 100 % ACN in an ultrasonic bath for 5 min. The supernatant was discarded, the gel pieces heated at 56 °C for 1 min and then 25 µL trypsin solution (dilution 1:100) were added. Incubation was performed over night at 37 °C and the supernatant was added in an ice cooled tube

in which all following supernatants were collected. Now, the remaining gel pieces were incubated in 50 µL 50 % ACN solution with 1 % formic acid (FA) in an ultrasonic bath for 15 min. This step was performed twice, each time the supernatant was collected in the before mentioned tube. 100 µL 100 % ACN were then added to the gel sample and again incubated in an ultrasonic bath for 15 min. The supernatant was collected again and the gel pieces were discarded, followed by an incubation of the collected supernatants for 30 min at -80 °C. The collected supernatants were then concentrated to a volume of 20 µL with a vacuum concentrator. and then centrifuged at 13 000 rpm for 15 min at 4 °C. 15 µL of the supernatant were then added to 5 µL Enolase (100 fmol) and 5 µL 1 % FA. This mixture was then ready for mass spectrometric measurements.

3.9.2 In-solution digestion

To obtain samples for mass spectrometric measurements after the pulldown assay described in section 3.8, an in-solution digestion was performed. Proteins were precipitated with the "ProteoExtract™Protein Precipitation Kit" (Merck Millipore, Darmstadt). 1 % RapiGest SF Surfactant solution were added ($\frac{1}{10}$ of sample volume) followed by an incubation for 15 min at 80 °C. 8 mM DTT were added to the sample, incubated for 15 min at 56 °C, followed by the addition of 15 mM IAA and an incubation at RT for 45 min. 1 µL trypsin and 8 mM DTT were added and incubated over night at 37 °C . The pH of the sample was lowered to 3 with 1 M HCl an the sample incubated for 10 min at 37 °C. After centrifugation for 30 min at 130 000 rpm and 4 °C, 10 µL supernatant were mixed with 5 µL Enolase (100 fmol) and 10 µL 1 % FA to yield samples ready for MS measurements.

3.9.3 Liquid Chromatography Mass Spectrometry

After tryptic digestion (see subsections 3.9.1 and 3.9.2) the peptides were separated via nanoUPLC with a nanoAcquity UPLC system (Waters Corporation, Milford) on an Acquity UPLC HSS-T3 reverse phase column (high silica strength, 75 µm $\times$ 250 µm 1.8 µm), which was equilibrated with Mobile Phase A (see table 2.2). In direct injection mode sample volumes between 0.7 µL and 0.6 µL were applied onto the reverse phase column, followed by a gradient flow of 5-40 % with Mobile Phase B over 90 min at a flow rate of 300 nL/min and a column temperature of

55 °C. Afterwards the column was washed with 90 % of Mobile Phase B and furthermore re-equilibrated.
A nano-ESI-Q-TOF mass spectrometer (Synapt G2-S HDMS, Waters Corporation) with an ion mobility separation (IMS) device was used for MS analysis performed in positive mode ESI. LC-MS data were collected in DIA mode using MS^E combined with IMS ($HDMS^E$) as well as in DDA mode using a top 10 method selecting the 10 most abundant ions for fragmentation.[63]

3.9.4 Data Processing and Protein Identification

LC-MS DIA data were processed and searched with ProteinLynx Global SERVER (PLGS) (version 3.02 built 5 from Waters Corporation). DDA data were processed using using the software package PEAKS (version 8, Bioinformatic Solution Inc., Waterloo, Canada). Protein identification was obtained searching a custom compiled database containing UniProtKB/SwissProt entries of the *E.coli* and human reference proteomes (entries: 4434 *E. coli*, 20 231 human) as well as the sequences of the N-terminal TRPV4 constructs. Sequence information for enolase (*Saccharomyces cerevisiae*) and common contaminants (e.g. human keratins, BSA, and trypsin) were added to the databases. Identified peptides had to match several search criteria:

1. Trypsin had to be the digestive enzyme.

2. Up to two missed cleavages were allowed.

3. Carbamidomethyl cysteine was defined as a fixed modification.

4. Methionine oxidation was defined as a variable modification.

5. Peptides had to have a minimum length of six amino acids.

The false discovery rate (FDR) for peptide and protein identification was assessed searching a reversed database. FDR was set to a 1 % threshold for database search in PLGS and PEAKS. $HDMS^E$ collected data were post-processed with the in-house software ISOQuant in order to facilitate the data analysis.[63]

3.10 Enzymatic assays

To validate the enzymatic activity of the recombinantly expressed and purified enzymes in the course of this work, enzymatic assays were performed as described below.

3.10.1 GTPase assay

Intrinsic GTPase activity of recombinantly expressed and purified human RhoA (see also subsection 3.7.5) was determined via the GTPase-Glo Assay (see also table 2.18) according to the manufacturers protocol. Luminescence was recorded with a FLUOStar Omega Microplate Reader (BMG Labtech). In this assay, GTPase activity is inversely correlated to the measured amount of luminescence.

3.10.2 ATPase assay

ATPase activity of recombinantly expressed and purified hsDDX3X (see als subsec3.7.6) was determined via an cuvette-based *in vitro*-ATPase assay. The ATPase assay used in this work is based on the enzyme-linked regeneration of ADP to ATP coupled to the oxidation of NADH to NAD^2.The decrease of NADH and therefore the ATPase dependent hydrolysis of ATP can be determined with photometric measurements at 340 nm.[84] For this, the components of table 3.16 were mixed together in a cuvette with HEPES buffer (pH = 7). After 30 s 1 mM ATP was added to the mixture and due to the ATPase-dependent RNA-Helicase Activity of DDX3X, the mixture was supplemented with 1 µM palindromic duplex RNA after 5 min (Sequence: 5′-UUUUUUUUUUUUUUUUUUUUGGCGGCCGCC-3′). As a control, the well-characterized *B. subtilis* ATPase BmrA was also supplemented with hsV4 ARD to rule out unspecific effects on the lactate dehydrogenase and pyruvate kinase involved in this assay. Measurements were carried out at RT with a Perkin-Elmer Lambda 25 Photometer.

Table 3.16: Sample composition for the *in vitro*-ATPase assay

Component	
$MgCl_2$	1 µM
Ascorbinic acid	1 µM

Component	
Phosphoenolpyruvate	3 µM
Pyruvate kinase	0.05-0.08 units/µL
Lactate dehydrogenase	0.08-0.12 units/µL
hsDDX3X	3 µM
BmrA	3 µM
hsV4N construct	12 µM
duplex RNA	1 µM
ATP	1 µM

3.10.3 Ubiquitinylation assay

To determine the E3 Ubiquitin ligase activity of recombinantly expressed and purified human ITCH (see also subsection 3.7.7) an *in vitro*-ubiquitinylation assay was performed. For this, the components of table 3.17 were incubated at 30 °C for up to 3 h in 10 mM Tris (pH=7.4) with 5 mM $MgCl_2$. Out of this mixture, samples were taken after several time points for subsequent SDS-PAGE and Coomassie staining.

Table 3.17: Sample composition for the *in vitro*-Ubiquitinylation assay

Component	Concentration [µM]
ATP	5000
Ubiquitin	100
E1 Ubiquitin ligase UBE1	2
E2 Ubiquitin ligase Ubc5Hc	1
E3 Ubiquitin ligase ITCH	10
hsV4N construct	20

3.11 Blue Native-PAGE (BN-PAGE)

BN-PAGE is a straight-forward way to identify direct protein-protein interactions, especially for proteins which isoelectrical points are > 8, as these proteins do not migrate in a PAGE under Laemmli-conditions.[85] Here, Coomassie G-250 is added into the discontinuous PAGE to create a net negative charge to allow protein migration towards the anode. In this work, BN-PAGE was used to determine the minimal binding side of ITCH at hsV4N. For this, 10 µM ITCH and 20 µM of the respective hsV4N construct were mixed in a tube with 10 mM Tris (pH=7.4) supplemented with 5 mM $MgCl_2$ as reaction buffer. The protein mixture was incubated at 30 °C for 1 h. After this, the protein mixture was supplemented with Coomassie G-250 to an end concentration 0.25 % (w/v). The PAGE were run with 4 - 15 % Mini-Protean® TGX™ Precast Protein Gels with a electrophoresis cathode buffer (see table 2.2) for 3 h at 4 °C.Ater this, Coomassie staining was performed and relevant bands were cut out to provide them for mass spectrometric verification (Mass Spectrometry Core Facility, Johns Hopkins School of Medicine, Baltimore, USA).

3.12 Circular dichroism (CD) spectroscopy

Circular dichroism (CD) measurements were performed on a Jasco-815 CD spectrometer with a spectral range between 195 and 260 nm at 20 °C. The scanning intervals were set to 1 nm, the scanning speed to 50 nm/min and the band-width to 5 nm. CD data are often reported as a mean residue ellipticity $[\Theta]_{mrw,\lambda}$ (deg cm^2 $dmol^{-1}$). The conversion from the measured ellipticity Θ (deg) to the mean residue ellipticity $[\Theta]_{mrw,\lambda}$ is described by equation 3.1.

$$[\Theta]_{mrw,\lambda} = \frac{MRW \cdot [\Theta]}{10 \cdot c \cdot d} \tag{3.1}$$

Mean residue weight (MRW) is calculated with $MRW = \frac{M}{N-1}$, were M is the molecular weight in Dalton and N is the amino acid number of the measured protein. The secondary structure content was predicted with analyzing the CD spectra with the CAPITO tool (`https://capito.uni-jena.de`).The Chou-Fassmann algorithm predicts secondary structures based on empiric data in which amino acids show preferences for distinct secondary structures. Furthermore,

CAPITO compares the measured spectra with basis spectra data sets. A nearest-neighbor approach determines the 25 best matching references curves defined by closest proximity. At last, the lowest area differences are compared to reference curves.

3.13 NMR spectroscopy

To obtain uniformly ^{15}N-labeled proteins for ^{15}N-HSQC spectra, *E. coli* BL21 Gold cells were transfected and the proteins expressed as described in sections 3.1.1 and 3.7, however, the cells were grown in M9 medium (see table 2.2) to ensure that $^{15}NH_4Cl$ is the only nitrogen source for protein expression. NMR spectra of respective proteins were recorded at 25 °C on Bruker AVANCE 600, 700 and 800 MHz spectrometers equipped with cryogenic triple resonance probes (Bruker, Karlsruhe) at the Centre for Biomolecular Magnetic Resonance (BMRZ) (Goethe-University, Frankfurt a.M.). ^{1}H,^{15}N-HSQC spectra were measured using standard pulse sequences and processed using TOPSPIN 3.5 (Bruker, Karlsruhe).[86]

3.14 Cross-linking mass spectrometry (XL-MS)

XL-MS is a powerful tool for investigations of protein-protein interactions (PPIs) and the interfaces of these interaction. Due to the chemical cross-linking between functional groups of amino acid side chains XL-MS is advantageous to capture and identify weak or transient PPIs. Here, H12/D12-disuccinimidyl suberate (H12/D12-DSS) was used, cross-linking between the amide groups of lysines. Purified (hsV4N and DDX3X as well as hsV4N and ITCH) proteins were mixed in a molar ratio of 1:1 to a final concentration of 1 mg/mL in 100 µL. H12/D12-DSS was freshly dissolved in DMF prior use and added to the protein mixture at a final concentration of 1.5 mM. The cross-linking reaction was incubated for 2 h on ice and quenched with the addition of ammonium bicarbonate at a final concentration of 500 mM. The mixture was further incubated on ice for additional 2 h. Samples were flash-frozen in liquid nitrogen and stored at -20 °C until further use. Sample processing, MS measurements and analysis were kindly carried out by M. Sc. Jasmin Jansen (Working group Stengel, University of Konstanz).[87]

4 Results

4.1 A beginning to elucidate the versatile TRPV4 N-terminal protein interactome - the tip of the iceberg

4.1.1 Purification of biotinylated TRPV4 N-terminal proteins

The protein interactome of a cell is not a static structure of probable binary protein-protein interactions (PPIs). It is a reflection of the cells state and therefore indicates protein abundance, post-translational modifications, cell cycle phase or the stress level of a cell. Due to this broad variety of possible conditions, the protein interactome of a cell is very dynamic and specific biochemical methods can only yield snapshots of protein interactions in certain biological situations. To obtain a comprehensive view of the protein interactome, shotgun mass spectrometry is the method of choice.[73,88] This work focuses on the protein interactome of the full-length TRPV4 N-terminus (here referred to as hsV4N), as this portion of the full-length ion channel is a notorious hot-spot for disease-causing point mutations.[27,56,89,90] Furthermore, hsV4N plays an integral role in channel sensitization as well as desensitization and harbors a number of pivotal protein, lipid and small molecule interaction sites, like a phosphoinositide binding domain (PBD) and a proline rich region (PRR), which are followed by six α-helical ankyrin repeats, the ankyrin repeat domain (ARD).[22,39] Previously, a protocol was established to obtain the hsV4N protein interactome after pulldown assays in HEK293 cell lysates followed by shotgun proteomics performed in cooperation with Dr. [redacted] (RG [redacted] University Medicine Mainz, JGU Mainz).[76] This protocol required recombinant expression, *in vivo* biotinylation as well as protein integrity investigations of several TRPV4 N-terminal constructs with an so-called avidin-tag (here referred as Avi). This tag allows side-specific *in vivo* biotinylation of a lysine in the avidin-tag itself (single letter code avidin-tag: GLNDIFEAQ**K**IEWHE).[91] In addition to

the already used and validated full-length hsV4N with avidin-tag (hsV4N wt Avi), before mentioned protocol was optimized for the TRPV4 ankyrin repeat domain (here referred as hsV4 ARD), including the selected disease-causing mutations R232C and K276E (figure 4.1). The TRPV4 R232C mutation leads to Charcot-Marie-Tooth Type 2C (CMT2C)[54], whereas TRPV4 K276E results in fetal akinesia - a combined phenotype of metatropic dysplasia with putative neurodegenerative symptoms.[92] Protein expression, *in vivo* biotinylation and purifications were performed as described in subsection 3.7.4. All size exclusion chromatograms (SEC) of used TRPV4 N-terminal constructs in figure 4.1 show narrow gaussian peaks with expected elution volumes for all biotinylated proteins (see section 6.2 for SEC purification of unbiotinylated proteins). Coomassie stained SDS-PAGEs show pure proteins and a Streptavidin-Peroxidase (Strep-POD) dot-blot confirms successful biotinylation. However, hsV4N wt Avi shows a significant stronger signal in the Strep-POD dot blot than the hsV4 ARD Avi constructs. Image analysis of the Strep-POD dot blots with Fiji shows a 90 % weaker biotinylation efficacy of the hsV4 ARD Avi constructs compared to hsV4N Avi (data not shown). Adjustment of the used hsV4 ARD Avi concentrations was sufficient enough for successful pulldowns due to the strong interaction between biotin and streptavidin with a K_D in the femtomolar range.[91,94–96] CD spectra show, as also previously reported[22], that hsV4N consists of a large α-helical part, which is contributed by the ARD (aa 149 - aa 398), and a large unstructured region (aa 1-aa 149). Comparison of the CD spectra between biotinylated and non-biotinylated hsV4 ARD Avi constructs shows no change in the α-helical structure, which is also underlined by secondary structure prediction via CAPITO[93]. Only biotinylated hsV4N wt Avi supposedly harbors a marginal β-sheet

Figure 4.1 *(facing page)*: **Purification of *in vivo* biotinylated and structural intact TRPV4 N-terminal constructs**. **A** Schematic topology model of TRPV4 N-terminal constructs used for protein interactome investigations via pulldown assays and subsequent mass spectrometry in this work. HsV4N represents the full-length human TRPV4 N-terminus with important interaction sites like the phosphoinositide binding site (PBD), proline rich region (PRR) and the ankyrin repeat domain (ARD). Avi = avidin tag (single letter code: GLNDIFEAQKIEWHE). His_6 = hexa-histidine tag (single letter code: HHHHHH). **B** SEC purifications of biotinylated hsV4N wt Avi and hsV4 ARD Avi constructs. SEC runs were either performed with a HiLoad Superdex 200 pg or a HiLoad Superdex 75 pg preparative SEC column. Inlets show Coomassie stained 15 % SDS-PAGEs of collected and concentrated fractions after SEC, furthermore a Strep-POD dot blot indicating biotinylated proteins of the respective proteins. x-axis: eluted volume in mL, y-axis: absorbance at 280 nm, M = marker in kilodalton (kDa). **C** Comparison of far UV CD spectra of purified biotinylated and non-biotiynlated hsV4N constructs. Spectra were measured at 293 K and proteins were used at 2 µM concentration in SEC buffer with a final concentration of 30 mM NaCl. Inlets show secondary structure prediction performed with CAPITO.[93] The predicted α-helix/β-sheet/random coil content of the purified proteins is for non-biotinylated hsV4N wt Avi 53 %/0 %/46 %, hsV4 ARD wt Avi 76 %/0 %/24 %, hsV4 ARD R232C Avi 74 %/0 %/26 % and hsV4 K276E Avi 76 %/0 %/24 %. Biotinylated proteins show the following secondary structure content distribution: hsV4N wt Avi 40 %/14 %/46 %, hsV4 ARD wt Avi 76 %/0 %/24 %, hsV4 ARD R232C Avi 74 %/0 %/26 % and hsV4 ARD K276E Avi 76 %/0 %/24 %. x-axis: mean residue ellipticity ($[\Theta]_{mrw,\lambda}$) in 10^{-3} deg cm^2 dmol^{-1}, y-axis: wavelength λ in nm.

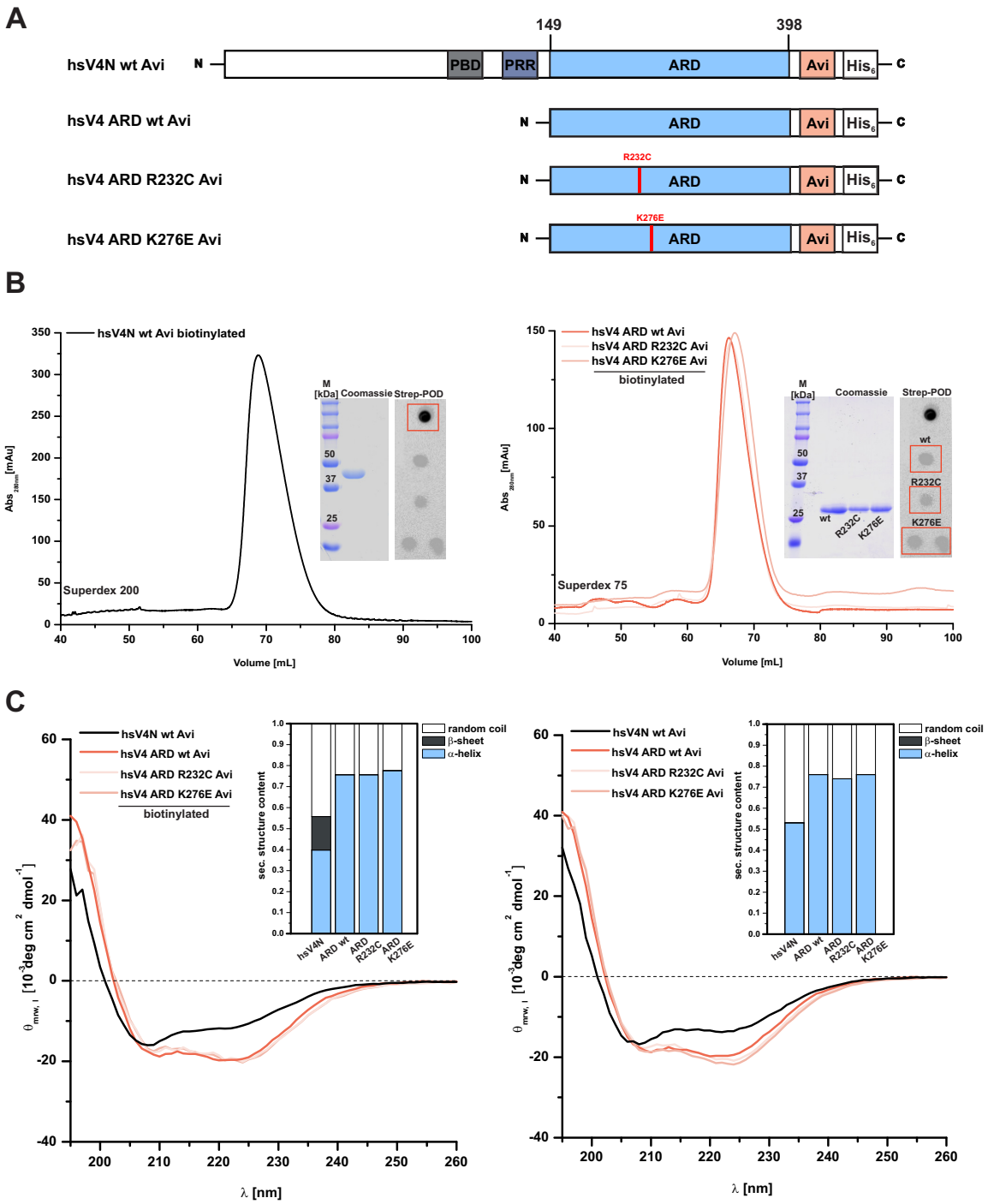
A
149
398
hsV4N wt Avi
N
PBD
PRR
ARD
Avi
His6
C
hsV4 ARD wt Avi
hsV4 ARD R232C Avi
R232C
hsV4 ARD K276E Avi
K276E
B
hsV4N wt Avi biotinylated
Superdex 200
Abs280nm [mAu]
Volume [mL]
M [kDa]
Coomassie
Strep-POD
hsV4 ARD wt Avi
hsV4 ARD R232C Avi
hsV4 ARD K276E Avi
biotinylated
Superdex 75
wt
R232C
K276E
C
hsV4N wt Avi
hsV4 ARD wt Avi
hsV4 ARD R232C Avi
hsV4 ARD K276E Avi
biotinylated
θmrw, l [10-3deg cm2 dmol-1]
λ [nm]
sec. structure content
random coil
β-sheet
α-helix
hsV4N
ARD wt
ARD R232C
ARD K276E

fold content compared to non-biotinylated hsV4N wt Avi.

4.1.2 The TRPV4 N-terminal protein interactome in HEK293 cells derived via mass spectrometry

For the elucidation of the TRPV4 N-terminal protein interactome, biotinylated and non-biotinylated constructs (see subsection 4.1.1) were subjected to streptavidin-dependent pulldowns with HEK293 cytosolic extracts. Table 4.1 lists all samples which were used in the pulldowns with HEK293 cytosolic protein extracts (see figure 4.2 for workflow and section 3.8 for protocol). Shortly, streptavidin-coated magnetic beads were incubated with the respective purified TRPV4 N-terminal construct (biotinylated or non-biotinylated), washed and then incubated with the cytosolic extract of HEK293 cells. Additionally, samples with biotinylated constructs were supplemented with 2 mM Ca^{2+} during the HEK293 cytosolic extract incubation step to mimic an increased intracellular Ca^{2+} concentration as it would be observed upon TRPV4 ion channel activation.

Table 4.1: Sample overview of hsV4N interactome pulldowns with HEK293 cytosolic protein extracts

Construct	Biotinylated	Sample supplement
hsV4N wt Avi	Yes	none
hsV4 ARD wt Avi	Yes	none
hsV4 ARD R232C Avi	Yes	none
hsV4 ARD K276E Avi	Yes	none
hsV4N wt Avi	Yes	2 mM Ca^{2+}
hsV4 ARD wt Avi	Yes	2 mM Ca^{2+}
hsV4 ARD R232C Avi	Yes	2 mM Ca^{2+}
hsV4 ARD K276E Avi	Yes	2 mM Ca^{2+}
Controls		
hsV4N wt Avi	No	none
hsV4 ARD wt Avi	No	none
hsV4 ARD R232C Avi	No	none
hsV4 ARD K276E Avi	No	none

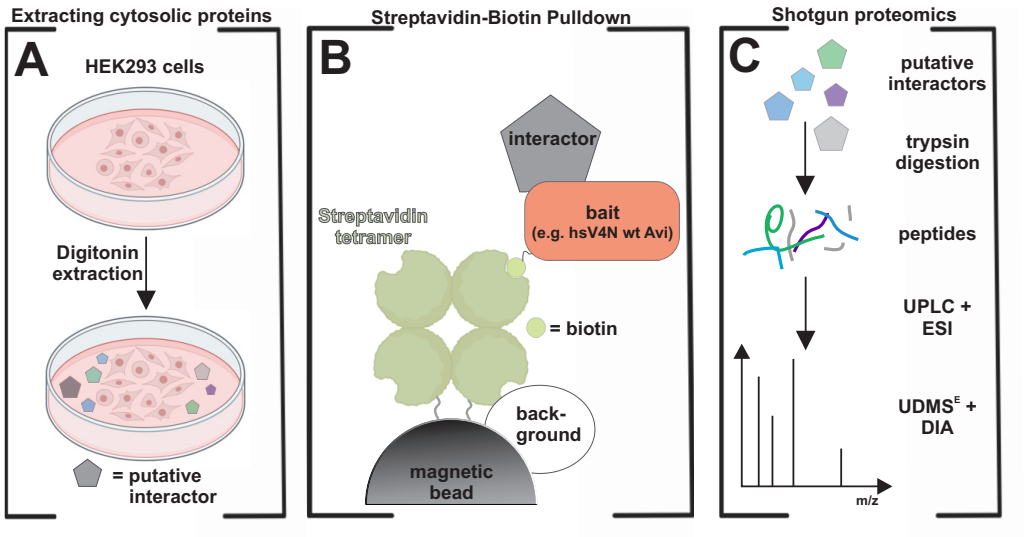

Figure 4.2: **Outline of the proteomics workflow performed in this work.** See sections 3.8 and 3.9 for protocols. **A** To enrich cytosolic proteins, plasma membranes of HEK293 cells were permebealized with digitonin. This detergent releases cytosolic proteins into the supernatant while contaminations by other cell compartments are reduced to a minimum.[83] **B** Schematic layout of the hsV4N interactome pulldown. Streptavidin-bound magnetic beads were loaded with respective purified hsV4N Avi construct (see also figure 4.1). Loaded beads were incubated in HEK293 protein extract containing cytosolic proteins. As a control, beads were also incubated with non-biotinylated TRPV4 N-terminal constructs to rule out unspecific interactors (background).**C** After elution, putative interactors were trypsin digested to peptides. These peptides were then separated by ultra high-performance liquid chromatography (UPLC) and directly supplied into the mass spectrometer via electron spray ionization (ESI). MS data were collected in data independent acquisition (DIA) mode. All steps in C were performed in cooperation with [redacted] University Medicine Mainz).[63,72,73]

The HEK293 protein interactome of the TRPV4 full-length N-terminus

Figure 4.3 shows the volcano plots of two independent ultra high-definition mass spectrometry^E (UDMS^E) measurements of hsV4N wt Avi. In these volcano plots, only significantly detected proteins are shown. All samples listed in table 4.1 were measured in technical quadruplicates. Proteins were considered as significant, if the p-value was ≤ 0.05 (Benjamini-Hochberg corrected Student's t-test) and the $\log_2$ fold change fo respective protein between biotinylated hsV4N wt Avi and non-biotinylated hsV4N Avi wt control sample was ≥ 1. Additionally, only proteins which appeared in both independent UDMS^E measurements were considered as highly probable hsV4N wt Avi protein interactome members. Significant proteins showed different fold changes between the two independent measurements (black and grey dots in figure 4.3), indicating a high sensitivity of the UDMS^E measurements towards different NaCl concentrations

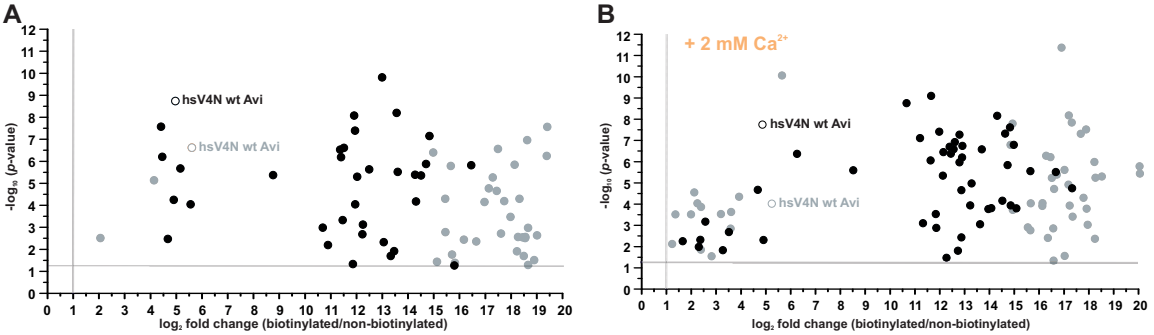

Figure 4.3: **UDMS^E measurements revealed up to 64 probable hsV4N protein interactors. A** Volcano plot of two independent HEK293 protein interactome UDMS^E measurements from hsV4N wt Avi. 34 proteins were considered as significant. **B** Volcano plot of two independent HEK293 protein interactome UDMS^E measurements from hsV4N wt Avi with 2 mM Ca^{2+} sample supplementation. 64 proteins were considered as significant. Black (hsV4N wt Avi, 300 mM NaCl buffer) and dark gray points (hsV4N wt Avi, 750 mM NaCl buffer) indicate significant, detected HEK293 protein interactome candidates in both independent experiments. Each pulldown was measured in quadruplicates. Horizontal light gray lines indicate the *p*-value = 0.05 (Benjamini-Hochberg corrected Student's *t*-test) of the quadruplicates of each UDMS^E measurement. Vertical light gray lines indicate a $\log_2$ fold change $\geq$ 1. For a full list of hsV4N interactors, see tables 6.3 and 6.4

supplemented in the hsV4N wt Avi SEC buffer. Data analysis resulted in 34 relevant hsV4N wt Avi interaction partners in samples without Ca^{2+} supplementation and 64 hsV4N wt Avi interaction partners in the samples with Ca^{2+} supplementation (see figures 4.4 A and 4.5 A), including the known direct TRPV4 interactor PACSIN3 in both conditions.[22,23,70,71] Gene Ontology enrichment analysis (GO enrichment analysis) is a technique to interpret high-throughput data in terms of over- or underrepresentation of certain genes in respective experiment. The Gene Ontology classification assigns genes to sets of predefined bins depending on their role in cellular processes or functional characteristics.[97] GO enrichment analysis with STRING[98] via Cytoscape 3.8.0 demonstrated that all detected proteins are associated with the cytoplasm, which is composed out of the cytosol and cytoskeleton, indicating successful extraction of mainly cytosolic proteins. Only HNRNPM_HUMAN represents an exception, as it is associated with the nucleoplasm but also with ribonucleoprotein complexes - like the majority of the cytosolic proteins in the here disclosed network. Like HNRNPM_HUMAN, a small portion of other proteins could also be associated with the nucleoplasm, but are known for their nucleocytoplasmic shuttling.[99] Additionally, GO enrichment analysis and manual data curation connected a considerable amount of detected proteins with cytoplasmic ribonucleoprotein or cytoplasmic stress granules (13 proteins, see figure 4.4 and table 6.3). *Cytoplasmic ribonucleoprotein granule* is a collective GO term for distinct RNA-binding protein-containing foci in the cytoplasm, including amongst others neuronal transport granules, P-bodies and stress granules. Stress granules, appearing as their name says after various stress factors like oxidative or hyperosmotic stress in the cytosol, form

via liquid-liquid phase separation of pre-existing RNA-binding protein (RBP) complexes.[100,101] The exact role of stress granules in neuronal (patho)physiological processes remains largely unknown. It is known that stress granule formation is accompanied by polysome disassembly and translational arrest.[102–105] Stress granules are mostly composed out of translation initiators, RBPs, 40S ribosomes and polyadenylated mRNAs and therefore are proposed to play a protective role in cells by promptly providing the undamaged translation machinery for important household proteins after their disassembly due to stress withdrawal.[106–110] Stress granules and other cytoplasmic ribonucleoprotein granules show major overlaps in their proteome but are also known for their highly variable and dynamic protein compositions, transitioning from one granule to the other in dependency of the cellular stress level.[101,107–109,111–114] Liu-Yesucevitz *et al.* showed that potassium chloride (KCl)-induced depolarization in primary neurons, leading to dramatically elevated cytoplasmic Ca^{2+} levels, induces a transformation of neuronal mRNA transport granules to stress granules.[115] Interestingly, it was shown that neuropathy-causing mutations of TRPV4 show an elevated baseline Ca^{2+}-influx activity of the channel, also leading to higher cytosolic Ca^{2+}-concentrations.[53,54] In the present work, upon Ca^{2+}-supplementation, the amount of ribosomal proteins in the hsV4N interactome considerably increased, but also the number of proteins associated with cytosolic ribonucleoprotein granules (20 proteins, figure 4.5 and table 6.4). In both conditions, without and with Ca^{2+}, known stress granule formation proteins are present, namely YBX1, IGF2BP1, PAPBC1 and DDX3X.[107,108,116–120] Furthermore, upon Ca^{2+} supplementation proteins associated with the GO term *supramolecular fiber* were detected. Supramolecular fibers are defined as protein complexes which form fiber-shaped structures, like microtubule or actin filaments. Fiber-like structures were shown to spur the maturation of phase-seperated droplets to more stable and less dynamic structures and therefore impair an important property of stress granules: the fast disassembly within minutes after stress removal.[101,102,117,121–130] Amyotrophic lateral sclerosis (ALS)-causing mutations in stress granule proteins, especially in the intrinsically disordered regions (IDRs) of RBPs, were shown *in cellulo* to lead to insoluble inclusions. This is particularly interesting, as the TRPV4-associated neuropathy Charcot-Marie-Tooth Type 2C is also referred as a so-called "ALS-mimic", due to the shared clinical symptoms.[131] Furthermore, insoluble inclusion formations were also observed

Figure 4.4 *(facing page)*: **The hsV4N protein interactome determined via UDMS^{E}. A** STRING interaction network of detected, significant hsV4N interactome proteins. Outer ring color of nodes represent Gene Ontology (GO) terms for cell components, also shown in B. For a full list of protein interactors see table 6.3 **B** Selected GO terms for cell components of significant, detected hsV4N interactome proteins via UDMS^{E} after GO enrichment analysis. **C** Selected GO terms for cell processes of significantly detected hsV4N interactome proteins via UDMS^{E} after GO enrichment analysis (Benjamini-Hochberg corrected, p<0.05)

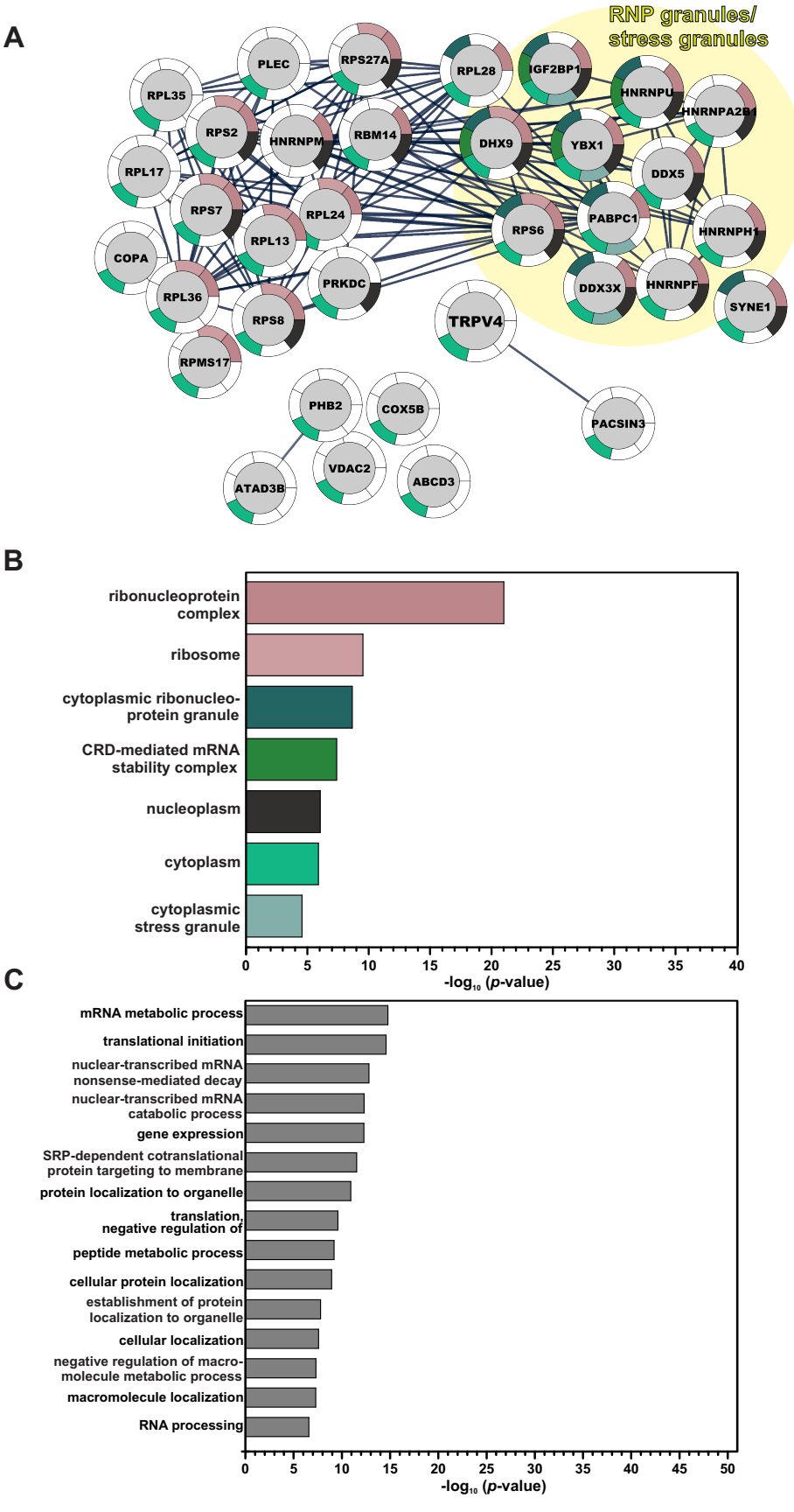
A
RNP granules/
stress granules
PLEC
RPS27A
RPL28
IGF2BP1
HNRNPU
HNRNPA2B1
RPL35
RPS2
HNRNPM
RBM14
DHX9
YBX1
DDX5
RPL17
RPS7
RPL24
RPS6
PABPC1
HNRNPH1
RPL13
COPA
PRKDC
DDX3X
HNRNPF
SYNE1
RPL36
RPS8
TRPV4
RPMS17
PHB2
COX5B
PACSIN3
VDAC2
ATAD3B
ABCD3
B
ribonucleoprotein complex
ribosome
cytoplasmic ribonucleo-protein granule
CRD-mediated mRNA stability complex
nucleoplasm
cytoplasm
cytoplasmic stress granule
0 5 10 15 20 25 30 35 40
-log10 (p-value)
C
mRNA metabolic process
translational initiation
nuclear-transcribed mRNA nonsense-mediated decay
nuclear-transcribed mRNA catabolic process
gene expression
SRP-dependent cotranslational protein targeting to membrane
protein localization to organelle
translation, negative regulation of
peptide metabolic process
cellular protein localization
establishment of protein localization to organelle
cellular localization
negative regulation of macro-molecule metabolic process
macromolecule localization
RNA processing
0 5 10 15 20 25 30 35 40 45 50
-log10 (p-value)

with wild-typic RBPs after induction of repeated cycles of stress granule assembly and disassembly in short time, mimicking chronic stress conditions.[100,132] Permanent Ca^{2+} influx, for example via neuropathy-causing mutations in TRPV4, could thus lead to a pathological switch from dynamic granules to aggregates, which then impair the important roles of ribonucleoprotein granule functions like dendritic and axonal mRNA transport and local translation. Due to the unique cellular structure of neurons, this cell type is more sensitive to the lacking clearance of these aggregates and therefore explain the high neurotoxicity of these inclusions.[133–135] Thus, TRPV4 and its disease-causing mutations provide multiple factors to be a part of the stress granule machinery. Neuropathy causing TRPV4 mutations, like TRPV4 R232C, lead to chronic stress levels due to increased Ca^{2+}-influx activity. Based on the data shown here, hsV4N itself could act as a direct interaction site for stress granule key proteins and in combination with the Ca^{2+}-dependent recruitment of proteins involved in supramolecular fiber formation, possibly leading to neurotoxic aggregates.

To narrow down the interaction sites of the previously identified hsV4N interactors, several hsV4 ARD constructs were probed in the same $UDMS^{E}$ experimental set-ups as hsV4N. The ARD of TRPV4 is a hot-spot for disease-causing mutations.[27,56] Here, besides the wild-typic hsV4 ARD, hsV4 ARD harboring the neuropathy-causing R232C mutation as well as the fetal-akinesia causing hsV4 ARD K276E mutation were investigated with regard to their HEK293 cells protein interactome. Figures 4.6 A-F show the STRING interaction map and GO enrichment analysis of the respective hsV4 ARD construct without and with Ca^{2+}-supplementation. To provide a better overview, only proteins associated with ribonucleoprotein granules and/or stress granules via GO analysis and/or manual data curation are shown in the interaction maps (figures 4.6 A-E). Upon Ca^{2+}-supplementation, the amount of RBPs increases in the case of hsV4 ARD wt (figures 4.6 A and B) and R232C (figures 4.6 C and D). Only for hsV4 ARD K276E the amount of riboluceoprotein granule associated proteins decreases upon Ca^{2+}-supplementation (figure 4.6 E and F). It should be noted that TRPV4 R232C showed elevated basal Ca^{2+}-influx level *in cellulo*.[53,54] Basal Ca^{2+}-influx activities of TRPV4 K276E were not evaluated until now, but due to the severe clinical outcome of this mutation it could be assumed that this mutation also leads to a gain-of-function phenotype of the channel.[48] It is therefore possible that the interactions after Ca^{2+} supplementation are more representative for the possible aberrant PPIs in the presence of disease-causing mutations (figures 4.6 C and D (hsV4 ARD R232C) as well as E and F (hsV4 ARD K276E), respectively).

Comparing the interactome composition between the different TRPV4 N-terminal constructs, it seems that the interactome is highly variable - not only between the samples without and with

Ca^{2+}-supplementation, but also between hsV4 ARD wt and mutated hsV4 ARDs, as well as between hsV4N and hsV4 ARD wt (see figure 4.7). These variations could thus hint towards an important regulatory role of the intrinsically disordered region (hsV4 IDR), preceding hsV4 ARD in hsV4N, on the protein interactions of hsV4 ARD. Interestingly, throughout all $UDMS^E$ measurements, the ATP-dependent RNA-helicase DDX3X was detected as a part of the hsV4N protein interactome, more precisely of hsV4 ARD protein interactome. DDX3X was shown to directly interact with full-length TRPV4 via a yeast-two hybrid screening (Y2H), although the species of used TRPV4 was not mentioned in the publication.[136] Due to the central role of DDX3X in stress granule formation and its role in neurodegeneration, section 4.2 gives a closer look on the probable direct interaction between DDX3X and hsV4N.[119,137–139]

The TRIP database (http://trpchannel.org/) is a manually curated database of PPIs for mammalian TRP channels and therefore gives an overview of known PPIs of TRPV4.[16,29,30] Most of the listed interactors in the TRIP database were determined via co-immunoprecipitations (co-IPs), co-immunofluorescence staining and/or FRET measurements with endogenous proteins and/or overexpressing HEK293 cells (see also table 6.1). The TRPV4 interacting protein classes which are represented in the TRIP databsae are very diverse, including amongst others, transmembrane proteins (TRPC1, AT1aR, AQP4 e.g.), kinases (FYN, LYN e.g.), E3 ubiquitin ligases (ITCH) and cytoskeletal proteins (α-actin and α-tubulins). Another reliable database for PPIs is BioGrid (https://thebiogrid.org/). BioGrid lists the same protein interactors as the TRIP database for human TRPV4.[140] In both databases, no RBPs or other proteins involved in cytoplasmic ribonucleoprotein granules are indicated. One reason for this could be that most of the PPI determinations were conducted via co-IPs of full-length TRPV4 and subsequent western blotting with immunostaining, only allowing to investigate pin-pointed PPIs with certain proteins. Comprehensive mass spectrometric proteomics analysis of isolated TRPV4 domains like the here used hsV4N as a bait were not published until now. Donate-Macian *et al.* used full-length TRPV4 as a bait for Y2H screening of direct TRPV4 interactors, the species of the used TRPV4 construct was not mentioned though, as pointed out above. Besides DDX3X, UBAP2L was also shown to directly interact with TRPV4.[136] In this thesis, UBAP2L was detected in $UDSM^E$

Figure 4.5 *(facing page)*: **The hsV4N wt Avi protein interactome determined via $UDMS^E$ with Ca^{2+} sample supplementation.** **A** STRING interaction network of detected, significant hsV4N interactome proteins. Outer ring color of nodes represent Gene Ontology (GO) terms for cell components, also shown in B. For a full list of protein interactors see table 6.4 **B** Selected GO terms for cell components of significant, detected hsV4N wt Avi interactome proteins via $UDMS^E$ after GO enrichment analysis. **C** Selected GO terms for cell processes of significant, detected hsV4N interactome proteins via $UDMS^E$ after GO enrichment analysis.

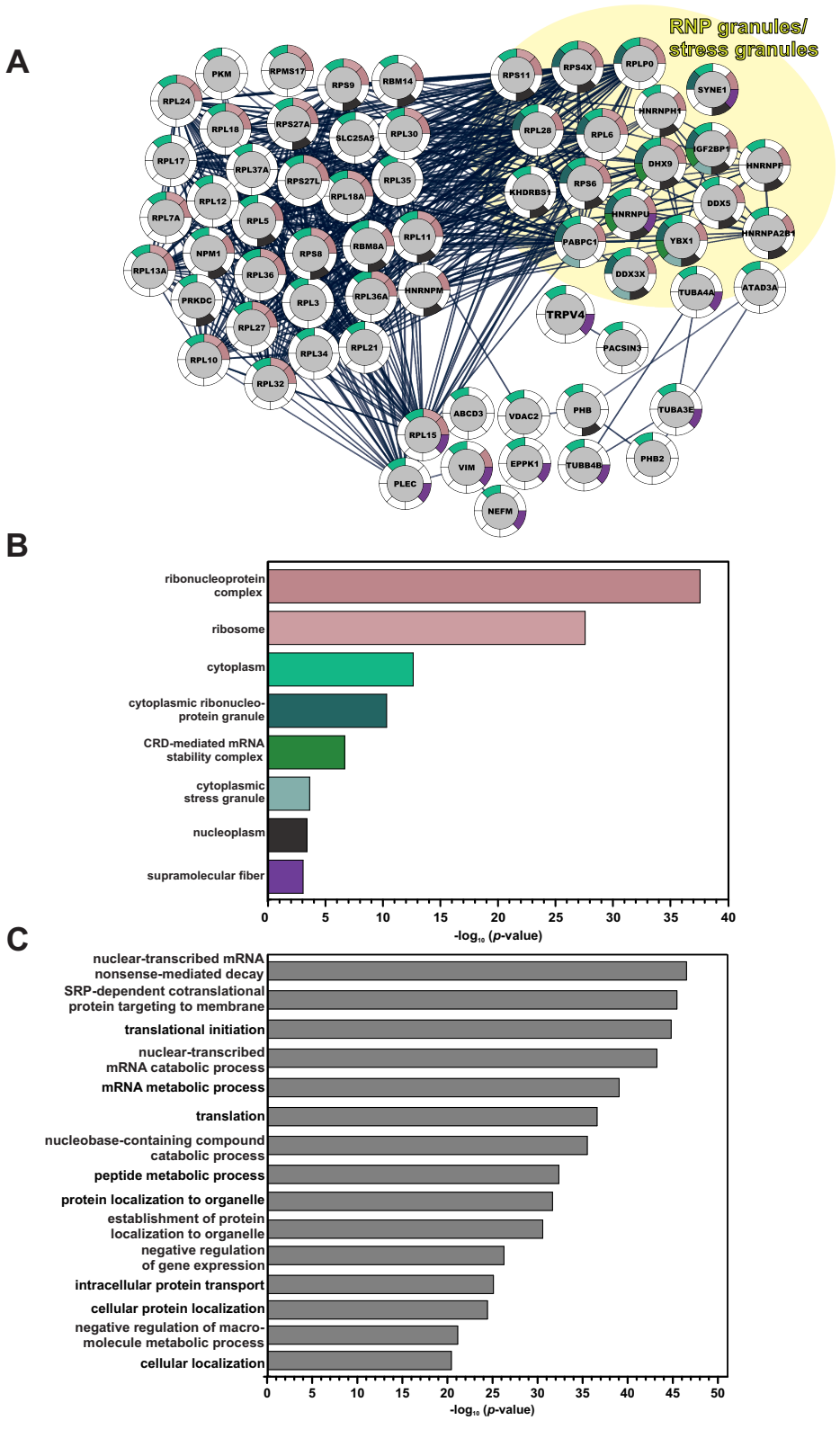
A
RNP granules/
stress granules
PKM
RPMS17
RPS9
RBM14
RPS11
RPS4X
RPLP0
SYNE1
RPL24
RPS27A
SLC25A5
RPL30
RPL28
RPL6
HNRNPH1
RPL18
RPL17
RPL37A
RPS27L
RPL18A
RPL35
KHDRBS1
RPS6
DHX9
IGF2BP1
HNRNPF
RPL12
RPL7A
RPL5
HNRNPU
DDX5
RPL11
PABPC1
YBX1
HNRNPA2B1
NPM1
RPS8
RBM8A
RPL13A
RPL36
DDX3X
TUBA4A
ATAD3A
PRKDC
RPL3
RPL36A
HNRNPM
TRPV4
RPL27
PACSIN3
RPL10
RPL34
RPL21
RPL32
ABCD3
VDAC2
PHB
TUBA3E
RPL15
VIM
EPPK1
TUBB4B
PHB2
PLEC
NEFM
B
ribonucleoprotein complex
ribosome
cytoplasm
cytoplasmic ribonucleo-protein granule
CRD-mediated mRNA stability complex
cytoplasmic stress granule
nucleoplasm
supramolecular fiber
0 5 10 15 20 25 30 35 40
-log10 (p-value)
C
nuclear-transcribed mRNA nonsense-mediated decay
SRP-dependent cotranslational protein targeting to membrane
translational initiation
nuclear-transcribed mRNA catabolic process
mRNA metabolic process
translation
nucleobase-containing compound catabolic process
peptide metabolic process
protein localization to organelle
establishment of protein localization to organelle
negative regulation of gene expression
intracellular protein transport
cellular protein localization
negative regulation of macro-molecule metabolic process
cellular localization
0 5 10 15 20 25 30 35 40 45 50
-log10 (p-value)

experiments conducted with hsV4 ARD wt (figures 4.6 A and B). However, the protein overlap between UDSM^{E} and Y2H is low, which was also already shown after comparison of other affinity purification MS (AP-MS) experiments with Y2H screens with the same bait protein. This emphasizes the highly complementary nature of both techniques: while MS approaches provide large-scale data on protein complexes, with additional Y2H results it is possible to break these complexes down into binary PPIs.[141]

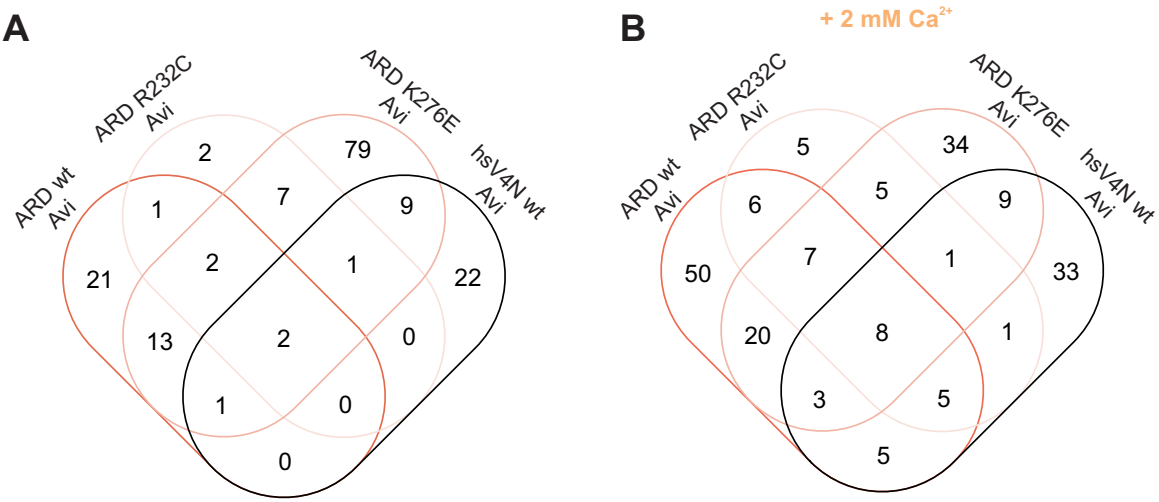

Figure 4.7: **Venn diagrams of overlapping proteins detected in respective UDMS^{E} experiments without (A) and with Ca^{2+} sample supplementation (B).** For full lists of detected proteins see tables 6.3, 6.4, 6.5, 6.6, 6.7, 6.8, 6.9 and 6.10

Figure 4.6 *(facing page)*: **Interaction map, volcano plots and enrichment analysis of Gene Ontology (GO) cell component and processes terms of hsV4 ARD wt Avi, hsV4 ARD R232C Avi and hsV4 ARD K276E Avi interactome proteins detected via UDMS^{E} without (A,C,E) and with Ca^{2+} sample supplementation (B,D,F)** For full lists of protein interactors see tables 6.5, 6.6, 6.7, 6.8, 6.9 and 6.10 **A** hsV4 ARD wt Avi *Upper left:* STRING interaction network of detected, significant hsV4 ARD wt Avi interactome proteins associated with cytoplasmic ribonucleoprotein granules and/or stress granules after manual data curation. For full list of interactors see section 6.3. Outer ring color of nodes represent GO cell component terms shown in the GO cell component enrichment graphic below. *Upper right:* Volcano plot of two independent HEK293 protein interactome UDMS^{E} experiments with hsV4 ARD wt Avi. Each pulldown was measured in quadruplicates. Horizontal light gray line indicates *p*-value = 0.05 (Benjamini-Hochberg corrected Student's *t*-test). Vertical light gray line indicates $\log_2$ fold change ≥ 1. *Lower left:* Selected GO terms for cell components of significant, detected hsV4 ARD wt Avi interactome proteins via UDMS^{E} after GO enrichment analysis (Benjamini-Hochberg corrected, $p<0.05$). *Lower Right:* Top 15 GO cell processes terms of significant, detected hsV4 ARD wt Avi interactome proteins via UDMS^{E} after GO enrichment analysis (Benjamini-Hochberg corrected, $p < 0.05$). **B** hsV4 ARD wt Avi with Ca^{2+}. **C** hsV4 ARD R232C Avi and **D** with Ca^{2+}. **E** hsV4 ARD K276 Avi and **F** with Ca^{2+}. Please note for graphs in E and F the range changing in the x-axis of the GO Enrichment Processes Graphs in comparison to A-D.

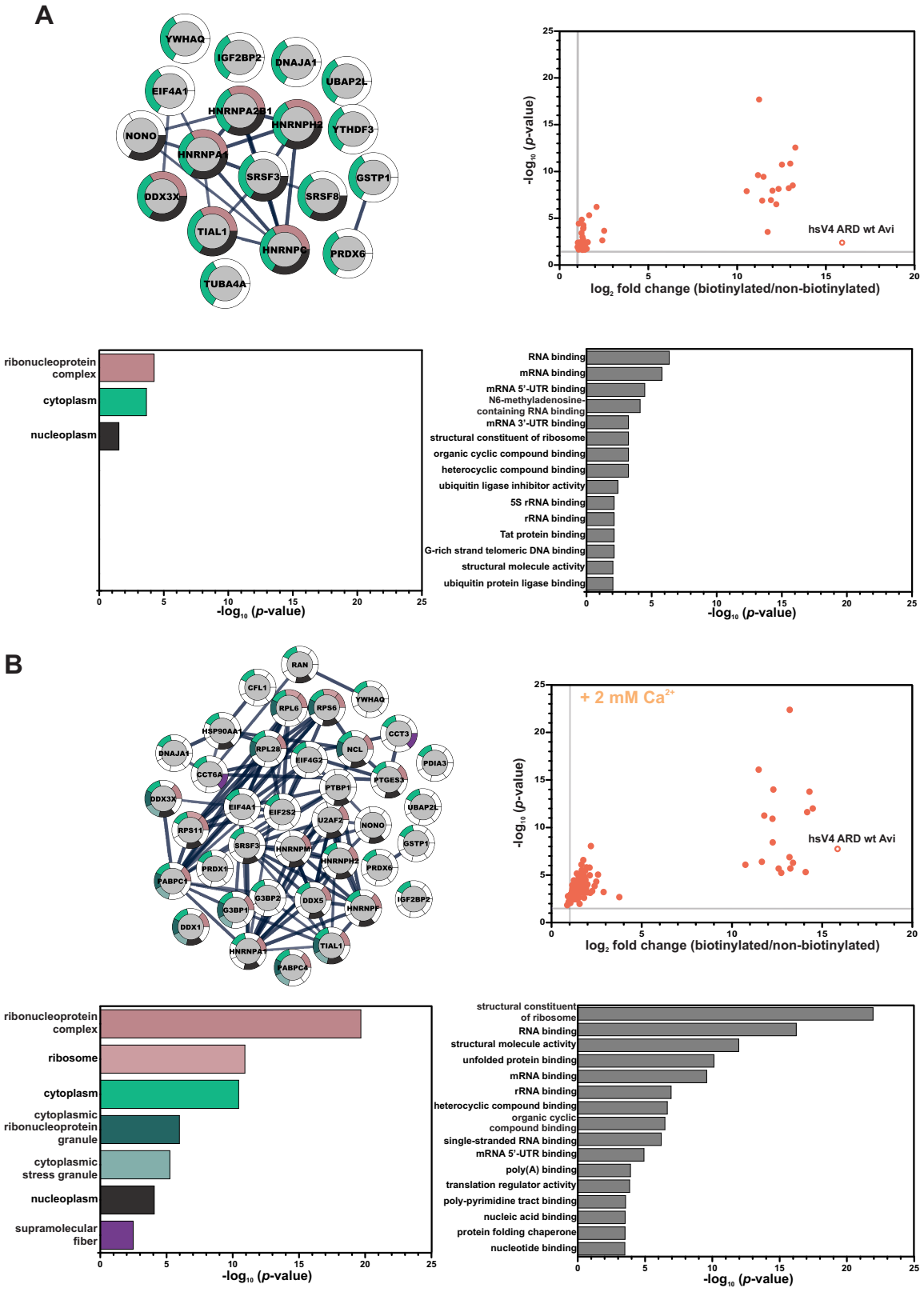
A
YWHAQ
IGF2BP2
DNAJA1
UBAP2L
EIF4A1
HNRNPA2B1
HNRNPH2
YTHDF3
NONO
HNRNPA1
SRSF3
GSTP1
DDX3X
SRSF8
TIAL1
HNRNPC
PRDX6
TUBA4A
-log10 (p-value)
log2 fold change (biotinylated/non-biotinylated)
hsV4 ARD wt Avi
ribonucleoprotein complex
cytoplasm
nucleoplasm
-log10 (p-value)
RNA binding
mRNA binding
mRNA 5'-UTR binding
N6-methyladenosine-containing RNA binding
mRNA 3'-UTR binding
structural constituent of ribosome
organic cyclic compound binding
heterocyclic compound binding
ubiquitin ligase inhibitor activity
5S rRNA binding
rRNA binding
Tat protein binding
G-rich strand telomeric DNA binding
structural molecule activity
ubiquitin protein ligase binding
-log10 (p-value)
B
RAN
CFL1
YWHAQ
RPL6
RPS6
HSP90AA1
CCT3
DNAJA1
RPL28
NCL
EIF4G2
PDIA3
CCT6A
PTBP1
PTGES3
DDX3X
EIF4A1
EIF2S2
UBAP2L
U2AF2
RPS11
NONO
SRSF3
HNRNPM
GSTP1
HNRNPH2
PRDX1
PRDX6
PABPC1
G3BP2
DDX5
IGF2BP2
G3BP1
HNRNPF
DDX1
TIAL1
HNRNPA1
PABPC4
+ 2 mM Ca2+
-log10 (p-value)
log2 fold change (biotinylated/non-biotinylated)
hsV4 ARD wt Avi
ribonucleoprotein complex
ribosome
cytoplasm
cytoplasmic ribonucleoprotein granule
cytoplasmic stress granule
nucleoplasm
supramolecular fiber
-log10 (p-value)
structural constituent of ribosome
RNA binding
structural molecule activity
unfolded protein binding
mRNA binding
rRNA binding
heterocyclic compound binding
organic cyclic compound binding
single-stranded RNA binding
mRNA 5'-UTR binding
poly(A) binding
translation regulator activity
poly-pyrimidine tract binding
nucleic acid binding
protein folding chaperone
nucleotide binding
-log10 (p-value)

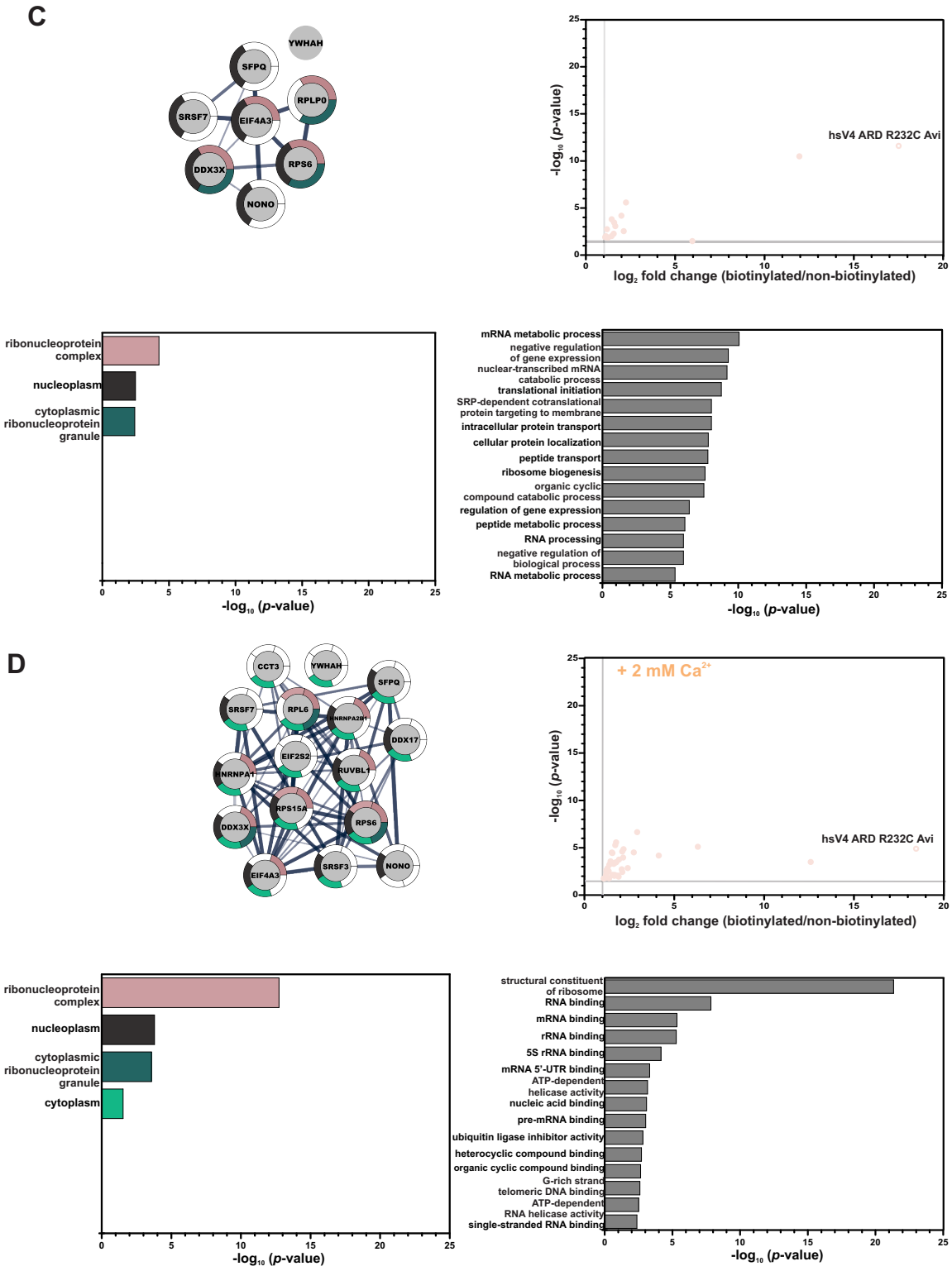
C
YWHAH
SFPQ
RPLP0
SRSF7
EIF4A3
RPS6
DDX3X
NONO
hsV4 ARD R232C Avi
-log10 (p-value)
log2 fold change (biotinylated/non-biotinylated)
ribonucleoprotein complex
nucleoplasm
cytoplasmic ribonucleoprotein granule
-log10 (p-value)
mRNA metabolic process
negative regulation of gene expression
nuclear-transcribed mRNA catabolic process
translational initiation
SRP-dependent cotranslational protein targeting to membrane
intracellular protein transport
cellular protein localization
peptide transport
ribosome biogenesis
organic cyclic compound catabolic process
regulation of gene expression
peptide metabolic process
RNA processing
negative regulation of biological process
RNA metabolic process
-log10 (p-value)
D
CCT3
YWHAH
SFPQ
SRSF7
RPL6
HNRNPA2B1
DDX17
EIF2S2
HNRNPA1
RUVBL1
RPS15A
DDX3X
RPS6
EIF4A3
SRSF3
NONO
+ 2 mM Ca2+
hsV4 ARD R232C Avi
-log10 (p-value)
log2 fold change (biotinylated/non-biotinylated)
ribonucleoprotein complex
nucleoplasm
cytoplasmic ribonucleoprotein granule
cytoplasm
-log10 (p-value)
structural constituent of ribosome
RNA binding
mRNA binding
rRNA binding
5S rRNA binding
mRNA 5'-UTR binding
ATP-dependent helicase activity
nucleic acid binding
pre-mRNA binding
ubiquitin ligase inhibitor activity
heterocyclic compound binding
organic cyclic compound binding
G-rich strand telomeric DNA binding
ATP-dependent RNA helicase activity
single-stranded RNA binding
-log10 (p-value)

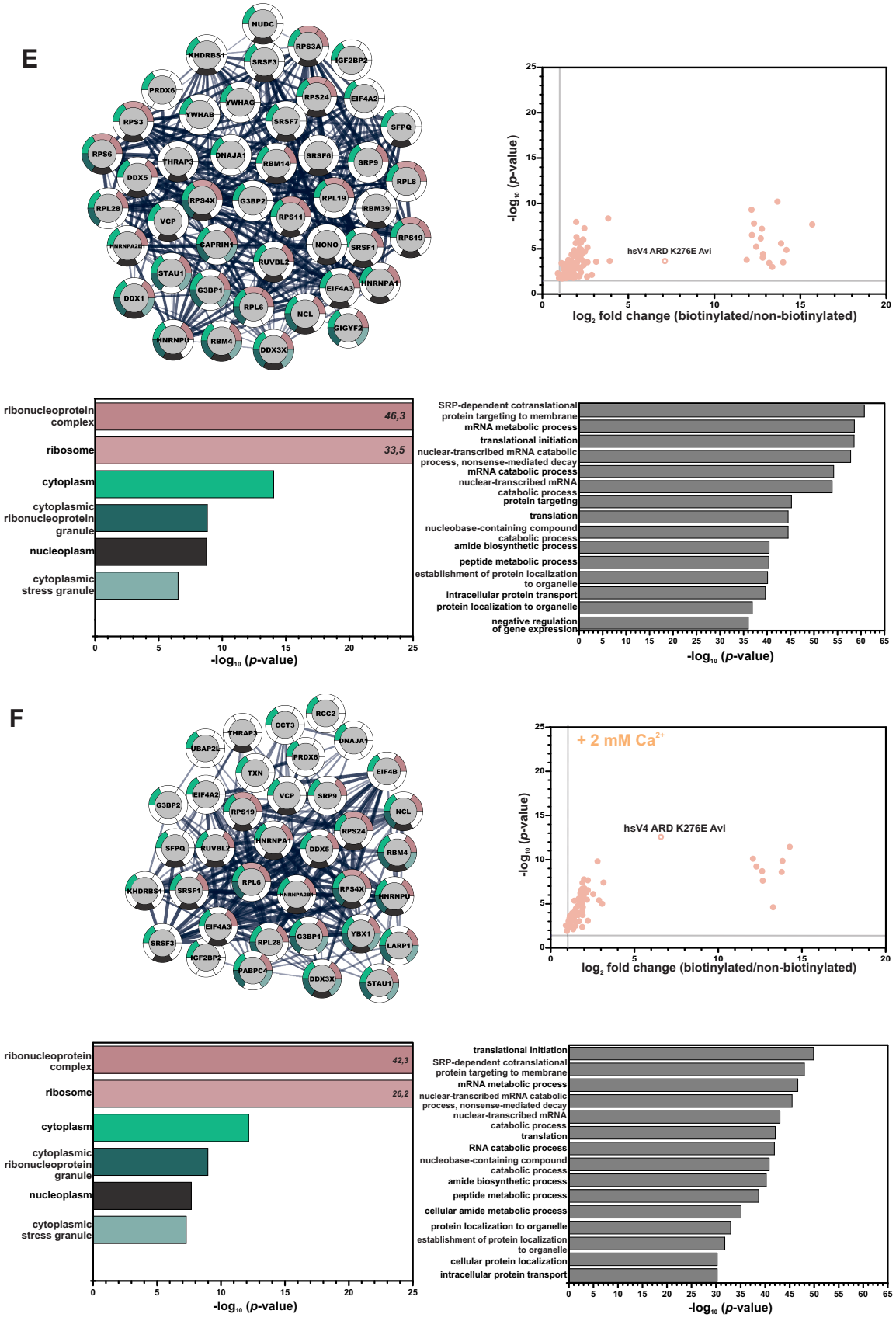
E
NUDC
KHDRBS1
SRSF3
RPS3A
IGF2BP2
PRDX6
YWHAG
RPS24
EIF4A2
RPS3
YWHAB
SRSF7
SFPQ
RPS6
THRAP3
DNAJA1
RBM14
SRSF6
SRP9
DDX5
RPL8
RPL28
RPS4X
G3BP2
RPL19
RBM39
VCP
RPS11
HNRNPA2B1
CAPRIN1
NONO
SRSF1
RPS19
STAU1
RUVBL2
G3BP1
EIF4A3
HNRNPA1
DDX1
RPL6
NCL
GIGYF2
HNRNPU
RBM4
DDX3X
-log10 (p-value)
log2 fold change (biotinylated/non-biotinylated)
hsV4 ARD K276E Avi
ribonucleoprotein complex
ribosome
cytoplasm
cytoplasmic ribonucleoprotein granule
nucleoplasm
cytoplasmic stress granule
46,3
33,5
-log10 (p-value)
SRP-dependent cotranslational protein targeting to membrane
mRNA metabolic process
translational initiation
nuclear-transcribed mRNA catabolic process, nonsense-mediated decay
mRNA catabolic process
nuclear-transcribed mRNA catabolic process
protein targeting
translation
nucleobase-containing compound catabolic process
amide biosynthetic process
peptide metabolic process
establishment of protein localization to organelle
intracellular protein transport
protein localization to organelle
negative regulation of gene expression
-log10 (p-value)
F
RCC2
CCT3
THRAP3
DNAJA1
UBAP2L
PRDX6
TXN
EIF4B
EIF4A2
VCP
SRP9
G3BP2
RPS19
NCL
RPS24
HNRNPA1
SFPQ
RUVBL2
DDX5
RBM4
KHDRBS1
SRSF1
RPL6
HNRNPA2B1
RPS4X
HNRNPU
EIF4A3
YBX1
SRSF3
RPL28
G3BP1
LARP1
IGF2BP2
PABPC4
DDX3X
STAU1
+ 2 mM Ca2+
hsV4 ARD K276E Avi
-log10 (p-value)
log2 fold change (biotinylated/non-biotinylated)
ribonucleoprotein complex
ribosome
cytoplasm
cytoplasmic ribonucleoprotein granule
nucleoplasm
cytoplasmic stress granule
42,3
26,2
-log10 (p-value)
translational initiation
SRP-dependent cotranslational protein targeting to membrane
mRNA metabolic process
nuclear-transcribed mRNA catabolic process, nonsense-mediated decay
nuclear-transcribed mRNA catabolic process
translation
RNA catabolic process
nucleobase-containing compound catabolic process
amide biosynthetic process
peptide metabolic process
cellular amide metabolic process
protein localization to organelle
establishment of protein localization to organelle
cellular protein localization
intracellular protein transport
-log10 (p-value)

The UDMS^{E} interactome results shown in this thesis revealed ribonucleotide binding proteins as a new potential class of TRPV4 interacting proteins and thus indicate TRPV4 as a until now unknown player in the regulatory mechanism of cytoplasmic ribonulceoprotein granule formation via its cytosolic N-terminus. The following sections take a closer look on chosen TRPV4 PPIs *in vitro* and *in cellulo*.

4.2 Birds of a feather flock together - the interaction between the two protean proteins TRPV4 and DDX3X

As described in sub chapter 4.1, elaborate mass spectrometry (MS)-based interactome studies of hsV4N showed a significant amount of RNA-binding proteins (RBPs) as a new class of potential TRPV4 binding partners. The composition of detected RBPs varied between different conditions, like the presence of disease-causing mutations and/or Ca^{2+}-supplementation. Intriguingly, the ATP-dependent RNA-helicase DDX3X was consistently detected in all samples. Recently, Donate-Macian *et al.*[136] showed via a Y2H screening that DDX3X is a direct interactor of full-length TRPV4. The MS-based interactome studies conducted in this work indicate that DDX3X possibly binds to the TRPV4 N-terminus with the ARD (hsV4 ARD) as a minimal binding site. Log_2 ratios of DDX3X in respective MS-measurements already suggested elevated DDX3X binding-levels with mutation-bearing hsV4 ARDs (hsV4 ARD R232C and K276E, respectively) in comparison to hsV4 ARD wt or hsV4N (see tables 6.3, 6.4, 6.5, 6.6, 6.7, 6.8, 6.9 and 6.10). To conduct *in vitro* experiments regarding the probable direct interaction between DDX3X and hsV4 ARD, recombinant DDX3X and TRPV4 N-terminal constructs were purified and their structural integrity confirmed as shown in figure 4.8 (see subsections 3.7.1 and 3.7.6 for purification protocols). hsV4 ARD K276E showed heavy precipitation behavior in all subsequent *in vitro* studies and is therefore not shown in following procedures and experiments.

Figure 4.8 *(facing page)*: **Purification of recombinant human TRPV4 N-terminal constructs and human DDX3X. A** Topology model of recombinantly expressed human TRPV4 N-terminal constructs and human DDX3X. The DDX3X construct was optimized for future nuclear magnetic resonance spectroscopy experiments, comprising supposedly unstructured regions which include residues aa 1 - 120 and aa 582 - 662. His_6 = hexa-histidine tag (single letter code: HHHHHH), TEV = Tobacco Etch Virus Cleavage Site (single letter code: ENLYFQG), DEAD = DEAD domain (RecA-like domain 1), HELICc = C-terminal helicase domain (RecA-like domain 2). See figure 4.14 A for full-length DDX3X. His_6-tags with preceding or subsequent TEV Cleveage Site were removed. **B** SEC purifications of human TRPV4 N-terminal constructs and human DDX3X. SEC runs were performed with either a HiLoad Superdex 200 or a HiLoad Superdex 75 pg preparative SEC column. Inlets show Coomassie stained 15 % SDS-PAGEs of collected and concentrated fractions after SEC. x-axis: eluted volume in mL, y-axis: absorbance at 280 nm, M = marker. **C** Comparison of far UV CD spectra of purified human TRPV4 N-terminal constructs and human DDX3X, respectively. Spectra were measured at 293 K and proteins were used at 1 µM concentration in either SEC Buffer with a final NaCl concentration of 30 mM (TRPV4 N-terminal constructs) or DDX3X SEC buffer with a final concentration of 12.5 mM NaCl (DDX3X). Inlets show secondary structure prediction performed with CAPITO.[93] The predicted α-helix/β-sheet/random coil content of the purified proteins is for hsV4N 53 %/0 %/47 %, hsV4N R232C 33 %/13 %/53 %, hsV4 ARD wt 68 %/0 %/32 %, hsV4 ARD R232C 78 %/0 %/32 % and DDX3X 40 %/14 %/46 %. y-axis: mean residue ellipticity ($[\Theta]_{mrw,\lambda}$) in 10^{-3} deg cm^2 dmol^{-1}, x-axis: wavelength λ in nm.

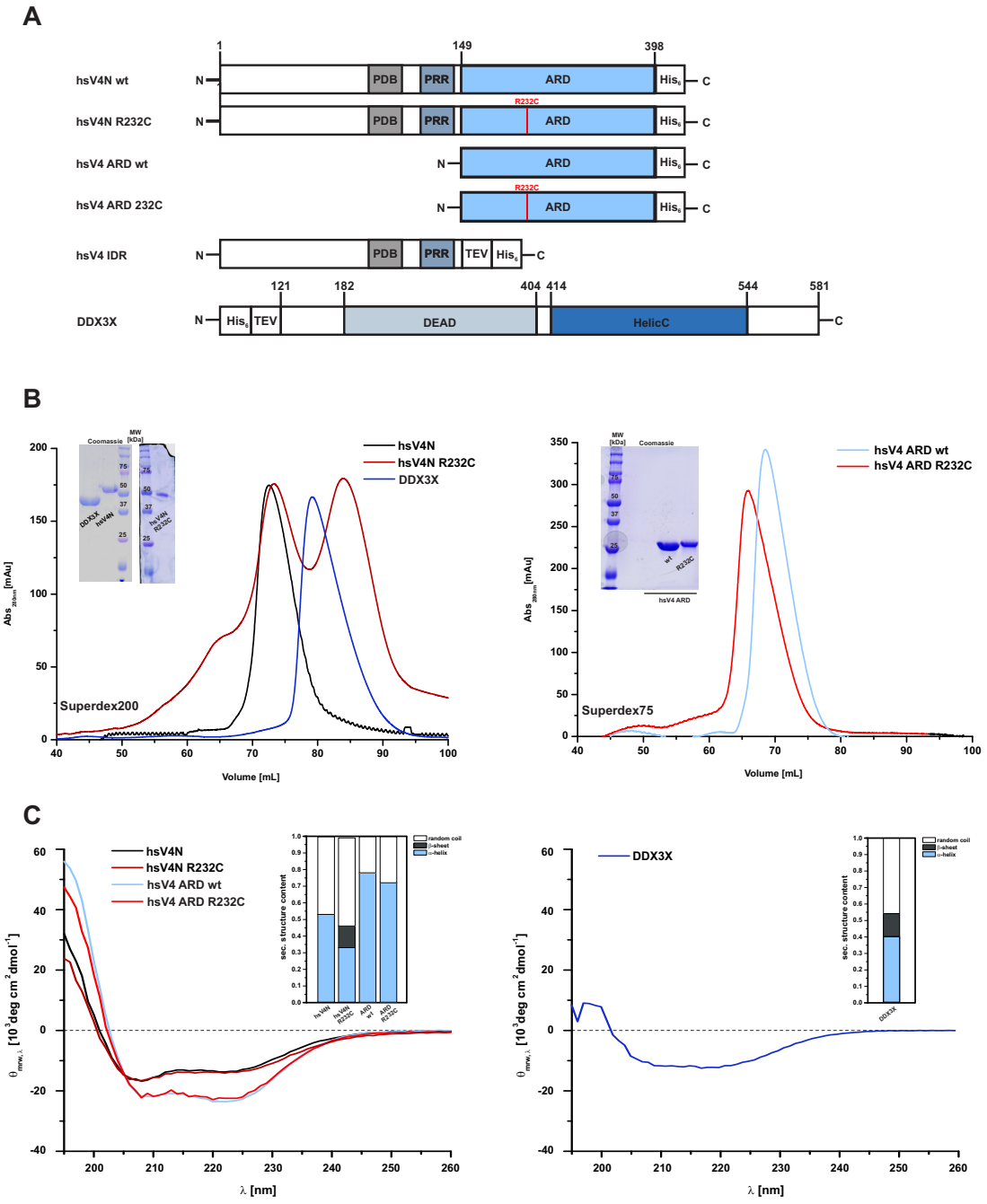
A
hsV4N wt
hsV4N R232C
hsV4 ARD wt
hsV4 ARD 232C
hsV4 IDR
DDX3X
PDB
PRR
ARD
TEV
DEAD
HelicC
R232C
B
hsV4N
hsV4N R232C
DDX3X
Superdex200
Volume [mL]
hsV4 ARD wt
hsV4 ARD R232C
Superdex75
C
hsV4N
hsV4N R232C
hsV4 ARD wt
hsV4 ARD R232C
DDX3X
λ [nm]
sec. structure content
random coil
β-sheet
α-helix

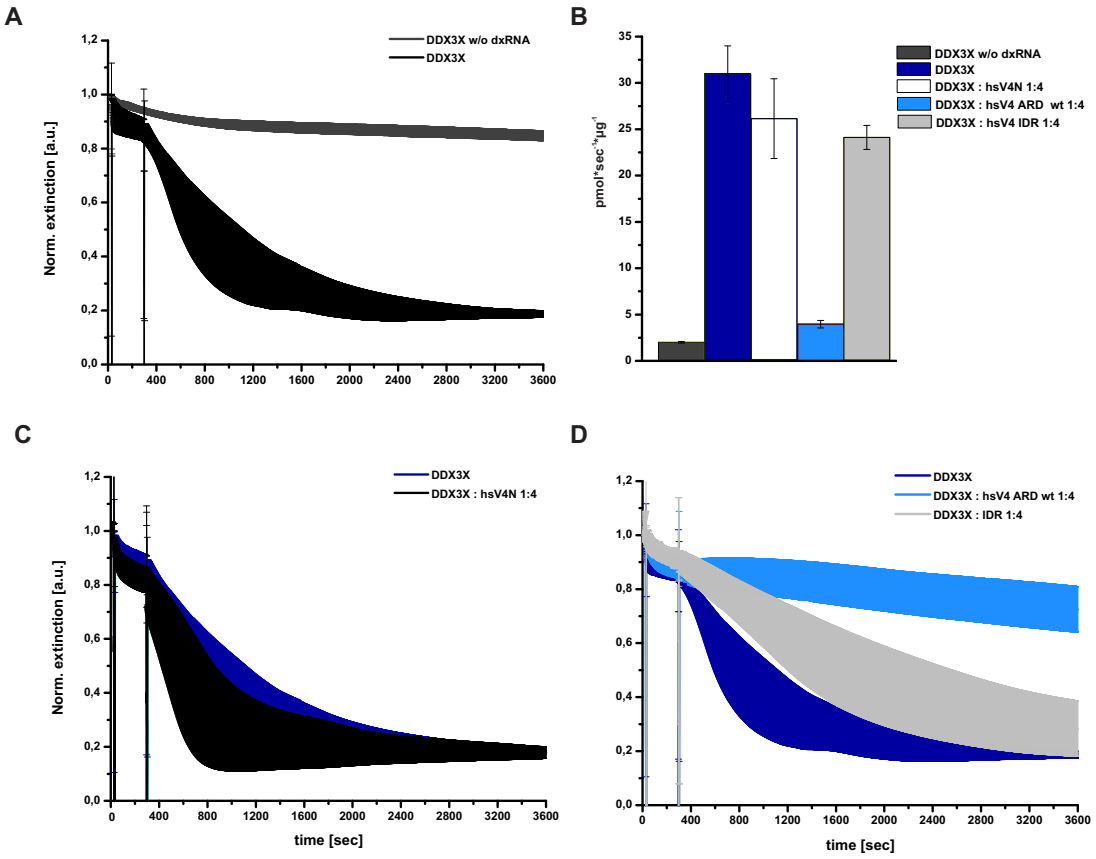

Figure 4.9: **hsV4 ARD, but not hsV4N, decreases the DDX3X ATPase activity. A** In an enzyme-coupled ATPase assay, DDX3X showed a time-dependent duplex RNA (dxRNA)-stimulated ATPase activity (black) and a negligible ATPase activity in the absence of dxRNA (DDX3X w/o dxRNA, dark gray), in agreement with the literature.[84,142] **B** DDX3X ATPase activity in the presence of several TRPV4 N-terminal constructs. Error bars indicate SDs of determined slopes after natural logarithmic conversion and linear regression. **C+D** DDX3X showed decreased ATPase activity in the presence of hsV4 ARD. Interestingly, hsV4N itself and the ARD preceding intrinsically disordered region (IDR) consisting of amino acids 1-149 of hsV4N do not demonstrate such an effect on DDX3X. DDX3X was used at a concentration of 3 µM and TRPV4 N-terminal constructs at 12 µM, resulting in a 1:4 ratio. After 30 s samples were supplemented with ATP and after 5 min with duplex RNA (dxRNA), both at a final concentration of 1 µM. ATPase activity was determined by an ATP-dependent enzyme-coupled oxidation from NADH to NAD^+, resulting in an time-dependent absorption decrease at 340 nm. Measurements were normalized to DDX3X ATPase activity. Error bars indicate SDs of three measurements of three independent DDX3X purifications for each condition. Used TRPV4 N-terminal constructs originated from one purification. x-axis = time in s, y-axis = extinction at 340 nm in arbitrary units. IDR was kindly provided and fully characterized by Dr[redacted] and[redacted].[143]

To ensure enzymatic activity of purified DDX3X, an enzyme-coupled ATPase assay was performed (see figures 4.13 C and D). In agreement with Epling *et al.*[142], DDX3X showed a time-dependent duplex RNA (dxRNA)-stimulated ATPase activity and a negligible ATPase activity in the absence of dxRNA (figure 4.9 A). When supplemented with hsV4 ARD, the ATPase activity of DDX3X significantly decreased, whereas no effect was observed upon hsV4N supplementation (see figure 4.9). Interestingly, DDX3X ATPase activity did not decrease in the presence

of the isolated TRPV4 intrinsic disordered region (hsV4 IDR), which consists of aa 1-149 of hsV4N, preceding the hsV4 ARD. As a control, the well-characterized *B. subtilis* ATPase BmrA was also supplemented with hsV4 ARD to rule out unspecific effects on the lactate dehydrogenase and pyruvate kinase involved in this assay. No decrease in BmrA ATPase activity was observed upon hsV4 ARD wt supplementation (see section 6.4, figure 6.3), supporting the direct interaction between hsV4 ARD and DDX3X. Nevertheless the question arose, why there is such a discrepancy between hsV4N and hsV4 ARD modulation of DDX3X ATPase activity. Cross-linking mass spectrometry (XL-MS) experiments with DSS-cross linked hsV4N and DDX3X (see figure 4.10) revealed cross-linking between K251 of hsV4 ARD and K511 in the C-terminal helicase domain (HelicC) of DDX3X in close proximity to motifs V (aa 501-505) and VI (aa 525-536), which are responsible for RNA recognition (motif V) and ATP-binding (motif VI).[144]

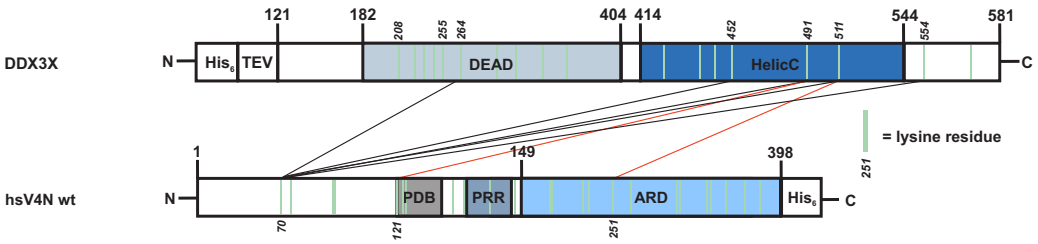

Figure 4.10: **Cross-linking mass spectrometry (XL-MS) confirms a direct interaction between hsV4N and DDX3X.** Green bars indicate native lysine residues, whereas lysine residues involved in DSS-mediated cross-linking are additionally numbered. Black lines show cross-links including hsV4N K70 and DDX3X lysine residues, red lines cross-links between hsV4N K121 and DDX3X K491 and hsV4N K251 and DDX3X K511, respectively. XL-MS measurements were kindly carried out by M.Sc. [redacted] University of Konstanz)

XL-MS experiments of Dr. Benedikt Goretzki demonstrated an IDR-ARD interaction in the *G. gallus* (chicken) TRPV4 N-terminus (ggV4N) between distinct lysine residues, indicating these interactions not to be arbitrary but rather following certain preferred contact sites of the IDR with the ARD.[23] Amongst others, ggV4N showed an intra-domain interaction between $K56^{IDR}$ and $K237^{ARD}$, which could be also detected in the corresponding lysine residues $K70^{IDR}$ and $K251^{ARD}$ in hsV4N (data not shown). It was previously shown that the TRPV4 N-termini of chicken and human share important conserved motifs like the prolines in the PRR and show overall similiar behavior and structural features (sharing 84.27 % amino acid identity), enabling to transfer *in vitro* studies of the N-termini between the species.[22] Regarding this folding behavior of the IDR back to the ARD, preventing the ARD to interact with a distinct contact site with the DDX3X HelicC domain, the difference of ATPase activity modulation between hsV4N, IDR and hsV4 ARD could be explained. The interaction of the IDR itself seems not to play a role in

ATPase modulation of DDX3X. Inada *et al.* showed that hsV4 ARD is able to bind ATP, which induces conformational changes in fingers 2 and 3.[27]

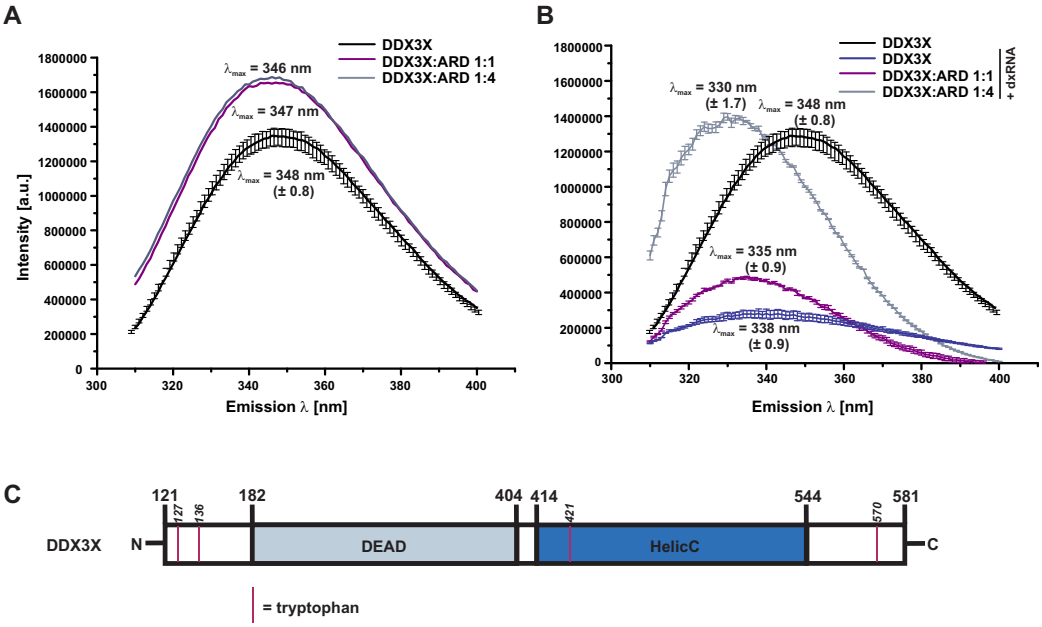

Figure 4.11: **hsV4 ARD interacts with duplex RNA (dxRNA)-bound DDX3X**.**A** Tryptophan fluorescence measurements of DDX3X and hsV4 ARD wt. **B** Tryptophan fluorescence measurements of DDX3X and hsV4 ARD wt in the presence of dxRNA. Each sample was additionally supplemented with 1 µM ATP, as DDX3X requires ATP for RNA binding.[144] hsV4 ARD does not harbor tryptophan residues. DDX3X was used at a concentration of 3 µM and hsV4 ARD at either 3 µM (1:1 ratio) or 12 µM (1:4 ratio). Indicated samples were supplemented with duplex RNA (dxRNA) to a final concentration of 1 µM. Measurements with dxRNA were corrected due to the inner filter effect of supplemented dxRNA (see equations 4.1 and 4.2).[145] Error bars indicate SDs of three measurements of three independent DDX3X purifications for each condition. Used TRPV4 N-terminal constructs originated from one purification. Emission maxima (λ_{max} in nm) are listed with SDs if applicable. x-axis = emission wavelength λ in nm, y-axis = fluorescence intensity in arbitrary units. **C** Topology model of recombinantly expressed and purified human DDX3X used for tryptophan fluoresence measurements, containing four tryptophan residues (indicated by pink bars). DEAD = DEAD domain (RecA-like domain 1), HELICc = C-terminal helicase domain (RecA-like domain 2). See figure 4.14 A for full-length DDX3X.

To exlcude unspecific DDX3X ATPase activity modulation via interactions between the dxRNA phosphate groups and the basic surfaces of hsV4 ARD, tryptophan fluorescence measurements were carried out (figure 4.11). The DDX3X construct used here harbors four tryptophan residues (W127, W137, W421 and W570), whereas hsV4 ARD does not include any tryptophan residues, resulting in the DDX3X tryptophan residues to be the only reporters in these measurements. With tryptophan fluorescence it is possible to investigate the polarity of tryptophan environments in proteins, displayed by the position of the tryptophan residue emission maxima. Polar environments result in redshifted emission maxima, hydrophobic environments therefore in blueshifted maxima. Furthermore, the quantum yield and thus the emission intensity also depends on the tryptophan's direct environment, displaying higher emission intensities

of tryptophan residues in more apolar surroundings.[145] Due to inner filter effects (quenching of tryptophan fluorescence) of the supplemented dxRNA, the obtained fluorescence spectra were corrected according to Hellmann *et al.* with the following equations:[145]

$$\text{Correction Factor (CF)} = \frac{F_W(x)}{F_W(0)} \tag{4.1}$$

The Correction Factor (CF) in equation 4.1 is obtained by the division of the fluorescence of a tryptophane solution with $1\,\mu M$ dxRNA ($F_W(x)$) by the fluorescence of a pure tryptophane solution ($F_W(0)$). The tryptophan concentration here was the same as used for DDX3X in the measurements ($3\,\mu M$). The corrected tryptophan fluorescence for DDX3X ($F_{DDX3X,\ corrected(x)}$) was then obtained by dividing the measured tryptophan fluorescence with dxRNA ($F_{DDX3X}(x)$) divided by CF (see 4.2).

$$F_{DDX3X,\ corrected(x)} = \frac{F_{DDX3X}(x)}{CF} \tag{4.2}$$

The displayed tryptophan fluorescence measurements suggest that hsV4 ARD binds to ATP and dxRNA-bound DDX3X. Intensity changes in figure 4.11 A are not considered significant, as more measurements have to be carried out to receive statistical relevant results with DDX3X and hsV4 ARD in the ratios 1:1 and 1:4, respectively. Emission spectra in figure 4.11 B hint to a dxRNA mediated interaction between DDX3X and hsV4 ARD. Upon dxRNA addition, the emission maximum significantly blueshifted in comparison to ATP-bound DDX3X in the absence of dxRNA from $348\,nm$ to $338\,nm$, which implies a considerable polarity change of the DDX3X tryptophan residues towards a more hydrophobic environment. The crystal structures shown in figure 4.12 visualize the dramatic structural change and therefore the tryptophane residues' environmental change upon RNA binding in DDX3X.[142,144] Addition of dxRNA lead to a significant emission intensity decrease, which can be explained by the quenching effect of RNA in tryptophane fluorescece measurements.[146,147] Interestingly, upon hsV4 ARD supplementation, the DDX3X emission maxima gradually redshifted, suggesting a direct interaction between DDX3X and hsV4 ARD. Additionally, a dramatic emission intensity increase upon hsV4 ARD supplementation was detected, especially at a DDX3X:hsV4 ARD ratio of 1:4. These tryptophan residues environment changes indicate a direct hsV4 ARD interaction with DDX3X and not unspecific binding of dxRNA by hsV4 ARD.

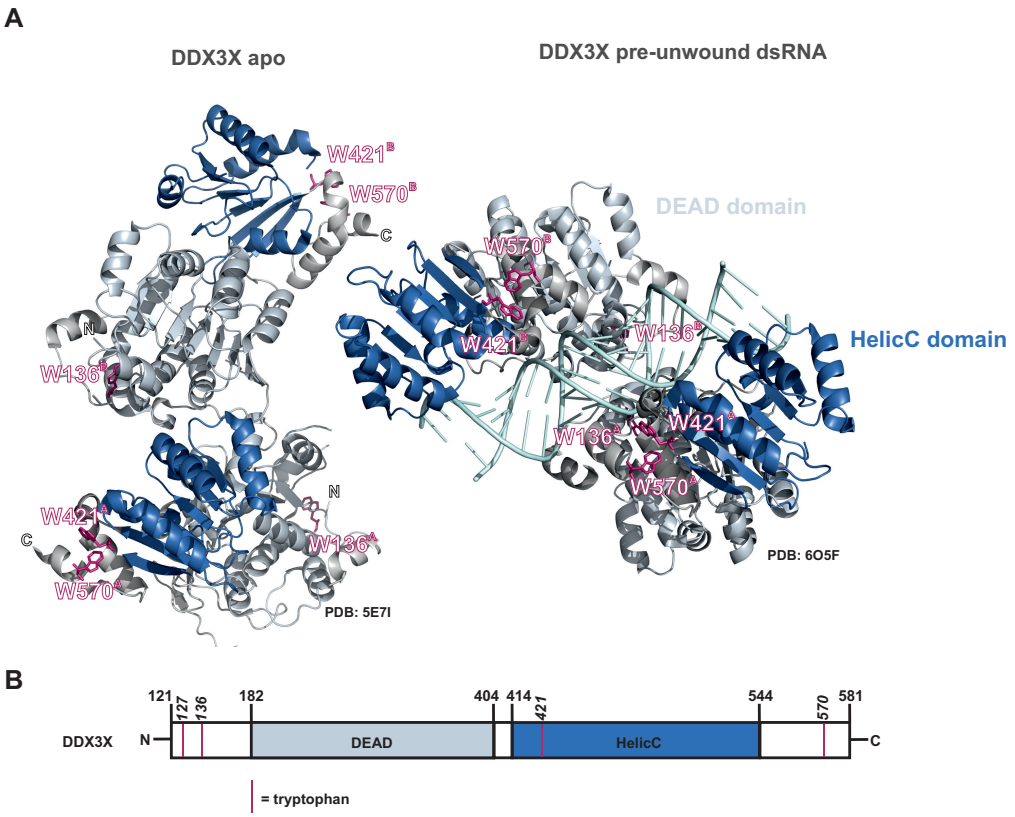

Figure 4.12: **dsRNA binding changes the tryptophan environment in DDX3X dramatically. A** Crystal structures of human DDX3X in the apo state (left, PDB: 5E7I)[142] and bound to double-stranded RNA (right, PDB: 6O5F)[144]. ATP-binding DEAD domain is colored in light blue, the c-terminal helicase domain (HelicC) in dark blue. **B** Topology model of recombinantly expressed and purified human DDX3X used for tryptophan fluoresence measurements, containing four tryptophan residues (indicated by pink bars). DEAD = DEAD domain (RecA-like domain 1), HELICc = C-terminal helicase domain (RecA-like domain 2). See figure 4.14 A for full-length DDX3X.

XL-MS measurements were carried out without any ATP or dxRNA supplementation, as these additions could have interfered the cross-linking reaction, showing that the DDX3X:hsV4 ARD interaction also occurs without these components. One main advantage of XL-MS is the possibility to capture PPIs, which are very weak and/or transient.[87] Therefore, the XL-MS results combined with the rather low-resolution spectroscopic and photometric measurements indicate that DDX3X also interacts with hsV4 ARD in the apo state *in vitro*, but that this interaction can be enhanced upon ATP- and dxRNA binding. As DDX3X showed higher $\log_2$ ratios in MS-measurements carried out in subchapter 4.1 with hsV4 ARD R232C compared to hsV4 ARD wt or hsV4N, suggesting elevated DDX3X-binding level in the presence of this mutation, complementary ATPase assays as in figure 4.9 were carried out with respective mutation bearing TRPV4 N-terminal constructs. Interestingly, both hsV4N R232C and hsV4 ARD R232C showed significantly higher ATPase inhibiting effects as their wild-typic complementaries (figure 4.13).

These results underline the trend that DDX3X ATPase activity inhibition by hsV4 ARD R232C is more enhanced than by hsV4N R232C. As Dr. Benedikt Goretzki suggested[23], the charge distribution in ggV4N probably modulates the interaction between IDR and ARD. The very N-terminal part of ggV4N is enriched with negatively charged residues, which could interact with the overall positively charged residues of the ARD finger 1 and 2. Arg232 in hsV4 ARD resides in finger 2 and furthermore builds a salt bridge to Glu183 in finger 1, which was observed in the crystal structure of the isolated hsV4 ARD.[27] The neutral mutation R232C could disrupt the overall basic patch in hsV4 ARD which might be required for the intra-domain IDR-ARD interaction. Additionally, the disruption of the R232-E183 salt bridge could influence the dynamics of finger 1 and 2 of hsV4 ARD, leading to altered conformational hierarchies in the IDR-ARD interaction. Thus, the R232C mutation could lead to a decreased IDR-mediated masking of the probable DDX3X interaction site of hsV4 ARD.

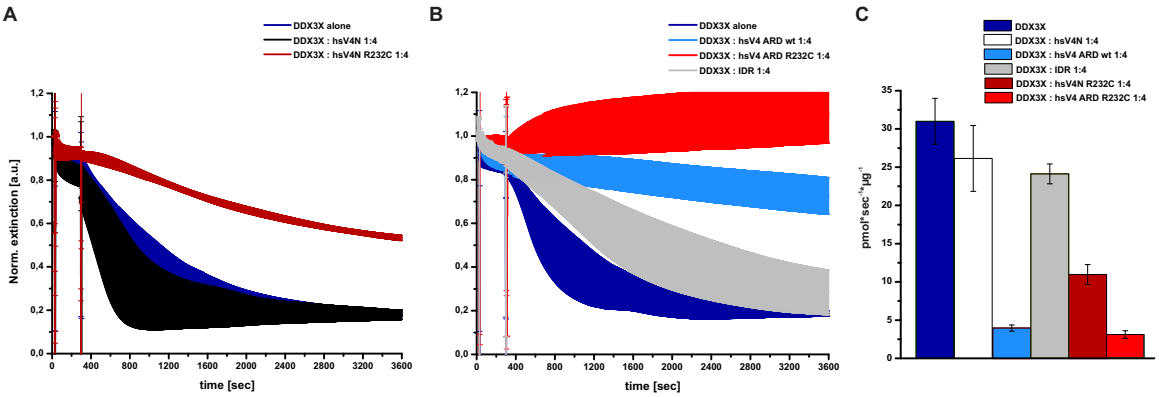

Figure 4.13: **DDX3X ATPase activity inhibition is enhanced in the presence of neuropathy-causing TRPV4 R232C mutation.** **A + B** An enzyme-coupled ATPase assay reveals an inhibitory effect of both, hsV4N R232C and hsV4 ARD R232C, onto the ATPase activity of DDX3X.[84] DDX3X was used at a concentration of 3 µM and TRPV4 N-terminal constructs at 12 µM, resulting into a 1:4 ratio. After 30 s samples were supplemented with ATP and after 5 min with duplex RNA (dxRNA), both at a final concentration of 1 µM. ATPase activity was determined by an ATP-dependent enzyme-coupled oxidation from NADH to NAD^+, resulting in an time-dependent absorption decrease at 340 nm. Measurements were normalized to DDX3X ATPase activity (DDX3X). Error bars indicate SDs of three measurements of three independent DDX3X purifications for each condition. Used TRPV4 N-terminal constructs originated from one purification. The TRPV4 intrinsic disordered region (IDR), consisting of aa 1-149 preceding the ARD of hsV4N, was kindly provided and fully characterized by Dr. [redacted] i[23] and M. Sc. [redacted].[143] x-axis = time in s, y-axis = extinction at 340 nm in arbitrary units **C** DDX3X ATPase activity in the presence of several TRPV4 N-terminal constructs. Error bars indicate SDs of determined slopes after natural logarithmic conversion and linear regression.

Additionally to the Y2H screen showing direct interaction between the full-length TRPV4 channel and DDX3X, Donate-Macian *et al.* performed co-IPs with full-length TRPV4 and DDX3X co-transfected in HEK293 cells. It was shown that DDX3X immunoprecipitates with TRPV4 and *vice versa*. To evaluate these *in cellulo* experiments, co-IPs were performed with HEK293T

cells co-transfected with full length human TRPV4 with a c-terminal GFP-tag (hsTRPV4-cGFP) and full-length human DDX3X with a n-terminal V5-tag (hsDDX3X-nV5, see figure 4.14 A for a full-length DDX3X topology model of the here used construct compared to the recombinantly expressed and purified DDX3X used for the here shown *in vitro* experiments). Furthermore, to investigate the effects of TRPV4 disease-causing mutations on DDX3X interaction *in cellulo*, co-transfection and -IPs with hsTRPV4 R232C-cGFP and hsDDX3X-nV5 were also performed. Transfections with hsTRPV4 K276E-cGFP resulted in severe cell death (data not shown). Figure 4.14 B and C show two western blots after co-IPs. Both western blots showed co-IP of hsDDX3X-nV5 with hsTRPV4 R232C-cGFP. With hsTRPV4-cGFP, only a weak band for hsDDX3X-nV5 in figure 4.14 B was detected.

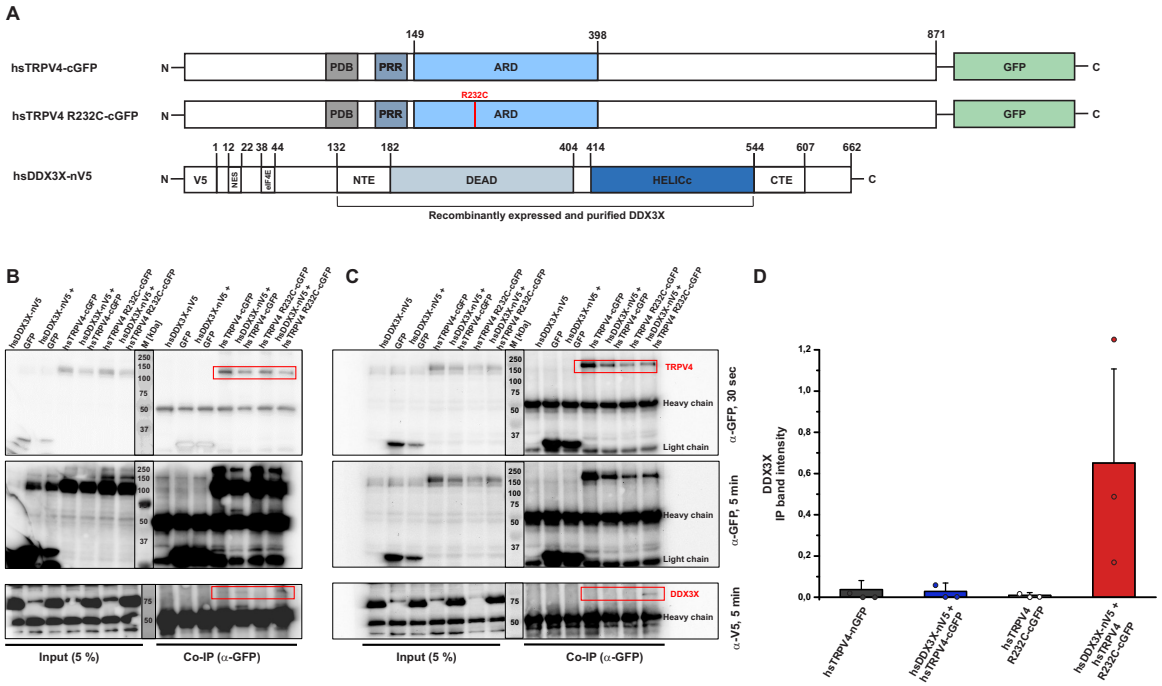

Figure 4.14: **Co-Immunoprecipitations (co-IPs) of full-length human TRPV4-cGFP and TRPV4 R232C-cGFP, respectively, in HEK293T cells show an increased DDX3X-V5 pulldown with the neuropathy-causing TRPV4-R232C mutation. A** Topology models of human full-length TRPV4 constructs and DDX3X used for co-expression in HEK293T cells. For TRPV4, important N-terminal domains, namely the proline rich region (PRR), phosphoinositide-binding domain (PBD) and ankyrin repeat domain (ARD), are highlighted. GFP = Green-fluorescent protein, V5= V5-tag (single letter code: GKPIPNPLLGLDST), NES = nuclear export sequence, eIF4E = binding site of transcription factor eIF4E, NTE= N-terminal extension, DEAD = DEAD domain (RecA-like domain 1), HELICc = C-terminal helicase domain (RecA-like domain 2), CTE = C-terminal extension.[148] **B + C** Two α-GFP co-IPs with full-length human TRPV4-cGFP and TRPV4 R232C-cGFP, respectively, co-transfected with hsDDX3X-nV5 in HEK293T cells show an increased hsDDX3X-nV5 pulldown with the neuropathy-causing TRPV4-R232C mutation. To rule out unspecific interactions, soluble GFP was co-transfected with respective TRPV4 construct. **D** Densitometric quantification of co-immunoprecipiated hsDDX3X-nV5, normalized to immunoprecipitated hsTRPV4-cGFP of respective condition. Error bars indicate SD. Densitometry was performed with Fiji.

Even though the amount of co-immunoprecipitated hsDDX3X-nV5 is low, the in the ATPase assays (figure 4.13) observed trend of a stronger DDX3X-TRPV4 R232C interaction compared to wild-type TRPV4 persisted. In the last few years, pathological stress granule formation more and more emerged to be one possible cause of neurodegenerative diseases such as the TRPV4-associated Charcot-Marie-Tooth Type 2C disease. These membraneless organelles form *in cellulo* upon oxidative and hyperosmotic stress, amongst others, as a consequence of stress-induced translational shutdown and polysome disassembly.[121,149] Stress granules are composed mainly from RNA-binding proteins like DDX3X and form highly dynamic structures upon acute stress, whereas chronic cellular stress is proposed to induce pathologically stable complexes that might promote the formation of aggregates.[149–151]

Based on the elevated DDX3X-TRPV4 R232C interaction shown in subchapter 4.1.2 and in figures 4.13 and 4.14, fluorescence microscopy experiments with HEK293T cells co-transfected with the same constructs used as in the co-IPs in figure 4.14 were performed to investigate probable foci formations of DDX3X in the presence of TRPV4 and/or neuropathy causing TRPV4 R232C (figure 4.15). Transiently transfected HEK293T cells showed expected subcellular localization of respective proteins, namely hsDDX3X-nV5 in the cytosol and hsTRPV4-cGFP in the plasma membrane. In the case of hsTRPV4 R232C-cGFP, beside the plasma membrane localization also GFP-containing foci were observed. For hsDDX3X-nV5 alone an uniform cytosolic distribution was observed, whereas in the presence of hsTRPV4-cGFP densifications formed. These hsDDX3X-nV5 densifications were more pronounced and spatially distinct as foci in the presence of hsTRPV4 R232C-cGFP. hsDDX3X-nV5 and hsTRPV4-cGFP or hsTRPV4 R232C-cGFP co-expression did not alter the subcellular localization of both TRPV4 constructs. These results indicate an influence of TRPV4 on DDX3X-containing foci formation *in cellulo*. Valentin-Vega *et al.* showed that medulloblastoma-associated mutations in DDX3X, leading to deficiency in RNA-stimulated ATP-hydrolysis of DDX3X, spur stress granule hyperassembly.[119,142] Therefore, not only the increased basal Ca^{2+} influx levels due to the neuropathy causing R232C mutation could lead to abnormal stress granule formations, but also the elevated ATPase inhibition due to an increased DDX3X interaction with the mutated hsV4 ARD. Donate-Macian *et al.* showed a decreased DDX3X co-IP with TRPV4 in Huh7 cells

Figure 4.15 *(facing page)*: **Fluorescence microscopy images of HEK293T cells co-transfected with TRPV4-GFP (green) and DDX3X-V5 (magenta) reveal cytosolic DDX3X densifications (white arrow heads), especially in the presence of TRPV4-R232C-GFP.** V5-tag of DDX3X was detected via mouse anti-V5 primary antibody and subsequent Alexa Fluor™647-coupled anti-mouse secondary antibody staining. Nuclei were stained with DAPI. Scale bar = 10 µm. Images were taken with a Zeiss Axio Observer Z1 inverted widefield microscope.

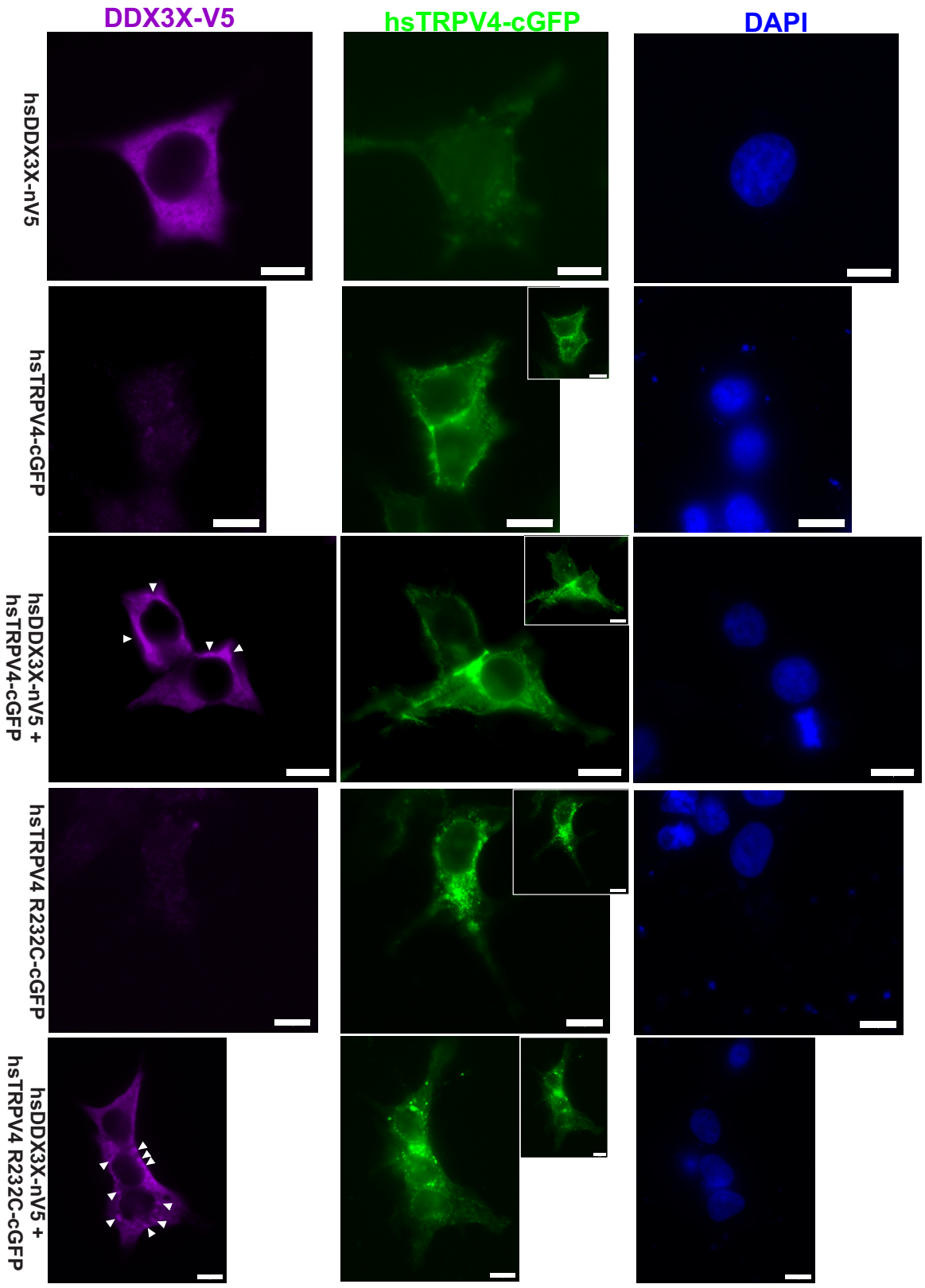
DDX3X-V5
hsTRPV4-cGFP
DAPI
hsDDX3X-nV5
hsTRPV4-cGFP
hsDDX3X-nV5 + hsTRPV4-cGFP
hsTRPV4 R232C-cGFP
hsDDX3X-nV5 + hsTRPV4 R232C-cGFP

upon treatment with the TRPV4 activator GSK1016790A (GSK-101), inducing TRPV4-mediated Ca^{2+}-influx. Additionally, TRPV4-mediated Ca^{2+}-influx, activated either via hypotonicity or the TRPV4 agonist GSK-101, induced partial shuttling of DDX3X into the nucleus in HEK293 cells via a Ca^{2+}/Calmodulin-dependent pathway. This shuttling behavior was not observed with the gain-of-function R232C mutation in TRPV4 in this thesis (figure 4.15).[54,136] In summary, the results by Donate-Macian *et al.* indicate a disruption of the TRPV4-DDX3X PPI upon TRPV4 activation.[136] In combination with the results shown in this thesis, the increased TRPV4 R232C-DDX3X PPI seems to be Ca^{2+}-influx independent, as TRPV4 R232C was previously shown to exhibit elevated basal Ca^{2+}-influx activity.[54] The TRPV4 R232C-DDX3X PPI seems to be elevated due to mutation-induced electrostatic and structural changes within and between the two proteins. These findings underline the importance of stress granule homeostasis and the severe consequences of dysregulation in stress granule dynamics, which ultimately leads to neuronal cell death.[119] The data shown in this thesis reveal TRPV4 as a potential communication hub for downstream processes involved in stress granule formation.

4.3 It is all about humanity - an *in cellulo* study of the interaction between human TRPV4 and PACSIN1-3

Besides the six ankyrin repeats organized in an ankyrin repeat domain (ARD), the hsV4N contains a proline rich region (PRR, aa 132 – 144) which is necessary for the interaction with PACSIN3 (Protein kinase C and casein kinase substrate in neurons 3), one of the few known direct interactors of TRPV4.[70] All three PACSIN isoforms consist of a F-BAR domain, a linker domain and a SH3 domain, of which the latter interacts with the TRPV4 PRR (see figure 4.16 F).[22,70,71] Previous experiments evaluated the physiological role of PACSIN3 in TRPV4 modulation, where it was shown that the relative plasma membrane amount of TRPV4 is enhanced by PACSIN3, but not by PACSIN1 and 2, despite of co-IPs of all three mouse PACSINs with rat TRPV4.[70] Furthermore, D'hoedt *et al.* showed that PACSIN3 desensitizes TRPV4 and inhibits its activation by cell swelling induced via a hypoosmotic solution and heat, but not by chemical stimuli like the known TRPV4 activator 4α-phorbol 12,13-didecanoate (4α-PDD). Although these previous experiments comprehensively evaluated the physiological role of PACSIN3 in TRPV4 modulation, data about the roles of PACSIN1 and PACSIN2 are lacking.[70,71] Also, before mentioned experiments where performed with rodent proteins (mouse PACSINs and rat TRPV4 or mouse TRPV4) in a human expression system (HEK293T cells). To elucidate the role of all PACSINs in TRPV4 modulation, in this work human full-length PACSINs and TRPV4 were co-expressed in HEK293T cells to gain a comprehensive and species consistent view on the physiological role of these PPIs. Following the initial studies of D'hoedt *et al.*[71] showing dampened TRPV4-mediated Ca^{2+}-influx upon hypotonicity by PACSIN3 in HEK293T cells, a Fura-2 AM-based Ca^{2+}-influx assay was performed (see figure 4.16 A). HEK293T cells co-transfected with human full-length TRPV4 and PACSIN1 or PACSIN3, respectively, show significant dampened TRPV4-mediated Ca^{2+}-influx in comparison to cells transfected with TRPV4 alone or co-transfected with PACSIN2. Furthermore, PACSIN1 and PACSIN3 dampen the basal Ca^{2+}-influx activity of TRPV4 (t=0). Figure 4.16 B shows that PACSIN1 and 3, but not PACSIN2, co-immunoprecipitate with TRPV4, which is in disagreement with the co-IPs performed with the rodent PACSIN orthologues and TRPV4.[70] As expression levels of all three PACSINs in figure 4.16 are on a comparable level, these results underline the difference of PPIs between protein orthologues across species, even in the context of high protein identities (see section 6.5).

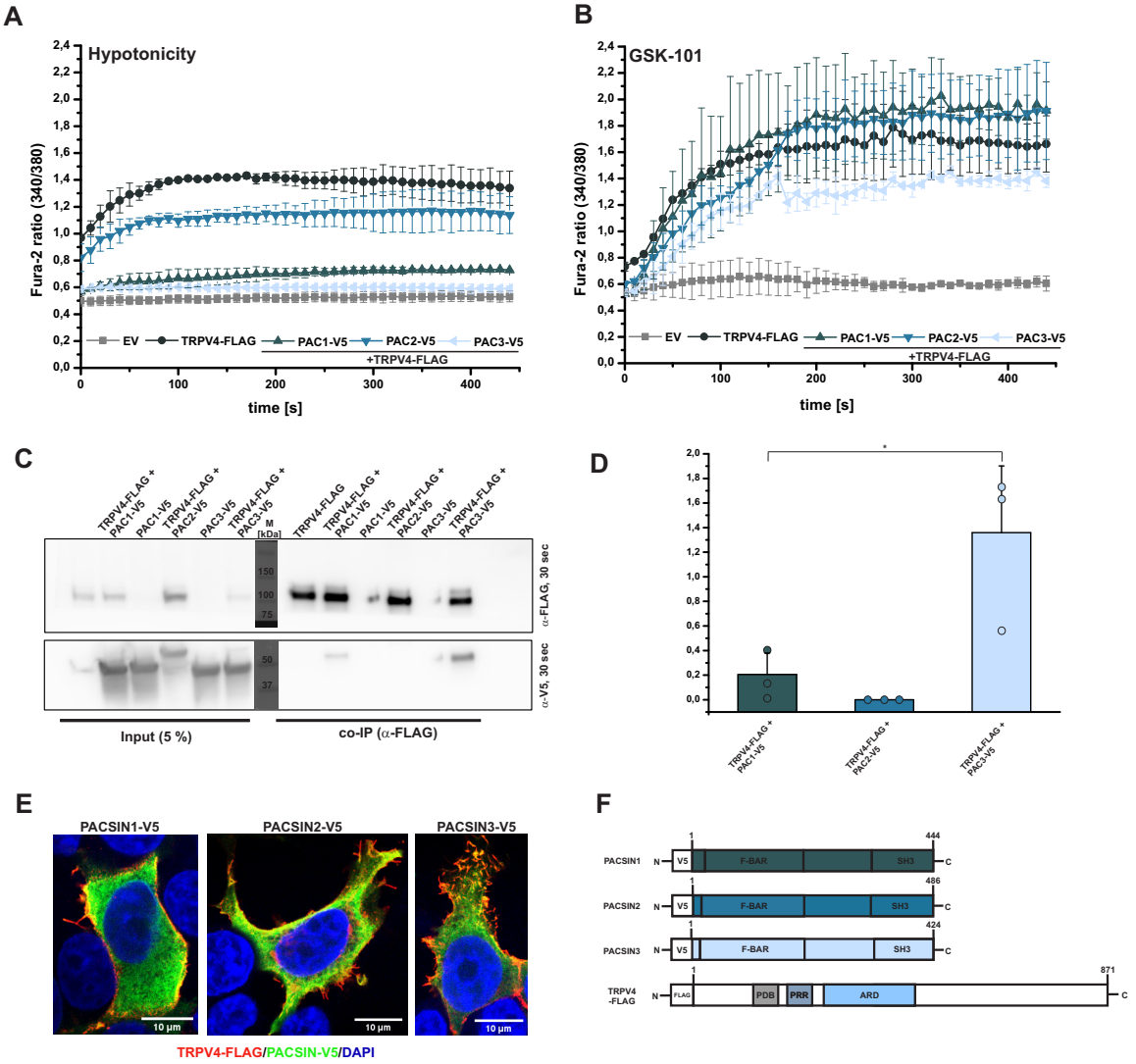

Figure 4.16: **Human PACSIN1 and 3, but not PACSIN2, dampen human TRPV4-mediated Ca^{2+}-influx in transiently co-transfected HEK293T cells upon hypotonicity**. **A** HEK293T cells transiently co-transfected with TRPV4-FLAG and PACSIN1-3-V5, respectively, were loaded with the calcium indicator Fura-2 AM and treated with hypotonic saline (30 mM NaCl) at time = 0. Intracellular calcium levels were measured by acquiring 340 nm/380 nm ratio images every 10 s for 480 s. EV = transfection with empty vector. Averages represent n = 3, where each measurement was conducted with 4 coverslips with 20-30 cells per coverslip per condition. Error bars indicate SD. x-axis = time in s, y-axis = Fura 2-AM 340 nm/380 nm wavelength ratio. **B** HEK293T cells transiently co-transfected with TRPV4-FLAG and PACSIN1-3-V5, respectively, were loaded with the calcium indicator Fura-2 AM and treated with 30 nM of the TRPV4 agonist GSK-101 at t = 0. Fore more experimental details see subfigure A. **C** Representative α-FLAG co-immunoprecipitation of TRPV4-FLAG and PACSIN1-3-V5, respectively, co-transfected in HEK293T cells show co-immunoprecipitation of PACSIN1 and 3, but not PACSIN2, with TRPV4-FLAG.**D** Densitometric quantification of co-immunoprecipiated PACSINs, normalized to immunoprecipitated TRPV4-FLAG of respective condition. Paired two-tailed t-test, n=3 from three independent co-IPs, *p $\leq$ 0.05. Error bars indicate SD. Densitometry was performed with Fiji. **E** Immunofluorescence images of HEK293T cells co-transfected with TRPV4-FLAG (red) and PACSIN1-3-V5 (green), respectively, show proper cellular distribution of overexpressed constructs with TRPV4-FLAG in the plasma membrane and PACSIN1-3-V5 in the cytosol. FLAG-tag was detected with rabbit α-FLAG and subsequent α-rabbit Alexa Fluor 555 staining. V5-tag was detected with mouse α-V5 and subsequent α-mouse Alexa Fluor 488 staining. Nuclei were stained with DAPI. Scale bar = 10 µm. Images were taken with a Zeiss LSM800 Confocal Microscope. **F** Topology model of expressed PACSIN constructs. V5= V5-tag (single letter code: GKPIPNPLLGLDST), FLAG = FLAG tag (single letter code: DYKDDDDK)

To confirm functional expression of TRPV4, complementary Ca^{2+}-influx experiments were performed with the potent TRPV4 agonist GSK-101, showing no PACSIN-mediated TRPV4 Ca^{2+}-influx dampening (see figure 4.16 C).[70,152,153] Additionally, immunofluorescence images in figure 4.16 D show proper subcellular distributions of expressed constructs *in cellulo*.

PACSIN3 mRNA transcripts were mainly found in skeletal and heart muscle tissue, whereas PACSIN2 transcripts were detected ubiquitously and PACSIN1 transcripts showed neurospecificity.[154] Interestingly, co-expression of the neuropathy-causing TRPV4 R269C mutation and PACSIN1 showed a strong trend towards a loss of TRPV4-mediated Ca^{2+}-influx inhibition in HEK293T cells upon hypotonicity, whereas PACSIN3 still retained its desensitizing role in TRPV4 regulation (figure 4.17). In agreement with Woolums *et al.*, Ca^{2+}-influx experiments indicate higher basal TRPV4 R269C Ca^{2+}-influx activity compared to wild-typic TRPV4 (t = 0) .[53] Despite the loss of the PACSIN1-desensitizing function upon stimuli induced TRPV4 R269C activation, co-expression of PACSIN1 with TRPV4 R269C still seems to dampen basal TRPV4 mediated Ca^{2+}-influx (t=0). To substantiate these trends, additional Ca^{2+}-influx assays are required. A first co-IP hints towards a loss of PACSIN1-binding to TRPV4 R269C (figure 4.17 B). These results indicate a neuron-specific consequence of the neuropathy-causing TRPV4 R269C mutation, also regarding the above mentioned tissue specific mRNA transcription of the three PACSIN isoforms. The mechanisms of PACSIN-mediated TRPV4 modulation still remain elusive until this date. Neurons are more vulnerable towards chronic Ca^{2+}-influx compared to other cell types due to their unique cellular structure, which lead to higher sensitivity towards Ca^{2+}-dyshomeostasis with excitotoxicity as a possible consequence .[155] As the desensitizing function of PACSIN1 precedes upon the TRPV4 R269C mutation in neurons, other tissues are possibly still able to regulate TRPV4-mediated Ca^{2+}-influx via PACSIN3 and/or other until now not known TRPV4 regulating mechanisms.

To shed light on the PPI between the PACSINs and the TRPV4 PRR, in chemical shift perturbation assays using nuclear magnetic resonance (NMR) spectroscopy, Goretzki *et al.* probed structural changes of the different PACSIN SH3 domains upon interacting with the TRPV4-PRR.[22] All three SH3 domains interact with the TRPV4-PRR in a highly comparable manner. These experiments showed that the SH3 domains of PACSIN1, 2 and 3 interact with the TRPV4-PRR through the same binding interfaces and have highly similar binding affinities. However, co-IPs (figure 4.16 B) showed that PACSIN3 binds better to TRPV4 than PACSIN1, and that PACSIN2 does not bind to TRPV4 *in cellulo* at all. This strongly hints towards a difference in the TRPV4-PACSIN3 interaction compared to its interaction with PACSIN1 in the context of full-length PACSINs and full-length TRPV4.

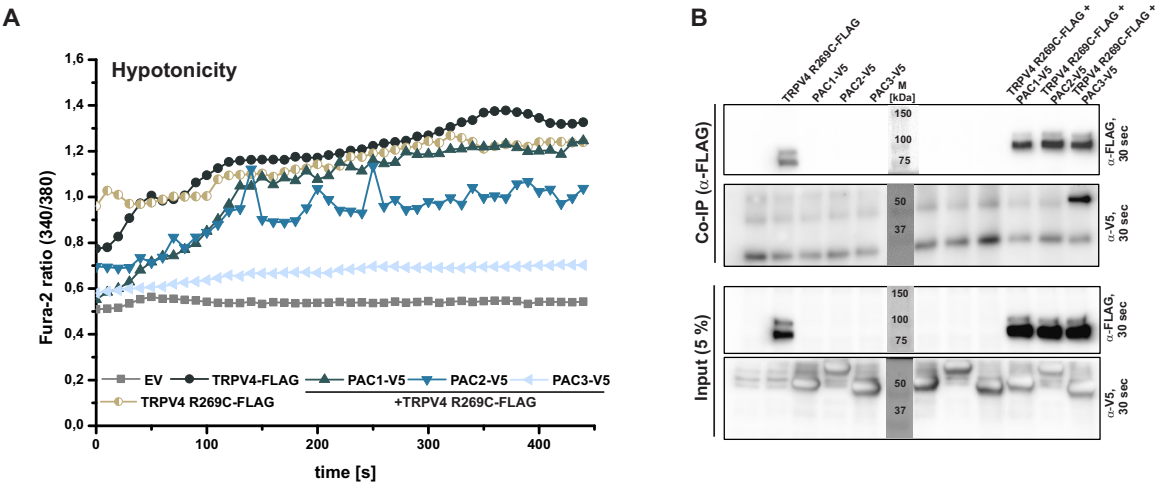

Figure 4.17: **Human PACSIN1 does not dampen TRPV4-mediated Ca^{2+}-influx in HEK293T cells transiently transfected with TRPV4 R269C upon hypotonicity. A** HEK293T cells transiently co-transfected with TRPV4-FLAG or neuropathy-causing TRPV4 R269C-FLAG and PACSIN1-3-V5, respectively, were loaded with the calcium indicator Fura-2 AM and treated with hypotonic saline (30 mM NaCl) at time = 0. Intracellular calcium levels were measured by acquiring 340 nm/380 nm ratio images every 10 s for 480 s. EV = transfection with empty vector. Averages represent n = 2, where each measurement was conducted with 4 coverslips with 20-30 cells per coverslip per condition. x-axis = time in s, y-axis = Fura 2-AM 340 nm/380 nm wavelength ratio. **B** α-FLAG co-immunoprecipitation of neuropathy-causing TRPV4 R269C-FLAG and PACSIN1-3-V5, respectively, co-transfected in HEK293T cells show only co-immunoprecipitation of PACSIN3 with TRPV4, but not PACSIN1 and 2.

Since Goretzki *et al.* have excluded the SH3 domain as the origin of these differences, the next step was to focus on the F-BAR domains.For this, the three F-BAR domains of PACSIN1-3 where exchanged while retaining the linker and SH3 domain of the original PACSIN via Gibson Assembly.[79,80] Of these originally six cloned constructs, only three showed expression in HEK293T cells (see figure 4.18 C for detailed chimera construct composition). Figure 4.18 A shows the results of Fura-2 AM-based Ca^{2+}-influx assays performed with HEK293T cells co-transfected with TRPV4 and respective PACSIN chimeras treated with hypotonic saline. Both PACSIN chimeras that combine the PACSIN1 linker and SH3 domain with either the PACSIN2 or PACSIN3 F-BAR domain (PACSIN2+1 and PACSIN3+1, figure 4.18 C), respectively, show no regulation of TRPV4-mediated Ca^{2+}-influx upon hypotonicity. Strikingly, PACSIN chimera PACSIN2+3, consisting of the PACSIN2 F-BAR domain with PACSIN3 linker and SH3 domain, shows comparable Ca^{2+}-influx dampening to PACSIN3-mediated dampening (figure 4.16 A). Co-IPs with TRPV4-FLAG and N-terminally V5-tagged PACSIN chimeras could not show a pulldown of any PACSIN chimera with TRPV4. Immunofluorescence images (figure 4.18 D) confirmed proper cellular distribution of the PACSIN chimeras in the cytosol and TRPV4 in the plasma membrane.

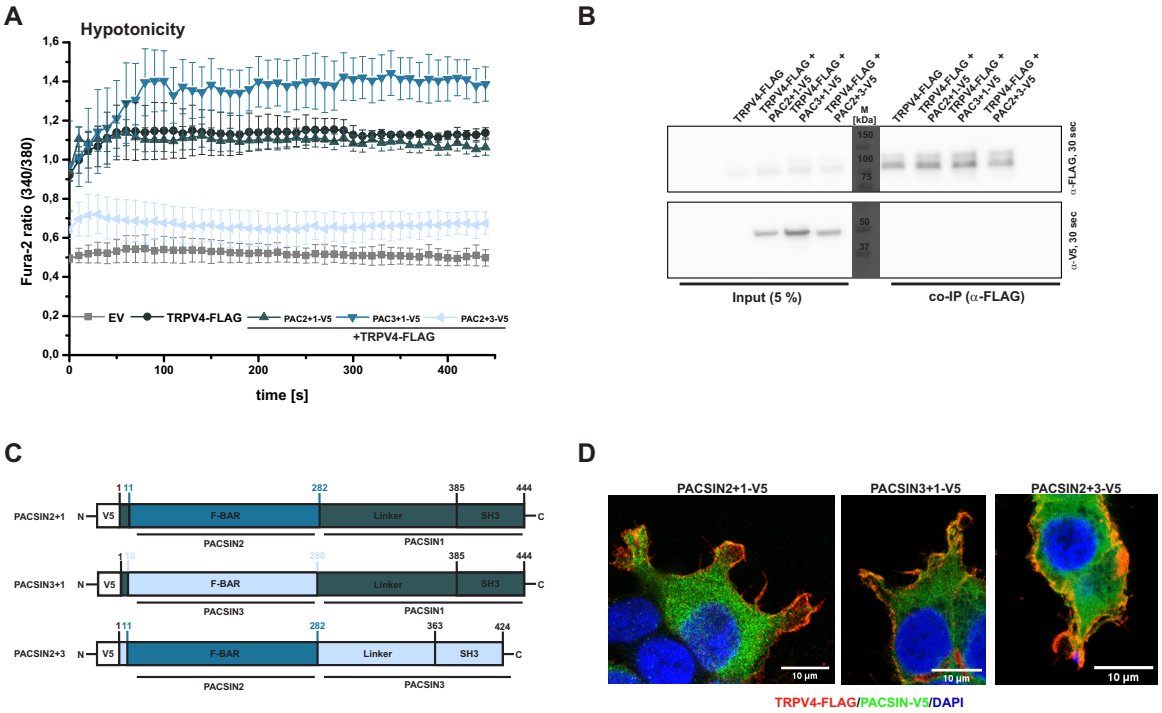

Figure 4.18: **PACSIN chimeras hint towards different regulation modes between PACSIN1 and PACSIN3 on TRPV4-mediated Ca^{2+}-influx in HEK293T cells**. **A** HEK293T cells transiently co-transfected with TRPV4-FLAG and respective PACSIN chimera shown in subfigure C, respectively, were loaded with the calcium indicator Fura-2 AM and treated with hypotonic saline (30 mM NaCl) at time = 0. Intracellular calcium levels were measured by acquiring 340 nm/380 nm ratio images every 10 s for 480 s. EV = transfection with empty vector. Averages represent n = 3, where each measurement was conducted with 4 coverslips with 20-30 cells per coverslip per condition. Error bars indicate SD. x-axis = time in s, y-axis = Fura 2-AM 340 nm/380 nm wavelength ratio. **B** Representative α-FLAG co-immunoprecipitation of TRPV4-FLAG and respective PACSIN chimera (see subfigure C) co-transfected in HEK293T cells show no co-immunoprecipitation of the PACSIN chimeras with TRPV4-FLAG. **C** Topology model of expressed PACSIN chimeras. For this the three F-BAR domains of PACSIN1-3 where exchanged while retaining the linker and SH3 domain of the original PACSIN. Of these originally six cloned constructs, only the pictured three showed expression in HEK293T cells. V5= V5-tag (single letter code: GKPIPNPLLGLDST), FLAG = FLAG tag (single letter code: DYKDDDDK). **D** Immunofluorescence images of HEK293T cells co-transfected with TRPV4-FLAG (red) and respective PACSIN chimera show proper cellular distribution of overexpressed constructs with TRPV4-FLAG in the plasma membrane and the PACSIN chimeras in the cytosol. FLAG-tag was detected with rabbit α-FLAG and subsequent α-rabbit Alexa Fluor 555 staining. V5-tag was detected with mouse α-V5 and subsequent α-rabbit Alexa Fluor 488 staining. Nuclei were stained with DAPI. Scale bar = 10 µm. Images were taken with a Zeiss LSM800 Confocal Microscope.

These results indicate different TRPV4-regulation modes between PACSIN1 and PACSIN3. Whereas PACSIN1 seems to need its F-BAR domain, PACSIN3 seems to regulate TRPV4-mediated Ca^{2+}-influx either F-BAR-independently or the PACSIN2 F-BAR domain is sufficient enough to substitute the PACSIN3 F-BAR domain (see also section 6.5 for mutliple sequence alignment between human PACSIN F-BAR domains, indicating a higher sequence identity between the PACSIN2 F-BAR domain and PACSIN3 F-BAR domain than between the PACSIN1 F-BAR domain and PACSIN3 F-BAR domain). Cuajungco *et al.* showed that PACSIN3 lacking

the F-BAR domain lost its ability to dampen TRPV4-mediated Ca^{2+}-influx upon hypotonicity in HEK293T cells.[70] This would hint towards the ability of the PACSIN2 F-BAR domain to substitute the PACSIN3 F-BAR domain. BAR domain-containing proteins like PACSIN1-3 are known to induce various forms of membrane deformations.[156,157] Membrane deformation experiments conducted by Goh *et al.* showed that the isolated F-BAR domains of PACSIN2 and PACSIN3 produced similar membrane morphologies after incubation with liposomes. Whereas PACSIN2 and 3 F-BAR proteins mainly induced formation of vesicular structures and wide tubules, the PACSIN1 F-BAR domain additionally induced narrow tubule formation. Additionally, Bai *et al.* showed in liposome tubulation assays that PACSIN3 induced low curvature tubulation with mainly tubule formation diameters from 90 nm to 110 nm, whereas PACSIN1 also additionally formed high curvature tubules, ranging from 10 nm to 200 nm. In this case, PACSIN2 again showed an intermediate behavior between PACSIN1 and 3, where PACSIN2-induced tubules showed a diameter range like PACSIN1, but the relative number of low-curvature tubes is higher compared to PACSIN1. It was shown previously that TRPV4-activation indeed is dependent from the surrounding membrane fluidity and stiffness and thus different degrees of membrane curvatures could also play a regulatory role in TRPV4 regulation.[158] As the different PACSIN isoforms serve different levels and forms of membrane deformations, PACSIN isoform dependent TRPV4 regulation via the F-BAR mediated membrane microenvironment seems to be an explanation for the possible different TRPV4-regulation modes between PACSIN1 and 3.[156,157,159,160] These findings also underline the probable ability of the PACSIN2 F-BAR domain to induce similar membrane curvatures like the PACSIN3 F-BAR domain. Therefore the PACSIN2 F-BAR domain may probably serve comparable local membrane environments for TRPV4 in the context of the PACSIN chimera 2+3.[156,160] Membrane deformation activity assays with all three murine full-length PACSIN isoforms showed reduced membrane deformation activity compared to the isolated F-BAR domains, whereby full-length PACSIN1 showed a significantly higher activity loss than PACSIN3. PACSIN2 showed again an intermediate behavior, where an activity decrease was also observed, but this decrease was not as pronounced as for PACSIN1. Membrane deformation activity reduction might occur due to the autoinhibition by the SH3 domain binding on the F-BAR domain, preventing the F-BAR domain to interact with membranes. This particular autoinhibition was shown for PACSIN1 in a X-ray crystal structure of murine PACSIN1 (PDB: 2X3X), where a negatively charged triple motif (Q396, E397, E400) in the SH3 domain interacts with a basic lysine patch (K141, K145, K148) in the F-BAR domain. This was confirmed with site-directed mutagenesis with subsequent pull-down assays *in cellulo*.[156,157] As the substrate-binding site of the SH3 domain overlaps with the SH3/F-BAR

domain interacting site, it was shown that the dynamin-PRR interrupts PACSIN1 autoinhibition and induces PACSIN1-mediated lipid tubulation.[156] This autoinhibition mechanism was also proposed for PACSIN2 and 3, as the SH3 and F-BAR domains amongst the isoforms are highly conserved, including the SH3/F-BAR domain interaction sites. Indeed, Goretzki *et al.* could show via NMR spectroscopy that the PACSIN3 SH3 domain interacts with the PACSIN3 F-BAR domain and that a QEE/RRR mutation in the PACSIN3 SH3 domain abrogated this interaction. Furthermore, the interaction between PACSIN3 SH3 and F-BAR seemed to be comparably weak and could be released with a TRPV4-PRR containing peptide in a similar manner to the dynamin-PRR-mediated autoinhibition-release of PACSIN1.[23,156] The strength between the SH3 and F-BAR domain interaction of PACSIN1 and 2 still have to be determined and variations in respective K_D values could serve as another explanation for the different TRPV4-mediated behaviors between the three PACSIN isoforoms and the possible ability of the PACSIN2 F-BAR domain to substitute the PACSIN3 F-BAR domain in the chimera PACSIN2+3. Expression of the PACSIN chimera consisting of PACSIN1 F-BAR domain and PACSIN3 linker and SH3 domain was not possible. Therefore it remains elusive, if the PACSIN1 F-BAR domain could also substitute the PACSIN3 F-BAR domain like occured in PACSIN chimera 2+3.

Another explanation for the different TRPV4-regulation outcomes of the PACSIN chimeras could be different protein interactomes of PACSIN1 and 3, due to their different tissue distributions and minor differences in amino acid sequences.[154] Goretzki *et al.* proposed that PACSIN3 possibly binds to TRPV4 as a dimer, where the F-BAR domains mediate the PACSIN3 dimerization. One SH3 domain therefore would interact with the TRPV4 PRR, whereas the other SH3 domain could recruit additional TRPV4 binding partners.

Furthermore, PACSIN3 is the only PACSIN isoform that contains a proline rich region in its linker region (aa 337-345), with which other proteins could interact with. PACSIN chimera 3+2 thus seems still to be able to bind to the TRPV4 PRR via its SH3 domain, exposing the PACSIN3 PRRs in the linker domains and the other SH3 domain for further protein interactions to form a multicomponent TRPV4 signaling complex. This could be an additional determinant for a PACSIN3- and therefore tissue specific protein interactome, which leads to a robust PACSIN3-TRPV4 interaction, whereas PACSIN1 loses its binding and consequently TRPV4 regulation ability in the presence of the neuropathy-causing TRPV4 R269C mutation. Expression levels of the PACSIN chimeras in HEK293T cells were significantly lower compared to wild-type PACSIN1-3 (see figure 4.16 B), which could also be a reason for the missing co-IP of any of the PACSIN chimeras with TRPV4. Low-affinity or transient PPIs may not be detected in co-IPs, as extensive washing and mechanical/chemical stresses during the experiment could

disrupt the PPI of the target complex. Therefore it would still be possible that the chimera PACSIN2+3 still directly binds to TRPV4 via its SH3 domain *in cellulo*, leading to a TRPV4 regulation. This would indicate that already low amounts of a TRPV4-regulating PACSIN isoforms/chimera are sufficient to achieve TRPV4-mediated Ca^{2+}-influx dampening and also explain the similar Ca^{2+}-influx dampening effect of PACSIN1 and PACSIN3 (figure 4.16 A) even though the TRPV4-PACSIN1 interaction seems to be weaker in the context of HEK293T cells (figure 4.16 B).

4.4 Small but powerful - the small GTPase RhoA interacts with the TRPV4 Ankyrin Repeat Domain

Parts of this chapter were published in: McCray, B.A., Diehl, E. *et al*. Neuropathy-causing TRPV4 mutations disrupt TRPV4-RhoA interactions and impair neurite extension. *Nat Commun* **12**, 1444 (2021).[69] The author of the present thesis (Erika Diehl) contributed purification, characterization and nuclear magnetic resonance (NMR) spectroscopy-based PPI studies between recombinantly expressed ^{15}N-RhoA and hsV4 ARD wt as well as hsV4 ARD R269C.

TRPV4 modulates cell morphology and stiffness via cytoskeleton components, namely microtubules and actin scaffolds.[69,161–165] A generic bottom-up proteomics approach, conducted by MD [redacted] (RG [redacted], Department of Neurology, Johns Hopkins University School of Medicine) with immunopurified human TRPV4-FLAG overexpressed in HEK293T cells indicated the small GTPase RhoA as a putative direct TRPV4 interactor.[69] These data complemented the recently published TRPV4-RhoA interaction identified via a Y2H screen.[136] RhoA itself is a pivotal regulator of the actin cytoskeleton, inducing stress fiber formation, for example.[166–168] Therefore a possible direct PPI and actin regulating interplay between TRPV4 and RhoA was investigated and if these putative interactions were aberrant in the presence of disease-causing mutations of TRPV4. MD [redacted] could show with comprehensive co-IP studies in HEK293T and MN-1 (a murine cholinergic motor neuron cell line) cells, that TRPV4 pulls down RhoA and *vice versa*. Furthermore, co-IPs of MN-1 cells transiently transfected with TRPV4 and inactive RhoA-GFP (T19N), or constitutively active RhoA-GFP (Q63L) demonstrated that TRPV4 interacts with inactive, GDP-bound RhoA T19N, but not active, GTP-

Figure 4.19 *(facing page)*: **Purification of hsV4 ARD wt, hsV4 ARD R269C and ^{15}N-isotope labeled human RhoA (^{15}N-RhoA). A** Schematic topology model of hsV4 ARD wt, hsV4 ARD R269C and ^{15}N-RhoA used for NMR spectroscopy measurements. His_6 = hexa-histidine tag (single letter code: HHHHHH), TEV = Tobacco Etch Virus Cleavage Site (single letter code: ENLYFQG). His_6-tags with preceding or subsequent TEV Cleveage Site were removed. **B** SEC purifications of ^{15}N-RhoA, hsV4 ARD wt and R269C. SEC runs were performed with a HiLoad Superdex 75 pg preparative SEC column. Inlets show Coomassie stained 15 % SDS-PAGEs of collected and concentrated fractions after SEC. x-axis: eluted volume in mL, y-axis: absorbance at 280 nm, M = marker. **C** For ^{15}N-RhoA, the intrinsic GTPase activity was determined via the luminescence-based GTPase-Glo Assay. GTPase activity is inversely correlated to measured luminescence intensity. A paired two-tailed t-test with 3 independent measurements including 4 technical replicates was performed, ***p < 0.001. Error bars indicate SD. **D + E** Far UV CD spectra of purified hsV4 ARD wt and hsV4 ARD R269C as well as ^{15}N-RhoA, respectively. Spectra were measured at 293 K and proteins were used at 1 µM concentration in RhoA SEC buffer with a final concentration of 20 mM NaCl. **F** Secondary structure prediction of shown far UV CD spectra shown in subfigures D and E, performed with CAPITO.[93] The predicted α-helix/β-sheet/random coil content of the purified proteins is for hsV4 ARD wt 78 %/0 %/22 %, hsV4 ARD R269C 68 %/0 %/32 % and ^{15}N-RhoA 27 %/24 %/49 %. y-axis: mean residue ellipticity ($[\Theta]_{mrw,\lambda}$) in 10^{-3} deg cm^2 dmol^{-1}, x-axis: wavelength λ in nm.

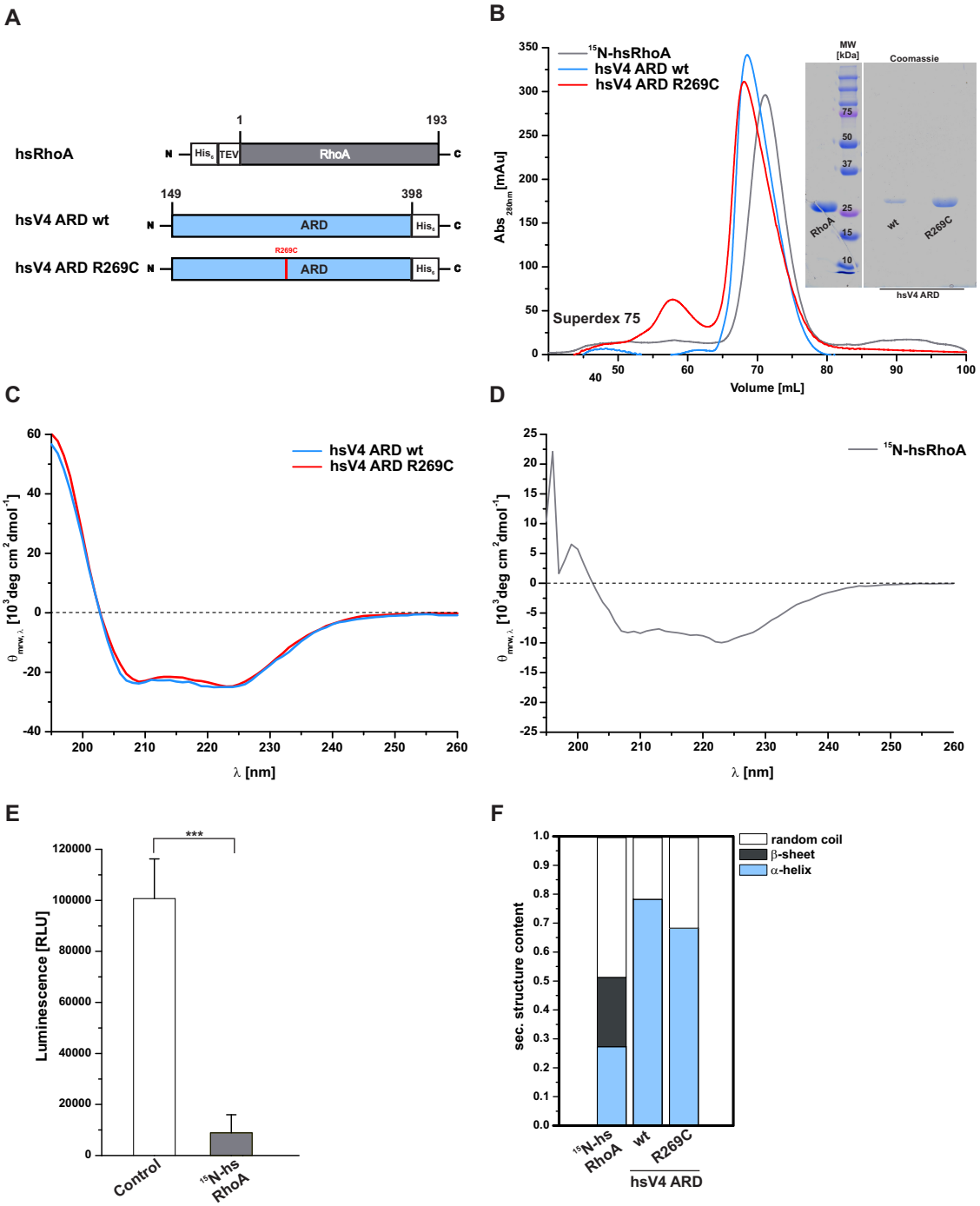
A
hsRhoA
hsV4 ARD wt
hsV4 ARD R269C
RhoA
ARD
TEV
R269C
B
15N-hsRhoA
hsV4 ARD wt
hsV4 ARD R269C
Superdex 75
Abs 280nm [mAu]
Volume [mL]
MW [kDa]
Coomassie
RhoA
wt
R269C
hsV4 ARD
C
hsV4 ARD wt
hsV4 ARD R269C
θ mrw,λ [10³deg cm²dmol⁻¹]
λ [nm]
D
15N-hsRhoA
θ mrw,λ [10³deg cm²dmol⁻¹]
λ [nm]
E
***
Luminescence [RLU]
Control
15N-hs RhoA
F
random coil
β-sheet
α-helix
sec. structure content
15N-hs RhoA
wt
R269C
hsV4 ARD

bound RhoA Q63L.[169] These results were further confirmed with Co-IPs in the presence of either excess GDP or an unhydrolyzable GTP analog (GTPγS) to favor the inactive or active form of RhoA. Additionally, co-IPs with immunopurified RhoA-myc and recombinantly expressed, purified human TRPV4 N-terminus (hsV4N) and ARD (hsV4 ARD), respectively, indicated a direct interaction between these proteins. Further co-IPs in transiently transfected MN-1 cells showed an abolished TRPV4-RhoA PPI in the presence of neuropathy-causing TRPV4 mutants (R232C, R237L, R269C, R315W), but not skeletal dyplasia-causing mutations (I331F, D333G). These neuropathy-mutant PPI disruptions were shown to be TRPV4-channel activity independent, as neither the TRPV4 anatgonist HC-067047 (HC-067) nor the pore-blocking M680K mutation restored the PPI between RhoA and TRPV4 harboring respective neuropathy-causing mutations.

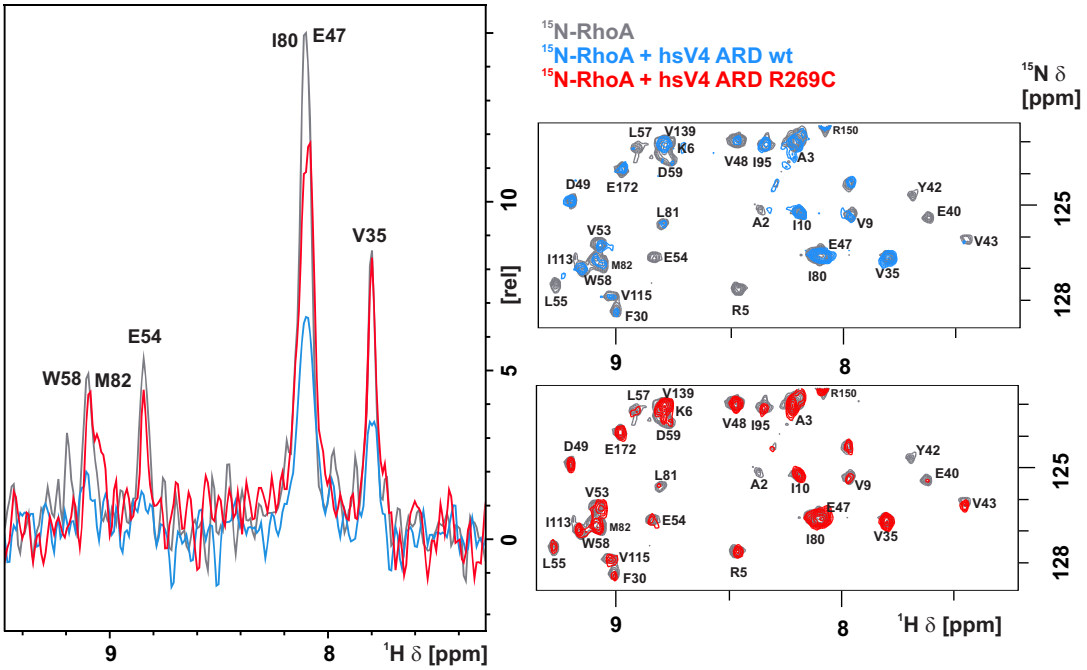

Figure 4.20: **NMR experiments revealed an decreased PPI between ^{15}N-RhoA and the neuropathy-causing mutation R269C in hsV4 ARD.** ***Left***: Representative 1D projection of ^{1}H resonances from 2D ^{1}H-^{15}N NMR spectra of ^{15}N-RhoA (grey) and in the presence of either hsV4 ARD (blue) or hsV4 ARD R269C (red). Stronger signal decreases for ^{15}N-RhoA in the presence of hsV4 ARD versus neuropathy mutant R269C indicate a decreased interaction between ^{15}N-RhoA and mutant ARD. ***Right***: Sections of 2D ^{1}H-^{15}N-NMR HSQC spectra of ^{15}N-RhoA: Overlay of spectra of ^{1}H-^{15}N-RhoA 2D HSCQs of ^{15}N-RhoA on its own (grey) in the presence of hsV4 ARD (blue, upper right) show line broadening, indicating the formation of a high molecular weight complex. In contrast, addition of hsV4 ARD R269C (red, lower right) shows only minor effects on the ^{15}N-RhoA spectrum. ^{15}N-RhoA backbone NMR assignments were transferred from previously published data[170]. NMR spectra were recorded on a Bruker 600 MHz spectrometer equipped with a cryogenic triple probe at 298.15 K and processed using Bruker TopSpin 3.2.

Due to the clustering of investigated neuropathy-causing TRPV4 mutations in the TRPV4 ARD (hsV4 ARD), the author of this thesis examined the direct PPI between recombinantly expressed and purified ^{15}N-RhoA and wild-type hsV4 ARD (hsV4 ARD wt) as well as hsV4 ARD R269C neuropathy mutant (hsV4 ARD R269C) via nuclear magnetic resonance (NMR) spectroscopy. To characterize this PPI in detail, ^{1}H,^{15}N NMR measurements of RhoA in the presence of hsV4 ARD and hsV4 ARD harboring the neuropathy-causing mutation R269C (hsV4 ARD R269C) were performed. For this, recombinantly expressed hsV4 ARD and hsV4 ARD R269C, as well as ^{15}N-labeled human GDP-bound RhoA (hereafter referred to as ^{15}N-RhoA) were purified (see subsection 3.7.5). Recombinant proteins showed the expected molecular weights via SDS-PAGE with subsequent Coomassie-staining (figure 4.19 **A** inlet) and secondary structures determined by CD spectroscopy (figure 4.19 **D** and **E**). Additionally, ^{15}N-RhoA showed enzymatic functionality in a luminescence-based GTPase assay (figure 4.19 **F**). After confirmation of the protein integrity, two-dimensional ^{1}H,^{15}N-NMR spectra of ^{15}N-RhoA were recorded (see section 6.6 figures 6.4 and 6.5 for full spectra). The obtained spectra agreed with previously published NMR data (BMRB:16668)[170] and allowed a backbone resonance assignment transfer of 93.6 %.

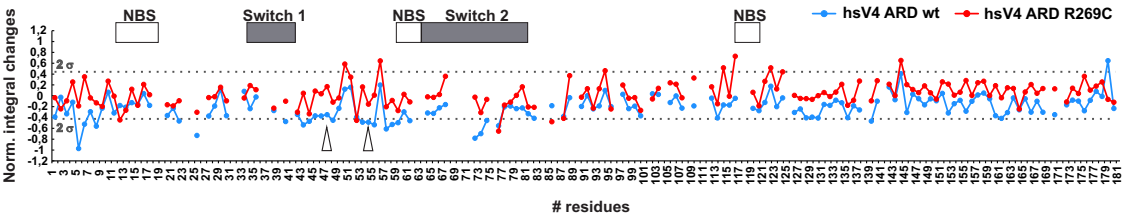

Figure 4.21: **Relative signal intensity changes of RhoA in the presence of unlabeled hsV4 ARD wt and R269C, respectively**. The largest decrease in signal intensity accounted for the E54 residue in ^{15}N-RhoA, and a smaller decrease in E47, indicated by arrow heads. NBS = Nucleotide binding site, Switch 1 and 2 = Switch 1 and 2 loop, 2σ = two SDs

To map the hsV4 ARD binding site on ^{15}N-RhoA, spectra were recorded in the presence of either hsV4 ARD or hsV4 ARD R269C (see figure 4.20). Signal intensities of ^{15}N-RhoA resonances decreased significantly in the presence of hsV4 ARD, indicating formation of a large molecular complex between hsV4 ARD (29.3 kDa) and RhoA (21.8 kDa). Addition of hsV4 ARD R269C did not lead to such strong signal intensity decreases, indicating a reduced affinity for ^{15}N-RhoA. To identify the ^{15}N-RhoA residues that are strongly affected by the interaction with hsV4 ARD, the relative signal intensity for every residue in the ^{15}N-RhoA NMR spectra were determined (figure 4.21). In total, peaks corresponding to 20 residues in ^{15}N-RhoA exhibited peak

integral decreases greater than two standard deviations (2σ) in the presence of hsV4 ARD, whereas only two residues showed this decrease with hsV4 ARD R269C. This is also reflected in the mean relative signal intensity change of ^{15}N-RhoA in the presence of hsV4 ARD versus hsV4 ARD R269C (figure 4.22, right).

Mapping the affected residues onto the crystal structure of GDP-bound RhoA (PDB: 1FTN)[171] revealed that the interswitch and switch II regions of ^{15}N-RhoA are primarily involved in hsV4 ARD binding (figure 4.22, left). The switch regions of RhoA are important regulatory sites within the small GTPase which are sensors whether RhoA is in its GDP or GTP-bound state by changing their conformational state upon the presence of hydrogen bonds to the γ-phosphate in GTP ("loading-spring" mechanism). Depending on the switch conformations, interaction of downstream effectors like Rho GDP dissociation inhibitors (RhoGDIs) and Rho guanine nucleotide exchange factors (RhoGEFs) are regulated.[169] The largest decrease in signal intensity accounted for the E54 residue in ^{15}N-RhoA, and a smaller decrease in E47, suggesting these residues might be particularly important in TRPV4 binding (see figure 4.21, indicated by arrow heads). These glutamic acids are unique to RhoA and are not present in the related Rho GTPases Rac1 and Cdc42, consistent with the results demonstrating specificity for interaction of TRPV4 with RhoA and not Rac1 or Cdc42.[69] Mutation of E54 to A completely abolished the interaction of RhoA with TRPV4 in co-IPs conducted by MD Brett A. McCray, suggesting that E54 may be important for electrostatic interaction with positively charged arginine residues within the hsV4 ARD that appear to be critical for RhoA binding.[69] Both mutants, E47 and E54, showed preserved interaction with RhoGDI, indicating that they were properly folded and functional. Our observations thus provide a potential structural explanation for the disruption of RhoA interaction by neuropathogenic mutations within hsV4 ARD. MD Brett A. McCray showed

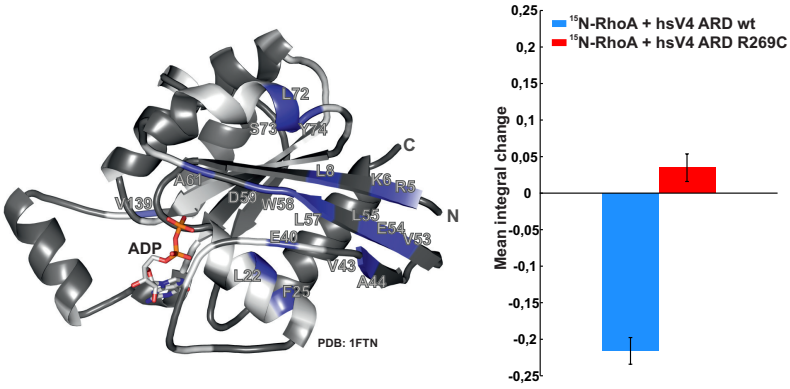

Figure 4.22: **Interaction sites of hsV4 ARD with ^{15}N-RhoA.** *Left*: NMR signal intensities in the presence of hsV4 ARD mapped on a crystal structure of GDP-bound human RhoA (PDB: 1FTN)[171]. Residues with significant decreases in signal intensity (indicated in dark purple) are predominantly localized in the RhoA switch regions. White parts correspond to residues for which no peaks could be identified in the measured ^{1}H-^{15}N 2D HSQC spectra. *Right*: Average integral change of ^{15}N-RhoA residues in the presence of hsV4 ARD or hsV4 ARD R269C. Error bars indicate SEM.

via live Ca^{2+}-influx assays and co-IPs with transiently transfected MN-1 cells, that RhoA binding results in suppression of TRPV4 channel activity but also to RhoA inhibition. Activation of TRPV4 with the potent TRPV4 agonist GSK-101 in transfected HEK293T cells lead to RhoA activation and cytoskeletal changes. The regulation of cell morphology by an interplay between TRPV4 and RhoA was furthermore investigated by neurite-like outgrowth length quantification of MN-1 cells. MN-1 cells transfected with TRPV4 alone showed pronounced neurite-like outgrowth, whereas the neuro-pathy-causing R237L mutation failed to promote neurite-like outgrowth in MN-1 cells. Co-expression of RhoA with TRPV4 therefore strongly inhibited this TRPV4-mediated neurite-like outgrowth, which was rescued by RhoA inhibition of the potent and specific RhoA inhibitor exoenzyme C3 transferase. Strikingly, also the neuropathy-causing mutation TRPV4 R237L phenotype could be partially rescued via RhoA inhibition, indicating that elevated RhoA activity due to interrupted RhoA-TRPV4 interaction contributes to pathological neurite-growth outcomes in TRPV4-caused neuropathies. This hypothesis was tested *in vivo* with a *D. melanogaster* model where it was found that expression of the *Drosophila* RhoA ortholog Rho1 by expression of dominant negative Rho1 T19N rescued neuronal degeneration with expression of neuropathy mutant TRPV4 R269C.

Within this cooperation, RhoA was identified as a direct interactor of TRPV4 with its ankyrin repeat domain, a notorious hot-spot for disease-causing mutations in TRPV4. RhoA was indentified as a mediator of TRPV4-induced cell structure changes and the here described findings strongly hint towards that disruption of TRPV4-RhoA binding is one determinant of tissue-specific toxicity of TRPV4 neuropathy mutations.

4.5 All or nothing - interaction of ITCH requires the full TRPV4 N-terminus *in vitro*

Ubiquitination and deubiquitination of transmembrane proteins are key mechanisms in regulating their surface expression. Wegierski *et al.* showed that ITCH-mediated TRPV4 ubiquitination does not increase TRPV4 degradation but decreases the TRPV4 amount in the plasma membrane.[172] It was shown that this ubiquitination took place at the TRPV4 N-terminus and not the C-terminus by overexpressing the respective FLAG-tagged cytosolic TRPV4 domain along with ITCH in HEK293T cells with subsequent western blotting of the cell lysates against FLAG and ubiquitin. As ITCH harbors four WW domains which are hypothetically able to interact with the TRPV4 PRR, these results suggested a direct interaction between ITCH and TRPV4, even though the cell lysate could have provided additionally required adaptor proteins for a proper PPI between ITCH and the TRPV4 N-terminus. Shukla *et al.* showed a β-arrestin 1 mediated ubiquitination and functional down-regulation of TRPV4 via an angiotensin I mediated AT1aR activation in HEK293T cells, indicating that β-arrestin 1 is required for a GPCR-regulated ITCH-mediated TRPV4 ubiquitination.[173]

To investigate a possible direct interaction between ITCH and the human TRPV4 N-terminus (hsV4N) *in vitro*, recombinantly expressed human full-length ITCH was successfully purified for the first time to date (see figure 4.23 and subsection 3.7.7). To distinguish possible minimal binding sites within hsV4N, hsV4N ARD and hsV4N ARD with the PRR (hsV4 ARD-PRR) were also recombinantly expressed and purified (see subsection 3.7.1 and 3.7.2). All proteins showed expected molecular weights and secondary structures determined by CD spectroscopy

Figure 4.23 *(facing page)*: **Purification of recombinant TRPV4 N-terminal constructs and human ITCH. A** Topology model of recombinantly expressed TRPV4 N-terminal constructs and human ITCH. His_6 = hexa-histidine tag (single letter code: HHHHHH), TEV = Tobacco Etch Virus Cleavage Site (single letter code: ENLYFQG), C2 = C2 domain, WW1+2 = WW domains 1 and 2, WW3+2 = WW domains 3 and 4, HECT = homologous to E6-AP C-terminus domain. His_6-tags with preceding or subsequent TEV Cleveage Site were removed. **B** SEC purification of full-length human ITCH. **C** SEC purifications of TRPV4 N-terminal constructs and ITCH. SEC runs were performed with either a HiLoad Superdex 200 or a HiLoad Superdex 75 pg preparative SEC column. Inlets show Coomassie stained 15 % SDS-PAGEs of collected and concentrated fractions after SEC. x-axis: eluted volume in mL, y-axis: absorbance at 280 nm, M = marker. **D** Far UV CD spectrum of full-length human ITCH. **E** Comparison of far UV CD spectra of purified TRPV4 N-terminal constructs. Spectra were measured at 293 K and proteins were used at 1 µM concentration in either SEC Buffer with a final NaCl concentration of 30 mM (TRPV4 N-terminal constructs) or ITCH SEC buffer with a final concentration of 20 mM NaCl (ITCH). Inlets show secondary structure prediction performed with CAPITO.[93] The predicted α-helix/β-sheet/random coil content of the purified proteins is for hsV4N 53 %/0 %/.47 %,hsV4 ARD-PRR 60 %/0 %/ 40 %, hsV4 ARD 68 %/0 %/32 % and ITCH 29 %/20 %/51 %. x-axis: mean residue ellipticity ($[\Theta]_{mrw,\lambda}$) in 10^{-3} deg cm^2 dmol^{-1}, y-axis: wavelength λ in nm.

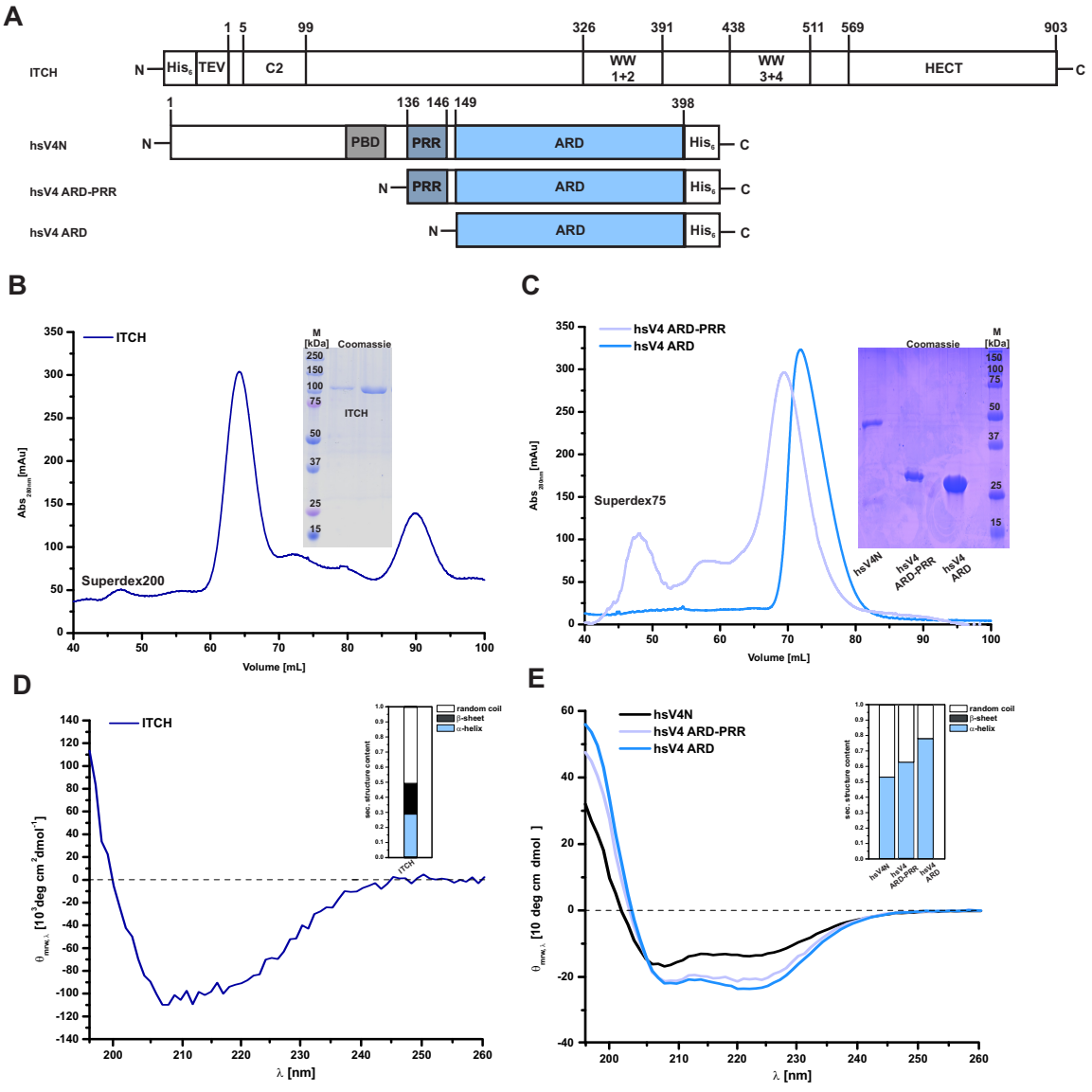
A
ITCH
hsV4N
hsV4 ARD-PRR
hsV4 ARD
His6
TEV
C2
WW 1+2
WW 3+4
HECT
PBD
PRR
ARD
B
ITCH
Superdex200
Coomassie
Volume [mL]
C
hsV4 ARD-PRR
hsV4 ARD
Superdex75
Coomassie
hsV4N
hsV4 ARD-PRR
hsV4 ARD
Volume [mL]
D
ITCH
λ [nm]
random coil
β-sheet
α-helix
E
hsV4N
hsV4 ARD-PRR
hsV4 ARD
λ [nm]

(see figures 4.23 A-E). The topology model in figure 4.23 A shows the domains full-length ITCH is harboring. Besides the already mentioned WW-domains, ITCH consists of a C2 and catalytically active HECT (homologous to E6-AP C-terminus) domain. C2 domains bind phospholipids for (plasma) membrane localization, either in Ca^{2+} dependent or Ca^{2+} independent manner, depending on the C2 domain family.[174] The catalytic HECT domain interacts with E2 ligases to obtain ubqiquitin via trans-thioesterification and ultimately carries out the ubiquitination of substrate proteins.[174,175] Zhu *et al.* provided the until to date only near-full length structure of ITCH via X-ray crystallography. However, the murine construct is lacking the N-terminal C2 domain (ΔC2-ITCH) and WW3+4 are not resolved (PDB:5XMC).[175] Nevertheless, this murine ΔC2-ITCH structure is consistent with individual resolved structures of WW1+2 and HECT domains. The structure of Zhu *et al.*, combined with several resolved structures of the isolated domains, revealed an overall α-helical fold for the HECT domain, whereas the C2 and WW domains exhibit β-sheet folds.[175–177] Enzymatic activity of purified ITCH was shown in an *in vitro*-ubiquitination assay (figure 4.25 A). The putative complex formation between ITCH and respective TRPV4 N-terminal construct was probed via Blue-native PAGE (BN-PAGE). For hsV4N a complex at approx.150 kDa could be observed, which corresponds to an ITCH (approx.100 kDa)-hsV4N (approx.50 kDa) complex with a stoichiometry of 1:1. To confirm this, respective band was cut out (figure 4.24 B, red square) and mass spectrometric measurements were carried out (Johns Hopkins Mass Spectrometry and Proteomics Facility), confirming the presence of both proteins in indicated band. These results show that ITCH physically interacts with hsV4N, but not with hsV4 ARD and hsV4 ARD-PRR. Cross-link mass spectrometry (XL-MS) measurements with hsV4N and ITCH confirmed this direct PPI and also hint towards the requirement of full hsV4N for the interaction with ITCH (figure 4.24 C). Surprisingly, no lysine residues between hsV4N and the ITCH HECT domain were cross-linked. The ITCH HECT domain harbors the enzymatic activity site to receive ubiquitin from E2 ligases and to transfer this ubiquitin via trans-thioesterification to the target protein.[178,179] Also, no cross-links between the hsV4N PRR and ITCH were detected, underlining the results of shown BN-PAGE results, that the full hsV4N is involved in the PPI (figure 4.24). To determine if ITCH is also able to ubiquitinate hsV4N *in vitro*, an ubiquitination assay with subsequent SDS-PAGE and Coomassie staining was performed with ITCH and respective hsV4N constructs (figure 4.25).

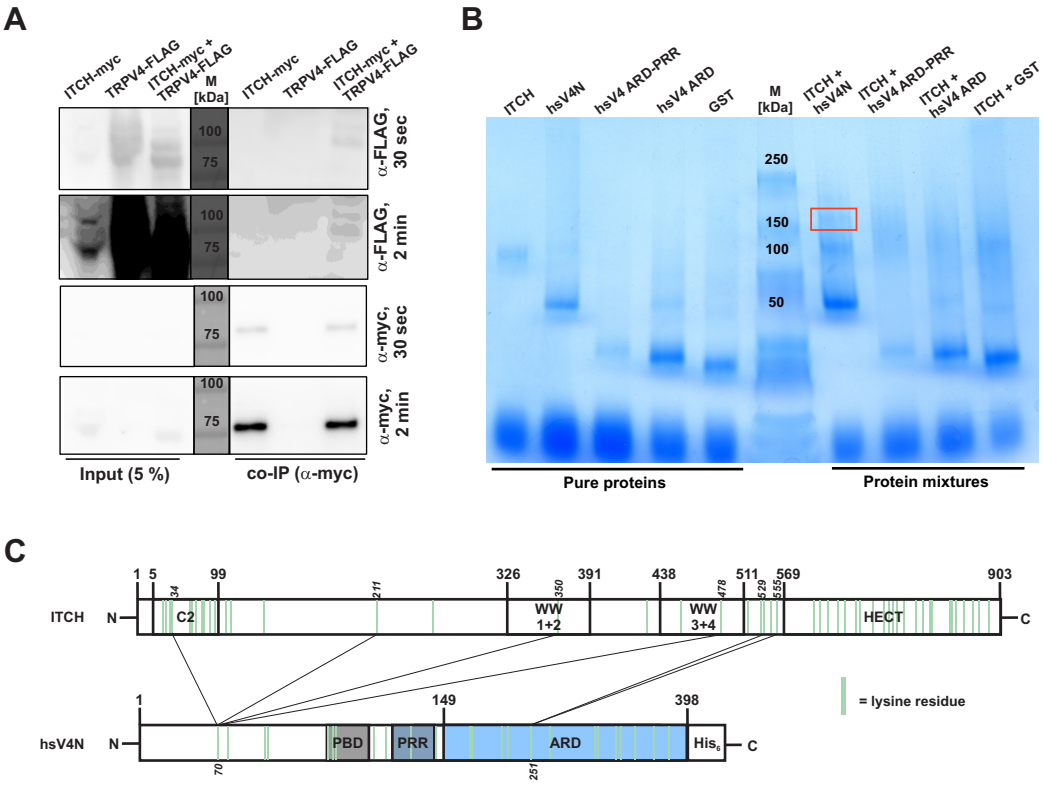

Figure 4.24: **ITCH and hsV4N are direct interaction partners**. **A** α-myc immunoprecipitation of ITCH-myc shows co-immunoprecipitation of TRPV4-FLAG co-transfected in HEK293T cells and confirms ITCH as a part of the TRPV4 interactome[172,173] **B** Blue-native PAGE with purified TRPV4 N-terminal constructs and ITCH (see figure 4.23) shows complex formation at approx. 150 kDa (red square) between ITCH and hsV4N, confirmed by mass-spectrometric measurements. **C** Cross-link mass spectrometry (XL-MS) confirms a direct interaction between ITCH and hsV4N. Green bars indicate native lysine residues, whereas lysine residues involved in DSS-mediated cross-linking are additionally numbered. Black lines show cross-links between respective lysine residues. XL-MS measurements were kindly carried out by M.Sc. [redacted], University of Konstanz)

At time point 60 min a band of approx.10 kDa (figure 4.25 A, red square) above the unmodified hsV4N band was observed, indicating an ubiquitination as ubiquitin has a molecular weight of 8.6 kDa. For better visualization, the time point 90 min is also shown. hsV4 ARD and hsV4 ARD-PRR showed no higher molecular weight bands and therefore no ubiquitination. For subsequent mass spectrometric identification of hsV4N ubiquitinaton sites, the red squared band after 60 min was cut out to rule out time-dependent unspecific ubiquitinations, as this was the earliest time point with a visible band for modified hsV4N. Four lysine residues in the intrinsically disordered region (IDR) of hsV4N were identified as ubiquitination sites: K77, K101, K130 and K136. The IDR alone includes 11 lysine residues and the whole hsV4N a total of 23 lysine residues, depicting a high lysine specificity of ITCH-mediated ubiquitination. As mentioned above, ubiquitin has a molecular weight of 8.6 kDa.

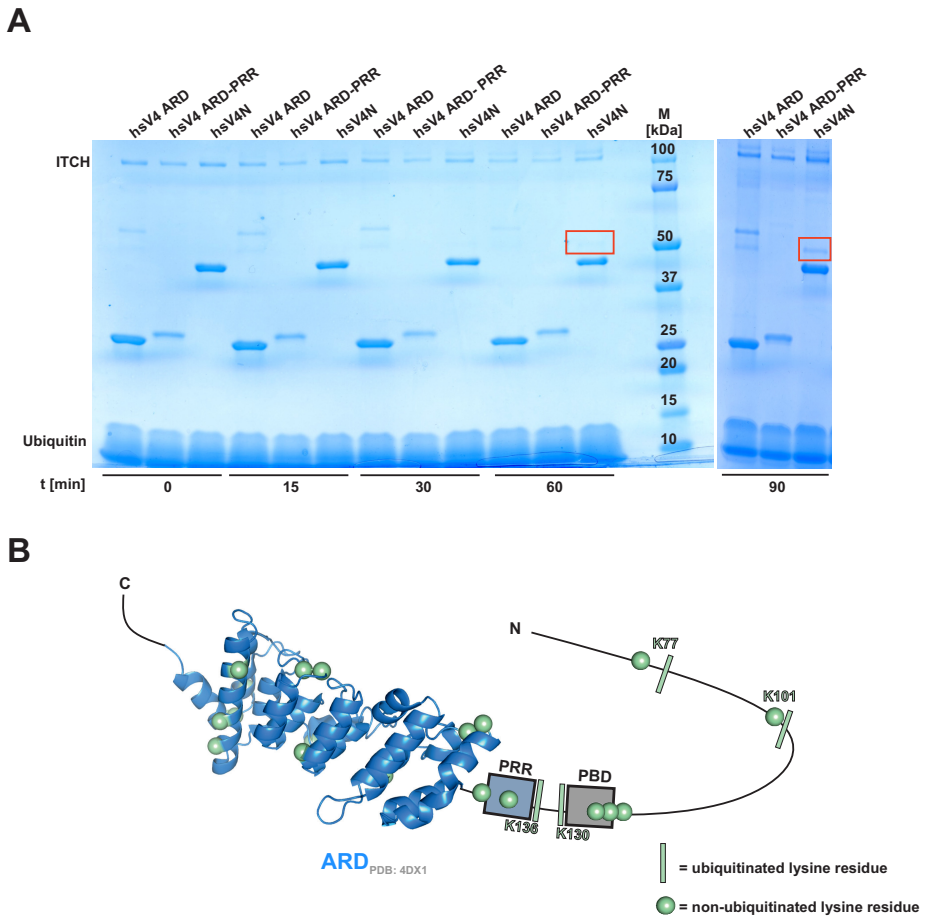

Figure 4.25: **ITCH ubiquitinates hsV4N directly. A** *In vitro* ubiquitination assay shows ubiquitination of hsV4N by ITCH, indicated by the bands in red squares at time points 60 min and 90 min. The band at time point 60 min was cut out and supplied to mass spectrometric detection for ubiquitination (Johns Hopkins Mass Spectrometry and Proteomics Facility). See subsection 3.10.3 for a protocol of the assay. **B** Mass spectrometry revealed the direct ubiquitination of four lysine residues (K77, K101, K130 and K136) in the hsV4 IDR by ITCH, indicated by green bars.

Therefore, hsV4N is present in a monoubiquitinated state in this assay, where each of above mentioned lysine residues is ubiquitinated once, respectively. The detected relative abundances of respective monoubiquitinated lysine harboring peptides decrease from K101>K77>K136>K130 (see section 6.7). Monoubiquination does not target proteins for proteosomal degradation, but rather serves as a signal for membrane trafficking and endocytosis.[172,180,181] These findings also underline the results of Wegierski *et al.*, who determined TRPV4 to be rather multi- than polyubiquitinated.[172] Furthermore it was shown that the amount of internalized TRPV4 increased in the presence of ITCH, suggesting an increased ITCH-mediated TRPV4-endocytosis via monoubiquitination.[172,173] But why is there no HECT-hsV4N IDR interaction in the shown XL-MS data in figure 4.24 C?

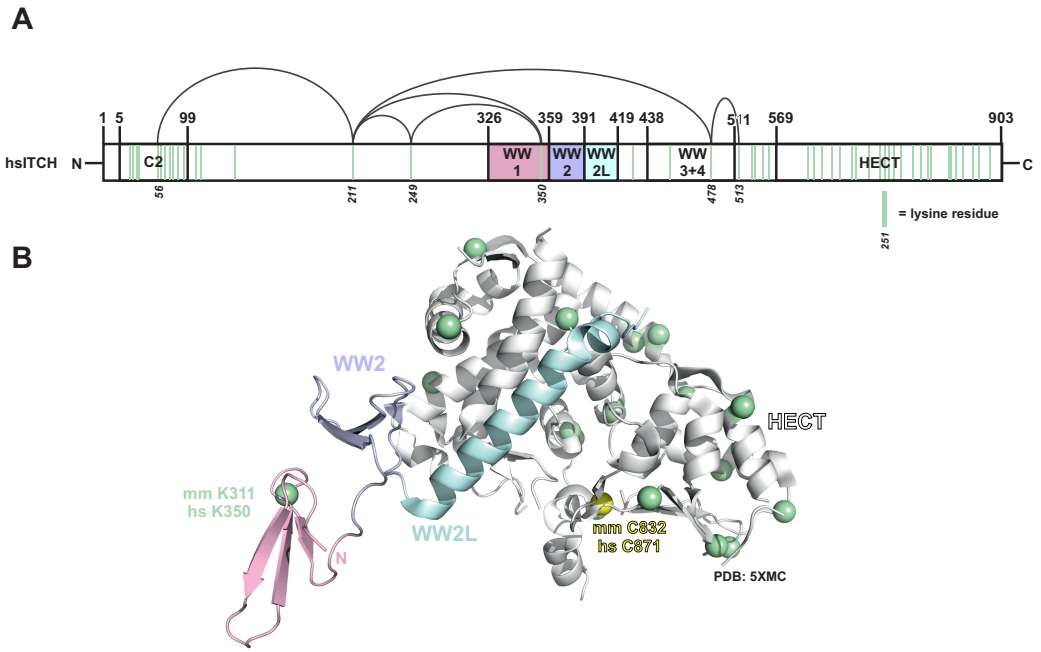

Figure 4.26: **Cross-link mass spectrometry (XL-MS) measurements showing inter- and/or intramolecular interactions between ITCH molecules. A** Topology model of full-length human ITCH with respective inter- and/or intramolecular self-crosslinks of ITCH. Green bars indicate native lysine residues, whereas lysine residues involved in DSS-mediated cross-linking are additionally numbered. Dark arches show cross-links between respective lysine residues. XL-MS measurements were kindly carried out by M. Sc. Jasmin Jansen (Working group Stengel, University of Konstanz).**B** Crystal structure of autoinhibited mouse ITCH (mmITCH) (PDB:5XMC). For better comparison with the used human constructs in this theses, highlighted residues are indicated for mouse (mm) with the corresponding human (hs) residue below. lysine residues are indicated as light green spheres. Mouse cysteine 832 (mm C832) is shown as yellow sphere, indicating the position of the catalytic active site for ubiquitin transthiolation in the HECT domain. The structure here is lacking the C2 domain, furthermore the WW3 and 4 domains were not resolved. The only structurally resolved lysine in shown murinal structure which is involved in cross-links shown in A mouse lysine 311 (mm K311),which is the corresponding lysine for human lysine 350 (hs K350).[175]

It is known that HECT E3 ligases like ITCH exist in an autoinhibited state.[175,179] In this autoinhibited state, the WW2 domain and a part of the linker region connecting WW2 and WW3 (referred as WW2L) bind to a hydrophobic surface opposite to the catalytic active site of the ITCH HECT domain, therefore allosterically locking the HECT domain in an inactive state (figure 4.26 A). However, binding of the ITCH interaction partner Ndfip1 to the ITCH WW2 domain releases ITCH out of its autoinhibited state.[175] The XL-MS data thus could represent the initiation step of the ITCH-hsV4N interaction, where hsV4N releases ITCH out of its autoinhibitory state and ITCH would be ready to receive an ubiquitin from an E2 ligase in its HECT domain. The presence of ITCH in this autoinhibited state could not be determined via self-link (inter- or intramolecular between ITCH) XL-MS data (figure 4.26), as the WW2 domain and WW2L does not harbor any lysine residues which could have been cross-linked to lysine residues in the

HECT domain. Furthermore, neither in intermolecular cross-links between hsV4N and ITCH (figure 4.24 C) nor in self-linked cross-links between or within ITCH (see 4.26 B) any HECT lysine participated in cross-linking. This could be due to the location of most HECT lysine residues, as they are buried in the N- and C-lobe of the HECT domain and therefore are unreachable for DSS for cross-linking (figure 4.26 B). Ubiquitin binding itself leads to dramatic conformational changes in the HECT domain. HECT domains consists of a so-called N- and C-lobe, with the C-lobe harboring the catalytically active site. These lobes change their overall orientation from a "closed" T-shape to an "open" L-shape upon ubiquitin binding, enabled via a flexible hinge region between the two lobes. Therefore the data suggests, that hsV4N probably releases ITCH from its autoinhibited state, enabling ubiquitin binding to the HECT domain via an E2 ligase. Due to the ubiquitin-binding, the HECT domain changes from a "closed" T-shape to an "open" L-shape, enabling an interaction of the hsV4N IDR with the HECT domain for IDR ubiquitination.[182]

Interestingly, two of the ubiquitinated TRPV4 lysine residues are in close proximity to the proline rich region (PRR, K136) and the phosphoinositide-binding domain (PBD, K130) of hsV4N, two important regulatory sites in TRPV4. These modifications could thus lead to an altered binding behavior between hsV4N and other proteins, for example, between PACSIN3 and the TRPV4 PRR. As already described in section 4.3, co-expression of PACSIN 1 and 3, respectively, with TRPV4 lead to a dampened hypoosmolarity induced TRPV4-mediated Ca^{2+}-influx in HEK293T cells (figure 4.16). Furthermore, it was shown that the presence of PACSIN3 increases the plasma membrane amount of TRPV4 by probably inhibiting endocytosis, whereas ITCH decreases the TRPV4 amount in the plasma membrane via endocytosis.[70,172] Here, two different regulating mechanisms lead to a decreased basal TRPV4 activity. The ubiquitination close to the TRPV4 PRR thus could therefore be a regulating switch between these two mechanisms: whereas PACSIN3 could provide a transient and fast TRPV4 desensitization, ITCH could disrupt this interaction via the K130 and K136 monoubiquitinations, therefore sterically hindering the PACSIN3 SH3 domain to interact with the TRPV4 PRR. This then could lead to a TRPV4 endocytosis, serving a TRPV4 "inactivation" for a longer time range.[172] Furthermore, the monoubiquination of K136 next to the PBD could lead to an impaired TRPV4-PIP_2 interaction, resulting in an altered TRPV4 regulation. Opposite consequences for the TRPV4 activity were shown upon PIP_2 binding, pointing out the need for further investigations of the consequences of TRPV4-lipid interactions.[39,183,184]

Goretzki *et al.* showed via elaborate and comprehensive biophysical studies a structural and dynamic coupling between the TRPV4 IDR and ARD.[23] Consequently, comparably large post-

translational modifications (PTMs) in the TRPV4 IDR could thus lead to modified interactions with the TRPV4 ARD with impacts on ARD-mediated PPIs, for example. The results shown here therefore contribute to a further understanding of the PPI between hsV4N and ITCH.

4.6 TRPV4 and the actin cytoskeleton - connecting scientific disciplines

In preceding MS studies of the hsV4N interactome, conducted in the authors master thesis, a possible Ca^{2+}-dependent interaction between smooth muscle α-actin and hsV4N was observed, where α-actin amounts were higher in the samples with Ca^{2+}-supplementation.[76] This findings were especially intriguing, as TRPV4 is known to influence the microtubule and actin cytoskeleton, with consequences for cell stiffness, migratory behavior and morphogenesis.[185–187] Goswami *et al.* showed a direct interaction between the TRPV4 C-terminus and actin in cosedimentation assays, but left out hsV4N in these studies due to expression problems. Therefore, Goswami *et al.* argue that hsV4N could also play an important regulatory role in the shown colocalization between TRPV4-GFP and F-actin in transiently transfected F11 cells.[185] This possible cytoskeletal mediating role of hsV4N is underlined by the direct interaction between hsV4 ARD and the small GTPase RhoA shown in this thesis (section 4.4). RhoA is a prominent cytoskeleton regulator, playing a key role in stress fiber formation and actin polymerization.[166,167,169]. As a starting point to elucidate the role of hsV4N in actin regulation, the potential Ca^{2+}-dependent colocalization between the actin cytoskeleton and TRPV4 was investigated with fluorescence microscopy. HEK293 cells stably expressing human TRPV4-cGFP were treated either with 200 nM HC067 (TRPV4 antagonist) for 15 min at 37 °C, 30 nM GSK-101 for 1 min at 37 °C or left at 37 °C for 15 min without any supplementation. F-actin was visualized by subsequent phalloidin-TRITC staining (figure 4.27, for full immunostaining procedure see section 3.3).
Although plenty of colocalization programs are available, either as ImageJ plugins or as commercial softwares, the algorithms and parameters of these programs are poorly described.[188] Furthermore, most of the programs do not provide automated image analysis, making statistical evaluations of colocalization quantification tedious and time-consuming. To circumvent the usage of "black box" programs and to provide large-scale image analysis, the theoretical chemist B. Sc. [redacted] joined this project to contribute an in-house software for colocalization studies: ELSEXY, short for Efficient Large Scale Evaluation of cross(X)-correlation Yields. Figure 4.27 shows representative fluorescence images of stably transfected HEK293 cells expressing hsTRPV4-cGFP after various treatments.

Figure 4.27: **Fluorescence microscopy images reveal stress fiber formation upon TRPV4 activation in stably transfected HEK293 cells.** Stress fiber formation was especially pronounced upon treatment with 30 nM GSK-101 for 1 min at 37 °C, with clearly visible dorsal and ventral stress fibers as well as transverse arcs, whereas only temperature activation of TRPV4 at 37 °C lead to a milder phenotype with some ventral stress fibers visible. Treatment with 200 nM of the TRPV4 antagonist HC-067 for 15 min at 37 °C showed no stress fiber development. F-actin was visualized via phalloidin-TRITC staining (see section 3.3). Scale bar = 10 µm. Images were taken with a Zeiss Axio Observer Z1 inverted widefield microscope.

Upon chemical compound activation with the potent TRPV4 activator GSK1016790A (GSK-101), cells showed explicit stress fiber formation, hinting towards a hsV4N involvement in cellular actin reassembly, as hsV4 ARD was shown to directly interact with inactive GDP-bound RhoA, the key regulator of stress fibers in cells (see section4.4).[166,167,169] TRPV4 activation activates RhoA, leading to a loss-of-interaction between TRPV4 and RhoA.[69] Activated, GTP-bound RhoA then mediates stress fiber formation by downstream interactors like ROCK and mDIA1.[166] The mild stress fiber phenotype of cells after TRPV4 temperature activation hints towards a Ca^{2+}-concentration dependency of stress fiber formation, as more physiological stimuli lead to lower amount of Ca^{2+}-influx compared to GSK-101 treatment (see also section 4.3, figure 4.16). To determine if TRPV4-mediated Ca^{2+} influx leads to an increased TRPV4-actin colocalization, fluorescence images were subjected to ELSEXY.

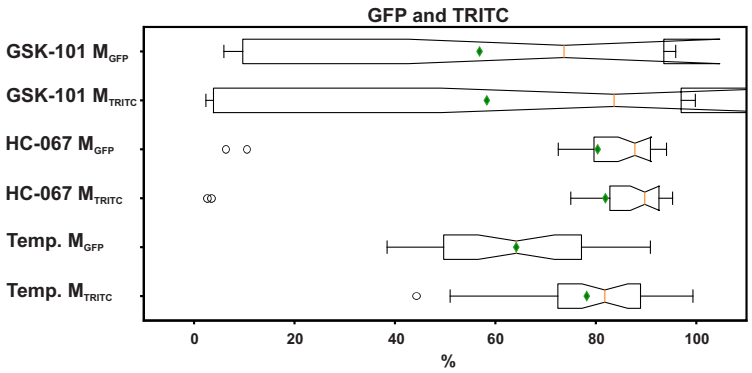

Figure 4.28: **Calculated M-values of GFP (TRPV4-cGFP) and TRITC (F-actin stained with Phalloidin-TRITC) images show decreased TRPV4 and F-actin colocalization upon TRPV4-mediated Ca^{2+}-influx in HEK293 cells.** For description of M-values see equation 4.4 and corresponding text. Box plot whiskers indicate values inside 1.5-fold interquartile range, green diamonds the arithmetic mean. Notches show 95 % confidence intervall of mode. Outliers are shown as circles. $n_{GSK\text{-}101}$=18, $n_{HC\text{-}067}$=28, n_{Temp}=33.

Shortly described, after hot-pixel and non-uniform background correction, ELSEXY calculates the Pearson Colocalization Coefficient (PCC) r of subjected fluorescence images (figure 6.8). The PCC is a measure for the linear dependency of two measured values. To obtain the PCC of the here obtained imgages, the measured values here are the fluorescence intensities of a pair of corresponding pixels in two fluorescence microscopy images (I_A and I_B, see equation 4.3).[189]

$$r_{A,B} = \frac{\overline{I_A \times I_B} - \overline{I_A} \times \overline{I_B}}{\sqrt{(\overline{I_A^2} - \overline{I_A}^2) \times (\overline{I_B^2} - \overline{I_B}^2)}} \tag{4.3}$$

Due to this linear dependency, the PCC not always perfectly describes the probable colocalization in two images. Additionally, so-called M-values can improve the colocalization quantification, by calculating the fraction of colocalized intensities. This is conducted by defining thresholds for intensities. Pixel intensities above the defined thresholds in respective images

are considered as colocalized. These thresholds (T_A, T_B) result from a limit intensity (I_{lim}) dependent evaluation of the PCC for pixels which are smaller than I_{lim}. M-values thereby depend on the PCC r, as the thresholds depend on each other, shown in equation 4.4.[189]

$$M_A = \frac{\sum_{I_A > T_A \wedge I_B > T_B}}{\sum I_A} \tag{4.4}$$

with $I_B = m \cdot I_B + b$.

Statistical evaluation of the colocalization between hsTRPV4-cGFP and F-actin via phalloidin-TRITC with ELSEXY showed a decreased colocalization upon TRPV4-mediated Ca^{2+}-influx (figure 4.28 and also see figures 6.9 for negative controls). These results seem to oppose the above mentioned increased actin-levels detected in hsV4N MS samples upon Ca^{2+}-supplementation.[76] One possible explanation could serve the sample preparation for subsequent MS experiments conducted by Diehl *et al.*, which differ from the protocol conducted in this work (section 3.8). Whereas in the present work a digitonin solution was used to release cytosolic proteins into the supernatant of dish-cultured HEK293 cells, the previous protocol included whole-cell lysis of HEK293 cells with a CHAPS-containing buffer. It was shown that detergents like CHAPS lead to actin depolymerization from F-actin to G-actin, therefore hinting towards the possibility that G-actin binds in a Ca^{2+}-dependent manner to hsV4N.[190] This hypothesis is underlined by the results of Becker *et al.* who showed that the TRPV4 C-terminus is also capable of binding G-actin in co-sedimentation assays.[185] The possible interaction between G-actin and hsV4N could represent a regulatory loop between TRPV4, RhoA and F-actin. TRPV4 activation leads to a reduced binding of RhoA to hsV4 ARD and activation of RhoA via GTP binding.[69] RhoA activation leads ultimately to stress fiber formation, while G-actin possibly now interacts with hsV4N. In the course of this work it was tried to clone a TRPV4 construct lacking the C-terminus to determine if only hsV4N is responsible for stress fiber formation via RhoA, but until to this date, the cloning was not successful. However, above mentioned experimental set-ups should be conducted to get a more detailed view on the hsV4N-actin interaction. Overall it could be shown that different TRPV4 activators lead to Ca^{2+} concentration dependent stress fiber formation in stably TRPV4-cGFP transfected HEK293 cells. Furthermore, the in house software ELSEXY generated preliminary Ca^{2+}-dependent colocalization data between TRPV4-cGFP and F-actin. However, ELSEXY is still in the refinement process and will give raise to a comprehensive, high-throughput colocalization studies in the future.

5 Conclusion & Outlook

Meeting at the hot-spot of disease causing TRPV4 mutations - the TRPV4 ARD and its interaction partners DDX3X and RhoA

Inada *et al.* proposed altered tissue-specific protein-protein interactions (PPIs) as a reason for the disease pathology and tissue specificity of respective TRPV4 mutations.[27] First results in this thesis underline before mentioned hypothesis by showing both, increased and abolished PPIs between TRPV4 harboring neuropathy-causing mutations and several cytosolic proteins. CMT2C-causing TRPV4 R232C showed increased interaction with DDX3X compared to TRPV4 wt *in vitro* and *in cellulo*, leading to decreased dxRNA-stimulated ATP-hydrolysis of DDX3X upon this interaction *in vitro* (see sections 4.1 and 4.2). This altered PPI is particularly interesting, as mutations leading to ATP-hydrolysis deficiency in DDX3X are connected to the emergence of medulloblastoma, a rapidly growing and metastasizing form of infant cerebellum tumor, and can be the cause of so-called X-linked intellectual development disorder Snijder Broks type (MRXSSB, OMIM: 300958). MRXSSB patients show a spectrum of neuropathological symptoms, but the most shared among patients are muscle hypotonia, movement disorders and aberrant intellectual development.[139,191–195] These symptoms, especially the intellectual disability, hint towards a pivotal role of DDX3X in neuronal fetal development of the central nervous system (CNS). DDX3X mutations were shown to affect CNS neurogenesis during fetal development of the cerebral cortex. Additionally, it was shown that DDX3X plays a role in the induction of the neuronal crest during fetal development, the progenitor structure from which the peripheral nervous systems (PNS) develops from.[196] TRPV4-associated neuropathies affect the PNS, underlining the possible key role of the TRPV4-DDX3X interaction in PNS development and maintenance and ultimately pathological consequences due to a TRPV4 mutation induced aberrant TRPV4-DDX3X PPI, probably leading to stress granule (SG) hyperassembly in the PNS.[31,137,197]

Pharmacological inhibition of ATP-hydrolysis or RNA-helicase activity in DDX3X via the small

molecules RK-33 or D16, respectively, showed diminished SG assembly upon arsenite induced oxidative stress in UO2S cells. Already formed SGs upon stress treatment showed no altered disassembly behavior upon RK-33 or D16 treatment, respectively.[117] Especially regarding the ATP hydrolysis inhibition, these findings seem to contradict the results of Valentin-Vega *et al.* and in this thesis, indicating that impaired DDX3X ATP hydrolysis, either due to DDX3X mutations or altered PPIs, spur SG assembly.[119] Yang *et al.* confirmed direct binding of RK-33 to recombinant DDX3X (aa 1-508) with isothermal calorimetry (ITC) and proposed an impaired RK-33 interaction via the active site of ATP hydrolysis due to the depletion of RK-33 binding to DDX3X K230E in sedimentation velocity assays. This mutation resides within the DDX3X Walker A motif, which is essential for DDX3X's ability to hydrolyze ATP.[198] However, the exact binding mode of RK-33 to DDX3X still remains elusive and therefore the overall possible structural consequences within DDX3X upon RK-33 binding. Thus, disease-causing mutations which lead to impaired ATP hydrolysis in DDX3X still could be the cause of altered PPIs and subsequent SG hyperassemblies, while pharmacological ATP hydrolysis inhibition influences DDX3X in such a manner, that pathological SG-inducing PPIs are also impaired.

To shed more light in the consequences between the here shown elevated TRPV4 R232C-DDX3X PPI, a multi-pronged approach should be performed. On one hand, NMR chemical shift perturbation assays, corresponding to the experiments in section 4.4 with hsV4 ARD and ^{15}N-labled RhoA, should be conducted to gain detailed insights in the direct interaction between DDX3X and hsV4 ARD and hsV4 ARD R232C, respectively. Furthermore, the influence of RK-33 on possible structural changes in DDX3X could be also investigated via NMR and compared to before mentioned NMR perturbation assays with hsV4 ARD and hsV4 ARD R232C to reveal possible difference in ATP hydrolysis inhibition via a PPI or a pharmacological inhibition. Additional *in vitro* experiments should include further ATPase assays with ARDs of other TRP channels or even other protein superfamilies to distinguish if this interaction exclusively accounts for hsV4 ARD or also other ARDs. Furthermore, functional studies of DDX3X interaction for TRPV4 should be conducted *in cellulo* via Ca^{2+}-influx assays as shown in 4.3. To underline the hypothesis of SG hyperassembly due to aberrant TRPV4 R232C-DDX3X interaction, *in cellulo* experiments with transfected cells should be conducted to investigate a TRPV4 (R232C)-mediated influence upon stress granule formation with DDX3X participation via immunofluorescence staining and subsequent microscopy, for example.

Additionally, the binary TRPV4 PPIs shown in this thesis should be expanded into ternary and even quaternary PPI investigations. One starting point could be the possible ternary PPI between TRPV4, DDX3X and RhoA. For both proteins, a direct interaction with hsV4 ARD was

shown in this thesis. Furthermore it was shown that GSK-101 activation of TRPV4 wt *in cellulo* leads to a decreased PPI between TRPV4 and RhoA or DDX3X, respectively, shown by co-IPs.[69,136] Furthermore, Phung *et al.* indicated a possible DDX3X-RhoA interplay by showing elevated levels of GTP-bound (active) RhoA in human liver cancer cell lines (HT-144 and A2058) upon DDX3X siRNA treatment, lowering but not depleting DDX3X levels in respective cell lines.[199] In the course of this thesis, upon the presence of a neuropathy-causing mutation, DDX3X showed an increased TRPV4 PPI, whereas RhoA showed a decreased TRPV4 PPI. It should be noted that two different neuropathy-causing mutations were used (TRPV4 R232C with DDX3X and TRPV4 R269C with RhoA). Both mutations should be investigated in the context of the ternary TRPV4-DDX3X-RhoA interaction.

Disorder matters - PPIs of the TRPV4 N-terminus underlines the pivotal role of the intrinsically disordered region

Another possible ternary PPI which could be relevant in the context of neuropathy-causing TRPV4 mutations includes TRPV4, PACSIN1 and ITCH. In this thesis it was shown that ITCH directly interacts with only the full TRPV4 N-terminus (hsV4N), but not with the TRPV4 ankyrin repeat domain (hsV4 ARD) or hsV4 ARD with the preceding proline rich region (hsV4 ARD-PRR). Furthermore it was shown, that ITCH ubiquitinates four distinct lysines in the intrinsically disordered region (IDR) of hsV4N (K77, K101, K130 and K136, see section 4.5). This is particularly interesting, as such post-translational modifications (PTMs) could interfere with possible TRPV4 PPIs. With regard of the known interaction of PACSIN SH3 domains with the TRPV4 PRR (aa 136-144), ubiquitination of lysines K130 and K136 are especially interesting with regard to possible disrupted PACSIN1/3 interactions with the TRPV4 PRR due to steric hindrance after ubiquitination of respective lysine. But also, interaction of PACSIN1/3 could prevent TRPV4 IDR ubiquitination, resulting in two different regulating mechanism leading to a decreased basal TRPV4 activity (see section 4.5). Desrochers *et al.* furthermore showed that the PACSIN1 SH3 domain interacts with the ITCH PRR located between the C2 and WW1 domain (aa 252 - 267). With the shown loss-of-interaction between PACSIN1 and TRPV4 harboring the neuropathy-causing R269C mutation with vanished TRPV4-mediated Ca^{2+}-influx dampening by PACSIN1 as a consequence *in cellulo* (see section 4.3), this loss-of-interaction could also lead to an increased interaction between PACSIN1 and ITCH in neurons. The physiological consequences of this interaction still remain elusive, but one scenario could be an impaired interaction of ITCH with other proteins - TRPV4 for example. Due to the location of the ITCH PRR between two other

important regulatory domains, namely the ITCH C2 domain and the ITCH WW1 domain, interaction with PACSIN1 could therefore impair possible interactions of at least these two domains, hypothetically impairing plasma membrane localization via the ITCH C2 domain and other PPIs of the ITCH WW1 domain, if not also of the other WW domains regarding the compact structure of ITCH in its autoinhibited state (shown in figure 4.26 B). As ITCH is known to mediate TRPV4 endocytosis, a loss of interaction between PACSIN1 and TRPV4 R269C could therefore induce a vicious cycle where PACSIN1 and ITCH-mediated negative TRPV4 regulation are both abolished. This would lead then to elevated neurotoxic Ca^{2+} levels due to the elevated basal Ca^{2+} influx activity of this TRPV4 mutation (see also figure 4.17) in addition to the here showed lost interaction between TRPV4 R269C and RhoA with the cytoskeletal consequences (see 4.4).[53,69]

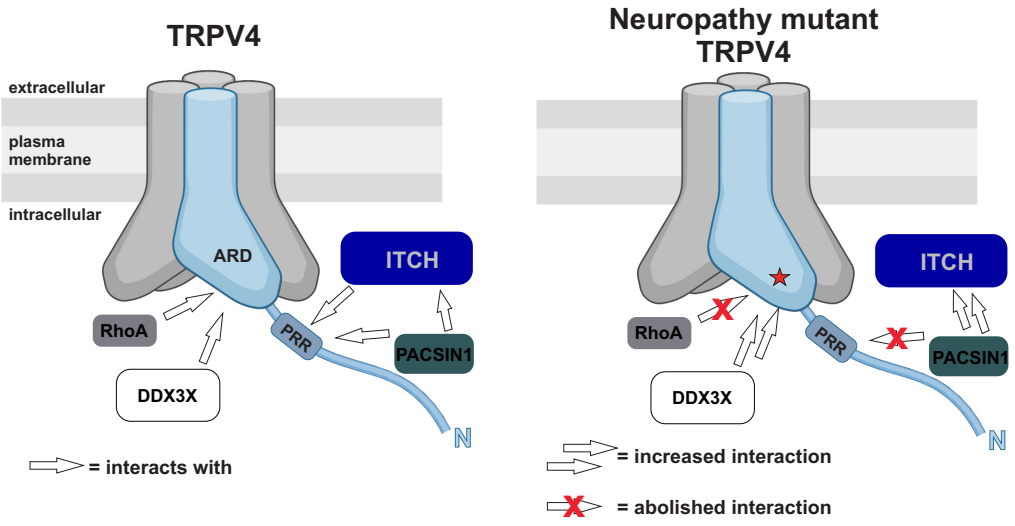

Figure 5.1: **Tissue specificity of neuropathy-causing TRPV4 mutations occur due to aberrant tissue specific protein-protein interactions** Schematic representation of how TRPV4 neuropathy mutations lead to aberrant protein-protein interactions investigated in the course of this thesis. It was shown that RhoA and DDX3X specifically interact with the a-helical TRPV4 ankyrin repeat domain (ARD), whereas PACSIN1 is known to interact with the TRPV4 proline rich (PRR) region within the unstructured intrinsically disordered region (IDR) and ITCH requires the full TRPV4 N-terminus, with a possible interaction with the TRPV4 PRR.[22,69] In the presence of a neuropathy-causing TRPV4 mutation the interactions with RhoA and PACSIN1 are abolished, with a possible consequence for the ITCH-TRPV4 interaction due to a putative increased PACSIN1-ITCH interaction. An increased interaction between neuropathy mutant TRPV4 and DDX3X was also shown in this thesis.

To elucidate this, co-IPs with cells transfected with TRPV4 (R269C), ITCH and PACSIN1 should be conducted to investigate the proposed binding competition between ITCH and PACSIN1 to TRPV4. After getting details of the interaction between ITCH and TRPV4, either with NMR studies including the ITCH WW domains and a peptide including the TRPV4 PRR or via cryo-EM with full length ITCH and hsV4N, latter experiment should be complemented with the TRPV4

R269C mutation. If both before mentioned methods should not be applicable, XL-MS studies could be conducted including hsV4N R269C with ITCH and PACSIN1, respectively, to get a detailed insight into the mutation-dependent altered PPIs.

With the comprehensive interactome study shown in this thesis, future investigations should further validate the identified putative TRPV4 interactors shown in section 4.1, especially considering the proposed role of TRPV4 in cytoplasmic granule and/or stress granule formation via its cytosolic N-terminus. Co-IPs with cells transfected with (mutated) TRPV4 and other here detected prominent SG formation proteins like TIA-1 and IGF2BP2 (figure 4.6) should be conducted, as well a possible TRPV4 mediation of altered stress granule formations under stress conditions *in cellulo*.

6 Appendix

6.1 Appendix - Introduction

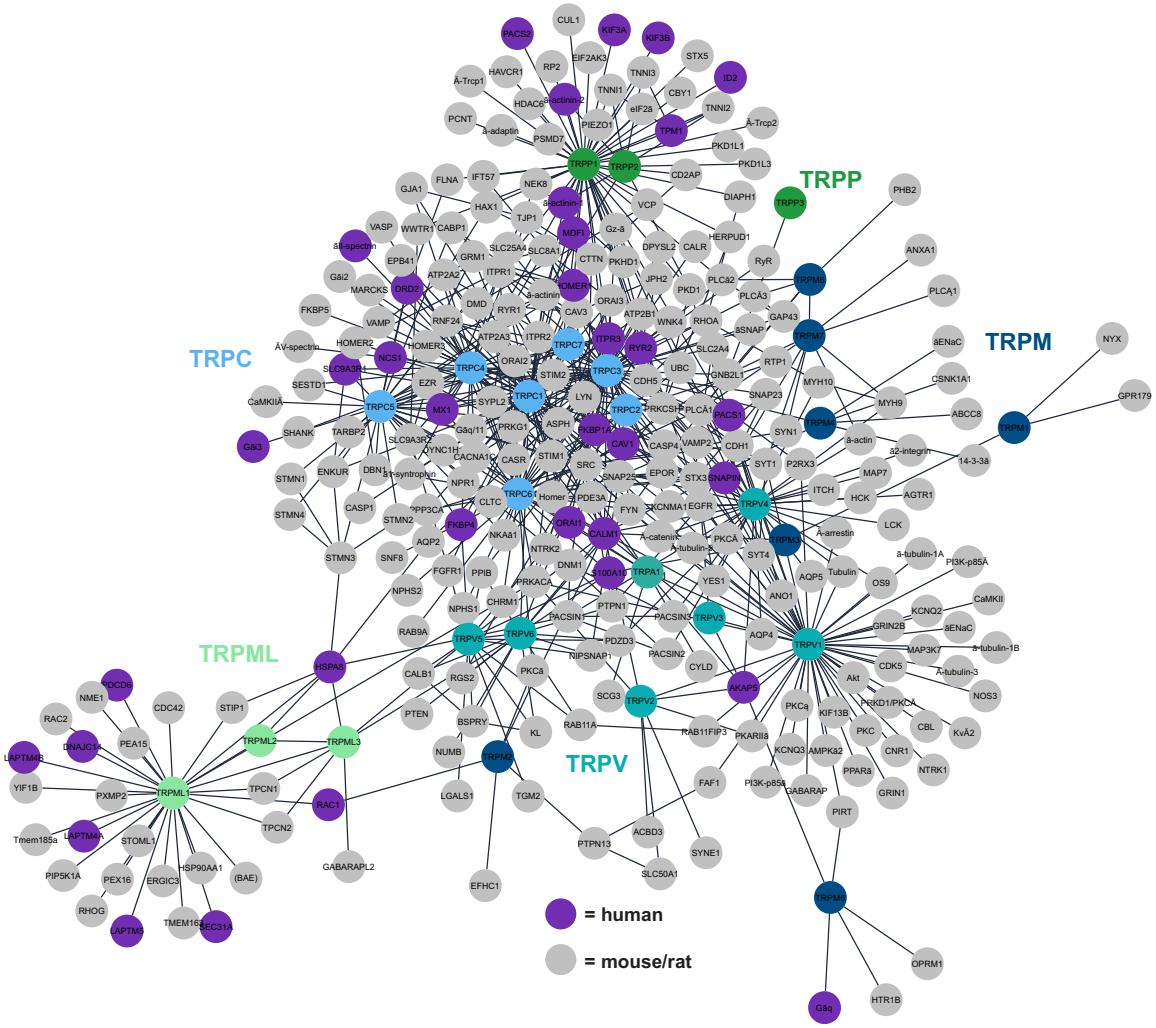

Figure 6.1: **TRP channel PPI network extracted from the TRIP Database.** The majority of the shown PPIs are with rodent proteins (grey nodes), whereas only a minority depicts PPIs with human proteins (purple nodes). Node colors of TRP subfamilies are indicated in the figure. Network was rendered with Cytoscape 3.8.0.[29,30]

Table 6.1: List of human TRP channel protein interactors deposited in the TRIP database.[29,30] Note, that not all TRP channels are represented, as the most experiments did not use human proteins for PPI investigations.

TRP channel	Protein interactor	Experiment
TRPC1	Calmodulin	Fusion protein-pull down assay
TRPC1	Caveolin-1	Fusion protein-pull down assay
TRPC1	D2R	Fusion protein-pull down assay
TRPC1	FKBP52/FKBP4	Co-immunoprecipitation
TRPC1	FKBP52/FKBP4	Fusion protein-pull down assay
TRPC1	I-MFA	Fusion protein-pull down assay
TRPC1	NCS-1	Fusion protein-pull down assay
TRPC1	TRPP1	Fusion protein-pull down assay
TRPC3	Calmodulin	Fusion protein-pull down assay
TRPC3	FKBP12	Co-immunoprecipitation
TRPC3	Homer-1	Fusion protein-pull down assay
TRPC3	IP3R3	Fusion protein-pull down assay
TRPC3	MxA	Fusion protein-pull down assay
TRPC3	NCX1	Fusion protein-pull down assay
TRPC3	Orai1	Fusion protein-pull down assay
TRPC3	TRPC1	Fusion protein-pull down assay
TRPC3	TRPM4	Yeast two-hybrid
TRPC4	αII-spectrin	Fusion protein-pull down assay
TRPC4	αII-spectrin	Fusion protein-pull down assay
TRPC4	D2R	Fusion protein-pull down assay
TRPC4	MxA	Fusion protein-pull down assay
TRPC4	NHERF1	Fusion protein-pull down assay
TRPC5	D2R	Fusion protein-pull down assay
TRPC5	Gαqi3	Fusion protein-pull down assay
TRPC5	MxA	Fusion protein-pull down assay
TRPC5	NCS-1	Yeast two-hybrid
TRPC5	NCS-1	Fusion protein-pull down assay
TRPC6	MxA	Fusion protein-pull down assay
TRPC7	MxA	Fusion protein-pull down assay

TRP channel	Protein interactor	Experiment
TRPM3	Calmodulin	Fluorescence probe labeling
TRPM3	S100A10	Fluorescence probe labeling
TRPM4	TRPC3	Yeast two-hybrid
TRPM7	SNAPIN	Fusion protein-pull down assay
TRPM8	Gαq	Fusion protein-pull down assay
TRPML1	ALG-2/PDCD6	Fusion protein-pull down assay
TRPML1	HSC70	Fusion protein-pull down assay
TRPML1	HSP40/DNAJC14	Fusion protein-pull down assay
TRPML1	LAPTM4a	Yeast two-hybrid
TRPML1	LAPTM4b	Yeast two-hybrid
TRPML1	LAPTM5	Yeast two-hybrid
TRPML1	SEC31A	Fusion protein-pull down assay
TRPP1	ID2	Yeast two-hybrid
TRPP1	KIF3A	Yeast two-hybrid
TRPP1	KIF3A	Fusion protein-pull down assay
TRPP1	KIF3B	Fusion protein-pull down assay
TRPP1	PACS-1	Fusion protein-pull down assay
TRPP1	PACS-2	Fusion protein-pull down assay
TRPP1	TRPP1	Yeast two-hybrid
TRPP1	RyR2	Fusion protein-pull down assay
TRPP1	Tropomyosin 1	Fusion protein-pull down assay
TRPP1	Troponin I 3	Fusion protein-pull down assay
TRPP1	TRPC1	Fusion protein-pull down assay
TRPP2	α-actinin-1	Yeast two-hybrid
TRPP2	α-actinin-1	Yeast two-hybrid
TRPP2	α-actinin-2	Yeast two-hybrid
TRPP2	α-actinin-2	Yeast two-hybrid
TRPP2	Troponin I 1	Fusion protein-pull down assay
TRPP2	Troponin I 2	Fusion protein-pull down assay
TRPP2	Troponin I 3	Fusion protein-pull down assay
TRPP3	RACK1	Fusion protein-pull down assay
TRPV1	AKAP5/AKAP150	Fusion protein-pull down assay

TRP channel	Protein interactor	Experiment
TRPV4	Calmodulin	Fusion protein-pull down assay

Table 6.2: List of known TRPV4 interactors deposited in the TRIP database.[29,30]

TRP channel	Protein interactor	Experiment
TRPV4	LYN	Co-immunoprecipitation
TRPV4	LYN	Co-immunofluorescence staining
TRPV4	LYN	In vitro PTM assay
TRPV4	LYN	Calcium measurement
TRPV4	SRC	Co-immunoprecipitation
TRPV4	SRC	In vitro PTM assay
TRPV4	SRC	Calcium measurement
TRPV4	FYN	Co-immunoprecipitation
TRPV4	FYN	Co-immunoprecipitation
TRPV4	FYN	In vitro PTM assay
TRPV4	FYN	Calcium measurement
TRPV4	HCK	Co-immunoprecipitation
TRPV4	HCK	In vitro PTM assay
TRPV4	HCK	Calcium measurement
TRPV4	LCK	Co-immunoprecipitation
TRPV4	LCK	In vitro PTM assay
TRPV4	LCK	Calcium measurement
TRPV4	YES	Co-immunoprecipitation
TRPV4	YES	In vitro PTM assay
TRPV4	YES	Calcium measurement
TRPV4	LYN	Inference
TRPV4	SRC	Inference
TRPV4	FYN	Inference
TRPV4	HCK	Inference
TRPV4	LCK	Inference

TRP channel	Protein interactor	Experiment
TRPV4	YES	Inference
TRPV4	Calmodulin	Fusion protein-pull down assay
TRPV4	Calmodulin	Fusion protein-pull down assay
TRPV4	Calmodulin	Fusion protein-pull down assay
TRPV4	Calmodulin	Patch clamp
TRPV4	Calmodulin	Inference
TRPV4	MAP7	Yeast two-hybrid
TRPV4	MAP7	Co-immunoprecipitation
TRPV4	MAP7	Co-immunoprecipitation
TRPV4	MAP7	Co-immunofluorescence staining
TRPV4	MAP7	Co-immunofluorescence staining
TRPV4	MAP7	Co-immunofluorescence staining
TRPV4	MAP7	Cell surface biotinylation
TRPV4	MAP7	Patch clamp
TRPV4	PACS-1	Co-immunoprecipitation
TRPV4	PACS-1	Co-immunoprecipitation
TRPV4	PACS-1	Inference
TRPV4	NHERF4	Inference
TRPV4	AQP-5	Co-immunoprecipitation
TRPV4	AQP-5	Co-immunoprecipitation
TRPV4	AQP-5	Inference
TRPV4	Pacsin1	Yeast two-hybrid
TRPV4	Pacsin1	Co-immunoprecipitation
TRPV4	Pacsin1	Co-immunoprecipitation
TRPV4	Pacsin2	Inference
TRPV4	Pacsin2	Co-immunoprecipitation
TRPV4	Pacsin2	Co-immunoprecipitation
TRPV4	Pacsin3	Yeast two-hybrid
TRPV4	Pacsin3	Co-immunoprecipitation
TRPV4	Pacsin3	Co-immunoprecipitation
TRPV4	Pacsin3	Co-immunoprecipitation
TRPV4	Pacsin3	Co-immunoprecipitation

TRP channel	Protein interactor	Experiment
TRPV4	Pacsin3	Co-immunofluorescence staining
TRPV4	Pacsin3	Co-immunofluorescence staining
TRPV4	Pacsin3	Co-immunofluorescence staining
TRPV4	Pacsin3	Co-immunofluorescence staining
TRPV4	ITCH/AIP4	Co-immunoprecipitation
TRPV4	ITCH/AIP4	Co-immunofluorescence staining
TRPV4	ITCH/AIP4	Co-immunofluorescence staining
TRPV4	UBC	In vivo PTM assay
TRPV4	ITCH/AIP4	Inference
TRPV4	UBC	Inference
TRPV4	UBC	In vivo PTM assay
TRPV4	OS-9	Yeast two-hybrid
TRPV4	OS-9	Co-immunoprecipitation
TRPV4	OS-9	Co-immunoprecipitation
TRPV4	OS-9	Co-immunofluorescence staining
TRPV4	OS-9	Cell surface biotinylation
TRPV4	Pacsin3	Co-immunoprecipitation
TRPV4	Pacsin2	Co-immunofluorescence staining
TRPV4	Pacsin3	Co-immunofluorescence staining
TRPV4	Pacsin3	Patch clamp
TRPV4	LYN	Co-immunoprecipitation
TRPV4	α2-integrin	Co-immunoprecipitation
TRPV4	α2-integrin	Inference
TRPV4	IP3R3	Calcium measurement
TRPV4	IP3R3	Patch clamp
TRPV4	IP3R3	Co-immunoprecipitation
TRPV4	IP3R3	Inference
TRPV4	TRPP1	Co-immunoprecipitation
TRPV4	TRPP1	Co-immunofluorescence staining
TRPV4	TRPP1	Fluorescence resonance energy transfer
TRPV4	TRPP1	Inference
TRPV4	TRPP1	Patch clamp

TRP channel	Protein interactor	Experiment
TRPV4	AKAP5/AKAP150	Co-immunoprecipitation
TRPV4	AKAP5/AKAP150	Speculation
TRPV4	IP3R3	Co-immunoprecipitation
TRPV4	IP3R3	Co-immunoprecipitation
TRPV4	IP3R3	Calcium measurement
TRPV4	IP3R3	Patch clamp
TRPV4	α-actin	Fluorescence resonance energy transfer
TRPV4	α-actin	Co-immunofluorescence staining
TRPV4	α-actin	Inference
TRPV4	SRC	In vivo PTM assay
TRPV4	SRC	In vivo PTM assay
TRPV4	SRC	Calcium measurement
TRPV4	80K-H	Co-immunoprecipitation
TRPV4	80K-H	Speculation
TRPV4	Calmodulin	Fusion protein-pull down assay
TRPV4	α-arrestin 2	Affinity purification-mass spectrometry
TRPV4	α-arrestin 1	Co-immunoprecipitation
TRPV4	α-arrestin 1	Inference
TRPV4	α-arrestin 1	Co-immunoprecipitation
TRPV4	AT1aR	Inference
TRPV4	AT1aR	Co-immunoprecipitation
TRPV4	AT1aR	Co-immunofluorescence staining
TRPV4	AT1aR	Co-immunoprecipitation
TRPV4	ITCH/AIP4	Co-immunoprecipitation
TRPV4	α-catenin	Co-immunoprecipitation
TRPV4	E-cadherin	Co-immunoprecipitation
TRPV4	α-catenin	Yeast two-hybrid
TRPV4	E-cadherin	Inference
TRPV4	α-catenin	Co-immunoprecipitation
TRPV4	α-catenin	Co-immunoprecipitation
TRPV4	Calmodulin	Fusion protein-pull down assay
TRPV4	Caveolin-1	Co-immunofluorescence staining

TRP channel	Protein interactor	Experiment
TRPV4	TRPC1	Inference
TRPV4	Caveolin-1	Inference
TRPV4	TRPC1	Co-immunofluorescence staining
TRPV4	TRPC1	Fluorescence resonance energy transfer
TRPV4	TRPC1	Co-immunoprecipitation
TRPV4	TRPC1	Calcium measurement
TRPV4	TRPC1	Co-immunoprecipitation
TRPV4	TRPC1	Co-immunofluorescence staining
TRPV4	TRPC1	Co-immunofluorescence staining
TRPV4	TRPC1	Calcium measurement
TRPV4	TRPC1	Cell surface biotinylation
TRPV4	TRPC1	Fluorescence resonance energy transfer
TRPV4	AQP-4	Inference
TRPV4	AQP-4	Co-immunofluorescence staining
TRPV4	AQP-4	Co-immunoprecipitation
TRPV4	AQP-4	Co-immunoprecipitation
TRPV4	TRPP1	Co-immunoprecipitation
TRPV4	TRPP1	Atomic force microscopy(AFM) analysis
TRPV4	TRPC1	Fluorescence resonance energy transfer
TRPV4	TRPC1	Fluorescence resonance energy transfer
TRPV4	Calmodulin	Fusion protein-pull down assay
TRPV4	α-actin	Co-immunoprecipitation
TRPV4	α-actin	Fusion protein-pull down assay
TRPV4	Tubulin	Co-immunoprecipitation
TRPV4	Tubulin	Fusion protein-pull down assay
TRPV4	α-actin	Inference
TRPV4	α-actin	Fusion protein-pull down assay
TRPV4	Tubulin	Fusion protein-pull down assay
TRPV4	α-tubulin-5	Inference
TRPV4	α-tubulin-5	Co-immunoprecipitation
TRPV4	α-tubulin-5	Co-immunofluorescence staining
TRPV4	E-cadherin	Co-immunoprecipitation

TRP channel	Protein interactor	Experiment
TRPV4	α-catenin	Co-immunoprecipitation
TRPV4	TRPP1	Co-immunoprecipitation
TRPV4	TRPP1	Co-immunofluorescence staining
TRPV4	TRPP1	Co-immunoprecipitation
TRPV4	TRPP1	Co-immunofluorescence staining
TRPV4	TRPP1	Calcium measurement
TRPV4	RPS27A	Affinity purification-mass spectrometry
TRPV4	Myosin-HIIA	Affinity purification-mass spectrometry
TRPV4	Myosin-10	Affinity purification-mass spectrometry
TRPV4	Calmodulin	Fusion protein-pull down assay
TRPV4	Myosin-HIIA	Co-immunofluorescence staining
TRPV4	Myosin-10	Co-immunofluorescence staining
TRPV4	TRPP1	Co-immunofluorescence staining
TRPV4	TRPP1	Co-immunoprecipitation
TRPV4	TRPP1	Co-immunoprecipitation
TRPV4	Pacsin3	Fluorescence resonance energy transfer
TRPV4	TMEM16A/ANO1	Inference
TRPV4	TMEM16A/ANO1	Co-immunoprecipitation
TRPV4	AKAP5/AKAP150	Co-immunofluorescence staining
TRPV4	AKAP5/AKAP150	Patch clamp
TRPV4	TRPP1	Co-immunoprecipitation
TRPV4	TRPC1	Co-immunoprecipitation
TRPV4	TRPP1	Co-immunoprecipitation
TRPV4	TRPC1	Co-immunoprecipitation
TRPV4	TRPP1	Fluorescence resonance energy transfer
TRPV4	TRPC1	Fluorescence resonance energy transfer
TRPV4	TRPP1	Patch clamp
TRPV4	TRPC1	Patch clamp
TRPV4	Bkca	Inference
TRPV4	Bkca	Co-immunoprecipitation
TRPV4	TRPC1	Co-immunoprecipitation

6.2 Appendix - Purification of biotinylated TRPV4 N-terminal proteins

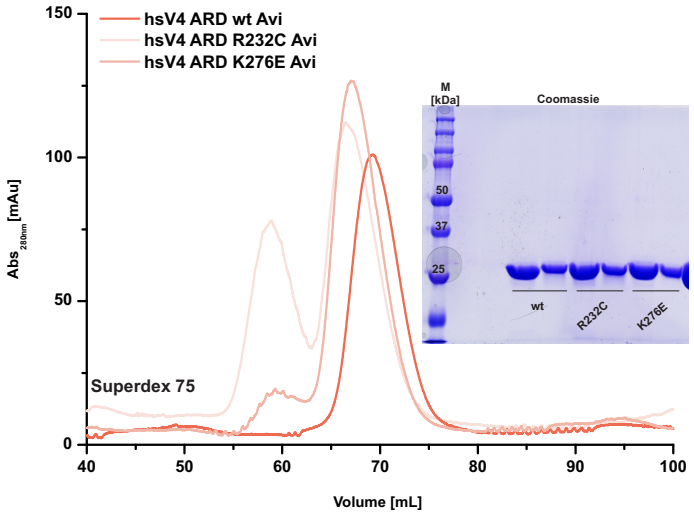

Figure 6.2: **Purification of unbiotinylated hsV4 ARD Avi constructs**. **A** SEC purifications of unbiotinylated hsV4 ARD Avi constructs. For biotinylated constructs see figure 4.1. SEC runs were either performed with a HiLoad Superdex 75 pg preparative SEC column. Inlet shows Coomassie stained 15 % SDS-PAGE of collected and concentrated fractions after SEC. x-axis: eluted volume in mL, y-axis: absorbency at 280 nm, M = marker.

6.3 Appendix - A beginning to elucidate the versatile TRPV4 interatcome

Following tables contain the mass spec data of all significant identified protein interactome members of respective TRPV4 N-terminal construct. With gene ontology and manual curation, each protein was investigated upon a possible role in RNP and/or stress granules. These tables present the current data situation in April 2021 and do not claim any comprehensiveness.

Table 6.3: List of cytoplasmic RNP granule and stress granule proteins found in the hsV4N wt Avi protein interactome determined via two independent UDMS^E in this work. *p*-values (Benjamini-Hochberg corrected Student's *t*-test) were determined of the quadruplicates of each of the two UDMS^E measurements, $\log_2$ fold change ($\log_2$ FC) between biotinylated and non-biotinylated hsV4N Avi wt (control) of each UDMS^E measurement. Bold numbers assign *p*- and $\log_2$ FC values to respective UDMS^E measurement. Manual data curation was performed to determine association of detected proteins with cytosolic ribonucleoprotein (RNP) and/or stress granules (see also figure 4.4). Respective literature is appended (Lit.).

UniProt ID	-$\log_{10}$ (*p*-value) **1**	$\log_2$ FC **1**	-$\log_{10}$ (*p*-value) **2**	$\log_2$ FC **2**	RNP granules	Stress granules	Lit.
TRPV4_HUMAN	6.69	5.59	8.81	4.95	no	no	
ABCD3_HUMAN	2.49	16.10	8.15	11.86	no	no	
ATD3B_HUMAN	6.31	19.30	1.38	11.81	no	no	
COPA_HUMAN	4.36	15.38	1.32	15.73	no	no	
COX5B_HUMAN	4.25	17.66	5.43	8.72	no	no	
DDX3X_HUMAN	4.83	17.06	2.38	13.00	yes	yes	107–109,120,127,200–203
DDX5_HUMAN	2.77	17.53	5.94	14.63	no	yes	107,203,204
DHX9_HUMAN	1.49	15.05	7.22	14.77	yes	yes	108,120
HNRH1_HUMAN	7.02	18.54	6.60	11.31	no	yes	108,200,205
HNRPF_HUMAN	4.35	18.24	6.25	11.34	no	yes	108,205
HNRPM_HUMAN	3.03	18.57	6.27	4.44	no	no	
HNRPU_HUMAN	5.91	18.05	1.75	13.27	yes	yes	108,200,206
IF2B1_HUMAN	2.84	15.38	9.89	12.93	yes	yes	107,108,120,200
PABP1_HUMAN	4.21	16.89	5.45	14.21	yes	yes	107–109,207–209
PACN3_HUMAN	5.85	15.59	4.10	11.90	no	no	
PHB2_HUMAN	5.20	4.12	4.10	5.54	no	no	
PLEC_HUMAN	2.60	18.36	4.23	14.25	no	no	
PRKDC_HUMAN	1.34	18.58	5.88	16.38	no	no	

UniProt ID	-$\log_{10}$ (*p*-value) **1**	$\log_2$ FC **1**	-$\log_{10}$ (*p*-value) **2**	$\log_2$ FC **2**	RNP granules	Stress granules	Lit
RBM14_HUMAN	3.53	17.89	2.74	12.17	no	no	
RL13_HUMAN	2.69	18.92	5.41	14.44	no	no	
RL17_HUMAN	1.56	18.81	5.58	13.53	no	no	
RL24_HUMAN	1.96	18.14	3.18	12.19	no	no	
RL28_HUMAN	6.63	17.41	1.97	13.40	yes	no	[210]
RL35_HUMAN	2.41	16.58	3.39	11.41	no	no	
RL36_HUMAN	1.44	15.75	7.46	11.89	no	no	
ROA2_HUMAN	5.33	17.21	5.69	12.44	yes	yes	[107,108,126,200,206,211]
RS2_HUMAN	2.57	2.05	4.31	4.89	no	no	
RS27A_HUMAN	2.56	18.47	6.68	11.46	no	no	
RS6_HUMAN	2.62	18.19	5.73	5.14	yes	yes	[113,210,212]
RS7_HUMAN	1.81	15.64	5.36	11.97	no	no	
RS8_HUMAN	2.61	18.47	2.53	4.66	no	no	
RT17_HUMAN	6.47	14.91	2.24	10.84	no	no	
SYNE1_HUMAN	1.74	18.41	7.64	4.40	yes	no	[210]
VDAC2_HUMAN	7.64	19.32	3.04	10.64	no	no	
YBOX1_HUMAN	4.72	17.37	8.27	13.50	yes	yes	[107,108,116,120,206,213]

Table 6.4: List of cytoplasmic hRNP granule and stress granule proteins found in the hsV4N protein interactome in the presence of $2\,\mathrm{mM}$ Ca^{2+} determined via UDMS^{E} in this work. *p*-values (Benjamini-Hochberg corrected Student's *t*-test) were determined of the quadruplicates of each of the two UDMS^{E} measurements, $\log_2$ fold change ($\log_2$ FC) between biotinylated and non-biotinylated hsV4N wt Avi (control) of each UDMS^{E} measurement. Bold numbers assign *p*- and $\log_2$ FC values to respective UDMS^{E} measurement. Manual data curation was performed to determine association of detected proteins with cytosolic ribonucleoprotein (RNP) and/or stress granules (see also figure 4.5)

UniProt ID	-$\log_{10}$ (*p*-value) **1**	$\log_2$ FC **1**	-$\log_{10}$ (*p*-value) **2**	$\log_2$ FC **2**	RNP granules	Stress granules	Lit.
TRPV4_HUMAN	4.09	5.22	7.84	4.84	no	no	
ABCD3_HUMAN	2.83	15.59	7.01	12.56	no	no	
ADT2_HUMAN	4.12	2.23	5.92	14.68	no	no	
ATD3A_HUMAN	2.92	3.57	4.01	14.81	no	yes	[107]
DDX3X_HUMAN	4.12	16.08	4.74	12.83	no	yes	[107–109,120,127,200–203]
DDX5_HUMAN	11.47	16.85	3.87	15.03	no	yes	[107,203,204]
DHX9_HUMAN	6.87	14.80	5.64	15.59	yes	yes	[108,120]
EPIPL_HUMAN	5.86	19.97	5.59	16.62	no	no	
HNRH1_HUMAN	5.38	18.46	9.19	11.61	no	yes	[108,200]
HNRPF_HUMAN	3.10	17.89	6.14	11.59	no	yes	[108]
HNRPM_HUMAN	4.38	17.72	4.75	4.66	no	no	
HNRPU_HUMAN	7.60	17.83	2.39	2.35	yes	yes	[108,200,206]
IF2B1_HUMAN	7.88	14.88	2.50	12.83	yes	yes	[107,108,120,200]
KHDR1_HUMAN	6.30	16.40	3.18	11.28	no	yes	[107,124]
KPYM_HUMAN	1.92	2.38	2.32	1.65	no	no	
NFM_HUMAN	10.16	5.63	1.89	3.25	no	no	
NPM_HUMAN	3.49	17.29	3.24	2.55	no	no	
PABP1_HUMAN	2.93	16.51	4.24	14.47	yes	yes	[107–109,207–209]
PACN3_HUMAN	3.80	14.89	3.61	11.80	no	no	
PHB_HUMAN	5.52	19.99	6.46	12.40	no	no	

UniProt ID	-$\log_{10}$ (*p*-value) **1**	$\log_2$ FC **1**	-$\log_{10}$ (*p*-value) **2**	$\log_2$ FC **2**	RNP granules	Stress granules	Lit
PHB2_HUMAN	4.42	3.91	6.45	6.23	no	no	
PLEC_HUMAN	4.01	17.17	3.89	14.02	no	no	
PRKDC_HUMAN	2.43	18.18	4.82	17.27	no	no	
RBM14_HUMAN	5.47	16.65	1.54	12.23	no	no	
RBM8A_HUMAN	2.98	15.49	6.78	12.36	no	no	
RL10_HUMAN	6.07	18.16	7.41	14.58	no	no	
RL11_HUMAN	3.94	2.38	6.05	12.75	no	yes	[108]
RL12_HUMAN	7.93	17.25	7.36	12.75	no	no	
RL13A_HUMAN	4.63	2.11	6.83	12.87	no	no	
RL15_HUMAN	4.99	17.13	3.12	13.58	no	no	
RL17_HUMAN	7.40	17.62	6.28	12.85	no	no	
RL18_HUMAN	3.86	17.85	4.01	13.18	no	no	
RL18A_HUMAN	3.59	1.98	7.71	14.77	no	no	
RL21_HUMAN	1.41	16.53	6.67	13.64	no	no	
RL24_HUMAN	5.33	18.21	7.50	11.93	no	no	
RL27_HUMAN	2.48	16.29	2.96	11.82	no	no	
RL28_HUMAN	5.31	16.46	5.06	13.23	yes	no	[210]
RL3_HUMAN	3.59	1.35	2.75	3.50	no	no	
RL30_HUMAN	1.63	16.97	2.37	4.89	no	no	
RL32_HUMAN	6.36	16.23	6.67	12.51	no	no	
RL34_HUMAN	3.70	3.59	1.87	12.69	no	no	
RL35_HUMAN	3.99	16.07	5.67	8.49	no	no	
RL36_HUMAN	4.11	15.61	7.19	11.17	no	no	
RL36A_HUMAN	2.19	1.22	5.42	12.08	no	no	
RL37A_HUMAN	8.27	17.13	8.85	10.63	no	no	
RL5_HUMAN	1.61	2.81	8.25	14.26	no	no	

UniProt ID	-log$_{10}$ (*p*-value) **1**	log$_2$ FC **1**	-log$_{10}$ (*p*-value) **2**	log$_2$ FC **2**	RNP granules	Stress granules	Lit
RL6_HUMAN	3.60	3.18	6.88	14.93	yes	no	[210]
RL7A_HUMAN	5.69	16.96	3.85	13.91	no	no	
RLA0_HUMAN	4.79	16.54	6.53	12.11	yes	no	[206,214]
ROA2_HUMAN	8.18	17.08	2.05	2.29	yes	yes	[107,108,126,200,206,211]
RS11_HUMAN	4.41	19.00	5.67	10.46	no	no	
RS27A_HUMAN	5.65	17.35	8.03	11.64	no	no	
RS27L_HUMAN	4.80	15.97	2.52	3.21	no	no	
RS4X_HUMAN	6.93	17.79	8.12	13.23	yes	no	[206]
RS6_HUMAN	5.88	17.81	2.69	5.23	yes	yes	[113,210,212]
RS8_HUMAN	9.09	18.15	4.79	4.53	no	no	
RS9_HUMAN	2.51	17.21	4.21	12.63	no	no	
RT17_HUMAN	1.72	14.63	3.27	11.15	no	no	
SYNE1_HUMAN	2.91	18.11	2.85	3.09	yes	no	[210]
TBA3E_HUMAN	4.46	19.93	8.46	14.18	no	no	
TBA4A_HUMAN	4.55	17.05	2.41	3.24	no	yes	[107]
TBB4B_HUMAN	5.07	20.09	3.35	4.00	no	no	
VDAC2_HUMAN	5.26	17.83	6.93	11.54	no	no	
VIME_HUMAN	6.02	3.60	3.37	5.48	no	no	
YBOX1_HUMAN	12.38	17.03	1.50	12.50	yes	yes	[107,108,116,120,206,213]

Table 6.5: List of cytoplasmic hRNP granule and stress granule proteins found in the hsV4 ARD wt protein interactome determined via UDMS^E in this work. *p*-values (Benjamini-Hochberg corrected Student's *t*-test) were determined of the quadruplicates of each of the two UDMS^E measurements, $\log_2$ fold change ($\log_2$ FC) between biotinylated and non-biotinylated hsV4 ARD wt Avi (control) of each UDMS^E measurement. Manual data curation was performed to determine association of detected proteins with cytosolic ribonucleoprotein (RNP) and/or stress granules (see also figure 4.6 A)

UniProt ID	-$\log_{10}$ (*p*-value) **1**	$\log_2$ FC	RNP granules	Stress granules	Lit.
TRPV4_HUMAN	2,13	15,77	no	no	
1433E_HUMAN	8,32	13,01	no	no	
1433T_HUMAN	12,43	13,15	no	no	
ACLY_HUMAN	3,74	1,30	no	no	
AK1A1_HUMAN	17,63	11,13	no	no	
BOLA2_HUMAN	7,94	12,21	no	no	
CAH2_HUMAN	3,41	2,46	no	no	
COPD_HUMAN	6,28	12,09	no	no	
DDX3X_HUMAN	2,13	0,98	no	yes	107–109,120,127,200–203
DNJA1_HUMAN	2,74	1,24	no	yes	107
ENOG_HUMAN	6,00	2,03	no	no	
ERF3A_HUMAN	3,28	11,60	no	no	
GSTP1_HUMAN	2,38	2,36	no	no	
H31T_HUMAN	1,33	1,24	no	no	
HNRH2_HUMAN	10,58	12,40	no	yes	107
HNRPC_HUMAN	2,03	1,35	no	no	
IF2B2_HUMAN	10,69	12,87	yes	yes	107–109,120,204,215
IF4A1_HUMAN	3,16	1,19	no	yes	107,108,216
MDHC_HUMAN	4,61	1,20	no	no	
NONO_HUMAN	3,62	1,28	yes	yes	107,217

UniProt ID	-log$_{10}$ (*p*-value) **1**	log$_2$ FC	Lit.		
NPM_HUMAN	1,93	1,14	no	no	
PEBP1_HUMAN	9,26	11,37	no	no	
POTEE_HUMAN	8,02	12,79	no	no	
POTEJ_HUMAN	7,70	10,43	no	no	
PRDX6_HUMAN	6,73	11,79	no	yes	[107]
PUR6_HUMAN	2,17	1,54	no	no	
PUR9_HUMAN	9,44	11,06	no	no	
RL11_HUMAN	1,92	1,39	no	no	
RL27A_HUMAN	1,37	1,03	no	no	
RL4_HUMAN	1,77	1,22	no	no	
RL5_HUMAN	1,45	1,48	no	no	
ROA2_HUMAN	1,65	0,97	no	yes	[107,108,126,211]
RS13_HUMAN	1,86	1,36	no	no	
SRSF3_HUMAN	1,60	1,02	no	yes	[211]
SRSF8_HUMAN	4,03	1,29	no	no	
TBA4A_HUMAN	4,19	1,04	no	yes	[107,129,130]
TBB4A_HUMAN	6,67	11,30	no	no	
TCPD_HUMAN	5,09	1,61	no	no	
TIAR_HUMAN	7,76	11,87	no	yes	[107–109,205,207,218–220]
UBP2L_HUMAN	1,36	1,38	no	yes	[107–109,221]
YTHD3_HUMAN	2,49	1,28	no	yes	[107–109,222]

Table 6.6: List of cytoplasmic hRNP granule and stress granule proteins found in the hsV4 ARD wt protein interactome in the presence of 2 mM Ca^{2+} determined via $UDMS^E$ in this work. *p*-values (Benjamini-Hochberg corrected Student's *t*-test) were determined of the quadruplicates of each of the two $UDMS^E$ measurements, $\log_2$ fold change ($\log_2$ FC) between biotinylated and non-biotinylated hsV4 ARD wt Avi (control) of each $UDMS^E$ measurement. Manual data curation was performed to determine association of detected proteins with cytosolic ribonucleoprotein (RNP) and/or stress granules (see also figure 4.6 B).

UniProt ID	-$\log_{10}$ (*p*-value)	$\log_2$ FC	RNP granules	Stress granules	Lit.
TRPV4_HUMAN	7,59	15,46	no	no	
1433E_HUMAN	22,08	12,87	no	no	
1433G_HUMAN	4,82	2,04	no	no	
1433T_HUMAN	13,78	11,98	no	no	
ACLY_HUMAN	2,68	1,82	no	no	
AK1A1_HUMAN	6,24	11,36	no	no	
ALDOA_HUMAN	2,14	1,39	no	no	
BOLA2_HUMAN	6,14	13,05	no	no	
CAH2_HUMAN	4,08	2,50	no	no	
COF1_HUMAN	1,69	1,19	no	no	
COF2_HUMAN	2,19	2,08	no	no	
COPD_HUMAN	5,54	12,27	no	no	
DDX1_HUMAN	1,38	0,96	no	yes	[107–109,116]
DDX3X_HUMAN	2,36	1,09	no	yes	[107–109,120,127,200–203]
DDX5_HUMAN	2,14	1,22	yes	yes	[203,204]
DNJA1_HUMAN	2,74	1,24	no	yes	[107]
DNJC7_HUMAN	2,82	1,45	no	no	
DUT_HUMAN	3,92	1,75	no	no	
ENOG_HUMAN	2,27	2,80	no	no	
ENPL_HUMAN	2,04	1,02	no	no	

UniProt ID	-$\log_{10}$ (p-value)	$\log_2$ FC	RNP granule	Stress granules	Lit.
ERF3A_HUMAN	8,27	11,95	no	no	
FKB1A_HUMAN	2,36	2,19	no	no	
G3BP1_HUMAN	3,06	1,93	no	yes	107–109,123,126,135,204,205,211,223
G3BP2_HUMAN	1,52	1,22	no	yes	223,224
GSTP1_HUMAN	2,90	2,32	no	no	
H31T_HUMAN	1,64	0,97	no	no	
HNRH2_HUMAN	5,55	12,90	no	yes	107
HNRPF_HUMAN	1,63	1,13	no	yes	108
HNRPM_HUMAN	1,54	1,08	no	yes	108
HS90A_HUMAN	1,04	1,50	no	no	
HSP76_HUMAN	3,27	1,28	no	no	
IF2B_HUMAN	2,66	1,85	no	yes	107
IF2B2_HUMAN	11,80	14,12	yes	yes	107–109,120,204,215
IF4A1_HUMAN	1,74	3,65	no	yes	107,108,205,216
IF4G2_HUMAN	1,86	0,96	no	yes	107,109
IF5A2_HUMAN	1,54	1,14	no	yes	225
KCD12_HUMAN	2,71	1,31	no	no	
LC7L2_HUMAN	1,13	1,00	no	no	
LDHA_HUMAN	2,77	1,60	no	no	
LDHB_HUMAN	2,26	1,48	no	no	
MDHC_HUMAN	3,07	1,89	no	no	
NONO_HUMAN	2,67	1,76	yes	yes	107,217
NPM_HUMAN	3,15	1,62	no	no	
NUCL_HUMAN	1,73	1,15	no	no	
PABP1_HUMAN	1,92	1,15	no	yes	107–109,127,202,226
PABP4_HUMAN	1,30	1,01	no	no	

UniProt ID	-$\log_{10}$ (*p*-value)	$\log_2$ FC	RNP granule	Stress granules	Lit.
PDIA3_HUMAN	1,67	1,75	no	yes	[108]
PEBP1_HUMAN	10,73	11,94	no	no	
POTEE_HUMAN	13,55	13,94	no	no	
POTEJ_HUMAN	11,06	11,50	no	no	
PRDX1_HUMAN	2,66	1,21	no	yes	[107,108]
PRDX2_HUMAN	11,42	13,82	no	no	
PRDX6_HUMAN	5,10	12,41	no	yes	[107]
PTBP1_HUMAN	2,05	1,45	no	no	
PUR6_HUMAN	3,35	2,40	no	no	
PUR9_HUMAN	15,84	11,19	no	no	
RAN_HUMAN	1,69	1,22	no	no	
RBM39_HUMAN	0,91	0,83	no	no	
RL11_HUMAN	4,04	1,58	no	no	
RL12_HUMAN	2,51	1,19	no	no	
RL13_HUMAN	2,62	1,12	no	no	
RL15_HUMAN	2,66	1,24	no	no	
RL18A_HUMAN	2,61	1,31	no	no	
RL21_HUMAN	3,30	1,38	no	no	
RL23A_HUMAN	3,20	1,24	no	no	
RL27A_HUMAN	1,65	0,95	no	no	
RL28_HUMAN	2,12	1,49	no	no	
RL3_HUMAN	4,54	1,62	no	no	
RL34_HUMAN	1,61	1,22	no	no	
RL36L_HUMAN	4,02	2,06	no	no	
RL37A_HUMAN	3,38	1,37	no	no	
RL4_HUMAN	5,13	1,61	no	no	

UniProt ID	-log$_{10}$ (*p*-value)	log$_2$ FC	RNP granule	Stress granules	Lit.
RL5_HUMAN	4,83	1,88	no	no	
RL6_HUMAN	2,00	1,10	no	no	
RL7A_HUMAN	2,42	1,29	no	no	
RLA0L_HUMAN	3,55	1,54	no	no	
ROA1_HUMAN	2,99	1,10	no	yes	[107,108,219]
RS11_HUMAN	3,84	1,45	no	no	
RS13_HUMAN	3,88	1,63	no	no	
RS15A_HUMAN	7,06	2,12	no	no	
RS20_HUMAN	1,67	1,24	no	no	
RS21_HUMAN	1,98	1,02	no	no	
RS23_HUMAN	1,48	1,38	no	no	
RS28_HUMAN	1,54	1,10	no	no	
RS30_HUMAN	3,49	1,19	no	no	
RS5_HUMAN	4,20	1,35	no	no	
RS6_HUMAN	1,24	0,91	no	no	
SRSF3_HUMAN	1,84	0,87	no	yes	[211]
SRSF8_HUMAN	4,38	1,70	no	no	
TAGL2_HUMAN	2,92	1,25	no	no	
TBB3_HUMAN	2,23	1,92	no	yes	[107]
TBB4A_HUMAN	5,94	10,47	no	no	
TBB6_HUMAN	1,73	1,49	no	no	
TCPA_HUMAN	2,21	1,72	no	no	
TCPB_HUMAN	2,17	1,37	no	no	
TCPD_HUMAN	3,32	1,75	no	no	
TCPG_HUMAN	3,53	1,82	no	no	
TCPH_HUMAN	1,94	1,29	no	no	

UniProt ID	-log$_{10}$ (*p*-value)	log$_2$ FC	RNP granule	Stress granules	Lit.
TCPZ_HUMAN	4,15	1,61	no	no	
TEBP_HUMAN	4,49	1,80	no	no	
TIAR_HUMAN	6,73	12,86	no	yes	[107–109,205,207,218–220]
TPIS_HUMAN	2,68	1,71	no	no	
U2AF2_HUMAN	5,17	13,73	no	yes	[107]
UBP2L_HUMAN	5,60	1,71	no	yes	[107–109,205,221]

Table 6.7: List of cytoplasmic hRNP granule and stress granule proteins found in the hsV4 ARD R232C protein interactome determined via UDMS^E in this work. *p*-values (Benjamini-Hochberg corrected Student's *t*-test) were determined of the quadruplicates of each of the two UDMS^E measurements, $\log_2$ fold change ($\log_2$ FC) between biotinylated and non-biotinylated hsV4 ARD wt Avi (control) of each UDMS^E measurement. Manual data curation was performed to determine association of detected proteins with cytosolic ribonucleoprotein (RNP) and/or stress granules (see also figure 4.6 C).

UniProt ID	-$\log_{10}$ (*p*-value)	$\log_2$ FC	RNP granules	Stress granules	Lit.
TRPV4_HUMAN	11,53	17,45	no	no	
1433F_HUMAN	1,33	1,18	no	no	
DDX3X_HUMAN	5,06	2,18	no	yes	107–109,120,127,200–203
IF4A3_HUMAN	10,43	11,91	no	yes	108
NONO_HUMAN	2,01	2,05	yes	yes	107,217
POTEJ_HUMAN	1,42	5,94	no	no	
RL11_HUMAN	3,27	1,38	no	no	
RL3_HUMAN	1,74	1,49	no	no	
RL35A_HUMAN	2,93	1,51	no	no	
RLA0_HUMAN	1,37	1,01	no	no	
RS15A_HUMAN	2,22	1,12	no	no	
RS6_HUMAN	1,48	1,05	no	no	
SFPQ_HUMAN	3,65	1,92	no	yes	107,217
SRSF7_HUMAN	1,49	1,38	no	yes	227
U2AF2_HUMAN	2,55	1,58	no	yes	107

Table 6.8: List of cytoplasmic hRNP granule and stress granule proteins found in the hsV4 ARD R232C protein interactome in the presence of 2 mM Ca^{2+} determined via $UDMS^E$ in this work. *p*-values (Benjamini-Hochberg corrected Student's *t*-test) were determined of the quadruplicates of each of the two $UDMS^E$ measurements, $\log_2$ fold change ($\log_2$ FC) between biotinylated and non-biotinylated hsV4 ARD wt Avi (control) of each $UDMS^E$ measurement. Manual data curation was performed to determine association of detected proteins with cytosolic ribonucleoprotein (RNP) and/or stress granules (see also figure 4.6 C).

UniProt ID	-$\log_{10}$ (*p*-value)	$\log_2$ FC	RNP granules	Stress granules	Lit.
TRPV4_HUMAN	4,89	18,44	no	no	
1433F_HUMAN	3,02	1,98	no	no	
DDX17_HUMAN	3,17	1,73	no	yes	[204]
DDX3X_HUMAN	6,12	2,94	no	yes	[107–109,120,127,200–203]
IF2B_HUMAN	2,19	1,49	no	yes	[107]
IF4A3_HUMAN	2,94	12,58	no	yes	[108]
KCD12_HUMAN	1,63	1,47	no	no	
NONO_HUMAN	4,48	2,45	yes	yes	[107,217]
POTEE_HUMAN	3,80	4,40	no	no	
POTEJ_HUMAN	4,74	6,57	no	no	
RL11_HUMAN	3,36	2,19	no	no	
RL12_HUMAN	2,41	1,56	no	no	
RL13_HUMAN	1,34	1,64	no	no	
RL15_HUMAN	4,91	1,99	no	no	
RL18A_HUMAN	1,63	2,13	no	no	
RL24_HUMAN	1,72	1,83	no	no	
RL29_HUMAN	4,07	1,83	no	no	
RL3_HUMAN	3,57	2,42	no	no	
RL34_HUMAN	3,07	2,04	no	no	
RL37A_HUMAN	5,22	2,03	no	no	

UniProt ID	-$\log_{10}$ (p-value)	$\log_2$ FC	RNP granule	Stress granules	Lit.
RL4_HUMAN	2,02	2,38	no	no	
RL5_HUMAN	2,31	2,34	no	no	
RL6_HUMAN	1,64	1,91			
RL7A_HUMAN	1,62	1,95	no	no	
ROA1_HUMAN	2,89	1,90	no	yes	[107,108,219]
ROA2_HUMAN	1,38	1,43	no	yes	[107,108,126,211]
RS13_HUMAN	2,99	1,75	no	no	
RS15A_HUMAN	4,13	1,79	no	no	
RS2_HUMAN	1,31	1,34	no	no	
RS20_HUMAN	2,06	1,56	no	no	
RS26L_HUMAN	1,71	1,96	no	no	
RS6_HUMAN	1,52	2,17	no	no	
RUVB1_HUMAN	2,12	1,62	no	no	
SFPQ_HUMAN	4,23	2,37	no	yes	[107,217]
SRSF2_HUMAN	2,44	2,68	no	no	
SRSF3_HUMAN	2,80	1,66	no	yes	[211]
SRSF7_HUMAN	4,13	3,02	no	yes	[227]
TCPG_HUMAN	1,81	1,48	no	no	

Table 6.9: List of cytoplasmic hRNP granule and stress granule proteins found in the hsV4 ARD K276E protein interactome determined via UDMS^{E} in this work. *p*-values (Benjamini-Hochberg corrected Student's *t*-test) were determined of the quadruplicates of each of the two UDMS^{E} measurements, $\log_2$ fold change ($\log_2$ FC) between biotinylated and non-biotinylated hsV4 ARD wt Avi (control) of each UDMS^{E} measurement. Manual data curation was performed to determine association of detected proteins with cytosolic ribonucleoprotein (RNP) and/or stress granules (see also figure 4.6 C).

UniProt ID	-$\log_{10}$ (*p*-value)	$\log_2$ FC	RNP granules	Stress granules	Lit.
TRPV4_HUMAN	3,53	7,08	no	no	
1433B_HUMAN	5,12	12,38	no	no	
1433G_HUMAN	1,41	1,66	no	no	
ACTBL_HUMAN	7,69	12,25	no	no	
ACTS_HUMAN	5,49	13,82	no	no	
AK1A1_HUMAN	3,91	12,76	no	no	
ANXA5_HUMAN	6,41	12,13	no	no	
BOLA2_HUMAN	1,56	1,10	no	no	
CAPR1_HUMAN	4,12	1,70	no	no	
DDX1_HUMAN	1,73	0,98	no	yes	107–109,116
DDX17_HUMAN	3,21	1,37	no	yes	204
DDX3X_HUMAN	7,16	2,41	no	yes	107–109,120,127,200–203
DDX5_HUMAN	2,55	1,09	yes	yes	203,204
DNJA1_HUMAN	2,86	0,93	no	yes	107
ENSA_HUMAN	3,33	13,13	no	no	
FKB1A_HUMAN	1,74	1,41	no	no	
G3BP1_HUMAN	1,62	1,31	no	yes	107–109,123,126,135,204,205,211,223
G3BP2_HUMAN	3,10	2,41	no	yes	223,224
GGYF2_HUMAN	2,53	1,26	no	no	
HAP28_HUMAN	2,79	1,76	no	no	

UniProt ID	-log$_{10}$ (*p*-value)	log$_2$ FC	RNP granule	Stress granules	Lit.
HNRPU_HUMAN	1,94	1,23	yes	yes	[108,200,206]
HS71A_HUMAN	0,06	1,10	no	no	
HS74L_HUMAN	3,66	11,83	no	no	
HS904_HUMAN	6,04	12,64	no	no	
HSP72_HUMAN	4,49	2,04	no	no	
IF2B2_HUMAN	10,10	13,62	yes	yes	[107–109,120,204,215]
IF4A2_HUMAN	7,57	15,63	no	yes	[228]
IF4A3_HUMAN	3,23	3,69	no	yes	[108]
JUPI2_HUMAN	1,86	0,68	no	no	
KHDR1_HUMAN	5,59	2,13	no	yes	[107,124]
KR111_HUMAN	4,76	14,13	no	no	
LKHA4_HUMAN	5,22	1,72	no	no	
MDHC_HUMAN	1,90	1,38	no	no	
MDHM_HUMAN	9,21	12,11	no	no	
METK2_HUMAN	2,32	1,03	no	no	
MOES_HUMAN	1,35	1,16	no	no	
NOLC1_HUMAN	3,00	0,90	no	yes	[108]
NONO_HUMAN	5,42	1,97	yes	yes	[107,217]
NUCL_HUMAN	1,36	1,58	no	no	
NUDC_HUMAN	3,48	0,01	no	yes	[107]
PAL4A_HUMAN	1,69	2,65	no	no	
PAP1L_HUMAN	1,51	0,95	no	no	
PEBP1_HUMAN	4,28	2,25	no	no	
POTEF_HUMAN	1,79	1,63	no	no	
PRDX4_HUMAN	2,55	1,23	no	no	
PRDX6_HUMAN	4,31	12,78	no	yes	[107]

UniProt ID	-$\log_{10}$ (*p*-value)	$\log_2$ FC	RNP granule	Stress granules	Lit.
PUR9_HUMAN	5,26	2,02	no	no	
RBM14_HUMAN	1,28	0,92	no	no	
RBM39_HUMAN	1,34	0,75	no	no	
RBM4_HUMAN	2,29	1,07	no	no	
RL10A_HUMAN	2,30	1,95	no	no	
RL11_HUMAN	5,22	1,88	no	no	
RL12_HUMAN	1,70	0,97	no	no	
RL13_HUMAN	2,79	1,56	no	no	
RL15_HUMAN	4,42	1,63	no	no	
RL18_HUMAN	1,49	2,37	no	no	
RL18A_HUMAN	2,60	1,81	no	no	
RL19_HUMAN	3,16	1,82	no	no	
RL24_HUMAN	3,06	1,74	no	no	
RL27_HUMAN	1,58	1,94	no	no	
RL28_HUMAN	3,24	2,15	no	no	
RL29_HUMAN	2,91	1,14	no	no	
RL3_HUMAN	4,03	2,08	no	no	
RL34_HUMAN	3,00	1,72	no	no	
RL35A_HUMAN	2,70	1,47	no	no	
RL36_HUMAN	2,28	1,62	no	no	
RL36A_HUMAN	3,13	1,81	no	no	
RL36L_HUMAN	4,07	1,76	no	no	
RL4_HUMAN	4,62	1,95	no	no	
RL5_HUMAN	3,94	1,72	no	no	
RL6_HUMAN	2,81	1,32	no	no	
RL7_HUMAN	3,39	13,95	no	no	

UniProt ID	-$\log_{10}$ (p-value)	$\log_2$ FC	RNP granule	Stress granules	Lit.
RL7A_HUMAN	3,26	1,45	no	no	
RL8_HUMAN	1,37	1,20	no	no	
RLA0L_HUMAN	2,37	1,92	no	no	
RMXL1_HUMAN	7,10	12,71	no	no	
ROA1_HUMAN	4,19	1,80	no	yes	[107,108,219]
ROA2_HUMAN	2,09	1,44	no	yes	[107,108,219]
RS11_HUMAN	2,05	1,51	no	no	
RS12_HUMAN	7,86	1,93	no	no	
RS13_HUMAN	3,94	1,48	no	no	
RS15A_HUMAN	3,35	1,29	no	no	
RS16_HUMAN	1,55	1,14	no	no	
RS17_HUMAN	2,09	1,44	no	no	
RS19_HUMAN	1,67	1,92	no	no	
RS20_HUMAN	2,13	1,45	no	no	
RS23_HUMAN	3,59	1,80	no	no	
RS24_HUMAN	1,47	1,40	no	no	
RS26L_HUMAN	2,26	1,43	no	no	
RS3_HUMAN	2,99	1,40	no	no	
RS30_HUMAN	3,81	1,70	no	no	
RS3A_HUMAN	2,19	1,48	no	no	
RS4X_HUMAN	1,39	0,84	no	no	
RS5_HUMAN	2,83	1,43	no	no	
RS6_HUMAN	2,50	2,01	no	no	
RS7_HUMAN	2,99	1,47	no	no	
RS8_HUMAN	2,25	1,47	no	no	
RS9_HUMAN	2,56	1,32	no	no	

UniProt ID	-$\log_{10}$ (*p*-value)	$\log_2$ FC	RNP granule	Stress granules	Lit.
RUVB2_HUMAN	1,54	1,90	no	no	
SFPQ_HUMAN	3,76	1,61	no	yes	[107,217]
SRP09_HUMAN	1,98	2,02	no	no	
SRSF1_HUMAN	3,40	1,95	no	no	
SRSF3_HUMAN	1,95	1,09	no	yes	[211]
SRSF6_HUMAN	3,63	2,00	no	no	
SRSF7_HUMAN	4,73	2,40	no	yes	[227]
STAU1_HUMAN	1,58	0,93	no	yes	[207]
STK26_HUMAN	2,82	0,44	no	no	
SYNC_HUMAN	2,88	13,32	no	no	
TBB2B_HUMAN	5,59	2,16	no	no	
TBB6_HUMAN	1,82	1,11	no	no	
TERA_HUMAN	2,78	2,18	no	no	
TR150_HUMAN	3,15	2,90	no	no	
U2AF1_HUMAN	5,87	1,76	no	yes	[107]
U2AF2_HUMAN	8,24	3,79	no	no	

Table 6.10: List of cytoplasmic hRNP granule and stress granule proteins found in the hsV4 ARD K276E protein interactome in the presence of 2 mM Ca^{2+} determined via $UDMS^E$ in this work. *p*-values (Benjamini-Hochberg corrected Student's *t*-test) were determined of the quadruplicates of each of the two $UDMS^E$ measurements, $\log_2$ fold change ($\log_2$ FC) between biotinylated and non-biotinylated hsV4 ARD wt Avi (control) of each $UDMS^E$ measurement. Manual data curation was performed to determine association of detected proteins with cytosolic ribonucleoprotein (RNP) and/or stress granules (see also figure 4.6 C).

UniProt ID	-$\log_{10}$ (*p*-value)	$\log_2$ FC	RNP granules	Stress granules	Lit.
TRPV4_HUMAN	12,31	6,54	no	no	
ACLY_HUMAN	2,08	0,85	no	no	
AK1A1_HUMAN	9,88	12,05	no	no	
CAH2_HUMAN	4,39	1,19	no	no	
DDX17_HUMAN	4,46	1,40	no	yes	204
DDX3X_HUMAN	8,77	2,58	no	yes	107–109,120,127,200–203
DDX5_HUMAN	3,01	1,19	yes	yes	203,204
DNJA1_HUMAN	2,41	0,90	no	yes	107
ENOG_HUMAN	3,68	1,70	no	no	
G3BP1_HUMAN	1,53	0,95	no	yes	107–109,123,126,135,204,205,211,223
G3BP2_HUMAN	4,44	2,67	no	yes	223,224
GSTP1_HUMAN	1,50	1,05	no	no	
HNRPU_HUMAN	2,70	0,92	yes	yes	108,200,206
IF2B2_HUMAN	9,62	13,81	yes	yes	107–109,120,204,215
IF4A2_HUMAN	11,20	14,24	no	yes	228
IF4A3_HUMAN	6,41	2,94	no	yes	108
IF4B_HUMAN	1,63	0,94	no	yes	107,108,205
KCRB_HUMAN	3,11	1,32	no	no	
KHDR1_HUMAN	5,13	2,33	no	yes	107,124
LARP1_HUMAN	1,57	0,94	no	yes	107

UniProt ID	-$\log_{10}$ (*p*-value)	$\log_2$ FC	RNP granules	Stress granules	Lit.
LDHA_HUMAN	1,53	1,02	no	no	
NPM_HUMAN	1,20	1,13	no	no	
NUCL_HUMAN	2,76	1,09	no	no	
PABP4_HUMAN	1,49	0,84	no	yes	[107–109]
PAL4A_HUMAN	2,95	2,17	no	no	
PAP1L_HUMAN	2,73	1,01	no	no	
PGK1_HUMAN	2,99	1,06	no	no	
POTEF_HUMAN	2,18	1,21	no	no	
PRDX6_HUMAN	7,42	12,63	no	yes	[107]
PUR9_HUMAN	2,78	1,30	no	no	
RBM39_HUMAN	2,78	1,11	no	no	
RBM4_HUMAN	1,46	0,94	no	no	
RCC2_HUMAN	4,46	13,25	no	no	
RL10A_HUMAN	2,79	1,43	no	no	
RL11_HUMAN	5,27	1,89	no	no	
RL13_HUMAN	4,57	1,46	no	no	
RL15_HUMAN	4,64	1,47	no	no	
RL18_HUMAN	4,07	1,64	no	no	
RL18A_HUMAN	4,58	1,59	no	no	
RL19_HUMAN	5,36	1,68	no	no	
RL23A_HUMAN	1,02	0,75	no	no	
RL27_HUMAN	5,24	1,67	no	no	
RL28_HUMAN	5,55	2,00	no	no	
RL3_HUMAN	6,66	2,00	no	no	
RL35A_HUMAN	4,43	1,42	no	no	
RL36_HUMAN	4,32	1,63	no	no	

UniProt ID	-$\log_{10}$ (*p*-value)	$\log_2$ FC	RNP granules	Stress granules	Lit.
RL4_HUMAN	5,76	1,80	no	no	
RL5_HUMAN	4,90	1,75	no	no	
RL6_HUMAN	2,80	1,15	no	no	
RL7_HUMAN	8,39	13,76	no	no	
RLA0L_HUMAN	6,38	1,68	no	no	
RMXL1_HUMAN	8,49	12,60	no	no	
ROA1_HUMAN	5,32	1,57	no	yes	[107,108,219]
ROA2_HUMAN	5,20	1,56	no	yes	[107,108,219]
RS12_HUMAN	4,81	1,74	no	no	
RS13_HUMAN	5,45	1,57	no	no	
RS15A_HUMAN	5,70	1,66	no	no	
RS16_HUMAN	2,59	1,08	no	no	
RS19_HUMAN	2,57	1,17	no	no	
RS23_HUMAN	5,48	1,91	no	no	
RS24_HUMAN	3,12	1,64	no	no	
RS25_HUMAN	2,79	1,68	no	no	
RS26L_HUMAN	3,49	1,68	no	no	
RS27_HUMAN	1,45	1,67	no	no	
RS3A_HUMAN	2,98	1,23	no	no	
RS4X_HUMAN	2,43	1,00	no	no	
RS5_HUMAN	2,92	1,28	no	no	
RS7_HUMAN	3,80	1,38	no	no	
RS8_HUMAN	3,18	1,22	no	no	
RS9_HUMAN	3,51	1,29	no	no	
RUVB2_HUMAN	2,57	1,09	no	no	
SFPQ_HUMAN	6,76	1,77	no	yes	[107,217]

UniProt ID	-$\log_{10}$ (p-value)	$\log_2$ FC	RNP granules	Stress granules	Lit.
SRP09_HUMAN	2,09	1,48	no	no	
SRSF1_HUMAN	3,07	1,37	no	no	
SRSF2_HUMAN	2,79	1,23	no	no	
SRSF3_HUMAN	2,75	1,11	no	yes	[211]
SRSF6_HUMAN	5,30	2,11	no	no	
STAU1_HUMAN	2,51	1,15	no	no	
SYEP_HUMAN	1,99	0,89	no	no	
SYNC_HUMAN	9,01	12,25	no	no	
TCPG_HUMAN	2,40	0,94	no	no	
TERA_HUMAN	2,83	1,42	no	no	
THIO_HUMAN	1,91	0,90	no	no	
TR150_HUMAN	4,04	2,86	no	no	
TRFL_HUMAN	1,58	1,26	no	no	
UBP2L_HUMAN	1,62	0,69	no	yes	[107–109,205,221]
YBOX1_HUMAN	1,78	0,96	yes	yes	[107,108,116,120,206,213]

6.4 Appendix - The interaction between the two protean proteins TRPV4 and DDX3X

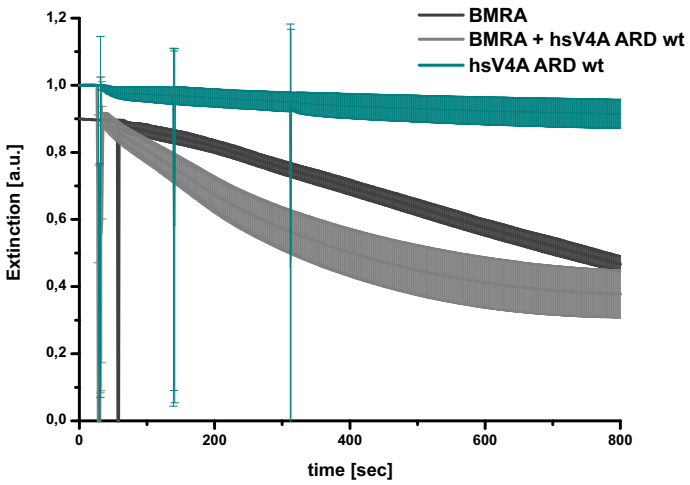

Figure 6.3: **hsV4 ARD does not influence or inhibit the assay components lactate dehydrogenase and pyruvate kinase**. As a control for the ATPase experiments shown in section 4.2, figures 4.9 and 4.13, the well-characterized *B. subtilis* ATPase BmrA was also supplemented with hsV4 ARD to rule out unspecific effects of hsV4 ARD on the lactate dehydrogenase and pyruvate kinase used in this assay. No decrease in BmrA ATPase activity was observed upon hsV4 ARD wt supplementation. Furthermore, hsV4 ARD alone did not show ATPase activity. BmrA was kindly provided by M. Sc. [redacted]

6.5 Appendix - An *in cellulo* study of the interaction between human TRPV4 and PACSIN1-3

Sequence alignment between rat and human TRPV4 performed with ClustalW.[2]

```
sp|Q9HBA0|TRPV4_HUMAN      MADSSEGPRAGPGEVAELPGDESGTPGGEAFPLSSLANLFEGEDGSLSPSPADASRPAGP 60
sp|Q9ERZ8|TRPV4_RAT        MADPGDGPRAAPGDVAEPPGDESGTSGGEAFPLSSLANLFEGEEGSSSLSPVDASRPAGP 60
                           *** .:****.**:*** ******* *****************:** * **.********

sp|Q9HBA0|TRPV4_HUMAN      GDGRPNLRMKFQGAFRKGVPNPIDLLESTLYESSVVPGPKKAPMDSLFDYGTYRHHSSDN 120
sp|Q9ERZ8|TRPV4_RAT        GDGRPNLRMKFQGAFRKGVPNPIDLLESTLYESSVVPGPKKAPMDSLFDYGTYRHHPSDN 120
                           ************************************************************ ***

sp|Q9HBA0|TRPV4_HUMAN      KRWRKKIIEKQPQSPKAPAPQPPPILKVFNRPILFDIVSRGSTADLDGLLPFLLTHKKRL 180
sp|Q9ERZ8|TRPV4_RAT        KRWRRKVVEKQPQSPKAPAPQPPPILKVFNRPILFDIVSRGSTADLDGLLSYLLTHKKRL 180
                           ****:*::*****************************************  :********

sp|Q9HBA0|TRPV4_HUMAN      TDEEFREPSTGKTCLPKALLNLSNGRNDTIPVLLDIAERTGNMREFINSPFRDIYYRGQT 240
sp|Q9ERZ8|TRPV4_RAT        TDEEFREPSTGKTCLPKALLNLSNGRNDTIPVLLDIAERTGNMREFINSPFRDIYYRGQT 240
                           ************************************************************

sp|Q9HBA0|TRPV4_HUMAN      ALHIAIERRCKHYVELLVAQGADVHAQARGRFFQPKDEGGYFYFGELPLSLAACTNQPHI 300
sp|Q9ERZ8|TRPV4_RAT        ALHIAIERRCKHYVELLVAQGADVHAQARGRFFQPKDEGGYFYFGELPLSLAACTNQPHI 300
                           ************************************************************

sp|Q9HBA0|TRPV4_HUMAN      VNYLTENPHKKADMRRQDSRGNTVLHALVAIADNTRENTKFVTKMYDLLLLKCARLFPDS 360
sp|Q9ERZ8|TRPV4_RAT        VNYLTENPHKKADMRRQDSRGNTVLHALVAIADNTRENTKFVTKMYDLLLLKCSRLFPDS 360
                           ************************************************:******

sp|Q9HBA0|TRPV4_HUMAN      NLEAVLNNDGLSPLMMAAKTGKIGIFQHIIRREVTDEDTRHLSRKFKDWAYGPVYSSLYD 420
sp|Q9ERZ8|TRPV4_RAT        NLETVLNNDGLSPLMMAAKTGKIGVFQHIIRREVTDEDTRHLSRKFKDWAYGPVYSSLYD 420
                           ***:*******************:***********************************

sp|Q9HBA0|TRPV4_HUMAN      LSSLDTCGEEASVLEILVYNSKIENRHEMLAVEPINELLRDKWRKFGAVSFYINVVSYLC 480
sp|Q9ERZ8|TRPV4_RAT        LSSLDTCGEEVSVLEILVYNSKIENRHEMLAVEPINELLRDKWRKFGAVSFYINVVSYLC 480
                           **********.************************************************

sp|Q9HBA0|TRPV4_HUMAN      AMVIFTLTAYYQPLEGTPPYPYRTTVDYLRLAGEVITLFTGVLFFFTNIKDLFMKKCPGV 540
sp|Q9ERZ8|TRPV4_RAT        AMVIFTLTAYYQPLEGTPPYPYRTTVDYLRLAGEVITLLTGVLFFFTSIKDLFMKKCPGV 540
                           ************************************:********.************

sp|Q9HBA0|TRPV4_HUMAN      NSLFIDGSFQLLYFIYSVLVIVSAALYLAGIEAYLAVMVFALVLGWMNALYFTRGLKLTG 600
sp|Q9ERZ8|TRPV4_RAT        NSLFVDGSFQLLYFIYSVLVVVSAALYLAGIEAYLAVMVFALVLGWMNALYFTRGLKLTG 600
                           ****:***************:****************************************

sp|Q9HBA0|TRPV4_HUMAN      TYSIMIQKILFKDLFRFLLVYLLFMIGYASALVSLLNPCANMKVCNEDQTNCTVPTYPSC 660
sp|Q9ERZ8|TRPV4_RAT        TYSIMIQKILFKDLFRFLLVYLLFMIGYASALVTLLNPCTNMKVCNEDQSNCTVPSYPAC 660
```

```
                         **********************************:*****:*********:*****:**:*

sp|Q9HBA0|TRPV4_HUMAN      RDSETFSTFLLDLFKLTIGMGDLEMLSSTKYPVVFIILLVTYIILTFVLLLNMLIALMGE 720
sp|Q9ERZ8|TRPV4_RAT        RDSETFSAFLLDLFKLTIGMGDLEMLSSAKYPVVFILLLVTYIILTFVLLLNMLIALMGE 720
                         *******:********************:*******:************************

sp|Q9HBA0|TRPV4_HUMAN      TVGQVSKESKHIWKLQWATTILDIERSFPVFLRKAFRSGEMVTVGKSSDGTPDRRWCFRV 780
sp|Q9ERZ8|TRPV4_RAT        TVGQVSKESKHIWKLQWATTILDIERSFPVFLRKAFRSGEMVTVGKSSDGTPDRRWCFRV 780
                         ************************************************************

sp|Q9HBA0|TRPV4_HUMAN      DEVNWSHWNQNLGIINEDPGKNETYQYYGFSHTVGRLRRDRWSSVVPRVVELNKNSNPDE 840
sp|Q9ERZ8|TRPV4_RAT        DEVNWSHWNQNLGIINEDPGKSEIYQYYGFSHTMGRLRRDRWSSVVPRVVELNKNSGTDE 840
                         ********************.* *********:**********************. **

sp|Q9HBA0|TRPV4_HUMAN      VVVPLDSMGNPRCDGHQQGYPRKWRTDDAPL 871
sp|Q9ERZ8|TRPV4_RAT        VVVPLDNLGNPNCDGHQQGYAPKWRAEDAPL 871
                         ******.:***.********  ***::****

Percent Identity  Matrix
1: sp|Q9HBA0|TRPV4_HUMAN  100.00   94.83
2: sp|Q9ERZ8|TRPV4_RAT     94.83  100.00
```

Sequence alignment between mouse and human PACSIN orthologues performed with ClustalW.[2]

```
sp|Q9BY11|PACN1_HUMAN      MSSSYDEASLAPEETTDSFWEVGNYKRTVKRIDDGHRLCNDLMNCVQERAKIEKAYGQQL 60
sp|Q61644|PACN1_MOUSE      MSGSYDEA---SEEITDSFWEVGNYKRTVKRIDDGHRLCNDLMSCVQERAKIEKAYAQQL 57
                         **.*****    ** ****************************.************.***

sp|Q9BY11|PACN1_HUMAN      TDWAKRWRQLIEKGPQYGSLERAWGAIMTEADKVSELHQEVKNNLLNEDLEKVKNWQKDA 120
sp|Q61644|PACN1_MOUSE      TDWAKRWRQLIEKGPQYGSLERAWGAMMTEADKVSELHQEVKNSLLNEDLEKVKNWQKDA 117
                         *************************:***************.****************

sp|Q9BY11|PACN1_HUMAN      YHKQIMGGFKETKEAEDGFRKAQKPWAKKMKELEAAKKAYHLACKEEKLAMTREMNSKTE 180
sp|Q61644|PACN1_MOUSE      YHKQIMGGFKETKEAEDGFRKAQKPWAKKMKELEAAKKAYHLACKEERLAMTREMNSKTE 177
                         ************************************************:************

sp|Q9BY11|PACN1_HUMAN      QSVTPEQQKKLQDKVDKCKQDVQKTQEKYEKVLEDVGKTTPQYMENMEQVFEQCQQFEEK 240
sp|Q61644|PACN1_MOUSE      QSVTPEQQKKLVDKVDKCRQDVQKTQEKYEKVLEDVGKTTPQYMEGMEQVFEQCQQFEEK 237
                         *********** ******:**************************.**************

sp|Q9BY11|PACN1_HUMAN      RLVFLKEVLLDIKRHLNLAENSSYIHVYRELEQAIRGADAQEDLRWFRSTSGPGMPMNWP 300
sp|Q61644|PACN1_MOUSE      RLVFLKEVLLDIKRHLNLAENSSYMHVYRELEQAIRGADAQEDLRWFRSTSGPGMPMNWP 297
                         ************************:***********************************

sp|Q9BY11|PACN1_HUMAN      QFEEWNPDLPHTTTKKEKQPKKAEGVALTNATGAVESTSQAGDRGSVSSYDRGQPYATEW 360
sp|Q61644|PACN1_MOUSE      QFEEWNPDLPHTTAKKEKQPKKAEGATLSNATGAVESTSQAGDRGSVSSYDRGQTYATEW 357
                         *************:***********.:*:************************* *****
```

```
sp|Q9BY11|PACN1_HUMAN      SDDESGNPFGGSETNGGANPFEDDSKGVRVRALYDYDGQEQDELSFKAGDELTKLGEEDE 420
sp|Q61644|PACN1_MOUSE      SDDESGNPFGGNEANGGANPFEDDAKGVRVRALYDYDGQEQDELSFKAGDELTKLGEEDE 417
                           ***********.*:**********:************************************

sp|Q9BY11|PACN1_HUMAN      QGWCRGRLDSGQLGLYPANYVEAI 444
sp|Q61644|PACN1_MOUSE      QGWCRGRLDSGQLGLYPANYVEAI 441
                           ************************

Percent Identity  Matrix
1: sp|Q9BY11|PACN1_HUMAN  100.00   95.46
2: sp|Q61644|PACN1_MOUSE   95.46  100.00



sp|Q9UNF0|PACN2_HUMAN      MSVTYDDSVGVEVSSDSFWEVGNYKRTVKRIDDGHRLCSDLMNCLHERARIEKAYAQQLT 60
sp|Q9WVE8|PACN2_MOUSE      MSVTYDDSVGVEVSSDSFWEVGNYKRTVKRIDDGHRLCGDLMNCLHERARIEKAYAQQLT 60
                           ************************************.**********************

sp|Q9UNF0|PACN2_HUMAN      EWARRWRQLVEKGPQYGTVEKAWMAFMSEAERVSELHLEVKASLMNDDFEKIKNWQKEAF 120
sp|Q9WVE8|PACN2_MOUSE      EWARRWRQLVEKGPQYGTVEKAWIAVMSEAERVSELHLEVKASLMNEDFEKIKNWQKEAF 120
                           ************************:*.********************:*************

sp|Q9UNF0|PACN2_HUMAN      HKQMMGGFKETKEAEDGFRKAQKPWAKKLKEVEAAKKAHHAACKEEKLAISREANSKADP 180
sp|Q9WVE8|PACN2_MOUSE      HKQMMGGFKETKEAEDGFRKAQKPWAKKLKEVEAAKKAHHTACKEEKLAISREANSKADP 180
                           ****************************************:*******************

sp|Q9UNF0|PACN2_HUMAN      SLNPEQLKKLQDKIEKCKQDVLKTKEKYEKSLKELDQGTPQYMENMEQVFEQCQQFEEKR 240
sp|Q9WVE8|PACN2_MOUSE      SLNPEQLKKLQDKIEKCKQDVLKTKDKYEKSLKELDQTTPQYMENMEQVFEQCQQFEEKR 240
                           *************************:********** **********************

sp|Q9UNF0|PACN2_HUMAN      LRFFREVLLEVQKHLDLSNVAGYKAIYHDLEQSIRAADAVEDLRWFRANHGPGMAMNWPQ 300
sp|Q9WVE8|PACN2_MOUSE      LRFFREVLLEVQKHLDLSNVASYKTIYRELEQSIKAADAVEDLRWFRANHGPGMAMNWPQ 300
                           ********************.**:**::*****:*************************

sp|Q9UNF0|PACN2_HUMAN      FEEWSADLNRTLSRREKKKATDGVTLTGINQTGDQSLPSKPSSTLNVPSNPAQSAQSQSS 360
sp|Q9WVE8|PACN2_MOUSE      FEEWSADLNRTLSRREKKKAVDGVTLTGINQTGDQSGQNKPGSNLSVPSNPAQSTQLQSS 360
                           ********************.***************  .**.*.*.********:* ***

sp|Q9UNF0|PACN2_HUMAN      YNPFEDEDDTGSTVSEKDDTKAKNVSSYEKTQSYPTDWSDDESNNPFSSTDANGDSNPFD 420
sp|Q9WVE8|PACN2_MOUSE      YNPFEDEDDTGSSISEKEDIKAKNVSSYEKTQTYPTDWSDDESNNPFSSTDANGDSNPFD 420
                           ************::***:* ************:**************************

sp|Q9UNF0|PACN2_HUMAN      DDATSGTEVRVRALYDYEGQEHDELSFKAGDELTKMEDEDEQGWCKGRLDNGQVGLYPAN 480
sp|Q9WVE8|PACN2_MOUSE      EDTTSGTEVRVRALYDYEGQEHDELSFKAGDELTKIEDEDEQGWCKGRLDSGQVGLYPAN 480
                           :*:*********************************:**************.*********

sp|Q9UNF0|PACN2_HUMAN      YVEAIQ 486
sp|Q9WVE8|PACN2_MOUSE      YVEAIQ 486
```

```
                          ******

Percent Identity  Matrix
1: sp|Q9UNF0|PACN2_HUMAN  100.00   93.83
2: sp|Q9WVE8|PACN2_MOUSE   93.83  100.00



sp|Q9UKS6|PACN3_HUMAN      MAPEEDAGGEALGGSFWEAGNYRRTVQRVEDGHRLCGDLVSCFQERARIEKAYAQQLADW 60
sp|Q99JB8|PACN3_MOUSE      MAPEEDAGGEVLGGSFWEAGNYRRTVQRVEDGHRLCGDLVSCFQERARIEKAYAQQLADW 60
                          **********.**************************************************

sp|Q9UKS6|PACN3_HUMAN      ARKWRGTVEKGPQYGTLEKAWHAFFTAAERLSALHLEVREKLQGQDSERVRAWQRGAFHR 120
sp|Q99JB8|PACN3_MOUSE      ARKWRGAVEKGPQYGTLEKAWHAFFTAAERLSELHLEVREKLHGPDSERVRTWQRGAFHR 120
                          ******:************************ *********:* ******:*********

sp|Q9UKS6|PACN3_HUMAN      PVLGGFRESRAAEDGFRKAQKPWLKRLKEVEASKKSYHAARKDEKTAQTRESHAKADSAV 180
sp|Q99JB8|PACN3_MOUSE      PVLGGFRESRAAEDGFRKAQKPWLKRLKEVEASKKSYHTARKDEKTAQTRESHAKADSSM 180
                          ************************************:******************::

sp|Q9UKS6|PACN3_HUMAN      SQEQLRKLQERVERCAKEAEKTKAQYEQTLAELHRYTPRYMEDMEQAFETCQAAERQRLL 240
sp|Q99JB8|PACN3_MOUSE      SQEQLRKLQERVGRCTKEAEKMKTQYEQTLAELNRYTPRYMEDMEQAFESCQAAERQRLL 240
                          *********** **:***** *:*********:***************:**********

sp|Q9UKS6|PACN3_HUMAN      FFKDMLLTLHQHLDLSSSEKFHELHRDLHQGIEAASDEEDLRWWRSTHGPGMAMNWPQFE 300
sp|Q99JB8|PACN3_MOUSE      FFKDVLLTLHQHLDLSSSDKFHELHRDLQQSIEAASDEEDLRWWRSTHGPGMAMNWPQFE 300
                          ****:*************:*********:*.*****************************

sp|Q9UKS6|PACN3_HUMAN      EWSLDTQRTISRKEKGGRSPDEVTLTSIVPTRDGTAPPPQSPGSPGTGQDEEWSDEESPR 360
sp|Q99JB8|PACN3_MOUSE      EWSLDTQRAISRKEKGGRSPDEVTLTSIVPTRDGTAPPPQSPSSPGSGQDEDWSDEESPR 360
                          ********:**********************************.***:****:********

sp|Q9UKS6|PACN3_HUMAN      KAATGVRVRALYDYAGQEADELSFRAGEELLKMSEEDEQGWCQGQLQSGRIGLYPANYVE 420
sp|Q99JB8|PACN3_MOUSE      KVATGVRVRALYDYAGQEADELSFRAGEELLKMSEEDEQGWCQGQLQSGRIGLYPANYVE 420
                          *.************************************************************

sp|Q9UKS6|PACN3_HUMAN      CVGA 424
sp|Q99JB8|PACN3_MOUSE      CVGA 424
                          ****

Percent Identity  Matrix
1: sp|Q9UKS6|PACN3_HUMAN  100.00   94.34
2: sp|Q99JB8|PACN3_MOUSE   94.34  100.00
```

Multiple sequence alignment between F-BARs of human PACSIN1-3 performed with ClustalW.[2]

```
sp|Q9UKS6|PACN3_F-BAR_HUMAN      ---MAPEEDAGGEALGGSFWEAGNYRRTVQRVEDGHRLCGDLVSCFQERARIEKAYAQQL 57
sp|Q9BY11|PACN1_F-BAR_HUMAN      MSSSYDEASLAPEETTDSFWEVGNYKRTVKRIDDGHRLCNDLMNCVQERAKIEKAYGQQL 60
```

```
sp|Q9UNF0|PACN2_F-BAR_HUMAN      MSVTYDD-SVGVEVSSDSFWEVGNYKRTVKRIDDGHRLCSDLMNCLHERARIEKAYAQQL 59
                                 : . . *   .****.***:***:*::******.**:.*.:***:*****.***

sp|Q9UKS6|PACN3_F-BAR_HUMAN      ADWARKWRGTVEKGPQYGTLEKAWHAFFTAAERLSALHLEVREKLQGQDSERVRAWQRGA 117
sp|Q9BY11|PACN1_F-BAR_HUMAN      TDWAKRWRQLIEKGPQYGSLERAWGAIMTEADKVSELHQEVKNNLLNEDLEKVKNWQKDA 120
sp|Q9UNF0|PACN2_F-BAR_HUMAN      TEWARRWRQLVEKGPQYGTVEKAWMAFMSEAERVSELHLEVKASLMNDDFEKIKNWQKEA 119
                                 ::**::**  :*******::*:** *::: *:::* ** **: .* .:* *::: **: *

sp|Q9UKS6|PACN3_F-BAR_HUMAN      FHRPVLGGFRESRAAEDGFRKAQKPWLKRLKEVEASKKSYHAARKDEKTAQTRESHAKAD 177
sp|Q9BY11|PACN1_F-BAR_HUMAN      YHKQIMGGFKETKEAEDGFRKAQKPWAKKMKELEAAKKAYHLACKEEKLAMTREMNSKTE 180
sp|Q9UNF0|PACN2_F-BAR_HUMAN      FHKQMMGGFKETKEAEDGFRKAQKPWAKKLKEVEAAKKAHHAACKEEKLAISREANSKAD 179
                                 :*: ::***:*:: ************ *::**:**:**::* * *:** * :** ::*::

sp|Q9UKS6|PACN3_F-BAR_HUMAN      SAVSQEQLRKLQERVERCAKEAEKTKAQYEQTLAELHRYTPRYMEDMEQAFETCQAAERQ 237
sp|Q9BY11|PACN1_F-BAR_HUMAN      QSVTPEQQKKLQDKVDKCKQDVQKTQEKYEKVLEDVGKTTPQYMENMEQVFEQCQQFEEK 240
sp|Q9UNF0|PACN2_F-BAR_HUMAN      PSLNPEQLKKLQDKIEKCKQDVLKTKEKYEKSLKELDQGTPQYMENMEQVFEQCQQFEEK 239
                                 ::. ** :***:::::* ::. **: :**: * :: : **:***:***.** **  *.:

sp|Q9UKS6|PACN3_F-BAR_HUMAN      RLLFFKDMLLTLHQHLDLSSSEKFHELHRDLHQGIEAASDEED 280
sp|Q9BY11|PACN1_F-BAR_HUMAN      RLVFLKEVLLDIKRHLNLAENSSYIHVYRELEQAIRGADAQED 283
sp|Q9UNF0|PACN2_F-BAR_HUMAN      RLRFFREVLLEVQKHLDLSNVAGYKAIYHDLEQSIRAADAVED 282
                                 ** *::::** :::**:*:.   :  ::::*.*.*..*.  **

Percent Identity  Matrix
1: sp|Q9UKS6|PACN3_HUMAN  100.00   50.71   56.27
2: sp|Q9BY11|PACN1_HUMAN   50.71  100.00   71.63
3: sp|Q9UNF0|PACN2_HUMAN   56.27   71.63  100.00
```

6.6 Appendix -The small GTPase RhoA interacts with the TRPV4 Ankyrin Repeat Domain

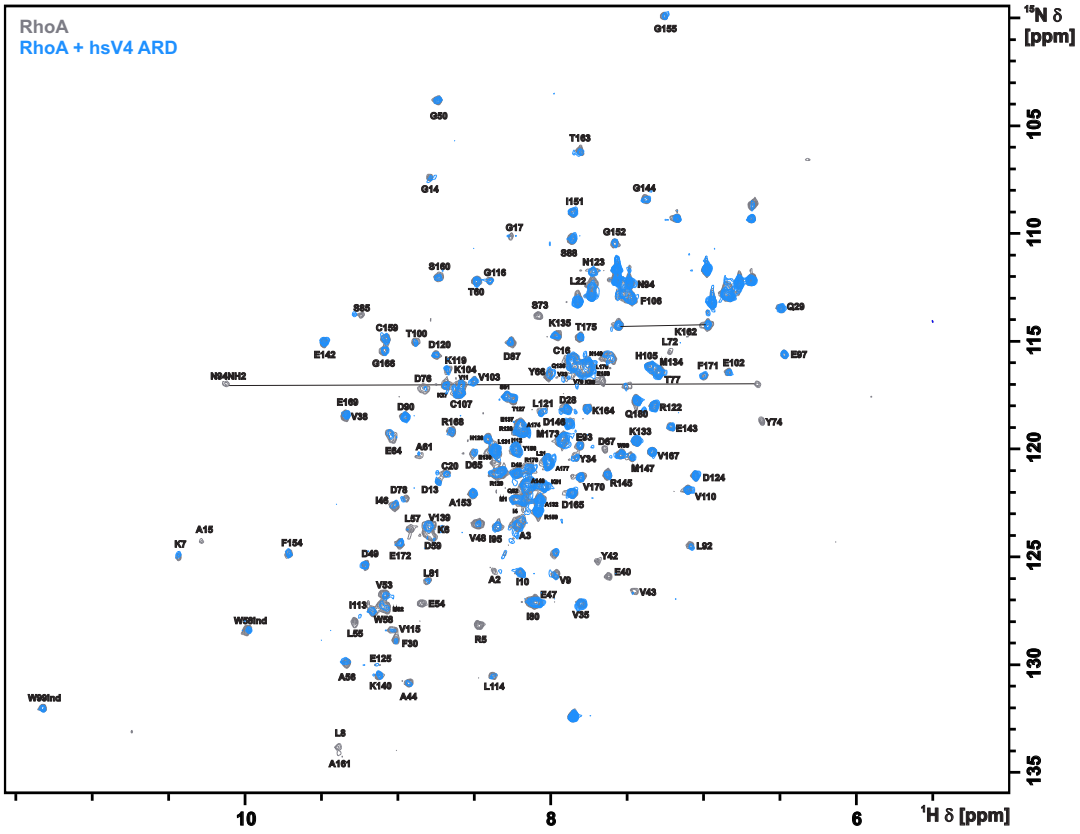

Figure 6.4: 2D ^{1}H-^{15}N-NMR spectrum of ^{15}N-RhoA: Overlay of spectra of ^{1}H-^{15}N RhoA 2D HSCQs of ^{15}N-RhoA on its own (grey) confirms presence of a well-folded protein in the GDP-bound state. In the presence of hsV4 ARD wt (blue), significant line broadening is observed indicative of the formation of a high molecular weight complex. RhoA backbone NMR assignments were transferred from previously published data.[170]

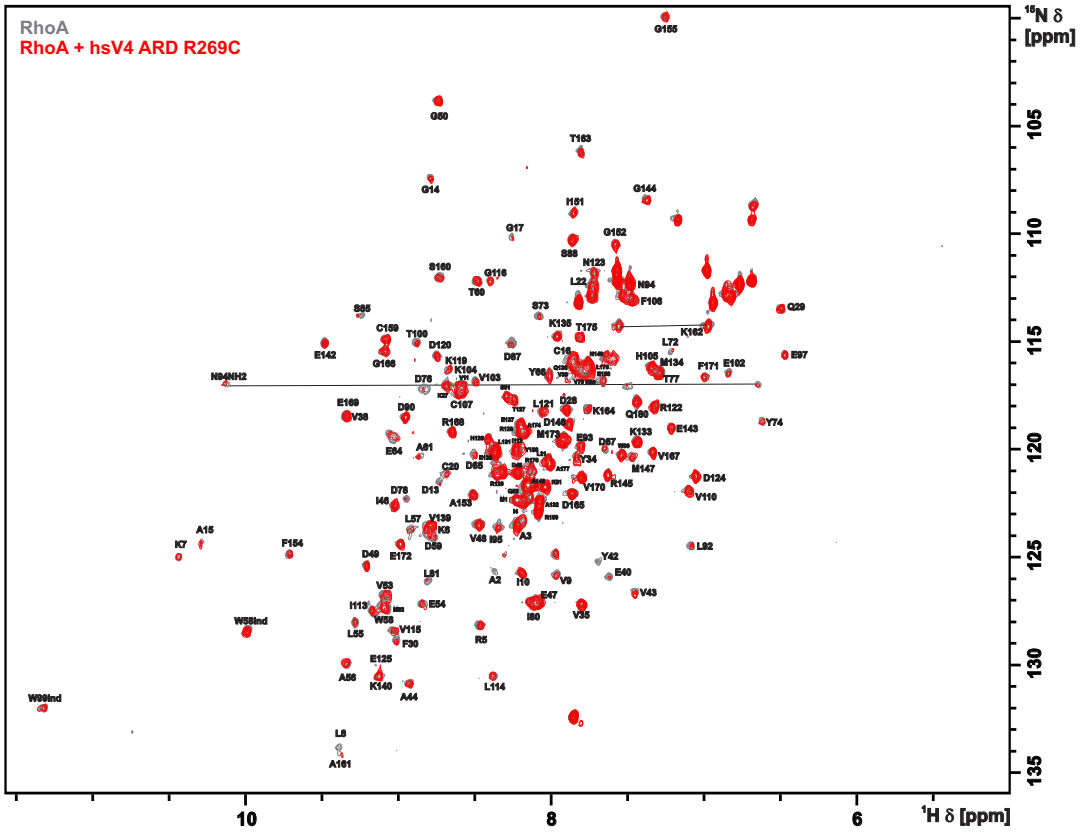

Figure 6.5: 2D ^{1}H-^{15}N-NMR spectrum of ^{15}N-RhoA: Overlay of spectra of ^{1}H-^{15}N RhoA 2D HSCQs of ^{15}N-RhoA on its own (grey) confirms presence of a well-folded protein in the GDP-bound state. Addition of hsV4 ARD R269C (red) shows only minor effects on the RhoA spectrum. RhoA backbone NMR assignments were transferred from previously published data.[170]

6.7 Appendix - Interaction of ITCH requires the full TRPV4 N-terminus *in vitro*

Following table contains MS data of ubiquitinated hsV4N after an *in vitro* ubiquitination assay with ITCH (see section 4.5, figure 4.25). MS experiments were carried out by the Johns Hopkins Mass Spectrometry and Proteomics Facility.

Table 6.11: MS data of ubiquitinated hsV4N after *in vitro* ubiquitination assay with ITCH (see section 4.5, figure 4.25). Ubiquitinated sequences are indicated in blue row color. # PSMs = peptide spectrum matches, total number of identified peptide sequences.

Annotated Sequence	Modifications	# Proteins	# PSMs	Positions in master proteins
(R).MKFQGAFR.(K)	1xOxidation [M1]	1	5	Q9HBA0 (69-76)
(R).LTDEEFR.(E)		1	36	Q9HBA0 (180-186)
(K).RLTDEEFR.(E)		2	52	Q9HBA0 (179-186)
(R).PAGPGDGRPNLR.(M)		2	182	Q9HBA0 (57-68)
(R).EFINSPFRDIYYRGQTALHIAIER.(R)		2	4	Q9HBA0 (225-248)
(K).IIEKQPQSPK.(A)		1	2	Q9HBA0 (127-136)
(K).TGKIGIFQHIIRR.(E)		2	43	Q9HBA0 (380-392)
(K).DEGGYFYFGELPLSLAACTNQ PHIVNYLTENPHK.(K)	1xMethylThiol (C18); 1xMethylthio (C18)	2	11	Q9HBA0 (277-310)
(R).CKHYVELLVAQGADVHAQAR.(G)	1xMethylthio (C1)	1	39	Q9HBA0 (250-269)
(R).GRFFQPK.(D)		2	13	Q9HBA0 (270-276)
(K).QPQSPK.(A)		2	5	Q9HBA0 (131-136)
(K).MYDLLLLK.(C)		1	19	Q9HBA0 (345-352)
(K).FQGAFR.(K)		2	8	Q9HBA0 (71-76)
(R).LFPDSNLEAVLNNDGLSPLMMAAK.(T)		2	26	Q9HBA0 (356-379)
(K).GVPNPIDLLESTLYESSVVPGPKK.(A)		1	13	Q9HBA0 (78-101)
(R).LFPDSNLEAVLNNDGLSPLMMAAK.(T)	1xDeamidated (N); 1xOxidation (M)	1	38	Q9HBA0 (356-379)
(R).PILFDIVSR.(G)		2	32	Q9HBA0 (152-160)
(R).ENTKFVTKMYDLLLLK.(C)	1xOxidation (M9)	1	1	Q9HBA0 (337-352)
(R).FFQPK.(D)		2	2	Q9HBA0 (272-276)
(K).IGIFQHIIRR.(E)		2	38	Q9HBA0 (383-392)
(R).LFPDSNLEAVLNNDGLSPLMMAAK.(T)	1xDeamidated (N); 2xOxidation (M20; M21)	1	95	Q9HBA0 (356-379)

Annotated Sequence	Modifications	# Proteins	# PSMs	Positions in master proteins
(K).GVPNPIDLLESTLYESSVVPGPK.(K)		2	53	Q9HBA0 (78-100)
(R).LFPDSNLEAVLNNDGLSPLMMAAK.(T)	2xOxidation (M20; M21)	1	276	Q9HBA0 (356-379)
(K).QPQSPKAPAPQPPPILK.(V)		2	7	Q9HBA0 (131-147)
(K).VFNRPILFDIVSR.(G)		2	206	Q9HBA0 (148-160)
(K).ALLNLSNGR.(N)	1xDeamidated (N7)	1	79	Q9HBA0 (198-206)
(R).NDTIPVLLDIAER.(T)	1xDeamidated (N1)	1	47	Q9HBA0 (207-219)
(R).GNTVLHALVAIADNTR.(E)	1xDeamidated (N)	1	76	Q9HBA0 (321-336)
(K).ALLNLSNGR.(N)		1	42	Q9HBA0 (198-206)
(R).NDTIPVLLDIAER.(T)		1	50	Q9HBA0 (207-219)
(R).GNTVLHALVAIADNTR.(E)		1	177	Q9HBA0 (321-336)
(K).ALLNLSNGR.(N)	2xDeamidated (N4; N7)	1	18	Q9HBA0 (198-206)
(K).KAPMDSLFDYGTYR.(H)		1	51	Q9HBA0 (101-114)
(K).KAPMDSLFDYGTYR.(H)	1xOxidation (M4)	1	467	Q9HBA0 (101-114)
(KR).GQTALHIAIER.(R)		3	153	Q9HBA0 (238-248)
(K).APAPQPPPILKVFNRPILFDIVSR.(G)		2	1	Q9HBA0 (137-160)
(K).HYVELLVAQGADVHAQAR.(G)		2	2595	Q9HBA0 (252-269)
(K).IGIFQHIIR.(R)		1	115	Q9HBA0 (383-391)
(R).EFINSPFR.(D)		2	62	Q9HBA0 (225-232)
(R).TGNMREFINSPFR.(D)	1xOxidation (M4)	1	3	Q9HBA0 (220-232)
(K).MYDLLLLK.(C)	1xOxidation (M1)	1	141	Q9HBA0 (345-352)
(K).APMDSLFDYGTYR.(H)	1xOxidation (M3)	1	166	Q9HBA0 (102-114)
(R).QDSRGNTVLHALVAIADNTRENTK.(F)		1	15	Q9HBA0 (317-340)
(K).VFNRPILFDIVSR.(G)	1xDeamidated (N3)	1	20	Q9HBA0 (148-160)
(R).LFPDSNLEAVLNNDGLSPLMMAAK.(T)	1xOxidation (M)	1	135	Q9HBA0 (356-379)

Annotated Sequence	Modifications	# Proteins	# PSMs	Positions in master proteins
(R).GSTADLDGLLPFLLTHKK.(R)		2	5	Q9HBA0 (161-178)
(K).TGKIGIFQHIIR.(R)		1	13	Q9HBA0 (380-391)
(KR).GQTALHIAIERR.(NC)		3	68	Q9HBA0 (238-249)
(R).AGPGEVAELPGDESGTPGGEAF		2	25	Q9HBA0 (10-56)
PLSSLANLFEGEDGSLSPSPADASR.(P)				
(R).EFINSPFRDIYYR.(G)		2	3	Q9HBA0 (225-237)
(R).EFINSPFR.(D)	1xDeamidated (N4)	1	42	Q9HBA0 (225-232)
(R).HHSSDNK.(R)		2	5	Q9HBA0 (115-121)
(K).ALLNLSNGRNDTIPVLLDIAER.(T)	1xDeamidated (N)	1	46	Q9HBA0 (198-219)
(K).APAPQPPPILK.(V)		1	128	Q9HBA0 (137-147)
(K).APAPQPPPILK.(V)	1xDeamidated (Q5)	1	8	Q9HBA0 (137-147)
(K).RLTDEEFREPSTGK.(T)		2	96	Q9HBA0 (179-192)
(R).LTDEEFREPSTGK.(T)		2	82	Q9HBA0 (180-192)
(R).QDSRGNTVLHALVAIADNTR.(E)		1	19	Q9HBA0 (317-336)
(R).GNTVLHALVAIADNTRENTK.(F)		1	11	Q9HBA0 (321-340)
(R).GSTADLDGLLPFLLTHK.(K)		1	96	Q9HBA0 (161-177)
(R).GNTVLHALVAIADNTRENTKFVTK.(M)		1	13	Q9HBA0 (321-344)
(R).LFPDSNLEAVLNNDGLSPLMMAAKTGK.(I)	2xOxidation (M20; M21)	1	6	Q9HBA0 (356-382)
(R).RQDSRGNTVLHALVAIADNTR.(E)		1	1	Q9HBA0 (316-336)
(M).ADSSEGPR.(A)		1	13	Q9HBA0 (2-9)
(K).DEGGYFYFGELPLSLAACTNQPHI	1xMethylthio (C18)	1	4	Q9HBA0 (277-311)
VNYLTENPHKK.(A)				
(K).GVPNPIDLLESTLYESSVVPGPKK.(A)	1xGG (K)	1	10	Q9HBA0 (78-101)
(K).IIEKQPQSPK.(A)	1xGG (K4)	1	1	Q9HBA0 (127-136)

Annotated Sequence	Modifications	# Proteins	# PSMs	Positions in master proteins
(K).KAPMDSLFDYGTYR.(H)	1xOxidation (M4); 1xGG (K1)	1	6	Q9HBA0 (101-114)
(R).AGPGEVAELPGDESGTPGGEA FPLSSLANLFEGEDGSLSPSPADASR.(P)		2	1	Q9HBA0 (10-56)
(R).KGVPNPIDLLESTLYESSVVPGPK.(K)		1	69	Q9HBA0 (77-100)
(K).QPQSPKAPAPQPPPILK.(V)	1xGlyGly (K6); 1xGG (K6)	2	2	Q9HBA0 (131-147)
(R).KGVPNPIDLLESTLYESSVVPGPK.(K)	1xGG (K1)	1	9	Q9HBA0 (77-100)

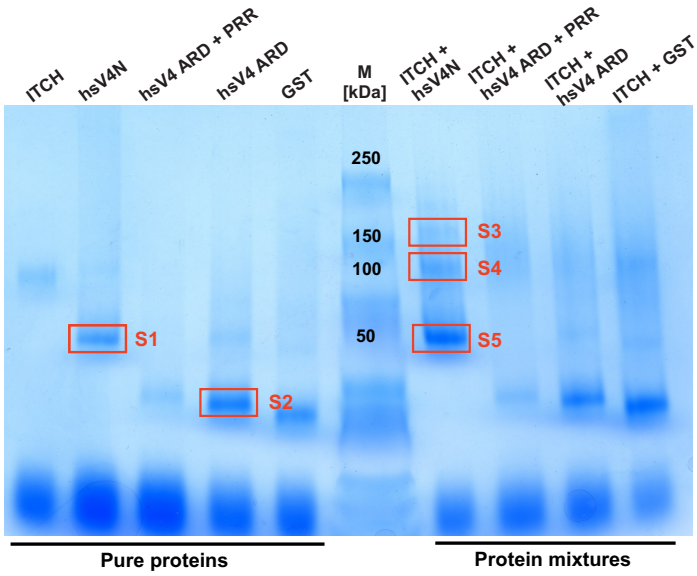

Figure 6.6: **Annotated BN PAGE samples submitted for MS measurements.** See tables 6.12 and 6.12 for MS data.

Tables 6.12 and 6.12 show MS data of BN PAGE complexes of ITCH and hsV4N (see section 4.5, figure 4.24). For sample annotation, see figure 6.6. MS experiments were carried out by the Johns Hopkins Mass Spectrometry and Proteomics Facility. Due to the omission of detergent in the BN PAGE procedure, protein mixtures lead to smearing and therefore also slight contaminations in bands which supposedly should only contain one protein.[85] This is also reflected in the quantitative values shown in tables 6.12 and 6.12.

Table 6.12: MS data of BN PAGE complexes of ITCH and hsV4N (see section 4.5, figure 4.24 and figure 6.6 for sample annotation). Indicated are quantitative values normalized to total MS spectra.

Accession Number	Molecular Weight	S1_NtermMono	S1_NtermMono	S2_ARD_mono	S2_ARD_mono
TRPV4_HUMAN	98 kDa	294,96	301,25	361,61	367,44
ITCH_HUMAN	103 kDa	0	0	0	0
K2C1_HUMAN	66 kDa	34,829	30,233	11,533	13,42
K1C10_HUMAN	59 kDa	25,033	21,595	10,855	10,224
K1C9_HUMAN	62 kDa	20,68	24,834	8,8197	5,1122
K22E_HUMAN	65 kDa	17,414	15,116	10,177	10,864
ALBU_HUMAN	69 kDa	0	0	0	0
K1C16_HUMAN	51 kDa	8,7072	8,6379	0	0
K1C14_HUMAN	52 kDa	5,442	5,3987	4,0706	0
K2C5_HUMAN	62 kDa	0	0	0	0
K2C6A_HUMAN (+1)	60 kDa	0	0	0	0
DSG1_HUMAN	114 kDa	0	0	0	0
K1C17_HUMAN	48 kDa	0	0	0	0
IGG1_HUMAN (+1)	49 kDa	0	0	0	0
DESP_HUMAN	332 kDa	0	0	0	0

Accession Number	Molecular Weight	S3_ITCH_complex2	S3_ITCH_complex2	S4_ITCH_alone	S4_ITCH_alone	S5_Nterm_alone	S5_Nterm_alone
TRPV4_HUMAN	98 kDa	164,67	170,2	179,41	189,14	367,54	369,73
ITCH_HUMAN	103 kDa	100,8	99,609	173,49	162,82	14,82	16,876
K2C1_HUMAN	66 kDa	31,549	32,157	15,233	18,092	11,856	7,6708
K1C10_HUMAN	59 kDa	31,549	35,294	14,387	14,802	4,9401	4,6025
K1C9_HUMAN	62 kDa	20,007	18,039	15,233	13,158	7,9041	5,1139
K22E_HUMAN	65 kDa	17,698	16,471	9,3091	6,5788	0	3,0683
ALBU_HUMAN	69 kDa	12,312	12,549	0	0	0	0
K1C16_HUMAN	51 kDa	6,9254	6,2746	0	2,467	0	0
K1C14_HUMAN	52 kDa	0	6,2746	0	0	0	0
K2C5_HUMAN	62 kDa	7,6949	7,8432	0	0	0	0
K2C6A_HUMAN (+1)	60 kDa	5,3865	0	0	0	0	0
DSG1_HUMAN	114 kDa	2,3085	0	0	0	0	0
K1C17_HUMAN	48 kDa	3,8475	0	0	0	0	0
IGG1_HUMAN (+1)	49 kDa	0	2,353	0	0	0	0
DESP_HUMAN	332 kDa	2,3085	0	0	0	0	0

6.8 Appendix - TRPV4 and the actin cytoskeleton - connecting scientific disciplines

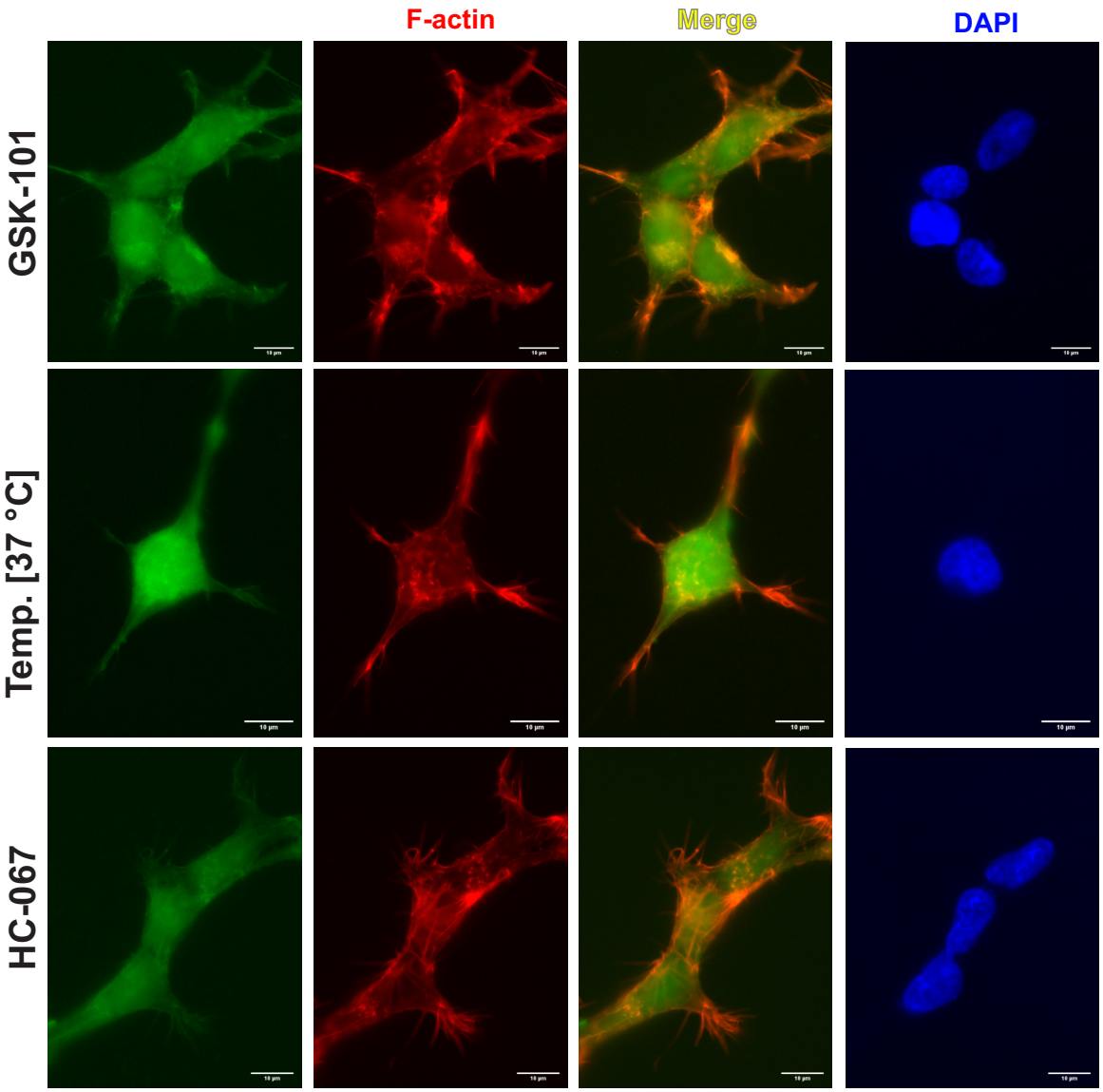

Figure 6.7: **Fluorescence microscopy images show no effect of GSK-101 or HC-067 on the cytoskeleton of unstransfected HEK293 cells.**

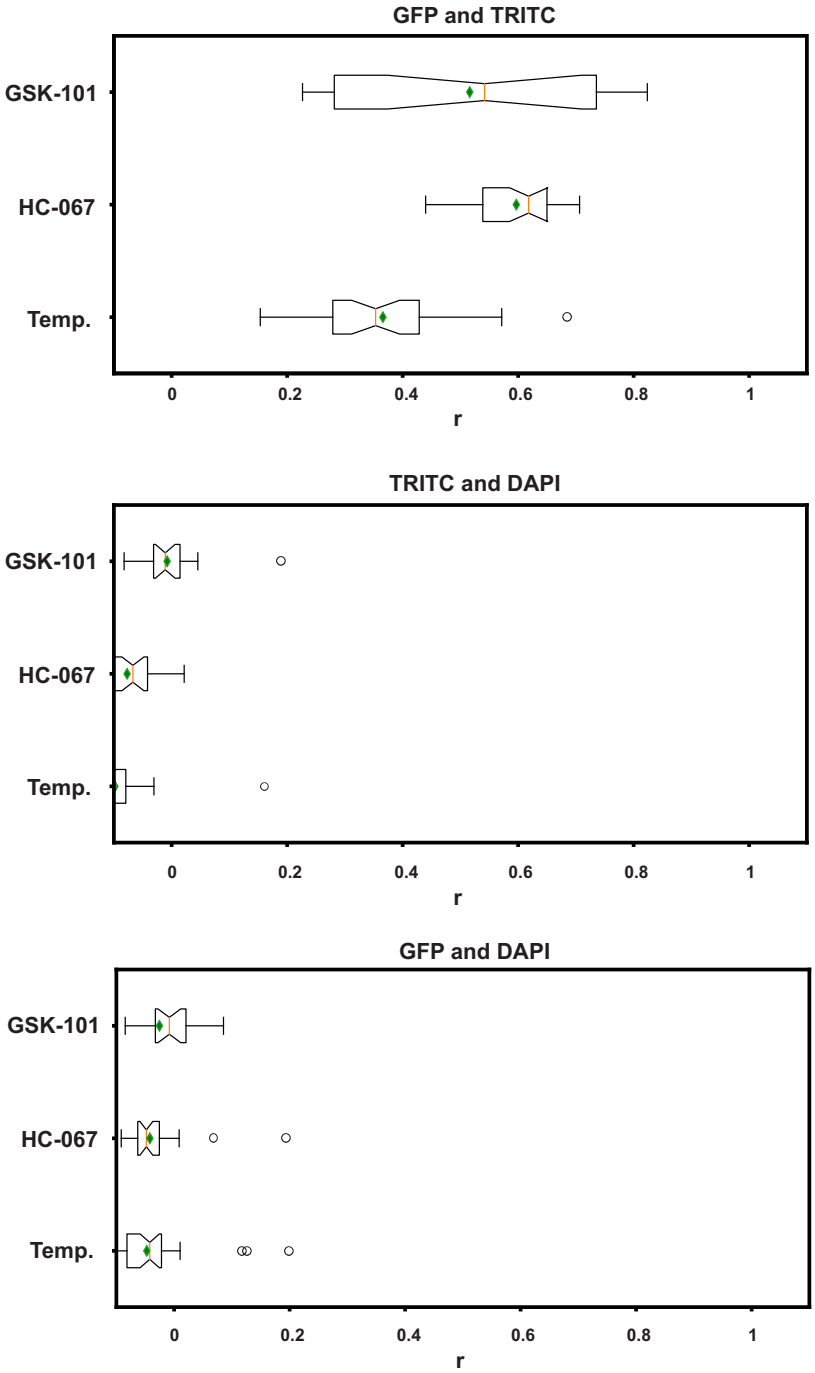

Figure 6.8: **Pearson Correlation Coefficients (PCC, r) of respective fluorescence marker pair.** GFP showed TRPV4-cGFP localization, F-actin was counter-stained with Phalloidin-TRITC and the nucleus with DAPI. Higher PCC values indicate stronger linear correlations of subjected images. See also 4.3. Box plot whiskers indicate values inside 1.5-fold interquartile range, green diamonds the arithmetic mean. Notches show 95% confidence intervall of mode. Outliers are shown as circles. $n_{GSK\text{-}101}$=18, $n_{HC\text{-}067}$=28, n_{Temp}=33.

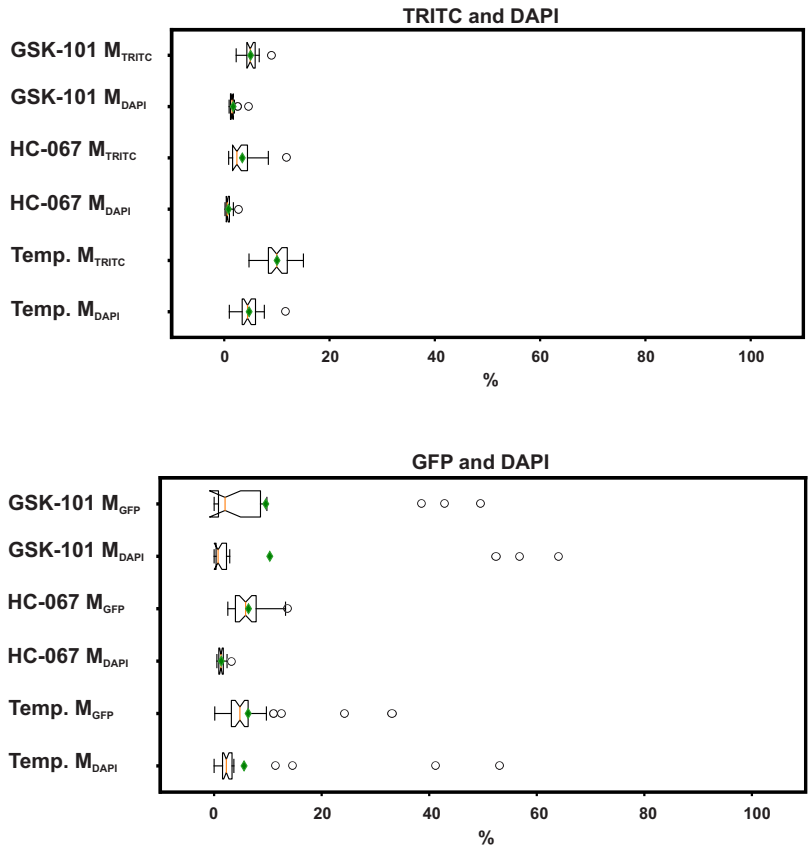

Figure 6.9: **Calculated M-values of respective fluorescence marker pairs as negative controls.** GFP showed TRPV4-cGFP localization, F-actin was counter-stained with Phalloidin-TRITC and the nucleus with DAPI. For description of M-values see equation 4.4 and corresponding text. Box plot whiskers indicate values inside 1.5-fold interquartile range, green diamonds the arithmetic mean. Notches show 95 % confidence intervall of mode. Outliers are shown as circles. $n_{GSK\text{-}101}$=18, $n_{HC\text{-}067}$=28, n_{Temp}=33.

Table 6.14: P and M-values of GFP (TRPV4-cGFP) and TRITC (F-actin stained with Phalloidon TRITC) images of stably transfected HEK293 cells upon various treatments, determined and calculated by ELSEXY (see also figures 4.28, 6.9 and 6.8). PCC = Pearson correlation coefficient r

Image IDs	PCC (r)	P-Value [%]	M_{GFP}-Value	M_{TRITC}-Value
GSK-101 treatment:				
Aufnahme-853-Aufnahme-854	0.5200	100.00	78.2787	86.0679
Aufnahme-857-Aufnahme-858	0.2732	100.00	62.2298	81.1937
Aufnahme-861-Aufnahme-862	0.4023	100.00	5.9401	4.2444
Aufnahme-867-Aufnahme-868	0.5681	100.00	9.9422	7.3226
Aufnahme-871-Aufnahme-873	0.7425	100.00	94.2158	97.9657
Aufnahme-876-Aufnahme-877	0.8212	100.00	93.5949	97.0998
Aufnahme-880-Aufnahme-881	0.6831	100.00	95.9003	97.4444
Aufnahme-884-Aufnahme-885	0.8237	100.00	92.8449	94.4432
Aufnahme-889-Aufnahme-890	0.5636	100.00	95.5037	99.8089
Aufnahme-893-Aufnahme-894	0.7147	100.00	94.6725	98.1046
Aufnahme-897-Aufnahme-898	0.7655	100.00	92.6020	96.5671
Aufnahme-901-Aufnahme-902	0.7937	100.00	93.3543	96.6338
Aufnahme-909-Aufnahme-910	0.2758	100.00	9.6166	3.1952
Aufnahme-913-Aufnahme-914	0.2837	100.00	7.1438	3.7441

Image IDs	PCC (r)	P-Value [%]	M_{GFP}-Value	M_{TRITC}-Value
Aufnahme-917-Aufnahme-918	0.2267	100.00	7.4609	2.3810
Aufnahme-921-Aufnahme-922	0.2634	100.00	69.0527	77.5663
Aufnahme-925-Aufnahme-926	0.2891	100.00	11.7675	3.1167
Aufnahme-930-Aufnahme-931	0.2809	100.00	9.1041	2.3597
Temperature treatment:				
Aufnahme-715-Aufnahme-717	0.2734	100.00	56.6989	81.8237
Aufnahme-722-Aufnahme-723	0.3650	100.00	57.1273	85.8436
Aufnahme-726-Aufnahme-727	0.3448	100.00	63.5204	82.0378
Aufnahme-730-Aufnahme-731	0.4119	100.00	74.7003	92.5601
Aufnahme-734-Aufnahme-735	0.5359	100.00	84.3648	98.6884
Aufnahme-738-Aufnahme-739	0.6848	100.00	90.3637	99.3332
Aufnahme-742-Aufnahme-743	0.1857	100.00	40.4781	50.9899
Aufnahme-746-Aufnahme-747	0.4916	100.00	66.8480	83.7768
Aufnahme-750-Aufnahme-751	0.1890	100.00	48.0745	54.6190
Aufnahme-754-Aufnahme-755	0.2810	100.00	47.5923	63.3100
Aufnahme-758-Aufnahme-759	0.3313	100.00	59.1588	75.0643
Aufnahme-763-Aufnahme-764	0.5716	100.00	80.0658	91.6231
Aufnahme-768-Aufnahme-769	0.3009	100.00	54.5052	76.3846
Aufnahme-772-Aufnahme-773	0.4322	100.00	66.4405	83.4705
Aufnahme-776-Aufnahme-777	0.2188	100.00	46.8050	44.2958
Aufnahme-780-Aufnahme-781	0.3458	100.00	50.2426	54.6213
Aufnahme-784-Aufnahme-785	0.4276	100.00	76.7970	78.3063
Aufnahme-788-Aufnahme-789	0.5264	100.00	87.7442	92.1042
Aufnahme-792-Aufnahme-793	0.5648	100.00	90.8593	95.6255
Aufnahme-796-Aufnahme-797	0.1653	100.00	43.9615	63.6713
Aufnahme-800-Aufnahme-801	0.1535	100.00	38.4351	57.4055
Aufnahme-804-Aufnahme-805	0.2361	100.00	44.8965	73.5039
Aufnahme-808-Aufnahme-809	0.3448	100.00	61.8572	81.7557
Aufnahme-812-Aufnahme-813	0.4092	100.00	78.1647	93.3742
Aufnahme-816-Aufnahme-817	0.4254	100.00	78.3585	74.6014
Aufnahme-820-Aufnahme-821	0.5456	100.00	88.8685	89.4498
Aufnahme-824-Aufnahme-825	0.2165	100.00	40.9267	69.2274
Aufnahme-828-Aufnahme-829	0.2849	100.00	59.3778	79.9833
Aufnahme-837-Aufnahme-838	0.2854	100.00	64.8022	75.1479
Aufnahme-841-Aufnahme-842	0.3744	100.00	75.0187	88.7091
Aufnahme-845-Aufnahme-846	0.3607	100.00	69.7550	85.6324
Aufnahme-849-Aufnahme-850	0.4218	100.00	66.0904	84.9898
HC-067 treatment:				
Aufnahme-1000-Aufnahme-1001	0.6449	100.00	92.2383	93.8185
Aufnahme-1004-Aufnahme-1005	0.6120	100.00	87.9697	89.9036
Aufnahme-1008-Aufnahme-1009	0.6150	100.00	88.5064	90.1036
Aufnahme-1012-Aufnahme-1013	0.5533	100.00	83.3883	85.0252
Aufnahme-1016-Aufnahme-1017	0.5419	100.00	81.3487	83.1448
Aufnahme-1020-Aufnahme-1021	0.5114	100.00	73.9040	77.9632
Aufnahme-1024-Aufnahme-1025	0.5629	100.00	78.7804	82.4833
Aufnahme-1028-Aufnahme-1029	0.6287	100.00	87.5814	90.4300

Image IDs	PCC (r)	P-Value [%]	M_{GFP}-Value	M_{TRITC}-Value
Aufnahme-1032-Aufnahme-1033	0.6687	100.00	92.2003	93.6834
Aufnahme-1036-Aufnahme-1037	0.6806	100.00	91.7884	92.6963
Aufnahme-1040-Aufnahme-1041	0.6476	100.00	92.9055	93.5310
Aufnahme-1045-Aufnahme-1046	0.6432	100.00	88.5934	89.5814
Aufnahme-1049-Aufnahme-1050	0.7043	100.00	90.0797	91.3065
Aufnahme-1053-Aufnahme-1054	0.6106	100.00	90.8049	92.5187
Aufnahme-1057-Aufnahme-1058	0.6569	100.00	90.5583	92.7421
Aufnahme-1061-Aufnahme-1062	0.6972	100.00	91.0875	92.3391
Aufnahme-1065-Aufnahme-1066	0.6118	100.00	88.4876	89.9069
Aufnahme-1069-Aufnahme-1070	0.6212	100.00	87.1519	89.3313
Aufnahme-938-Aufnahme-939	0.6324	100.00	10.5299	3.4553
Aufnahme-942-Aufnahme-943	0.6250	100.00	85.4327	87.9572
Aufnahme-946-Aufnahme-947	0.4504	100.00	6.3986	2.6539
Aufnahme-950-Aufnahme-951	0.4398	100.00	76.8892	81.2257
Aufnahme-954-Aufnahme-955	0.6594	100.00	91.6085	92.9828
Aufnahme-958-Aufnahme-959	0.7064	100.00	94.0716	95.2790
Aufnahme-962-Aufnahme-963	0.4668	100.00	72.5181	75.0115
Aufnahme-966-Aufnahme-967	0.5041	100.00	73.5635	76.5784
Aufnahme-972-Aufnahme-973	0.5297	100.00	81.9084	84.7888
Aufnahme-976-Aufnahme-977	0.4837	100.00	79.9120	82.8985

Table 6.15: P and M-values of TRITC (F-actin stained with Phalloidon TRITC) and DAPI (Nucleus) images of stably transfected HEK293 cells upon various treatments, determined and calculated by ELSEXY (see also figures 4.28, 6.9 and 6.8). PCC = Pearson correlation coefficient r

Image IDs	PCC (r)	P-Value [%]	M_{TRITC}-Value	M_{DAPI}-Value
GSK-101 treatment:				
Aufnahme-854-Aufnahme-855	0.0453	87.75	2.2698	1.9382
Aufnahme-858-Aufnahme-859	-0.0776	99.99	9.0303	4.6092
Aufnahme-862-Aufnahme-863	-0.0823	99.99	4.7414	1.0634
Aufnahme-868-Aufnahme-869	-0.0120	53.32	2.9750	1.7098
Aufnahme-873-Aufnahme-874	-0.1359	100.00	5.9047	1.5552
Aufnahme-877-Aufnahme-878	-0.0314	72.60	6.2035	1.4343
Aufnahme-881-Aufnahme-882	-0.0318	73.16	4.9780	1.1867
Aufnahme-885-Aufnahme-887	-0.0101	52.66	5.5307	1.1056
Aufnahme-890-Aufnahme-891	-0.0088	52.05	6.6444	1.4626
Aufnahme-894-Aufnahme-895	-0.0241	62.51	4.6918	0.9261
Aufnahme-898-Aufnahme-899	0.0112	53.11	5.7763	1.3593
Aufnahme-902-Aufnahme-903	0.0100	52.55	5.2710	1.1873
Aufnahme-910-Aufnahme-911	-0.0271	67.22	6.4353	2.6085

Image IDs	PCC (r)	P-Value [%]	M_{TRITC}-Value	M_{DAPI}-Value
Aufnahme-914-Aufnahme-915	-0.0308	70.34	4.9065	2.5552
Aufnahme-918-Aufnahme-919	0.0156	56.52	4.2131	1.5957
Aufnahme-922-Aufnahme-923	0.1897	100.00	3.3455	1.5303
Aufnahme-926-Aufnahme-927	0.0370	79.59	4.5315	1.7017
Aufnahme-931-Aufnahme-932	0.0225	62.21	2.7836	0.9981
Temperature treatment:				
Aufnahme-715-Aufnahme-720	-0.0279	69.65	3.6567	2.1010
Aufnahme-722-Aufnahme-724	0.0025	50.14	1.2990	0.5988
Aufnahme-726-Aufnahme-728	-0.0571	96.69	4.4134	2.3618
Aufnahme-730-Aufnahme-732	-0.0304	71.63	1.6476	0.8968
Aufnahme-734-Aufnahme-736	-0.1550	100.00	3.7128	2.6887
Aufnahme-738-Aufnahme-740	-0.0339	76.10	2.5587	1.5470
Aufnahme-742-Aufnahme-744	-0.1645	100.00	9.7233	3.3940
Aufnahme-746-Aufnahme-748	-0.1533	100.00	2.7878	1.5764
Aufnahme-750-Aufnahme-752	-0.0598	98.28	0.1225	0.0027
Aufnahme-754-Aufnahme-756	-0.0191	58.85	5.3142	2.1340
Aufnahme-758-Aufnahme-760	-0.0544	96.39	4.9039	2.5055
Aufnahme-763-Aufnahme-765	-0.0743	99.98	4.2717	2.2736
Aufnahme-768-Aufnahme-770	-0.0419	86.53	12.5606	14.5611
Aufnahme-772-Aufnahme-774	-0.1626	100.00	3.7872	3.3313
Aufnahme-776-Aufnahme-778	-0.1146	100.00	5.9939	2.2270
Aufnahme-780-Aufnahme-782	-0.0635	99.43	4.8804	3.6756
Aufnahme-784-Aufnahme-786	-0.0368	79.79	11.1294	3.5519
Aufnahme-788-Aufnahme-790	-0.1036	100.00	6.3836	3.2530
Aufnahme-792-Aufnahme-794	-0.1636	100.00	3.5069	2.2702
Aufnahme-796-Aufnahme-798	0.0103	52.55	24.3181	41.1005
Aufnahme-800-Aufnahme-802	0.1172	100.00	0.1573	0.0037
Aufnahme-804-Aufnahme-806	-0.0439	88.24	7.3157	11.4028
Aufnahme-808-Aufnahme-810	-0.0128	54.17	5.7927	2.2767
Aufnahme-812-Aufnahme-814	-0.0659	99.45	3.3155	1.0491
Aufnahme-816-Aufnahme-818	0.1985	100.00	0.4610	0.0281
Aufnahme-820-Aufnahme-822	-0.1803	100.00	5.3852	2.9802
Aufnahme-824-Aufnahme-826	-0.0228	61.88	5.1411	2.5597
Aufnahme-828-Aufnahme-830	0.1261	100.00	33.0759	53.0580
Aufnahme-837-Aufnahme-839	-0.0173	56.81	11.0905	3.3428
Aufnahme-841-Aufnahme-843	-0.0255	64.93	4.7149	1.9215
Aufnahme-845-Aufnahme-847	-0.0404	83.73	6.3069	2.0690
Aufnahme-849-Aufnahme-851	-0.0426	87.13	2.9024	1.4929
HC-067:				
Aufnahme-1001-Aufnahme-1002	-0.0259	67.38	1.9920	0.4166
Aufnahme-1005-Aufnahme-1006	-0.1626	100.00	2.1678	0.4999
Aufnahme-1009-Aufnahme-1010	-0.1890	100.00	1.5087	0.3787
Aufnahme-1013-Aufnahme-1014	-0.0232	64.10	3.6097	0.8075
Aufnahme-1017-Aufnahme-1018	-0.0244	67.30	2.5572	0.5483
Aufnahme-1021-Aufnahme-1022	-0.1046	100.00	8.3782	1.7364
Aufnahme-1025-Aufnahme-1026	-0.0623	99.29	7.2097	1.6761

Image IDs	PCC (r)	P-Value [%]	M_{TRITC}-Value	M_{DAPI}-Value
Aufnahme-1029-Aufnahme-1030	-0.0603	98.82	11.7791	2.7133
Aufnahme-1033-Aufnahme-1034	-0.0585	98.79	5.5796	1.3661
Aufnahme-1037-Aufnahme-1038	-0.0731	99.96	4.1914	0.8995
Aufnahme-1041-Aufnahme-1042	-0.0707	99.92	5.0806	1.1388
Aufnahme-1046-Aufnahme-1047	-0.0963	100.00	7.8957	1.5447
Aufnahme-1050-Aufnahme-1051	0.0217	62.47	5.5741	1.3416
Aufnahme-1054-Aufnahme-1055	-0.0581	97.64	3.9439	0.9346
Aufnahme-1058-Aufnahme-1059	-0.1628	100.00	3.5124	0.8515
Aufnahme-1062-Aufnahme-1063	-0.0444	89.74	2.3205	0.7769
Aufnahme-1066-Aufnahme-1067	-0.0325	74.71	2.2184	0.4525
Aufnahme-1070-Aufnahme-1071	-0.0152	56.12	1.1900	0.3502
Aufnahme-939-Aufnahme-940	-0.1093	100.00	1.3381	0.3299
Aufnahme-943-Aufnahme-944	-0.1054	100.00	0.8397	0.2275
Aufnahme-947-Aufnahme-948	-0.0382	83.89	1.6123	0.4816
Aufnahme-951-Aufnahme-952	-0.1044	100.00	0.9972	0.3373
Aufnahme-955-Aufnahme-956	-0.1044	100.00	2.4847	0.6036
Aufnahme-959-Aufnahme-960	-0.0634	99.80	1.7299	0.3815
Aufnahme-963-Aufnahme-964	-0.0429	87.90	2.5499	0.7984
Aufnahme-967-Aufnahme-968	-0.1261	100.00	1.6800	0.4122
Aufnahme-973-Aufnahme-974	-0.1074	100.00	1.2766	0.1771
Aufnahme-977-Aufnahme-978	-0.1154	100.00	0.9108	0.1482

Table 6.16: P and M-values of GFP (TRPV4-cGFP) and DAPI (Nucleus) images of stably transfected HEK293 cells upon various treatments, determined and calculated by ELSEXY (see also figures 4.28, 6.9 and 6.8). PCC = Pearson correlation coefficient r

Image IDs	PCC (r)	P-Value [%]	M_{GFP}-Value	M_{DAPI}-Value
GSK-101 treatment:				
Aufnahme-853-Aufnahme-855	-0.1403	100.00	0.0100	0.0041
Aufnahme-857-Aufnahme-859	-0.0333	76.46	0.5327	0.3642
Aufnahme-861-Aufnahme-863	-0.0847	100.00	3.2794	0.7690
Aufnahme-867-Aufnahme-869	0.0096	52.33	1.7832	0.9969
Aufnahme-871-Aufnahme-874	-0.0300	73.40	0.9859	0.4895
Aufnahme-876-Aufnahme-878	-0.0167	57.37	0.7300	0.3754
Aufnahme-880-Aufnahme-882	-0.0435	92.08	0.8073	0.3559
Aufnahme-884-Aufnahme-887	-0.0289	70.83	0.7969	0.3878
Aufnahme-889-Aufnahme-891	-0.0163	58.52	1.2954	0.7190
Aufnahme-893-Aufnahme-895	0.0280	72.08	42.9159	56.7900
Aufnahme-897-Aufnahme-899	0.0570	98.34	38.5048	52.4213
Aufnahme-901-Aufnahme-903	0.0855	100.00	49.5204	64.0538
Aufnahme-909-Aufnahme-911	0.0146	55.46	9.8164	2.9068
Aufnahme-913-Aufnahme-915	0.0367	77.81	2.8104	1.4889

Image IDs	PCC (r)	P-Value [%]	M_{GFP}-Value	M_{DAPI}-Value
Aufnahme-917-Aufnahme-919	0.0218	61.57	9.1948	2.5784
Aufnahme-921-Aufnahme-923	-0.3342	100.00	0.8344	0.2907
Aufnahme-925-Aufnahme-927	0.0168	57.13	6.9142	1.1782
Aufnahme-930-Aufnahme-932	-0.0003	50.00	2.2941	0.2445
Temperature treatment:				
Aufnahme-715-Aufnahme-720	-0.0279	69.65	3.6567	2.1010
Aufnahme-722-Aufnahme-724	0.0025	50.14	1.2990	0.5988
Aufnahme-726-Aufnahme-728	-0.0571	96.69	4.4134	2.3618
Aufnahme-730-Aufnahme-732	-0.0304	71.63	1.6476	0.8968
Aufnahme-734-Aufnahme-736	-0.1550	100.00	3.7128	2.6887
Aufnahme-738-Aufnahme-740	-0.0339	76.10	2.5587	1.5470
Aufnahme-742-Aufnahme-744	-0.1645	100.00	9.7233	3.3940
Aufnahme-746-Aufnahme-748	-0.1533	100.00	2.7878	1.5764
Aufnahme-750-Aufnahme-752	-0.0598	98.28	0.1225	0.0027
Aufnahme-754-Aufnahme-756	-0.0191	58.85	5.3142	2.1340
Aufnahme-758-Aufnahme-760	-0.0544	96.39	4.9039	2.5055
Aufnahme-763-Aufnahme-765	-0.0743	99.98	4.2717	2.2736
Aufnahme-768-Aufnahme-770	-0.0419	86.53	12.5606	14.5611
Aufnahme-772-Aufnahme-774	-0.1626	100.00	3.7872	3.3313
Aufnahme-776-Aufnahme-778	-0.1146	100.00	5.9939	2.2270
Aufnahme-780-Aufnahme-782	-0.0635	99.43	4.8804	3.6756
Aufnahme-784-Aufnahme-786	-0.0368	79.79	11.1294	3.5519
Aufnahme-788-Aufnahme-790	-0.1036	100.00	6.3836	3.2530
Aufnahme-792-Aufnahme-794	-0.1636	100.00	3.5069	2.2702
Aufnahme-796-Aufnahme-798	0.0103	52.55	24.3181	41.1005
Aufnahme-800-Aufnahme-802	0.1172	100.00	0.1573	0.0037
Aufnahme-804-Aufnahme-806	-0.0439	88.24	7.3157	11.4028
Aufnahme-808-Aufnahme-810	-0.0128	54.17	5.7927	2.2767
Aufnahme-812-Aufnahme-814	-0.0659	99.45	3.3155	1.0491
Aufnahme-816-Aufnahme-818	0.1985	100.00	0.4610	0.0281
Aufnahme-820-Aufnahme-822	-0.1803	100.00	5.3852	2.9802
Aufnahme-824-Aufnahme-826	-0.0228	61.88	5.1411	2.5597
Aufnahme-828-Aufnahme-830	0.1261	100.00	33.0759	53.0580
Aufnahme-837-Aufnahme-839	-0.0173	56.81	11.0905	3.3428
Aufnahme-841-Aufnahme-843	-0.0255	64.93	4.7149	1.9215
Aufnahme-845-Aufnahme-847	-0.0404	83.73	6.3069	2.0690
Aufnahme-849-Aufnahme-851	-0.0426	87.13	2.9024	1.4929
HC-067:				
Aufnahme-1000-Aufnahme-1002	-0.0451	90.68	3.1690	0.5565
Aufnahme-1004-Aufnahme-1006	-0.1631	100.00	4.8925	0.8189
Aufnahme-1008-Aufnahme-1010	-0.0314	75.59	3.7647	0.5352
Aufnahme-1012-Aufnahme-1014	0.0087	52.10	8.4618	1.4623
Aufnahme-1016-Aufnahme-1018	-0.0271	68.35	6.1828	1.0086
Aufnahme-1020-Aufnahme-1022	-0.0165	56.18	13.2830	2.1062
Aufnahme-1024-Aufnahme-1026	-0.0916	100.00	10.9515	1.8920
Aufnahme-1028-Aufnahme-1030	-0.0441	87.52	13.6688	3.2934

Image IDs	PCC (r)	P-Value [%]	M_{GFP}-Value	M_{DAPI}-Value
Aufnahme-1032-Aufnahme-1034	-0.0549	96.16	7.6856	1.7986
Aufnahme-1036-Aufnahme-1038	-0.0653	99.69	7.7639	1.8226
Aufnahme-1040-Aufnahme-1042	-0.0682	99.91	8.9296	2.1581
Aufnahme-1045-Aufnahme-1047	-0.0622	99.19	10.9042	2.4098
Aufnahme-1049-Aufnahme-1051	-0.0494	93.04	7.4204	1.5090
Aufnahme-1053-Aufnahme-1055	-0.0588	98.72	6.3371	1.6009
Aufnahme-1057-Aufnahme-1059	-0.0606	99.16	4.6242	1.3025
Aufnahme-1061-Aufnahme-1063	-0.0501	95.10	4.3516	1.0979
Aufnahme-1065-Aufnahme-1067	-0.1420	100.00	7.4282	1.2888
Aufnahme-1069-Aufnahme-1071	-0.0398	84.78	3.8079	0.7245
Aufnahme-938-Aufnahme-940	-0.1324	100.00	5.5320	0.8956
Aufnahme-942-Aufnahme-944	-0.0697	99.95	2.5526	0.5187
Aufnahme-946-Aufnahme-948	-0.0264	67.77	4.6858	0.9460
Aufnahme-950-Aufnahme-952	-0.0230	63.73	2.5941	0.6412
Aufnahme-954-Aufnahme-956	-0.0467	94.75	6.3291	1.3117
Aufnahme-958-Aufnahme-960	-0.0520	96.46	4.0165	0.8191
Aufnahme-962-Aufnahme-964	-0.0228	62.86	7.9805	1.6780
Aufnahme-966-Aufnahme-968	-0.0048	50.52	5.0571	1.1735
Aufnahme-972-Aufnahme-974	0.1943	100.00	3.7948	1.2591
Aufnahme-976-Aufnahme-978	0.0681	99.70	2.8181	0.9724

6.9 Appendix - Establishing HEK293 cell lines stably expressing TRP channels

In the course of this work, HEK293 cells stably expressing human TRPV4-cGFP and TRPML1-cGFP, respectively, were established (see section 3.2.3 for procedure). In both cases, fluorescence microscopy images showed expected subcellular localization, as shown for human TRPV4-cGFP in figure 6.10 and human TRPML1-cGFP 6.12. Furthermore, for HEK293 hsTRPV4-cGFP cells, functionality of hsTRPV4-cGFP was confirmed via a Ca^{2+}-influx assay, in agreement with McCray *et al.*[69]

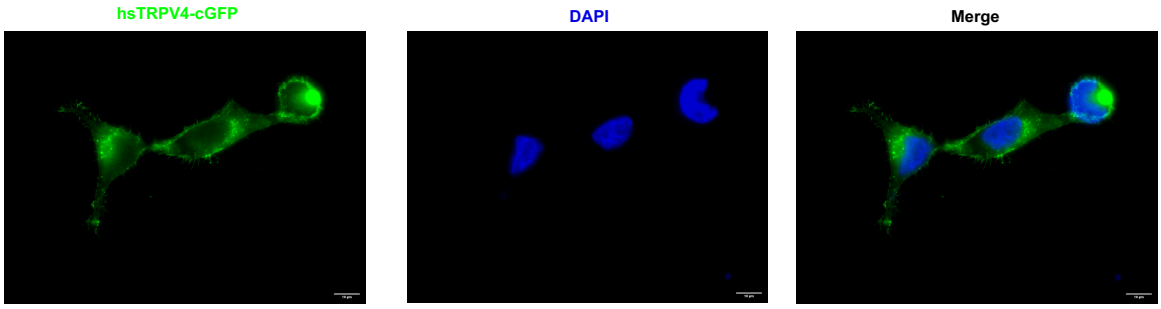

Figure 6.10: **Fluorescence microscopy images of HEK293 cells stably transfected with hsTRPV4-cGFP**. Stable transfection was achieved as described in subsection 3.2.3. hsTRPV4-cGFP shows expected plasma membrane localization.

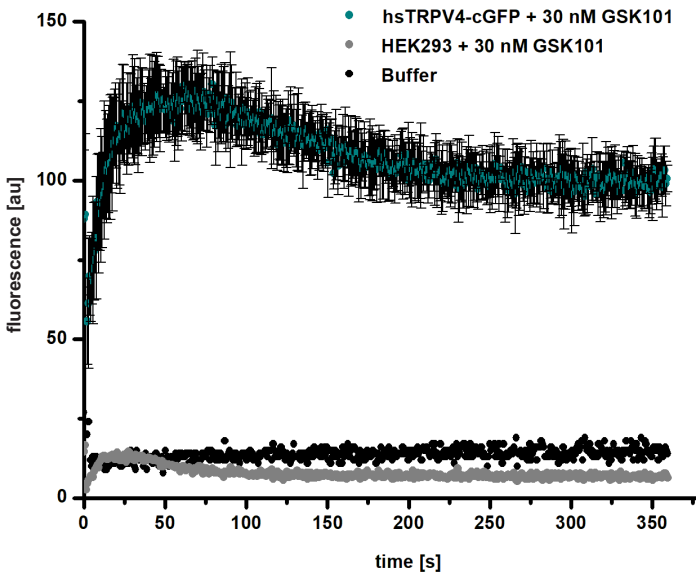

Figure 6.11: **Stably transfected HEK293 cells express funtional hsTRPV4-cGFP.** Functionality of expressed hsTRPV4-cGFP upon GSK101 activation, evaluated via a Ca^{2+}-influx assay performed with the Fluo-4 Direct Calcium Assay (see table 2.18). x-axis = time in seconds, y-axis: fluorescence in arbitrary units. Averages represent n = 3, error bars indicate SD.

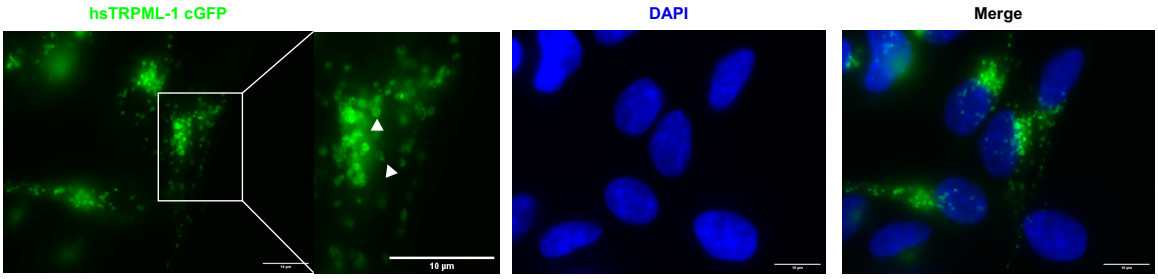

Figure 6.12: **Fluorescence microscopy images of HEK293 cells stabily transfected with hsTRPML1-cGFP**. Stable transfection was achieved as described in subsection 3.2.3. hsTRPML1-cGFP shows expected localization in vesicular structures (indicated by white arrow heads), which are most likely lysosomes.[229]

6.10 Appendix - Purification of ITCH WW domains

ITCH contains four WW domains (WW1-4), which could be possible interaction domains for the TRPV4 PRR.[230] To probe possible PPIs between the ITCH WW domains and TRPV4 PRR in detail recombinant expression of all four single WW domains and the tandem domains WW1+2 and 3+4 was established (see section 3.7.8). Furthermore, first purifications and characterizations of the WW1+2 and 2+3 tandem domains were carried out (figure 6.13).

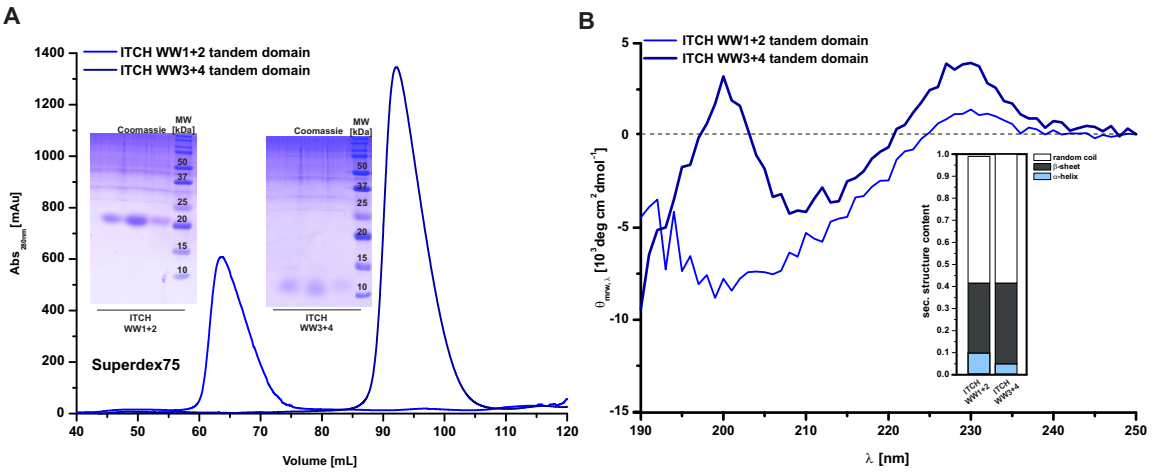

Figure 6.13: **Purification of recombinant human ITCH WW domains A** SEC purification of human ITCH WW1+2 and WW3+4 tandem domains. SEC runs were performed with a HiLoad Superdex 75 pg preparative SEC column. Inlet shows Coomassie stained 15 % SDS-PAGE of collected and concentrated fractions after SEC. x-axis: eluted volume in mL, y-axis: absorbency at 280 nm, M = marker. **B** Far UV CD spectrum of human WW1+2 and WW3+4 tandem domains. Spectra were measured at 293 K and proteins were used at 1 µM concentration in either SEC Buffer with a final NaCl concentration of 20 mM NaCl. Inlet shows secondary structure prediction performed with CAPITO.[93] The predicted α-helix/β-sheet/random coil content of the purified proteins is for ITCH WW1+2 tandem domain 10 %/32 %/58 % and ITCH WW3+4 tandem domain 5 %/37 %/59 %. x-axis: mean residue ellipticity ($[\Theta]_{mrw,\lambda}$) in 10^{-3} deg cm^2 dmol^{-1}, y-axis: wavelength λ in nm.

6.11 Appendix - Purification of YAP1 WW domains

YAP1 contains two WW domains, which could be possible interaction domains for the TRPV4 PRR.[230] To probe possible PPIs between the YAP1 WW domains and TRPV4 PRR in detail, recombinant expression of the YAP-1 WW1 domain and YAP1 WW1+2 tandem domain was established (see section 3.7.9). Furthermore, first purifications and characterizations of the YAP1 WW1 and WW1+2 tandem domain were carried out (figure 6.14). Expression conditions and subsequent purification of the YAP1 WW2 domain have still to be optimized.

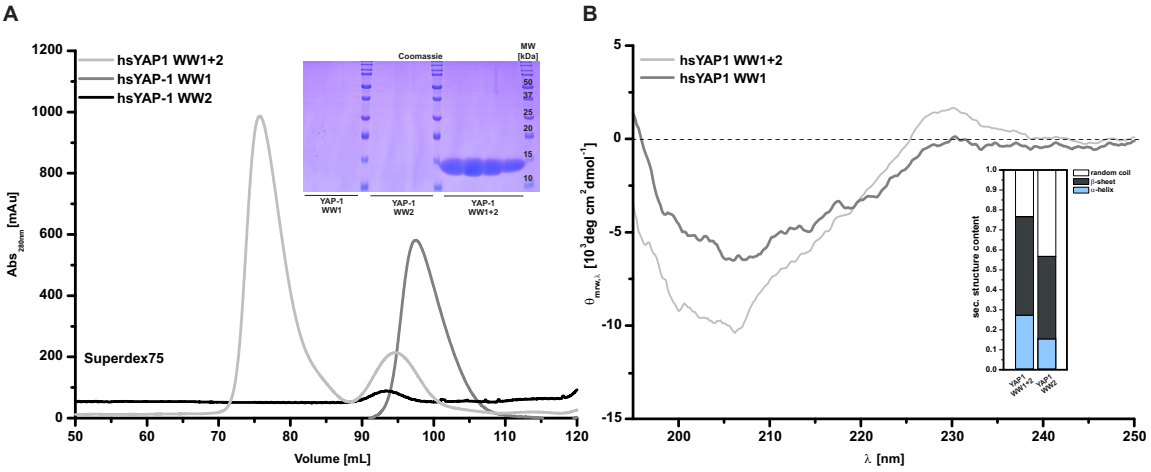

Figure 6.14: **Purification of recombinant human YAP1 WW domains A** SEC purification of human YAP1 WW1+2 tandem and YAP1 WW1 domain. SEC runs were performed with a HiLoad Superdex 75 pg preparative SEC column. Inlet shows Coomassie stained 15 % SDS-PAGE of collected and concentrated fractions after SEC. x-axis: eluted volume in mL, y-axis: absorbency at 280 nm, M = marker. **B** Far UV CD spectrum of human YAP1 WW1+2 tandem and YAP1 WW1 domain. Spectra were measured at 293 K and proteins were used at 1 µM concentration in either SEC Buffer with a final NaCl concentration of 20 mM NaCl. Inlet shows secondary structure prediction performed with CAPITO.[93] The predicted α-helix/β-sheet/random coil content of the purified proteins is for YAP WW1+2 tandem domain 3 %/50 %/47 % and YAP1 WW1 domain 2 %/42 %/56 %. x-axis: mean residue ellipticity ($[\Theta]_{mrw,\lambda}$) in 10^{-3} deg cm^2 dmol^{-1}, y-axis: wavelength λ in nm.

6.12 Appendix - Amino acid and DNA sequences

hsV4N

```
atggcggattccagcgaaggcccccgcgcggggcccggggaggtggctgagctccccggggatgagagtggcaccccaggtggggaggcttttcctctc
M  A  D  S  S  E  G  P  R  A  G  P  G  E  V  A  E  L  P  G  D  E  S  G  T  P  G  G  E  A  F  P  L
tcctccctggccaatctgtttgagggggaggatggctccctttcgccctcaccggctgatgccagtcgccctgctggcccaggcgatgggcgaccaaat
S  S  L  A  N  L  F  E  G  E  D  G  S  L  S  P  S  P  A  D  A  S  R  P  A  G  P  G  D  G  R  P  N
ctgcgcatgaagttccagggcgccttccgcaaggggggtgcccaaccccatcgatctgctggagtccaccctatatgagtcctcggtggtgcctgggccc
L  R  M  K  F  Q  G  A  F  R  K  G  V  P  N  P  I  D  L  L  E  S  T  L  Y  E  S  S  V  V  P  G  P
aagaaagcacccatggactcactgtttgactacggcacctatcgtcaccactccagtgacaacaagaggtggaggaagaagatcatagagaagcagccg
K  K  A  P  M  D  S  L  F  D  Y  G  T  Y  R  H  H  S  S  D  N  K  R  W  R  K  K  I  I  E  K  Q  P
cagagccccaaagcccctgcccctcagccgcccccatcctcaaagtcttcaaccggcctatcctctttgacatcgtgtcccggggctccactgctgac
Q  S  P  K  A  P  A  P  Q  P  P  P  I  L  K  V  F  N  R  P  I  L  F  D  I  V  S  R  G  S  T  A  D
ctggacgggctgctcccattcttgctgacccacaagaaacgcctaactgatgaggagtttcgagagccatctacggggaagacctgcctgcccaaggcc
L  D  G  L  L  P  F  L  L  T  H  K  K  R  L  T  D  E  E  F  R  E  P  S  T  G  K  T  C  L  P  K  A
ttgctgaacctgagcaatggccgcaacgacaccatccctgtgctgctggacatcgcggagcgcaccggcaacatgagggagttcattaactcgcccttc
L  L  N  L  S  N  G  R  N  D  T  I  P  V  L  L  D  I  A  E  R  T  G  N  M  R  E  F  I  N  S  P  F
cgtgacatctactatcgaggtcagacagccctgcacatcgccattgagcgtcgctgcaaacactacgtggaacttctcgtggcccagggagctgatgtc
R  D  I  Y  Y  R  G  Q  T  A  L  H  I  A  I  E  R  R  C  K  H  Y  V  E  L  L  V  A  Q  G  A  D  V
cacgcccaggcccgtgggcgcttcttccagcccaaggatgaggggggctacttctactttggggagctgcccctgtcgctggctgcctgcaccaaccag
H  A  Q  A  R  G  R  F  F  Q  P  K  D  E  G  G  Y  F  Y  F  G  E  L  P  L  S  L  A  A  C  T  N  Q
ccccacattgtcaactacctgacggagaaccccacaagaaggcggacatgcggcgccaggactcgcgaggcaacacagtgctgcatgcgctggtggcc
P  H  I  V  N  Y  L  T  E  N  P  H  K  K  A  D  M  R  R  Q  D  S  R  G  N  T  V  L  H  A  L  V  A
attgctgacaacacccgtgagaacaccaagtttgttaccaagatgtacgacctgctgctgctcaagtgtgcccgcctcttccccgacagcaacctggag
I  A  D  N  T  R  E  N  T  K  F  V  T  K  M  Y  D  L  L  L  L  K  C  A  R  L  F  P  D  S  N  L  E
gccgtgctcaacaacgacggcctctcgcccctcatgatggctgccaagacgggcaagattgggatctttcagcacatcatccggcgggaggtgacggat
A  V  L  N  N  D  G  L  S  P  L  M  M  A  A  K  T  G  K  I  G  I  F  Q  H  I  I  R  R  E  V  T  D
gaggcggccgctcatcatcaccatcatcattga
E  A  A  A  H  H  H  H  H  H  -
```

hsV4N wt Avi

```
atggcggattccagcgaaggcccccgcgcggggcccggggaggtggctgagctccccggggatgagagtggcaccccaggtggggaggcttttcctctc
M  A  D  S  S  E  G  P  R  A  G  P  G  E  V  A  E  L  P  G  D  E  S  G  T  P  G  G  E  A  F  P  L
tcctccctggccaatctgtttgagggggaggatggctccctttcgccctcaccggctgatgccagtcgccctgctggcccaggcgatgggcgaccaaat
S  S  L  A  N  L  F  E  G  E  D  G  S  L  S  P  S  P  A  D  A  S  R  P  A  G  P  G  D  G  R  P  N
ctgcgcatgaagttccagggcgccttccgcaaggggggtgcccaaccccatcgatctgctggagtccaccctatatgagtcctcggtggtgcctgggccc
L  R  M  K  F  Q  G  A  F  R  K  G  V  P  N  P  I  D  L  L  E  S  T  L  Y  E  S  S  V  V  P  G  P
aagaaagcacccatggactcactgtttgactacggcacctatcgtcaccactccagtgacaacaagaggtggaggaagaagatcatagagaagcagccg
K  K  A  P  M  D  S  L  F  D  Y  G  T  Y  R  H  H  S  S  D  N  K  R  W  R  K  K  I  I  E  K  Q  P
cagagccccaaagcccctgcccctcagccgcccccatcctcaaagtcttcaaccggcctatcctctttgacatcgtgtcccggggctccactgctgac
Q  S  P  K  A  P  A  P  Q  P  P  P  I  L  K  V  F  N  R  P  I  L  F  D  I  V  S  R  G  S  T  A  D
ctggacgggctgctcccattcttgctgacccacaagaaacgcctaactgatgaggagtttcgagagccatctacggggaagacctgcctgcccaaggcc
L  D  G  L  L  P  F  L  L  T  H  K  K  R  L  T  D  E  E  F  R  E  P  S  T  G  K  T  C  L  P  K  A
ttgctgaacctgagcaatggccgcaacgacaccatccctgtgctgctggacatcgcggagcgcaccggcaacatgagggagttcattaactcgcccttc
```

```
L  L  N  L  S  N  G  R  N  D  T  I  P  V  L  L  D  I  A  E  R  T  G  N  M  R  E  F  I  N  S  P  F
cgtgacatctactatcgaggtcagacagccctgcacatcgccattgagcgtcgctgcaaacactacgtggaacttctcgtggcccagggagctgatgtc
R  D  I  Y  Y  R  G  Q  T  A  L  H  I  A  I  E  R  R  C  K  H  Y  V  E  L  L  V  A  Q  G  A  D  V
cacgcccaggcccgtgggcgcttcttccagcccaaggatgaggggggctacttctactttggggagctgcccctgtcgctggctgcctgcaccaaccag
H  A  Q  A  R  G  R  F  F  Q  P  K  D  E  G  G  Y  F  Y  F  G  E  L  P  L  S  L  A  A  C  T  N  Q
ccccacattgtcaactacctgacggagaacccccacaagaaggcggacatgcggcgccaggactcgcgaggcaacacagtgctgcatgcgctggtggcc
P  H  I  V  N  Y  L  T  E  N  P  H  K  K  A  D  M  R  R  Q  D  S  R  G  N  T  V  L  H  A  L  V  A
attgctgacaacacccgtgagaacaccaagtttgttaccaagatgtacgacctgctgctgctcaagtgtgcccgcctcttccccgacagcaacctggag
I  A  D  N  T  R  E  N  T  K  F  V  T  K  M  Y  D  L  L  L  L  K  C  A  R  L  F  P  D  S  N  L  E
gccgtgctcaacaacgacggcctctcgcccctcatgatggctgccaagacgggcaagattgggatctttcagcacatcatccggcgggaggtgacggat
A  V  L  N  N  D  G  L  S  P  L  M  M  A  A  K  T  G  K  I  G  I  F  Q  H  I  I  R  R  E  V  T  D
gaggcggccgctggcctgaacgatatttttgaagcgcagaaaattgaatggcatgaacatcatcaccatcatcattga
E  A  A  A  G  L  N  D  I  F  E  A  Q  K  I  E  W  H  E  H  H  H  H  H  H  -
```

hsV4 ARD wt Avi

```
atgcttcaaccggcctatcctctttgacatcgtgtcccggggctccactgctgac
 M  F  N  R  P  I  L  F  D  I  V  S  R  G  S  T  A  D
ctggacgggctgctcccattcttgctgacccacaagaaacgcctaactgatgaggagtttcgagagccatctacggggaagacctgcctgcccaaggcc
L  D  G  L  L  P  F  L  L  T  H  K  K  R  L  T  D  E  E  F  R  E  P  S  T  G  K  T  C  L  P  K  A
ttgctgaacctgagcaatggccgcaacgacaccatccctgtgctgctggacatcgcggagcgcaccggcaacatgagggagttcattaactcgcccttc
L  L  N  L  S  N  G  R  N  D  T  I  P  V  L  L  D  I  A  E  R  T  G  N  M  R  E  F  I  N  S  P  F
cgtgacatctactatcgaggtcagacagccctgcacatcgccattgagcgtcgctgcaaacactacgtggaacttctcgtggcccagggagctgatgtc
R  D  I  Y  Y  R  G  Q  T  A  L  H  I  A  I  E  R  R  C  K  H  Y  V  E  L  L  V  A  Q  G  A  D  V
cacgcccaggcccgtgggcgcttcttccagcccaaggatgaggggggctacttctactttggggagctgcccctgtcgctggctgcctgcaccaaccag
H  A  Q  A  R  G  R  F  F  Q  P  K  D  E  G  G  Y  F  Y  F  G  E  L  P  L  S  L  A  A  C  T  N  Q
ccccacattgtcaactacctgacggagaacccccacaagaaggcggacatgcggcgccaggactcgcgaggcaacacagtgctgcatgcgctggtggcc
P  H  I  V  N  Y  L  T  E  N  P  H  K  K  A  D  M  R  R  Q  D  S  R  G  N  T  V  L  H  A  L  V  A
attgctgacaacacccgtgagaacaccaagtttgttaccaagatgtacgacctgctgctgctcaagtgtgcccgcctcttccccgacagcaacctggag
I  A  D  N  T  R  E  N  T  K  F  V  T  K  M  Y  D  L  L  L  L  K  C  A  R  L  F  P  D  S  N  L  E
gccgtgctcaacaacgacggcctctcgcccctcatgatggctgccaagacgggcaagattgggatctttcagcacatcatccggcgggaggtgacggat
A  V  L  N  N  D  G  L  S  P  L  M  M  A  A  K  T  G  K  I  G  I  F  Q  H  I  I  R  R  E  V  T  D
gaggcggccgctggcctgaacgatatttttgaagcgcagaaaattgaatggcatgaacatcatcaccatcatcattga
E  A  A  A  G  L  N  D  I  F  E  A  Q  K  I  E  W  H  E  H  H  H  H  H  H  -
```

hsV4 ARD R232C Avi

```
atgcttcaaccggcctatcctctttgacatcgtgtcccggggctccactgctgac
 M  F  N  R  P  I  L  F  D  I  V  S  R  G  S  T  A  D
ctggacgggctgctcccattcttgctgacccacaagaaacgcctaactgatgaggagtttcgagagccatctacggggaagacctgcctgcccaaggcc
L  D  G  L  L  P  F  L  L  T  H  K  K  R  L  T  D  E  E  F  R  E  P  S  T  G  K  T  C  L  P  K  A
ttgctgaacctgagcaatggccgcaacgacaccatccctgtgctgctggacatcgcggagcgcaccggcaacatgagggagttcattaactcgcccttc
L  L  N  L  S  N  G  R  N  D  T  I  P  V  L  L  D  I  A  E  R  T  G  N  M  R  E  F  I  N  S  P  F
tgtgacatctactatcgaggtcagacagccctgcacatcgccattgagcgtcgctgcaaacactacgtggaacttctcgtggcccagggagctgatgtc
 C  D  I  Y  Y  R  G  Q  T  A  L  H  I  A  I  E  R  R  C  K  H  Y  V  E  L  L  V  A  Q  G  A  D  V
cacgcccaggcccgtgggcgcttcttccagcccaaggatgaggggggctacttctactttggggagctgcccctgtcgctggctgcctgcaccaaccag
```

H A Q A R G R F F Q P K D E G G Y F Y F G E L P L S L A A C T N Q
ccccacattgtcaactacctgacggagaaccccacaagaaggcggacatgcggcgccaggactcgcgaggcaacacagtgctgcatgcgctggtggcc
P H I V N Y L T E N P H K K A D M R R Q D S R G N T V L H A L V A
attgctgacaacacccgtgagaacaccaagtttgttaccaagatgtacgacctgctgctgctcaagtgtgcccgcctcttccccgacagcaacctggag
I A D N T R E N T K F V T K M Y D L L L L K C A R L F P D S N L E
gccgtgctcaacaacgacggcctctcgcccctcatgatggctgccaagacgggcaagattgggatctttcagcacatcatccggcgggaggtgacggat
A V L N N D G L S P L M M A A K T G K I G I F Q H I I R R E V T D
gaggcggccgctggcctgaacgatatttttgaagcgcagaaaattgaatggcatgaacatcatcaccatcatcattga
E A A A G L N D I F E A Q K I E W H E H H H H H H -

hsV4 ARD K276E Avi

atgcttcaaccggcctatcctctttgacatcgtgtcccggggctccactgctgac
M F N R P I L F D I V S R G S T A D
ctggacgggctgctcccattcttgctgacccacaagaaacgcctaactgatgaggagtttcgagagccatctacggggaagacctgcctgcccaaggcc
L D G L L P F L L T H K K R L T D E E F R E P S T G K T C L P K A
ttgctgaacctgagcaatggccgcaacgacaccatccctgtgctgctggacatcgcggagcgcaccggcaacatgagggagttcattaactcgcccttc
L L N L S N G R N D T I P V L L D I A E R T G N M R E F I N S P F
cgtgacatctactatcgaggtcagacagccctgcacatcgccattgagcgtcgctgcaaacactacgtggaacttctcgtggcccagggagctgatgtc
R D I Y Y R G Q T A L H I A I E R R C K H Y V E L L V A Q G A D V
cacgcccaggcccgtgggcgcttcttccagcccaaggatgaggggggctacttctactttggggagctgcccctgtcgctggctgcctgcaccaaccag
H A Q A R G R F F Q P E D E G G Y F Y F G E L P L S L A A C T N Q
ccccacattgtcaactacctgacggagaaccccacaagaaggcggacatgcggcgccaggactcgcgaggcaacacagtgctgcatgcgctggtggcc
P H I V N Y L T E N P H K K A D M R R Q D S R G N T V L H A L V A
attgctgacaacacccgtgagaacaccaagtttgttaccaagatgtacgacctgctgctgctcaagtgtgcccgcctcttccccgacagcaacctggag
I A D N T R E N T K F V T K M Y D L L L L K C A R L F P D S N L E
gccgtgctcaacaacgacggcctctcgcccctcatgatggctgccaagacgggcaagattgggatctttcagcacatcatccggcgggaggtgacggat
A V L N N D G L S P L M M A A K T G K I G I F Q H I I R R E V T D
gaggcggccgctggcctgaacgatatttttgaagcgcagaaaattgaatggcatgaacatcatcaccatcatcattga
E A A A G L N D I F E A Q K I E W H E H H H H H H -

BirA ligase

atgaaggataacaccgtgccactgaaattgattgccctgttagcgaacggtgaatttcactctggcgagcagttgggtgaaacgctgggaatgagccgg
M K D N T V P L K L I A L L A N G E F H S G E Q L G E T L G M S R
gcggctattaataaacacattcagacactgcgtgactggggcgttgatgtctttaccgttccgggtaaaggatacagcctgcctgagcctatccagtta
A A I N K H I Q T L R D W G V D V F T V P G K G Y S L P E P I Q L
cttaatgctaaacagatattgggtcagctggatggcggtagtgtagccgtgctgccagtgattgactccacgaatcagtaccttcttgatcgtatcgga
L N A K Q I L G Q L D G G S V A V L P V I D S T N Q Y L L D R I G
gagcttaaatcgggcgatgcttgcattgcagaataccagcaggctggccgtggtcgccggggtcggaaatggttttcgccttttggcgcaaacttatat
E L K S G D A C I A E Y Q Q A G R G R R G R K W F S P F G A N L Y
ttgtcgatgttctggcgtctggaacaaggcccggcggcggcgattggtttaagtctggttatcggtatcgtgatggcggaagtattacgcaagctgggt
L S M F W R L E Q G P A A A I G L S L V I G I V M A E V L R K L G
gcagataaagttcgtgttaaatggcctaatgacctctatctgcaggatcgcaagctggcaggcattctggtggagctgactggcaaaactggcgatgcg
A D K V R V K W P N D L Y L Q D R K L A G I L V E L T G K T G D A
gcgcaaatagtcattggagccgggatcaacatggcaatgcgccgtgttgaagagagtgtcgttaatcaggggtggatcacgctgcaggaagcggggatc

A Q I V I G A G I N M A M R R V E E S V V N Q G W I T L Q E A G I
aatctcgatcgtaatacgttggcggccatgttaatacgtgaattacgtgctgcgttggaactcttcgaacaagaaggattggcaccttatctgtcgcgc
N L D R N T L A A M L I R E L R A A L E L F E Q E G L A P Y L S R
tgggaaaagctggataatttttattaatcgcccagtgaaacttatcattggtgataaagaaatatttggcatttcacgcggaatagacaaacaggggct
W E K L D N F I N R P V K L I I G D K E I F G I S R G I D K Q G A
ttattacttgagcaggatggaataataaaaccctggatgggcggtgaaatatccctgcgtagtgcagaaaaaggtggtctcgagtga
L L L E Q D G I I K P W M G G E I S L R S A E K G G L E -

hsV4 ARD+PRR

atgaaagcccctgcccctcagccgcccccccatcctcaaagtcttcaaccggcctatcctctttgacatcgtgtcccggggctccactgctgacctggac
M K A P A P Q P P P I L K V F N R P I L F D I V S R G S T A D L D
gggctgctcccattcttgctgacccacaagaaacgcctaactgatgaggagtttcgagagccatctacggggaagacctgcctgcccaaggccttgctg
G L L P F L L T H K K R L T D E E F R E P S T G K T C L P K A L L
aacctgagcaatggccgcaacgacaccatccctgtgctgctggacatcgcggagcgcaccggcaacatgagggagttcattaactcgcccttccgtgac
N L S N G R N D T I P V L L D I A E R T G N M R E F I N S P F R D
atctactatcgaggtcagacagccctgcacatcgccattgagcgtcgctgcaaacactacgtggaacttctcgtggcccagggagctgatgtccacgcc
I Y Y R G Q T A L H I A I E R R C K H Y V E L L V A Q G A D V H A
caggcccgtgggcgcttcttccagcccaaggatgagggggctacttctactttggggagctgcccctgtcgctggctgcctgcaccaaccagccccac
Q A R G R F F Q P K D E G G Y F Y F G E L P L S L A A C T N Q P H
attgtcaactacctgacggagaaccccccacaagaaggcggacatgcggcgccaggactcgcgaggcaacacagtgctgcatgcgctggtggccattgct
I V N Y L T E N P H K K A D M R R Q D S R G N T V L H A L V A I A
gacaacacccgtgagaacaccaagtttgttaccaagatgtacgacctgctgctgctcaagtgtgcccgcctcttccccgacagcaacctggaggccgtg
D N T R E N T K F V T K M Y D L L L L K C A R L F P D S N L E A V
ctcaacaacgacggcctctcgcccctcatgatggctgccaagacgggcaagattgggatctttcagcacatcatccggcgggaggtgacggatgaggcg
L N N D G L S P L M M A A K T G K I G I F Q H I I R R E V T D E A
gccgctcatcatcaccatcatcattga
A A H H H H H H -

hsV4 ARD wt

atgctcaaagtcttcaaccggcctatcctctttgacatcgtgtcccggggctccactgctgacctggacgggctgctcccattcttgctgacccacaag
M L K V F N R P I L F D I V S R G S T A D L D G L L P F L L T H K
aaacgcctaactgatgaggagtttcgagagccatctacggggaagacctgcctgcccaaggccttgctgaacctgagcaatggccgcaacgacaccatc
K R L T D E E F R E P S T G K T C L P K A L L N L S N G R N D T I
cctgtgctgctggacatcgcggagcgcaccggcaacatgagggagttcattaactcgcccttccgtgacatctactatcgaggtcagacagccctgcac
P V L L D I A E R T G N M R E F I N S P F R D I Y Y R G Q T A L H
atcgccattgagcgtcgctgcaaacactacgtggaacttctcgtggcccagggagctgatgtccacgcccaggcccgtgggcgcttcttccagcccaag
I A I E R R C K H Y V E L L V A Q G A D V H A Q A R G R F F Q P K
gatgaggggggctacttctactttggggagctgcccctgtcgctggctgcctgcaccaaccagccccacattgtcaactacctgacggagaaccccccac
D E G G Y F Y F G E L P L S L A A C T N Q P H I V N Y L T E N P H
aagaaggcggacatgcggcgccaggactcgcgaggcaacacagtgctgcatgcgctggtggccattgctgacaacacccgtgagaacaccaagtttgtt
K K A D M R R Q D S R G N T V L H A L V A I A D N T R E N T K F V
accaagatgtacgacctgctgctgctcaagtgtgcccgcctcttccccgacagcaacctggaggccgtgctcaacaacgacggcctctcgcccctcatg
T K M Y D L L L L K C A R L F P D S N L E A V L N N D G L S P L M
atggctgccaagacgggcaagattgggatctttcagcacatcatccggcgggaggtgacggatgaggcggccgctcatcatcaccatcatcattga

M A A K T G K I G I F Q H I I R R E V T D E A A A H H H H H H -

hsDDX3X_aa122-582

acc atg aaa cat cac cat cac cat cac ccc atg
M K H H H H H H P M
agc gat tac gac atc ccc act act gag aat ctt tat ttt cag ggc ggc aac agc cgc tgg
S D Y D I P T T E N L Y F Q G G N S R W
tgc gat aaa agc gat gag gat gac tgg agc aag ccg ctg ccg ccg agc gaa cgc ctg gag
C D K S D E D D W S K P L P P S E R L E
caa gaa ctg ttt agc ggt ggt aac acc ggt att aac ttt gaa aag tac gac gat atc ccg
Q E L F S G G N T G I N F E K Y D D I P
gtg gag gcg acc ggt aac aac tgc ccg ccg cac att gaa agc ttc agc gac gtt gag atg
V E A T G N N C P P H I E S F S D V E M
ggt gaa atc att atg ggc aac atc gag ctg acc cgt tat acc cgt ccg acc ccg gtg cag
G E I I M G N I E L T R Y T R P T P V Q
aag cat gcg att ccg atc att aag gaa aaa cgt gac ctg atg gcg tgc gcg cag acc ggt
K H A I P I I K E K R D L M A C A Q T G
agc ggt aaa acc gcg gcg ttt ctg ctg ccg atc ctg agc caa att tat agc gat ggt ccg
S G K T A A F L L P I L S Q I Y S D G P
ggt gaa gcg ctg cgt gcg atg aag gaa aac ggt cgt tac ggc cgt cgt aaa cag tat ccg
G E A L R A M K E N G R Y G R R K Q Y P
atc agc ctg gtg ctg gcg ccg acc cgt gag ctg gcg gtt caa att tac gag gaa gcg cgt
I S L V L A P T R E L A V Q I Y E E A R
aaa ttc agc tat cgt agc cgt gtg cgt ccg tgc gtg gtt tac ggt ggc gcg gac atc ggt
K F S Y R S R V R P C V V Y G G A D I G
cag caa att cgt gat ctg gaa cgt ggc tgc cac ctg ctg gtt gcg acc ccg ggt cgt ctg
Q Q I R D L E R G C H L L V A T P G R L
gtt gac atg atg gag cgt ggc aag atc ggc ctg gat ttc tgc aaa tat ctg gtt ctg gac
V D M M E R G K I G L D F C K Y L V L D
gaa gcg gat cgt atg ctg gac atg ggc ttt gag ccg cag atc cgt cgt att gtg gaa caa
E A D R M L D M G F E P Q I R R I V E Q
gat acc atg ccg cca aag ggt gtt cgt cac acc atg atg ttc agc gcg acc ttt ccg aaa
D T M P P K G V R H T M M F S A T F P K
gag atc cag atg ctg gcg cgt gac ttc ctg gat gaa tac att ttt ctg gcg gtg ggt cgt
E I Q M L A R D F L D E Y I F L A V G R
gtt ggc agc acc agc gag aac atc acc caa aag gtg gtt tgg gtg gag gaa agc gac aaa
V G S T S E N I T Q K V V W V E E S D K
cgt agc ttt ctg ctg gat ctg ctg aac gcg acc ggc aag gac agc ctg acc ctg gtg ttc
R S F L L D L L N A T G K D S L T L V F
gtt gaa acc aag aaa ggt gct gac agc ctg gag gat ttt ctg tac cac gaa ggt tat gcg
V E T K K G A D S L E D F L Y H E G Y A
tgc acc agc atc cac ggc gac cgt agc cag cgt gat cgt gag gaa gcg ctg cac caa ttc
C T S I H G D R S Q R D R E E A L H Q F
cgt agc ggc aag agc ccg att ctg gtg gcg acc gcg gtt gcg gcg cgt ggt ctg gat atc
R S G K S P I L V A T A V A A R G L D I
agc aac gtg aaa cac gtt att aac ttt gac ctg ccg agc gat atc gag gaa tat gtg cac

```
S   N   V   K   H   V   I   N   F   D   L   P   S   D   I   E   E   Y   V   H
cgt att ggt cgt acc ggc cgt gtt ggt aac ctg ggc ctg gcg acc agc ttc ttt aac gag
R   I   G   R   T   G   R   V   G   N   L   G   L   A   T   S   F   F   N   E
cgt aac atc aac att acc aaa gac ctg ctg gat ctg ctg gtt gaa gcg aag caa gag gtg
R   N   I   N   I   T   K   D   L   L   D   L   L   V   E   A   K   Q   E   V
ccg agc tgg ctg gag aat atg gcg tat gag cat cac tac aag ggc tga
P   S   W   L   E   N   M   A   Y   E   H   H   Y   K   G   -
```

hsDDX3X

```
atg gcc gga aaa cct atc cct aac cct ctg ctg ggg ctg gac tca acc gaa ctg
 M   A   G   K   P   I   P   N   P   L   L   G   L   D   S   T   E   L
att acc tct ctg tat aag aag gct gga act atg tcc cac gtg gca gtg gag aac gca ctg
I   T   S   L   Y   K   K   A   G   T   M   S   H   V   A   V   E   N   A   L
ggc ctg gac cag cag ttc gca ggc ctg gac ctg aac agc tcc gat aat cag tct gga ggc
G   L   D   Q   Q   F   A   G   L   D   L   N   S   S   D   N   Q   S   G   G
agc acc gcc tcc aag ggc agg tac atc ccc cct cac ctg cgg aat aga gag gcc aca aag
S   T   A   S   K   G   R   Y   I   P   P   H   L   R   N   R   E   A   T   K
ggc ttc tat gac aag gat tct agc ggc tgg tcc tct agc aag gac aag gat gcc tac tcc
G   F   Y   D   K   D   S   S   G   W   S   S   S   K   D   K   D   A   Y   S
tct ttt ggc tct agg agc gac tcc cgc ggc aag agc tcc ttc ttt tcc gat agg ggc tct
S   F   G   S   R   S   D   S   R   G   K   S   S   F   F   S   D   R   G   S
ggc agc agg ggc cgc ttt gac gat agg ggc aga agc gac tat gat ggc atc ggc tcc aga
G   S   R   G   R   F   D   D   R   G   R   S   D   Y   D   G   I   G   S   R
ggc gac agg tct ggc ttc ggc aag ttt gag agg gga gga aac agc agg tgg tgc gac aag
G   D   R   S   G   F   G   K   F   E   R   G   G   N   S   R   W   C   D   K
tcc gat gag gac gat tgg tct aag cca ctg cca cca agc gag cgg ctg gag cag gag ctg
S   D   E   D   D   W   S   K   P   L   P   P   S   E   R   L   E   Q   E   L
ttc agc gga ggc aac acc ggc atc aat ttt gag aag tac gac gat atc ccc gtg gag gcc
F   S   G   G   N   T   G   I   N   F   E   K   Y   D   D   I   P   V   E   A
aca ggc aac aat tgt cct cca cac atc gag tcc ttc tct gat gtg gag atg ggc gag atc
T   G   N   N   C   P   P   H   I   E   S   F   S   D   V   E   M   G   E   I
atc atg ggc aac atc gag ctg acc cgc tat aca cgg cca acc ccc gtg cag aag cac gcc
I   M   G   N   I   E   L   T   R   Y   T   R   P   T   P   V   Q   K   H   A
atc cct atc atc aag gag aag cgg gac ctg atg gca tgc gca cag aca ggc tcc ggc aag
I   P   I   I   K   E   K   R   D   L   M   A   C   A   Q   T   G   S   G   K
acc gca gcc ttt ctg ctg ccc atc ctg agc cag atc tac tcc gat gga cct gga gag gcc
T   A   A   F   L   L   P   I   L   S   Q   I   Y   S   D   G   P   G   E   A
ctg agg gca atg aag gag aat ggc cgc tac ggc cgg aga aag cag tat cct atc agc ctg
L   R   A   M   K   E   N   G   R   Y   G   R   R   K   Q   Y   P   I   S   L
gtg ctg gcc cca acc agg gag ctg gcc gtg cag atc tac gag gag gcc cgc aag ttc tct
V   L   A   P   T   R   E   L   A   V   Q   I   Y   E   E   A   R   K   F   S
tat agg agc cgc gtg cgg cct tgc gtg gtg tac gga gga gca gac atc gga cag cag atc
Y   R   S   R   V   R   P   C   V   V   Y   G   G   A   D   I   G   Q   Q   I
cgg gat ctg gag aga ggc tgt cac ctg ctg gtg gca acc cca ggc cgg ctg gtg gac atg
R   D   L   E   R   G   C   H   L   L   V   A   T   P   G   R   L   V   D   M
atg gag aga ggc aag atc ggc ctg gat ttc tgt aag tat ctg gtg ctg gac gag gcc gat
```

```
M   E   R   G   K   I   G   L   D   F   C   K   Y   L   V   L   D   E   A   D
cgg atg ctg gac atg ggc ttt gag ccc cag atc agg cgc atc gtg gag cag gat aca atg
R   M   L   D   M   G   F   E   P   Q   I   R   R   I   V   E   Q   D   T   M
ccc cct aag ggc gtg aga cac aca atg atg ttc agc gcc acc ttt cct aag gag atc cag
P   P   K   G   V   R   H   T   M   M   F   S   A   T   F   P   K   E   I   Q
atg ctg gcc cgg gac ttc ctg gat gag tac atc ttt ctg gcc gtg ggc aga gtg ggc agc
M   L   A   R   D   F   L   D   E   Y   I   F   L   A   V   G   R   V   G   S
aca tcc gag aac atc acc cag aag gtg gtg tgg gtg gag gag tct gac aag cgg agc ttt
T   S   E   N   I   T   Q   K   V   V   W   V   E   E   S   D   K   R   S   F
ctg ctg gat ctg ctg aat gcc aca ggc aag gac tcc ctg acc ctg gtg ttc gtg gag aca
L   L   D   L   L   N   A   T   G   K   D   S   L   T   L   V   F   V   E   T
aag aag ggc gcc gac tct ctg gag gat ttt ctg tac cac gag ggc tat gca tgc acc tcc
K   K   G   A   D   S   L   E   D   F   L   Y   H   E   G   Y   A   C   T   S
atc cac ggc gac cgg agc cag aga gat agg gag gag gcc ctg cac cag ttc cgc tcc ggc
I   H   G   D   R   S   Q   R   D   R   E   E   A   L   H   Q   F   R   S   G
aag tct cca atc ctg gtg gca aca gca gtg gca gca agg ggc ctg gat atc tct aac gtg
K   S   P   I   L   V   A   T   A   V   A   A   R   G   L   D   I   S   N   V
aag cac gtg atc aat ttt gac ctg ccc agc gat atc gag gag tat gtg cac aga atc gga
K   H   V   I   N   F   D   L   P   S   D   I   E   E   Y   V   H   R   I   G
agg acc gga agg gtg gga aac ctg ggc ctg gcc aca tcc ttc ttt aac gag aga aac atc
R   T   G   R   V   G   N   L   G   L   A   T   S   F   F   N   E   R   N   I
aac atc acc aag gac ctg ctg gat ctg ctg gtg gag gcc aag cag gag gtg ccc agc tgg
N   I   T   K   D   L   L   D   L   L   V   E   A   K   Q   E   V   P   S   W
ctg gag aat atg gcc tac gag cac cac tat aag ggc tct agc agg ggc cgg agc aag tcc
L   E   N   M   A   Y   E   H   H   Y   K   G   S   S   R   G   R   S   K   S
tct agg ttc tcc gga gga ttt gga gca agg gac tac aga cag agc tcc gga gcc tct agc
S   R   F   S   G   G   F   G   A   R   D   Y   R   Q   S   S   G   A   S   S
tcc tct ttc agc tcc tct cgg gcc agc tcc tct aga agc ggc ggc ggc ggc cac ggc agc
S   S   F   S   S   S   R   A   S   S   S   R   S   G   G   G   G   H   G   S
tcc cgc ggc ttc ggc ggc ggc ggc tat ggc ggc ttt tac aac tca gac ggc tac gga ggg
S   R   G   F   G   G   G   G   Y   G   G   F   Y   N   S   D   G   Y   G   G
aac tac aac tca cag ggc gtg gac tgg tgg gga aac tag
N   Y   N   S   Q   G   V   D   W   W   G   N   -
```

eGFP

```
atgagcaaaggcgaagaactgtttaccggcgtggtgccgattctggtggaactggatggcgatgtgaacggccataaatttagcgtgagcggcgaaggc
M   S   K   G   E   E   L   F   T   G   V   V   P   I   L   V   E   L   D   G   D   V   N   G   H   K   F   S   V   S   G   E   G
gaaggcgatgcgacctatggcaaactgaccctgaaatttatttgcaccaccggcaaactgccggtgccgtggccgaccctggtgaccacctttagctat
E   G   D   A   T   Y   G   K   L   T   L   K   F   I   C   T   T   G   K   L   P   V   P   W   P   T   L   V   T   T   F   S   Y
ggcgtgcagtgctttagccgctatccggatcatatgaaacagcatgatttttttaaaagcgcgatgccggaaggctatgtgcaggaacgcaccatttttt
G   V   Q   C   F   S   R   Y   P   D   H   M   K   Q   H   D   F   F   K   S   A   M   P   E   G   Y   V   Q   E   R   T   I   F
tttaaagatgatggcaactataaaaacccgcgcggaagtgaaatttgaaggcgataccctggtgaaccgcattgaactgaaaggcattgattttaaagaa
F   K   D   D   G   N   Y   K   T   R   A   E   V   K   F   E   G   D   T   L   V   N   R   I   E   L   K   G   I   D   F   K   E
gatggcaacattctgggccataaactggaatataactataacagccataacgtgtatattatggcggataaacagaaaaacggcattaaagtgaacttt
D   G   N   I   L   G   H   K   L   E   Y   N   Y   N   S   H   N   V   Y   I   M   A   D   K   Q   K   N   G   I   K   V   N   F
aaaattcgccataacattgaagatggcagcgtgcagctggcggatcattatcagcagaacaccccgattggcgatggcccggtgctgctgccggataac
```

```
K I R H N I E D G S V Q L A D H Y Q Q N T P I G D G P V L L P D N
cattatctgagcacccagagcgcgctgagcaaagatccgaacgaaaaacgcgatcatatggtgctgctggaatttgtgaccgcggcgggcattacccat
H Y L S T Q S A L S K D P N E K R D H M V L L E F V T A A G I T H
ggcatggatgaactgtataaa
G M D E L Y K
```

hsTRPV4-cGFP

```
atg gcg gat tcc agc gaa ggc ccc cgc gcg ggg ccc ggg gag gtg gct gag ctc ccc ggg
M  A  D  S  S  E  G  P  R  A  G  P  G  E  V  A  E  L  P  G
gat gag agt ggc acc cca ggt ggg gag gct ttt cct ctc tcc tcc ctg gcc aat ctg ttt
D  E  S  G  T  P  G  G  E  A  F  P  L  S  S  L  A  N  L  F
gag ggg gag gat ggc tcc ctt tcg ccc tca ccg gct gat gcc agt cgc cct gct ggc cca
E  G  E  D  G  S  L  S  P  S  P  A  D  A  S  R  P  A  G  P
ggc gat ggg cga cca aat ctg cgc atg aag ttc cag ggc gcc ttc cgc aag ggg gtg ccc
G  D  G  R  P  N  L  R  M  K  F  Q  G  A  F  R  K  G  V  P
aac ccc atc gat ctg ctg gag tcc acc cta tat gag tcc tcg gtg gtg cct ggg ccc aag
N  P  I  D  L  L  E  S  T  L  Y  E  S  S  V  V  P  G  P  K
aaa gca ccc atg gac tca ctg ttt gac tac ggc acc tat cgt cac cac tcc agt gac aac
K  A  P  M  D  S  L  F  D  Y  G  T  Y  R  H  H  S  S  D  N
aag agg tgg agg aag aag atc ata gag aag cag ccg cag agc ccc aaa gcc cct gcc cct
K  R  W  R  K  K  I  I  E  K  Q  P  Q  S  P  K  A  P  A  P
cag ccg ccc ccc atc ctc aaa gtc ttc aac cgg cct atc ctc ttt gac atc gtg tcc cgg
Q  P  P  P  I  L  K  V  F  N  R  P  I  L  F  D  I  V  S  R
ggc tcc act gct gac ctg gac ggg ctg ctc cca ttc ttg ctg acc cac aag aaa cgc cta
G  S  T  A  D  L  D  G  L  L  P  F  L  L  T  H  K  K  R  L
act gat gag gag ttt cga gag cca tct acg ggg aag acc tgc ctg ccc aag gcc ttg ctg
T  D  E  E  F  R  E  P  S  T  G  K  T  C  L  P  K  A  L  L
aac ctg agc aat ggc cgc aac gac acc atc cct gtg ctg ctg gac atc gcg gag cgc acc
N  L  S  N  G  R  N  D  T  I  P  V  L  L  D  I  A  E  R  T
ggc aac atg agg gag ttc att aac tcg ccc ttc cgt gac atc tac tat cga ggt cag aca
G  N  M  R  E  F  I  N  S  P  F  R  D  I  Y  Y  R  G  Q  T
gcc ctg cac atc gcc att gag cgt cgc tgc aaa cac tac gtg gaa ctt ctc gtg gcc cag
A  L  H  I  A  I  E  R  R  C  K  H  Y  V  E  L  L  V  A  Q
gga gct gat gtc cac gcc cag gcc cgt ggg cgc ttc ttc cag ccc aag gat gag ggg ggc
G  A  D  V  H  A  Q  A  R  G  R  F  F  Q  P  K  D  E  G  G
tac ttc tac ttt ggg gag ctg ccc ctg tcg ctg gct gcc tgc acc aac cag ccc cac att
Y  F  Y  F  G  E  L  P  L  S  L  A  A  C  T  N  Q  P  H  I
gtc aac tac ctg acg gag aac ccc cac aag aaa gcc gac atg agg agg cag gac agc agg
V  N  Y  L  T  E  N  P  H  K  K  A  D  M  R  R  Q  D  S  R
ggc aac acc gtg ctg cac gcc ctg gtg gcc atc gcc gac aac acc agg gag aac acc aag
G  N  T  V  L  H  A  L  V  A  I  A  D  N  T  R  E  N  T  K
ttc gtg acc aag atg tac gac ctg ctg ctg ctg aag tgc gcc agg ctg ttc ccc gac agc
F  V  T  K  M  Y  D  L  L  L  L  K  C  A  R  L  F  P  D  S
aac ctg gag gcc gtg ctg aac aac gac ggc ctg agc ccc ctg atg atg gcc gcc aag acc
N  L  E  A  V  L  N  N  D  G  L  S  P  L  M  M  A  A  K  T
ggc aag att ggg atc ttt cag cac atc atc cgg cgg gag gtg acg gat gag gac aca cgg
```

```
G  K  I  G  I  F  Q  H  I  I  R  R  E  V  T  D  E  D  T  R
cac ctg tcc cgc aag ttc aag gac tgg gcc tat ggg cca gtg tat tcc tcg ctt tat gac
H  L  S  R  K  F  K  D  W  A  Y  G  P  V  Y  S  S  L  Y  D
ctc tcc tcc ctg gac acg tgt ggg gaa gag gcc tcc gtg ctg gag atc ctg gtg tac aac
L  S  S  L  D  T  C  G  E  E  A  S  V  L  E  I  L  V  Y  N
agc aag att gag aac cgc cac gag atg ctg gct gtg gag ccc atc aat gaa ctg ctg cgg
S  K  I  E  N  R  H  E  M  L  A  V  E  P  I  N  E  L  L  R
gac aag tgg cgc aag ttc ggg gcc gtc tcc ttc tac atc aac gtg gtc tcc tac ctg tgt
D  K  W  R  K  F  G  A  V  S  F  Y  I  N  V  V  S  Y  L  C
gcc atg gtc atc ttc act ctc acc gcc tac tac cag ccg ctg gag ggc aca ccg ccg tac
A  M  V  I  F  T  L  T  A  Y  Y  Q  P  L  E  G  T  P  P  Y
cct tac cgc acc acg gtg gac tac ctg cgg ctg gct ggc gag gtc att acg ctc ttc act
P  Y  R  T  T  V  D  Y  L  R  L  A  G  E  V  I  T  L  F  T
ggg gtc ctg ttc ttc ttc acc aac atc aaa gac ttg ttc atg aag aaa tgc cct gga gtg
G  V  L  F  F  F  T  N  I  K  D  L  F  M  K  K  C  P  G  V
aat tct ctc ttc att gat ggc tcc ttc cag ctg ctc tac ttc atc tac tct gtc ctg gtg
N  S  L  F  I  D  G  S  F  Q  L  L  Y  F  I  Y  S  V  L  V
atc gtc tca gca gcc ctc tac ctg gca ggg atc gag gcc tac ctg gcc gtg atg gtc ttt
I  V  S  A  A  L  Y  L  A  G  I  E  A  Y  L  A  V  M  V  F
gcc ctg gtc ctg ggc tgg atg aat gcc ctt tac ttc acc cgt ggg ctg aag ctg acg ggg
A  L  V  L  G  W  M  N  A  L  Y  F  T  R  G  L  K  L  T  G
acc tat agc atc atg atc cag aag att ctc ttc aag gac ctt ttc cga ttc ctg ctc gtc
T  Y  S  I  M  I  Q  K  I  L  F  K  D  L  F  R  F  L  L  V
tac ttg ctc ttc atg atc ggc tac gct tca gcc ctg gtc tcc ctc ctg aac ccg tgt gcc
Y  L  L  F  M  I  G  Y  A  S  A  L  V  S  L  L  N  P  C  A
aac atg aag gtg tgc aat gag gac cag acc aac tgc aca gtg ccc act tac ccc tcg tgc
N  M  K  V  C  N  E  D  Q  T  N  C  T  V  P  T  Y  P  S  C
cgt gac agc gag acc ttc agc acc ttc ctc ctg gac ctg ttt aag ctg acc atc ggc atg
R  D  S  E  T  F  S  T  F  L  L  D  L  F  K  L  T  I  G  M
ggc gac ctg gag atg ctg agc agc acc aag tac ccc gtg gtc ttc atc atc ctg ctg gtg
G  D  L  E  M  L  S  S  T  K  Y  P  V  V  F  I  I  L  L  V
acc tac atc atc ctc acc ttt gtg ctg ctc ctc aac atg ctc att gcc ctc atg ggc gag
T  Y  I  I  L  T  F  V  L  L  L  N  M  L  I  A  L  M  G  E
aca gtg ggc cag gtc tcc aag gag agc aag cac atc tgg aag ctg cag tgg gcc acc acc
T  V  G  Q  V  S  K  E  S  K  H  I  W  K  L  Q  W  A  T  T
atc ctg gac att gag cgc tcc ttc ccc gta ttc ctg agg aag gcc ttc cgc tct ggg gag
I  L  D  I  E  R  S  F  P  V  F  L  R  K  A  F  R  S  G  E
atg gtc acc gtg ggc aag agc tcg gac ggc act cct gac cgc agg tgg tgc ttc agg gtg
M  V  T  V  G  K  S  S  D  G  T  P  D  R  R  W  C  F  R  V
gat gag gtg aac tgg tct cac tgg aac cag aac ttg ggc atc atc aac gag gac ccg ggc
D  E  V  N  W  S  H  W  N  Q  N  L  G  I  I  N  E  D  P  G
aag aat gag acc tac cag tat tat ggc ttc tcg cat acc gtg ggc cgc ctc cgc agg gat
K  N  E  T  Y  Q  Y  Y  G  F  S  H  T  V  G  R  L  R  R  D
cgc tgg tcc tcg gtg gta ccc cgc gtg gtg gaa ctg aac aag aac tcg aac ccg gac gag
R  W  S  S  V  V  P  R  V  V  E  L  N  K  N  S  N  P  D  E
gtg gtg gtg cct ctg gac agc atg ggg aac ccc cgc tgc gat ggc cac cag cag ggt tac
V  V  V  P  L  D  S  M  G  N  P  R  C  D  G  H  Q  Q  G  Y
ccc cgc aag tgg agg act gat gac gcc ccg ctc atg gtg tgc aag tat gag gag ctg ttc
```

```
P   R   K   W   R   T   D   D   A   P   L   M   V   C   K   Y   E   E   L   F
acc ggg gtg gtg ccc atc ctg gtc gag ctg gac ggc gac gta aac ggc cac aag ttc agc
T   G   V   V   P   I   L   V   E   L   D   G   D   V   N   G   H   K   F   S
gtg tcc ggc gag agc gag ggc gat gcc acg tac ggc aag ctg acc atg aag ttc atc tgc
V   S   G   E   S   E   G   D   A   T   Y   G   K   L   T   M   K   F   I   C
acc acc ggc aag ctg ccc gtg ccc tgg ccc acc ctc gtg acc acc ctg acg tac ggc gtg
T   T   G   K   L   P   V   P   W   P   T   L   V   T   T   L   T   Y   G   V
cag tgc ttc agc cgc tac ccc gac cac atg aag cag cac gac ttc ttc aag tcc gcc atg
Q   C   F   S   R   Y   P   D   H   M   K   Q   H   D   F   F   K   S   A   M
ccc gaa ggc tac gtc cag gag cgc acc atc ttc ttc aag gat gac ggc aac tac aag acc
P   E   G   Y   V   Q   E   R   T   I   F   F   K   D   D   G   N   Y   K   T
cgc gcc gag gtg aag ttc gag ggc gac acc ctg gtg aac cgc atc gag ctg aag ggc atc
R   A   E   V   K   F   E   G   D   T   L   V   N   R   I   E   L   K   G   I
gac ttc aag gag gac ggc aac atc ctg ggg cac aag ctg gag tac aac tac aac agc cac
D   F   K   E   D   G   N   I   L   G   H   K   L   E   Y   N   Y   N   S   H
aac gtc tat atc atg gcc gac aag cag aag aac ggc atc aag gtg aac ttc aag atc cgc
N   V   Y   I   M   A   D   K   Q   K   N   G   I   K   V   N   F   K   I   R
cac aac atc gag gac ggc agc gtg cag ctc gcc gac cac tac cag cag aac acc ccc atc
H   N   I   E   D   G   S   V   Q   L   A   D   H   Y   Q   Q   N   T   P   I
ggc gac ggc ccc gtg ctg ctg ccc gac aac cac tac ctg agc acc cag tcc aag ctg agc
G   D   G   P   V   L   L   P   D   N   H   Y   L   S   T   Q   S   K   L   S
aaa gac ccc aac gag aag cgc gat cac atg gtc ctg ctg gag ttc gtg acc gcc gcc ggg
K   D   P   N   E   K   R   D   H   M   V   L   L   E   F   V   T   A   A   G
atc act ctc ggc atg gac gag ctg tac aag tag
I   T   L   G   M   D   E   L   Y   K   -
```

hsTRPV4 R232C-cGFP

see hsTRPV4-cGFP, c.694C>T, p. Arg232C

hsTRPV4 R269C-cGFP

see hsTRPV4-cGFP, c.805C>T, p. Arg269C

hsTRPV4-cFLAG

```
atg gcg gat tcc agc gaa ggc ccc cgc gcg ggg ccc
M   A   D   S   S   E   G   P   R   A   G   P
ggg gag gtg gct gag ctc ccc ggg gat gag agt ggc acc cca ggt ggg gag gct ttt cct
G   E   V   A   E   L   P   G   D   E   S   G   T   P   G   G   E   A   F   P
ctc tcc tcc ctg gcc aat ctg ttt gag ggg gag gat ggc tcc ctt tcg ccc tca ccg gct
L   S   S   L   A   N   L   F   E   G   E   D   G   S   L   S   P   S   P   A
gat gcc agt cgc cct gct ggc cca ggc gat ggg cga cca aat ctg cgc atg aag ttc cag
D   A   S   R   P   A   G   P   G   D   G   R   P   N   L   R   M   K   F   Q
```

```
ggc gcc ttc cgc aag ggg gtg ccc aac ccc atc gat ctg ctg gag tcc acc cta tat gag
G   A   F   R   K   G   V   P   N   P   I   D   L   L   E   S   T   L   Y   E
tcc tcg gtg gtg cct ggg ccc aag aaa gca ccc atg gac tca ctg ttt gac tac ggc acc
S   S   V   V   P   G   P   K   K   A   P   M   D   S   L   F   D   Y   G   T
tat cgt cac cac tcc agt gac aac aag agg tgg agg aag aag atc ata gag aag cag ccg
Y   R   H   H   S   S   D   N   K   R   W   R   K   K   I   I   E   K   Q   P
cag agc ccc aaa gcc cct gcc cct cag ccg ccc ccc atc ctc aaa gtc ttc aac cgg cct
Q   S   P   K   A   P   A   P   Q   P   P   P   I   L   K   V   F   N   R   P
atc ctc ttt gac atc gtg tcc cgg ggc tcc act gct gac ctg gac ggg ctg ctc cca ttc
I   L   F   D   I   V   S   R   G   S   T   A   D   L   D   G   L   L   P   F
ttg ctg acc cac aag aaa cgc cta act gat gag gag ttt cga gag cca tct acg ggg aag
L   L   T   H   K   K   R   L   T   D   E   E   F   R   E   P   S   T   G   K
acc tgc ctg ccc aag gcc ttg ctg aac ctg agc aat ggc cgc aac gac acc atc cct gtg
T   C   L   P   K   A   L   L   N   L   S   N   G   R   N   D   T   I   P   V
ctg ctg gac atc gcg gag cgc acc ggc aac atg agg gag ttc att aac tcg ccc ttc cgt
L   L   D   I   A   E   R   T   G   N   M   R   E   F   I   N   S   P   F   R
gac atc tac tat cga ggt cag aca gcc ctg cac atc gcc att gag cgt cgc tgc aaa cac
D   I   Y   Y   R   G   Q   T   A   L   H   I   A   I   E   R   R   C   K   H
tac gtg gaa ctt ctc gtg gcc cag gga gct gat gtc cac gcc cag gcc cgt ggg cgc ttc
Y   V   E   L   L   V   A   Q   G   A   D   V   H   A   Q   A   R   G   R   F
ttc cag ccc aag gat gag ggg ggc tac ttc tac ttt ggg gag ctg ccc ctg tcg ctg gct
F   Q   P   K   D   E   G   G   Y   F   Y   F   G   E   L   P   L   S   L   A
gcc tgc acc aac cag ccc cac att gtc aac tac ctg acg gag aac ccc cac aag aaa
A   C   T   N   Q   P   H   I   V   N   Y   L   T   E   N   P   H   K   K
gcc gac atg agg agg cag gac agc agg ggc aac acc gtg ctg cac gcc ctg gtg gcc
A   D   M   R   R   Q   D   S   R   G   N   T   V   L   H   A   L   V   A
atc gcc gac aac acc agg gag aac acc aag
I   A   D   N   T   R   E   N   T   K
ttc gtg acc aag atg tac gac ctg ctg ctg ctg aag tgc gcc agg ctg ttc ccc gac agc
F   V   T   K   M   Y   D   L   L   L   L   K   C   A   R   L   F   P   D   S
aac ctg gag gcc gtg ctg aac aac gac ggc ctg agc ccc ctg atg atg gcc gcc aag acc
N   L   E   A   V   L   N   N   D   G   L   S   P   L   M   M   A   A   K   T
ggc aag att ggg atc ttt cag cac atc atc cgg cgg gag
G   K    I   G   I   F   Q   H   I   I   R   R   E
gtg acg gat gag gac aca cgg cac ctg tcc cgc aag ttc aag gac tgg gcc tat ggg cca
V   T   D   E   D   T   R   H   L   S   R   K   F   K   D   W   A   Y   G   P
gtg tat tcc tcg ctt tat gac ctc tcc tcc ctg gac acg tgt ggg gaa gag gcc tcc gtg
V   Y   S   S   L   Y   D   L   S   S   L   D   T   C   G   E   E   A   S   V
ctg gag atc ctg gtg tac aac agc aag att gag aac cgc cac gag atg ctg gct gtg gag
L   E   I   L   V   Y   N   S   K   I   E   N   R   H   E   M   L   A   V   E
ccc atc aat gaa ctg ctg cgg gac aag tgg cgc aag ttc ggg gcc gtc tcc ttc tac atc
P   I   N   E   L   L   R   D   K   W   R   K   F   G   A   V   S   F   Y   I
aac gtg gtc tcc tac ctg tgt gcc atg gtc atc ttc act ctc acc gcc tac tac cag ccg
N   V   V   S   Y   L   C   A   M   V   I   F   T   L   T   A   Y   Y   Q   P
ctg gag ggc aca ccg ccg tac cct tac cgc acc acg gtg gac tac ctg cgg ctg gct ggc
L   E   G   T   P   P   Y   P   Y   R   T   T   V   D   Y   L   R   L   A   G
gag gtc att acg ctc ttc act ggg gtc ctg ttc ttc ttc acc aac atc aaa gac ttg ttc
E   V   I   T   L   F   T   G   V   L   F   F   F   T   N   I   K   D   L   F
```

```
atg aag aaa tgc cct gga gtg aat tct ctc ttc att gat ggc tcc ttc cag ctg ctc tac
M   K   K   C   P   G   V   N   S   L   F   I   D   G   S   F   Q   L   L   Y
ttc atc tac tct gtc ctg gtg atc gtc tca gca gcc ctc tac ctg gca ggg atc gag gcc
F   I   Y   S   V   L   V   I   V   S   A   A   L   Y   L   A   G   I   E   A
tac ctg gcc gtg atg gtc ttt gcc ctg gtc ctg ggc tgg atg aat gcc ctt tac ttc acc
Y   L   A   V   M   V   F   A   L   V   L   G   W   M   N   A   L   Y   F   T
cgt ggg ctg aag ctg acg ggg acc tat agc atc atg atc cag aag att ctc ttc aag gac
R   G   L   K   L   T   G   T   Y   S   I   M   I   Q   K   I   L   F   K   D
ctt ttc cga ttc ctg ctc gtc tac ttg ctc ttc atg atc ggc tac gct tca gcc ctg gtc
L   F   R   F   L   L   V   Y   L   L   F   M   I   G   Y   A   S   A   L   V
tcc ctc ctg aac ccg tgt gcc aac atg aag gtg tgc aat gag gac cag acc aac tgc aca
S   L   L   N   P   C   A   N   M   K   V   C   N   E   D   Q   T   N   C   T
gtg ccc act tac ccc tcg tgc cgt gac agc gag acc ttc agc acc ttc ctc ctg gac ctg
V   P   T   Y   P   S   C   R   D   S   E   T   F   S   T   F   L   L   D   L
ttt aag ctg acc atc ggc atg ggc gac ctg gag atg ctg agc agc acc aag tac ccc
F   K   L   T   I   G   M   G   D   L   E   M   L   S   S   T   K   Y   P
gtg gtc ttc atc atc ctg ctg gtg acc tac atc atc ctc acc ttt gtg
V   V   F   I   I   L   L   V   T   Y   I   I   L   T   F   V
ctg ctc ctc aac atg ctc att gcc ctc atg ggc gag aca gtg ggc cag gtc tcc aag gag
L   L   L   N   M   L   I   A   L   M   G   E   T   V   G   Q   V   S   K   E
agc aag cac atc tgg aag ctg cag tgg gcc acc acc atc ctg gac att gag cgc tcc ttc
S   K   H   I   W   K   L   Q   W   A   T   T   I   L   D   I   E   R   S   F
ccc gta ttc ctg agg aag gcc ttc cgc tct ggg gag atg gtc acc gtg ggc aag agc tcg
P   V   F   L   R   K   A   F   R   S   G   E   M   V   T   V   G   K   S   S
gac ggc act cct gac cgc agg tgg tgc ttc agg gtg gat gag gtg aac tgg tct cac tgg
D   G   T   P   D   R   R   W   C   F   R   V   D   E   V   N   W   S   H   W
aac cag aac ttg ggc atc atc aac gag gac ccg ggc aag aat gag acc tac cag tat tat
N   Q   N   L   G   I   I   N   E   D   P   G   K   N   E   T   Y   Q   Y   Y
ggc ttc tcg cat acc gtg ggc cgc ctc cgc agg gat cgc tgg tcc tcg gtg gta ccc cgc
G   F   S   H   T   V   G   R   L   R   R   D   R   W   S   S   V   V   P   R
gtg gtg gaa ctg aac aag aac tcg aac ccg gac gag gtg gtg gtg cct ctg gac agc atg
V   V   E   L   N   K   N   S   N   P   D   E   V   V   V   P   L   D   S   M
ggg aac ccc cgc tgc gat ggc cac cag cag ggt tac ccc cgc aag tgg agg act gat gac
G   N   P   R   C   D   G   H   Q   Q   G   Y   P   R   K   W   R   T   D   D
gcc ccg ctc aat tcg tcg aca agc ttc tcg agc atg cat cta gat gac tat  gat gac
A   P   L     G   N   L   N   S   S   T   S   F   S   S   M   H   L   D   D
tat aaa gac gat gac gac tag
 Y   K   D   D   D   K   -
```

hsTRPV4 R232C-cFLAG

see hsTRPV4-cFLAG, c.694C>T, p. Arg232C

hsTRPV4 R269C-cFLAG

see hsTRPV4-cFLAG, c.805C>T, p. Arg269C

hsPACSIN1-nV5

```
atggcaggcaagccaatccctaaccctctgctgggcctggacagcaccgaattgatcacaagtttgtacaaaaaagcaggcacc
 M  A  G  K  P  I  P  N  P  L  L  G  L  D  S  T  E  L  I  T  S  L  Y  K  K  A  G  T
atg agc agc agc tac gac gag gcc agc ctg gcc ccc gag gag acc acc gac agc ttc tgg
M   S   S   S   Y   D   E   A   S   L   A   P   E   E   T   T   D   S   F   W
gag gtg ggc aac tac aag agg acc gtg aag agg atc gac gac ggc cac agg ctg tgc aac
E   V   G   N   Y   K   R   T   V   K   R   I   D   D   G   H   R   L   C   N
gac ctg atg aac tgc gtg cag gag agg gcc aag atc gag aag gcc tac ggc cag cag ctg
D   L   M   N   C   V   Q   E   R   A   K   I   E   K   A   Y   G   Q   Q   L
acc gac tgg gcc aag agg tgg agg cag ctg atc gag aag ggc ccc cag tac ggc agc ctg
T   D   W   A   K   R   W   R   Q   L   I   E   K   G   P   Q   Y   G   S   L
gag agg gcc tgg ggc gcc atc atg acc gag gcc gac aag gtg agc gag ctg cac cag gag
E   R   A   W   G   A   I   M   T   E   A   D   K   V   S   E   L   H   Q   E
gtg aag aac aac ctg ctg aac gag gac ctg gag aag gtg aag aac tgg cag aag gac gcc
V   K   N   N   L   L   N   E   D   L   E   K   V   K   N   W   Q   K   D   A
tac cac aag cag atc atg ggc ggc ttc aag gag acc aag gag gcc gag gac ggc ttc agg
Y   H   K   Q   I   M   G   G   F   K   E   T   K   E   A   E   D   G   F   R
aag gcc cag aag ccc tgg gcc aag aag atg aag gag ctg gag gcc gcc aag aag gcc tac
K   A   Q   K   P   W   A   K   K   M   K   E   L   E   A   A   K   K   A   Y
cac ctg gcc tgc aag gag gag aag ctg gcc atg acc agg gag atg aac agc aag acc gag
H   L   A   C   K   E   E   K   L   A   M   T   R   E   M   N   S   K   T   E
cag agc gtg acc ccc gag cag cag aag aag ctg cag gac aag gtg gac aag tgc aag cag
Q   S   V   T   P   E   Q   Q   K   K   L   Q   D   K   V   D   K   C   K   Q
gac gtg cag aag acc cag gag aag tac gag aag gtg ctg gag gac gtg ggc aag acc acc
D   V   Q   K   T   Q   E   K   Y   E   K   V   L   E   D   V   G   K   T   T
ccc cag tac atg gag aac atg gag cag gtg ttc gag cag tgc cag cag ttc gag gag aag
P   Q   Y   M   E   N   M   E   Q   V   F   E   Q   C   Q   Q   F   E   E   K
agg ctg gtg ttc ctg aag gag gtg ctg ctg gac atc aag agg cac ctg aac ctg gcc gag
R   L   V   F   L   K   E   V   L   L   D   I   K   R   H   L   N   L   A   E
aac agc agc tac atc cac gtg tac agg gag ctg gag cag gcc atc agg ggc gcc gac gcc
N   S   S   Y   I   H   V   Y   R   E   L   E   Q   A   I   R   G   A   D   A
cag gag gac ctg agg tgg ttc agg agc acc agc ggc ccc ggc atg ccc atg aac tgg ccc
Q   E   D   L   R   W   F   R   S   T   S   G   P   G   M   P   M   N   W   P
cag ttc gag gag tgg aac ccc gac ctg ccc cac acc acc acc aag aag gag aag cag ccc
Q   F   E   E   W   N   P   D   L   P   H   T   T   T   K   K   E   K   Q   P
aag aag gcc gag ggc gtg gcc ctg acc aac gcc acc ggc gcc gtg gag agc acc agc cag
K   K   A   E   G   V   A   L   T   N   A   T   G   A   V   E   S   T   S   Q
gcc ggc gac agg ggc agc gtg agc agc tac gac agg ggc cag ccc tac gcc acc gag tgg
A   G   D   R   G   S   V   S   S   Y   D   R   G   Q   P   Y   A   T   E   W
agc gac gac gag agc ggc aac ccc ttc ggc ggc agc gag acc aac ggc ggc gcc aac ccc
S   D   D   E   S   G   N   P   F   G   G   S   E   T   N   G   G   A   N   P
ttc gag gac gac agc aag ggc gtg agg gtg agg gcc ctg tac gac tac gac ggc cag gag
```

```
F   E   D   D   S   K   G   V   R   V   R   A   L   Y   D   Y   D   G   Q   E
cag gac gag ctg agc ttc aag gcc ggc gac gag ctg acc aag ctg ggc gag gag gac gag
Q   D   E   L   S   F   K   A   G   D   E   L   T   K   L   G   E   E   D   E
cag ggc tgg tgc agg ggc agg ctg gac agc ggc cag ctg ggc ctg tac ccc gcc aac tac
Q   G   W   C   R   G   R   L   D   S   G   Q   L   G   L   Y   P   A   N   Y
gtg gag gcc atc tag
V   E   A   I   -
```

hsPACSIN2-nV5

```
atggcaggcaagccaatccctaaccctctgctgggcctggacagcaccgaattgatcacaagtttgtacaaaaaagcaggc
M   A   G   K   P   I   P   N   P   L   L   G   L   D   S   T   E   L   I   T   S   L   Y   K   K   A   G
atg agc gtg acc tac gac gac agc gtg ggc gtg gag gtg agc agc gac agc ttc tgg gag
M   S   V   T   Y   D   D   S   V   G   V   E   V   S   S   D   S   F   W   E
gtg ggc aac tac aag agg acc gtg aag agg atc gac gac ggc cac agg ctg tgc agc gac
V   G   N   Y   K   R   T   V   K   R   I   D   D   G   H   R   L   C   S   D
ctg atg aac tgc ctg cac gag agg gcc agg atc gag aag gcc tac gcc cag cag ctg acc
L   M   N   C   L   H   E   R   A   R   I   E   K   A   Y   A   Q   Q   L   T
gag tgg gcc agg agg tgg agg cag ctg gtg gag aag ggc ccc cag tac ggc acc gtg gag
E   W   A   R   R   W   R   Q   L   V   E   K   G   P   Q   Y   G   T   V   E
aag gcc tgg atg gcc ttc atg agc gag gcc gag agg gtg agc gag ctg cac ctg gag gtg
K   A   W   M   A   F   M   S   E   A   E   R   V   S   E   L   H   L   E   V
aag gcc agc ctg atg aac gac gac ttc gag aag atc aag aac tgg cag aag gag gcc ttc
K   A   S   L   M   N   D   D   F   E   K   I   K   N   W   Q   K   E   A   F
cac aag cag atg atg ggc ggc ttc aag gag acc aag gag gcc gag gac ggc ttc agg aag
H   K   Q   M   M   G   G   F   K   E   T   K   E   A   E   D   G   F   R   K
gcc cag aag ccc tgg gcc aag aag ctg aag gag gtg gag gcc gcc aag aag gcc cac cac
A   Q   K   P   W   A   K   K   L   K   E   V   E   A   A   K   K   A   H   H
gcc gcc tgc aag gag gag aag ctg gcc atc agc agg gag gcc aac agc aag gcc gac ccc
A   A   C   K   E   E   K   L   A   I   S   R   E   A   N   S   K   A   D   P
agc ctg aac ccc gag cag ctg aag aag ctg cag gac aag atc gag aag tgc aag cag gac
S   L   N   P   E   Q   L   K   K   L   Q   D   K   I   E   K   C   K   Q   D
gtg ctg aag acc aag gag aag tac gag aag agc ctg aag gag ctg gac cag ggc acc ccc
V   L   K   T   K   E   K   Y   E   K   S   L   K   E   L   D   Q   G   T   P
cag tac atg gag aac atg gag cag gtg ttc gag cag tgc cag cag ttc gag gag aag agg
Q   Y   M   E   N   M   E   Q   V   F   E   Q   C   Q   Q   F   E   E   K   R
ctg agg ttc ttc agg gag gtg ctg ctg gag gtg cag aag cac ctg gac ctg agc aac gtg
L   R   F   F   R   E   V   L   L   E   V   Q   K   H   L   D   L   S   N   V
gcc ggc tac aag gcc atc tac cac gac ctg gag cag agc atc agg gcc gcc gac gcc gtg
A   G   Y   K   A   I   Y   H   D   L   E   Q   S   I   R   A   A   D   A   V
gag gac ctg agg tgg ttc agg gcc aac cac ggc ccc ggc atg gcc atg aac tgg ccc cag
E   D   L   R   W   F   R   A   N   H   G   P   G   M   A   M   N   W   P   Q
ttc gag gag tgg agc gcc gac ctg aac agg acc ctg agc agg agg gag aag aag aag gcc
F   E   E   W   S   A   D   L   N   R   T   L   S   R   R   E   K   K   K   A
acc gac ggc gtg acc ctg acc ggc atc aac cag acc ggc gac cag agc ctg ccc agc aag
T   D   G   V   T   L   T   G   I   N   Q   T   G   D   Q   S   L   P   S   K
ccc agc agc acc ctg aac gtg ccc agc aac ccc gcc cag agc gcc cag agc cag agc agc
```

```
P   S   S   T   L   N   V   P   S   N   P   A   Q   S   A   Q   S   Q   S   S
tac aac ccc ttc gag gac gag gac gac acc ggc agc acc gtg agc gag aag gac gac acc
Y   N   P   F   E   D   E   D   D   T   G   S   T   V   S   E   K   D   D   T
aag gcc aag aac gtg agc agc tac gag aag acc cag agc tac ccc acc gac tgg agc gac
K   A   K   N   V   S   S   Y   E   K   T   Q   S   Y   P   T   D   W   S   D
gac gag agc aac aac ccc ttc agc agc acc gac gcc aac ggc gac agc aac ccc ttc gac
D   E   S   N   N   P   F   S   S   T   D   A   N   G   D   S   N   P   F   D
gac gac gcc acc agc ggc acc gag gtg agg gtg agg gcc ctg tac gac tac gag ggc cag
D   D   A   T   S   G   T   E   V   R   V   R   A   L   Y   D   Y   E   G   Q
gag cac gac gag ctg agc ttc aag gcc ggc gac gag ctg acc aag atg gag gac gag gac
E   H   D   E   L   S   F   K   A   G   D   E   L   T   K   M   E   D   E   D
gag cag ggc tgg tgc aag ggc agg ctg gac aac ggc cag gtg ggc ctg tac ccc gcc aac
E   Q   G   W   C   K   G   R   L   D   N   G   Q   V   G   L   Y   P   A   N
tac gtg gag gcc atc cag tag
Y   V   E   A   I   Q   -
```

hsPACSIN3-nV5

```
atggcaggcaagccaatccctaaccctctgctgggcctggacagcaccgaattgatcacaagtttgtacaaaaaagcaggc
M   A   G   K   P   I   P   N   P   L   L   G   L   D   S   T   E   L   I   T   S   L   Y   K   K   A   G
atg gcc ccc gag gag gac gcc ggc ggc gag gcc ctg ggc ggc agc ttc tgg gag gcc ggc
M   A   P   E   E   D   A   G   G   E   A   L   G   G   S   F   W   E   A   G
aac tac agg agg acc gtg cag agg gtg gag gac ggc cac agg ctg tgc ggc gac ctg gtg
N   Y   R   R   T   V   Q   R   V   E   D   G   H   R   L   C   G   D   L   V
agc tgc ttc cag gag agg gcc agg atc gag aag gcc tac gcc cag cag ctg gcc gac tgg
S   C   F   Q   E   R   A   R   I   E   K   A   Y   A   Q   Q   L   A   D   W
gcc agg aag tgg agg ggc acc gtg gag aag ggc ccc cag tac ggc acc ctg gag aag gcc
A   R   K   W   R   G   T   V   E   K   G   P   Q   Y   G   T   L   E   K   A
tgg cac gcc ttc ttc acc gcc gcc gag agg ctg agc gcc ctg cac ctg gag gtg agg gag
W   H   A   F   F   T   A   A   E   R   L   S   A   L   H   L   E   V   R   E
aag ctg cag ggc cag gac agc gag agg gtg agg gcc tgg cag agg ggc gcc ttc cac agg
K   L   Q   G   Q   D   S   E   R   V   R   A   W   Q   R   G   A   F   H   R
ccc gtg ctg ggc ggc ttc agg gag agc agg gcc gcc gag gac ggc ttc agg aag gcc cag
P   V   L   G   G   F   R   E   S   R   A   A   E   D   G   F   R   K   A   Q
aag ccc tgg ctg aag agg ctg aag gag gtg gag gcc agc aag aag agc tac cac gcc gcc
K   P   W   L   K   R   L   K   E   V   E   A   S   K   K   S   Y   H   A   A
agg aag gac gag aag acc gcc cag acc agg gag agc cac gcc aag gcc gac agc gcc gtg
R   K   D   E   K   T   A   Q   T   R   E   S   H   A   K   A   D   S   A   V
agc cag gag cag ctg agg aag ctg cag gag agg gtg gag agg tgc gcc aag gag gcc gag
S   Q   E   Q   L   R   K   L   Q   E   R   V   E   R   C   A   K   E   A   E
aag acc aag gcc cag tac gag cag acc ctg gcc gag ctg cac agg tac acc ccc agg tac
K   T   K   A   Q   Y   E   Q   T   L   A   E   L   H   R   Y   T   P   R   Y
atg gag gac atg gag cag gcc ttc gag acc tgc cag gcc gcc gag agg cag agg ctg ctg
M   E   D   M   E   Q   A   F   E   T   C   Q   A   A   E   R   Q   R   L   L
ttc ttc aag gac atg ctg ctg acc ctg cac cag cac ctg gac ctg agc agc agc gag aag
F   F   K   D   M   L   L   T   L   H   Q   H   L   D   L   S   S   S   E   K
ttc cac gag ctg cac agg gac ctg cac cag ggc atc gag gcc gcc agc gac gag gag gac
```

```
F   H   E   L   H   R   D   L   H   Q   G   I   E   A   A   S   D   E   E   D
ctg agg tgg tgg agg agc acc cac ggc ccc ggc atg gcc atg aac tgg ccc cag ttc gag
L   R   W   W   R   S   T   H   G   P   G   M   A   M   N   W   P   Q   F   E
gag tgg agc ctg gac acc cag agg acc atc agc agg aag gag aag ggc ggc agg agc ccc
E   W   S   L   D   T   Q   R   T   I   S   R   K   E   K   G   G   R   S   P
gac gag gtg acc ctg acc agc atc gtg ccc acc agg gac ggc acc gcc ccc ccc ccc cag
D   E   V   T   L   T   S   I   V   P   T   R   D   G   T   A   P   P   P   Q
agc ccc ggc agc ccc ggc acc ggc cag gac gag gag tgg agc gac gag gag agc ccc agg
S   P   G   S   P   G   T   G   Q   D   E   E   W   S   D   E   E   S   P   R
aag gcc gcc acc ggc gtg agg gtg agg gcc ctg tac gac tac gcc ggc cag gag gcc gac
K   A   A   T   G   V   R   V   R   A   L   Y   D   Y   A   G   Q   E   A   D
gag ctg agc ttc agg gcc ggc gag gag ctg ctg aag atg agc gag gag gac gag cag ggc
E   L   S   F   R   A   G   E   E   L   L   K   M   S   E   E   D   E   Q   G
tgg tgc cag ggc cag ctg cag agc ggc agg atc ggc ctg tac ccc gcc aac tac gtg gag
W   C   Q   G   Q   L   Q   S   G   R   I   G   L   Y   P   A   N   Y   V   E
tgc gtg ggc gcc tag
C   V   G   A   -
```

PACSIN1+2-nV5

```
attt aag tgt cat tgg cag att acc acc atg gca ggc aag cca atc cct aac cct ctg ctg
F   K   C   H   W   Q   I   T   T   M   A   G   K   P   I   P   N   P   L   L
ggc ctg gac agc acc gaa ttg atc aca agt ttg tac aaa aaa gca ggc acc atg tcc agc
G   L   D   S   T   E   L   I   T   S   L   Y   K   K   A   G   T   M   S   S
tcc tac gat gag gcc tca ctg gta gaa gtg tcc agc gac agc ttc tgg gag gtc ggg aac
S   Y   D   E   A   S   L   V   E   V   S   S   D   S   F   W   E   V   G   N
tac aag cgg act gtg aag cgg atc gac gat ggc cac cgc ctg tgc agc gac ctc atg aac
Y   K   R   T   V   K   R   I   D   D   G   H   R   L   C   S   D   L   M   N
tgc ctg cat gag cgg gcg cgc atc gag aag gcg tat gcg cag cag ctc act gag tgg gcc
C   L   H   E   R   A   R   I   E   K   A   Y   A   Q   Q   L   T   E   W   A
cgg cgc tgg agg cag ctc gtg gag aaa ggg ccc cag tac ggg acc gtg gag aag gcc tgg
R   R   W   R   Q   L   V   E   K   G   P   Q   Y   G   T   V   E   K   A   W
atg gcc ttc atg tcc gag gca gag agg gtg agc gag ctg cac ctc gag gtg aag gcc tca
M   A   F   M   S   E   A   E   R   V   S   E   L   H   L   E   V   K   A   S
ctg atg aac gat gac ttc gag aag atc aag aac tgg cag aag gaa gcc ttt cac aag cag
L   M   N   D   D   F   E   K   I   K   N   W   Q   K   E   A   F   H   K   Q
atg atg ggc ggc ttc aag gag acc aag gaa gct gag gac ggc ttt cgg aag gca cag aag
M   M   G   G   F   K   E   T   K   E   A   E   D   G   F   R   K   A   Q   K
ccc tgg gcc aag aag ctg aaa gag gta gaa gca gca aag aaa gcc cac cat gca gcg tgc
P   W   A   K   K   L   K   E   V   E   A   A   K   K   A   H   H   A   A   C
aaa gag gag aag ctg gct atc tca cga gaa gcc aac agc aag gca gac cca tcc ctc aac
K   E   E   K   L   A   I   S   R   E   A   N   S   K   A   D   P   S   L   N
cct gaa cag ctc aag aaa ttg caa gac aaa ata gaa aag tgc aag caa gat gtt ctt aag
P   E   Q   L   K   K   L   Q   D   K   I   E   K   C   K   Q   D   V   L   K
acc aaa gag aag tat gag aag tcc ctg aaa gaa ctc gac cag ggc aca ccc cag tac atg
T   K   E   K   Y   E   K   S   L   K   E   L   D   Q   G   T   P   Q   Y   M
gag aac atg gag cag tgt ttg agc agt gcc agc agt tcg agg aga aaa cgc ctt cgc ttc
```

```
E   N   M   E   Q   C   L   S   S   A   S   S   S   R   R   K   R   L   R   F
ttc cgg gag gtt ctg ctg gag gtt cag aag cac cta gac ctg tcc aat gtg gct ggc tac
F   R   E   V   L   L   E   V   Q   K   H   L   D   L   S   N   V   A   G   Y
aaa gcc att tac cat gac ctg gag cag agc atc aga gca gct gat gca gtg gag gac ctc
K   A   I   Y   H   D   L   E   Q   S   I   R   A   A   D   A   V   E   D   L
aga tgg ttc cgc agc acc agt ggc ccc ggc atg ccc atg aac tgg ccc cag ttt gag gag
R   W   F   R   S   T   S   G   P   G   M   P   M   N   W   P   Q   F   E   E
tgg aac cca gac ctt cct cac acc acc acc aag aag gag aaa cag cct aag aag gca gag
W   N   P   D   L   P   H   T   T   T   K   K   E   K   Q   P   K   K   A   E
gga gtg gcg ctg acc aat gcc act ggg gcg gta gag tcc aca tcc cag gct ggg gac cgc
G   V   A   L   T   N   A   T   G   A   V   E   S   T   S   Q   A   G   D   R
ggc agt gtt agc agc tac gac aga ggc cag ccc tac gcc acc gag tgg tca gac gac gag
G   S   V   S   S   Y   D   R   G   Q   P   Y   A   T   E   W   S   D   D   E
agt ggg aac ccc ttt ggg ggc agt gag acc aac ggg ggc gcc aac ccc ttt gag gac gac
S   G   N   P   F   G   G   S   E   T   N   G   G   A   N   P   F   E   D   D
tcc aag gga gtg cgc gtg cgg gca ctc tac gac tat gac ggc cag gag cag gac gag ctc
S   K   G   V   R   V   R   A   L   Y   D   Y   D   G   Q   E   Q   D   E   L
agc ttt aag gcc gga gac gaa ctc acc aag ctg ggc gag gag gat gag cag ggc tgg tgc
S   F   K   A   G   D   E   L   T   K   L   G   E   E   D   E   Q   G   W   C
cgt ggg cgg ctg gac agc ggg cag ctg ggc ctc tac cct gcc aac tac gtg gag gct atc
R   G   R   L   D   S   G   Q   L   G   L   Y   P   A   N   Y   V   E   A   I
tag aac cca gct
-   N   P   A
```

PACSIN1+3-nV5

```
attt aag tgt cat tgg cag att acc acc atg gca ggc aag cca atc cct aac cct ctg ctg
F   K   C   H   W   Q   I   T   T   M   A   G   K   P   I   P   N   P   L   L
ggc ctg gac agc acc gaa ttg atc aca agt ttg tac aaa aaa gca ggc acc atg tcc agc
G   L   D   S   T   E   L   I   T   S   L   Y   K   K   A   G   T   M   S   S
tcc tac gat gag gcc tca ctg atg gcc ccc gag gag gac gcc ggc ggc gag gcc ctg ggc
S   Y   D   E   A   S   L   M   A   P   E   E   D   A   G   G   E   A   L   G
ggc agc ttc tgg gag gcc ggc aac tac agg agg acc gtg cag agg gtg gag gac ggc cac
G   S   F   W   E   A   G   N   Y   R   R   T   V   Q   R   V   E   D   G   H
agg ctg tgc ggc gac ctg gtg agc tgc ttc cag gag agg gcc agg atc gag aag gcc tac
R   L   C   G   D   L   V   S   C   F   Q   E   R   A   R   I   E   K   A   Y
gcc cag cag ctg gcc gac tgg gcc agg aag tgg agg ggc acc gtg gag aag ggc ccc cag
A   Q   Q   L   A   D   W   A   R   K   W   R   G   T   V   E   K   G   P   Q
tac ggc acc ctg gag aag gcc tgg cac gcc ttc ttc acc gcc gcc gag agg ctg agc gcc
Y   G   T   L   E   K   A   W   H   A   F   F   T   A   A   E   R   L   S   A
ctg cac ctg gag gtg agg gag aag ctg cag ggc cag gac agc gag agg gtg agg gcc tgg
L   H   L   E   V   R   E   K   L   Q   G   Q   D   S   E   R   V   R   A   W
cag agg ggc gcc ttc cac agg ccc gtg ctg ggc ggc ttc agg gag agc agg gcc gcc gag
Q   R   G   A   F   H   R   P   V   L   G   G   F   R   E   S   R   A   A   E
gac ggc ttc agg aag gcc cag aag ccc tgg ctg aag agg ctg aag gag gtg gag gcc agc
D   G   F   R   K   A   Q   K   P   W   L   K   R   L   K   E   V   E   A   S
aag aag agc tac cac gcc gcc agg aag gac gag aag acc gcc cag acc agg gag agc cac
```

```
K   K   S   Y   H   A   A   R   K   D   E   K   T   A   Q   T   R   E   S   H
gcc aag gcc gac agc gcc gtg agc cag gag cag ctg agg aag ctg cag gag agg gtg gag
A   K   A   D   S   A   V   S   Q   E   Q   L   R   K   L   Q   E   R   V   E
agg tgc gcc aag gag gcc gag aag acc aag gcc cag tac gag cag acc ctg gcc gag ctg
R   C   A   K   E   A   E   K   T   K   A   Q   Y   E   Q   T   L   A   E   L
cac agg tac acc ccc agg tac atg gag gac atg gag cag gcc ttc gag acc tgc cag gcc
H   R   Y   T   P   R   Y   M   E   D   M   E   Q   A   F   E   T   C   Q   A
gcc gag agg cag agg ctg ctg ttc ttc aag gac atg ctg ctg acc ctg cac cag cac ctg
A   E   R   Q   R   L   L   F   F   K   D   M   L   L   T   L   H   Q   H   L
gac ctg agc agc agc gag aag ttc cac gag ctg cac agg gac ctg cac cag ggc atc gag
D   L   S   S   S   E   K   F   H   E   L   H   R   D   L   H   Q   G   I   E
gcc gcc agc gac gag gag gac ctc aga tgg ttc cgc agc acc agt ggc ccc ggc atg ccc
A   A   S   D   E   E   D   L   R   W   F   R   S   T   S   G   P   G   M   P
atg aac tgg ccc cag ttt gag gag tgg aac cca gac ctt cct cac acc acc acc aag aag
M   N   W   P   Q   F   E   E   W   N   P   D   L   P   H   T   T   T   K   K
gag aaa cag cct aag aag gca gag gga gtg gcg ctg acc aat gcc act ggg gcg gta gag
E   K   Q   P   K   K   A   E   G   V   A   L   T   N   A   T   G   A   V   E
tcc aca tcc cag gct ggg gac cgc ggc agt gtt agc agc tac gac aga ggc cag ccc tac
S   T   S   Q   A   G   D   R   G   S   V   S   S   Y   D   R   G   Q   P   Y
gcc acc gag tgg tca gac gac gag agt ggg aac ccc ttt ggg ggc agt gag acc aac ggg
A   T   E   W   S   D   D   E   S   G   N   P   F   G   G   S   E   T   N   G
ggc gcc aac ccc ttt gag gac gac tcc aag gga gtg cgc gtg cgg gca ctc tac gac tat
G   A   N   P   F   E   D   D   S   K   G   V   R   V   R   A   L   Y   D   Y
gac ggc cag gag cag gac gag ctc agc ttt aag gcc gga gac gaa ctc acc aag ctg ggc
D   G   Q   E   Q   D   E   L   S   F   K   A   G   D   E   L   T   K   L   G
gag gag gat gag cag ggc tgg tgc cgt ggg cgg ctg gac agc ggg cag ctg ggc ctc tac
E   E   D   E   Q   G   W   C   R   G   R   L   D   S   G   Q   L   G   L   Y
cct gcc aac tac gtg gag gct atc tag aac cca gct
P   A   N   Y   V   E   A   I   -   N   P   A
```

PACSIN3+2-nV5

```
atg gca ggc aag cca atc cct aac cct ctg ctg ggc ctg gac agc acc gaa ttg atc aca
M   A   G   K   P   I   P   N   P   L   L   G   L   D   S   T   E   L   I   T
agt ttg tac aaa aaa gca ggc tcc acc gta gaa gtg tcc agc gac agc ttc tgg gag gtc
S   L   Y   K   K   A   G   S   T   V   E   V   S   S   D   S   F   W   E   V
ggg aac tac aag cgg act gtg aag cgg atc gac gat ggc cac cgc ctg tgc agc gac ctc
G   N   Y   K   R   T   V   K   R   I   D   D   G   H   R   L   C   S   D   L
atg aac tgc ctg cat gag cgg gcg cgc atc gag aag gcg tat gcg cag cag ctc act gag
M   N   C   L   H   E   R   A   R   I   E   K   A   Y   A   Q   Q   L   T   E
tgg gcc cgg cgc tgg agg cag ctc gtg gag aaa ggg ccc cag tac ggg acc gtg gag aag
W   A   R   R   W   R   Q   L   V   E   K   G   P   Q   Y   G   T   V   E   K
gcc tgg atg gcc ttc atg tcc gag gca gag agg gtg agc gag ctg cac ctc gag gtg aag
A   W   M   A   F   M   S   E   A   E   R   V   S   E   L   H   L   E   V   K
gcc tca ctg atg aac gat gac ttc gag aag atc aag aac tgg cag aag gaa gcc ttt cac
A   S   L   M   N   D   D   F   E   K   I   K   N   W   Q   K   E   A   F   H
```

```
aag cag atg atg ggc ggc ttc aag gag acc aag gaa gct gag gac ggc ttt cgg aag gca
K   Q   M   M   G   G   F   K   E   T   K   E   A   E   D   G   F   R   K   A
cag aag ccc tgg gcc aag aag ctg aaa gag gta gaa gca gca aag aaa gcc cac cat gca
Q   K   P   W   A   K   K   L   K   E   V   E   A   A   K   K   A   H   H   A
gcg tgc aaa gag gag aag ctg gct atc tca cga gaa gcc aac agc aag gca gac cca tcc
A   C   K   E   E   K   L   A   I   S   R   E   A   N   S   K   A   D   P   S
ctc aac cct gaa cag ctc aag aaa ttg caa gac aaa ata gaa aag tgc aag caa gat gtt
L   N   P   E   Q   L   K   K   L   Q   D   K   I   E   K   C   K   Q   D   V
ctt aag acc aaa gag aag tat gag aag tcc ctg aaa gaa ctc gac cag ggc aca ccc cag
L   K   T   K   E   K   Y   E   K   S   L   K   E   L   D   Q   G   T   P   Q
tac atg gag aac atg gag cag tgt ttg agc agt gcc agc agt tcg agg aga aaa cgc ctt
Y   M   E   N   M   E   Q   C   L   S   S   A   S   S   S   R   R   K   R   L
cgc ttc ttc cgg gag gtt ctg ctg gag gtt cag aag cac cta gac ctg tcc aat gtg gct
R   F   F   R   E   V   L   L   E   V   Q   K   H   L   D   L   S   N   V   A
ggc tac aaa gcc att tac cat gac ctg gag cag agc atc aga gca gct gat gca gtg gag
G   Y   K   A   I   Y   H   D   L   E   Q   S   I   R   A   A   D   A   V   E
gac ctg cgc tgg tgg cgc agc acc cac ggg cca ggc atg gcc atg aac tgg cca cag ttc
D   L   R   W   W   R   S   T   H   G   P   G   M   A   M   N   W   P   Q   F
gag gag tgg tcc ttg gac aca cag agg aca atc agc cgg aaa gag aag ggt ggc cgg agc
E   E   W   S   L   D   T   Q   R   T   I   S   R   K   E   K   G   G   R   S
cct gat gag gtt acc ctg acc agc att gtg cct aca aga gat ggc acc gca ccc cca ccc
P   D   E   V   T   L   T   S   I   V   P   T   R   D   G   T   A   P   P   P
cag tcc ccg ggg tcc cca ggc acg ggg cag gat gag gag tgg tca gat gaa gag agt ccc
Q   S   P   G   S   P   G   T   G   Q   D   E   E   W   S   D   E   E   S   P
cgg aag gct gcc acc ggg gtt cgg gtg agg gca ctc tat gac tac gct ggc cag gaa gct
R   K   A   A   T   G   V   R   V   R   A   L   Y   D   Y   A   G   Q   E   A
gat gag ctg agc ttc cga gca ggg gag gag ctg ctg aag atg agt gag gag gac gag cag
D   E   L   S   F   R   A   G   E   E   L   L   K   M   S   E   E   D   E   Q
ggc tgg tgc caa ggc cag ttg cag agt ggc cgc att ggc ctg tac cct gcc aac tac gtg
G   W   C   Q   G   Q   L   Q   S   G   R   I   G   L   Y   P   A   N   Y   V
gag tgt gtg ggc gcc tag
E   C   V   G   A   -
```

hsTRPML1-cGFP

```
atgaccgcgccggcgggcccgcgcggcagcgaaaccgaacgcctgctgaccccgaacccgggctatggcacccaggcgggcccgagcccggcgccgccg
M   T   A   P   A   G   P   R   G   S   E   T   E   R   L   L   T   P   N   P   G   Y   G   T   Q   A   G   P   S   P   A   P   P
accccgccggaagaagaagatctgcgccgccgcctgaaatatttttttatgagcccgtgcgataaatttcgcgcgaaaggccgcaaaccgtgcaaactg
T   P   P   E   E   E   D   L   R   R   R   L   K   Y   F   F   M   S   P   C   D   K   F   R   A   K   G   R   K   P   C   K   L
atgctgcaggtggtgaaaattctggtggtgaccgtgcagctgattctgtttggcctgagcaaccagctggcggtgacctttcgcgaagaaaacaccatt
M   L   Q   V   V   K   I   L   V   V   T   V   Q   L   I   L   F   G   L   S   N   Q   L   A   V   T   F   R   E   E   N   T   I
gcgtttcgccatctgtttctgctgggctatagcgatggcgcggatgataccttgcggcgtatacccgcgaacagctgtatcaggcgatttttcatgcg
A   F   R   H   L   F   L   L   G   Y   S   D   G   A   D   D   T   F   A   A   Y   T   R   E   Q   L   Y   Q   A   I   F   H   A
gtggatcagtatctggcgctgccggatgtgagcctgggccgctatgcgtatgtgcgcggcggcggcgatccgtggaccaacggcagcggcctggcgctg
V   D   Q   Y   L   A   L   P   D   V   S   L   G   R   Y   A   Y   V   R   G   G   G   D   P   W   T   N   G   S   G   L   A   L
tgccagcgctattatcatcgcggccatgtggatccggcgaacgataccttgatattgatccgatggtggtgaccgattgcattcaggtggatccgccg
C   Q   R   Y   Y   H   R   G   H   V   D   P   A   N   D   T   F   D   I   D   P   M   V   V   T   D   C   I   Q   V   D   P   P
```

```
gaacgcccgccgccgccgccgagcgatgatctgaccctgctggaaagcagcagcagctataaaaacctgaccctgaaatttcataaactggtgaacgtg
E R P P P P P S D D L T L L E S S S S Y K N L T L K F H K L V N V
accattcattttcgcctgaaaaccattaacctgcagagcctgattaacaacgaaattccggattgctatacctttagcgtgctgattacctttgataac
T I H F R L K T I N L Q S L I N N E I P D C Y T F S V L I T F D N
aaagcgcatagcggccgcattccgattagcctggaaacccaggcgcatattcaggaatgcaaacatccgagcgtgtttcagcatggcgataacagcttt
K A H S G R I P I S L E T Q A H I Q E C K H P S V F Q H G D N S F
cgcctgctgtttgatgtggtggtgattctgacctgcagcctgagctttctgctgtgcgcgcgcagcctgctgcgcggctttctgctgcagaacgaattt
R L L F D V V V I L T C S L S F L L C A R S L L R G F L L Q N E F
gtgggctttatgtggcgccagcgcggccgcgtgattagcctgtgggaacgcctggaatttgtgaacggctggtatattctgctggtgaccagcgatgtg
V G F M W R Q R G R V I S L W E R L E F V N G W Y I L L V T S D V
ctgaccattagcggcaccattatgaaaattggcattgaagcgaaaaacctggcgagctatgatgtgtgcagcattctgctgggcaccagcaccctgctg
L T I S G T I M K I G I E A K N L A S Y D V C S I L L G T S T L L
gtgtgggtgggcgtgattcgctatctgacctttttttcataactataacattctgattgcgaccctgcgcgtggcgctgccgagcgtgatgcgcttttgc
V W V G V I R Y L T F F H N Y N I L I A T L R V A L P S V M R F C
tgctgcgtggcggtgatttatctgggctattgcttttgcggctggattgtgctgggcccgtatcatgtgaaatttcgcagcctgagcatggtgagcgaa
C C V A V I Y L G Y C F C G W I V L G P Y H V K F R S L S M V S E
tgcctgtttagcctgattaacggcgatgatatgtttgtgacctttgcggcgatgcaggcgcagcagggccgcagcagcctggtgtggctgtttagccag
C L F S L I N G D D M F V T F A A M Q A Q Q G R S S L V W L F S Q
ctgtatctgtatagctttattagcctgtttatttatatggtgctgagcctgtttattgcgctgattaccggcgcgtatgataccattaaacatccgggc
L Y L Y S F I S L F I Y M V L S L F I A L I T G A Y D T I K H P G
ggcgcgggcgcggaagaaagcgaactgcaggcgtatattgcgcagtgccaggatagcccgaccagcggcaaatttcgccgcggcagcggcagcgcgtgc
G A G A E E S E L Q A Y I A Q C Q D S P T S G K F R R G S G S A C
agcctgctgtgctgctgcggccgcgatccgagcgaagaacatagcctgctggtgaacatgagcaaaggcgaagaactgtttaccggcgtggtgccgatt
S L L C C C G R D P S E E H S L L V N M S K G E E L F T G V V P I
ctggtggaactggatggcgatgtgaacggccataaatttagcgtgagcggcgaaggcgaaggcgatgcgacctatggcaaactgaccctgaaatttatt
L V E L D G D V N G H K F S V S G E G E G D A T Y G K L T L K F I
tgcaccaccggcaaactgccggtgccgtggccgaccctggtgaccacctttagctatggcgtgcagtgctttagccgctatccggatcatatgaaacag
C T T G K L P V P W P T L V T T F S Y G V Q C F S R Y P D H M K Q
catgatttttttaaaagcgcgatgccggaaggctatgtgcaggaacgcaccatttttttttaaagatgatggcaactataaaacccgcgcggaagtgaaa
H D F F K S A M P E G Y V Q E R T I F F K D D G N Y K T R A E V K
tttgaaggcgataccctggtgaaccgcattgaactgaaaggcattgattttaaagaagatggcaacattctgggccataaactggaatataactataac
F E G D T L V N R I E L K G I D F K E D G N I L G H K L E Y N Y N
agccataacgtgtatattatggcggataaacagaaaaacggcattaaagtgaacttaaaattcgccataacattgaagatggcagcgtgcagctggcg
S H N V Y I M A D K Q K N G I K V N F K I R H N I E D G S V Q L A
gatcattatcagcagaacaccccgattggcgatggcccggtgctgctgccggataaccattatctgagcacccagagcgcgctgagcaaagatccgaac
D H Y Q Q N T P I G D G P V L L P D N H Y L S T Q S A L S K D P N
gaaaaacgcgatcatatggtgctgctggaatttgtgaccgcggcgggcattacccatggcatggatgaactgtataaatag
E K R D H M V L L E F V T A A G I T H G M D E L Y K -
```

YAP1_WW1 domain-His$_6$

```
cat atg agc agc ttt gag atc ccg gac gac gtg ccg ctg ccg gcg ggt tgg gag atg gcg
H M S S F E I P D D V P L P A G W E M A
aag acc agc agc ggt cag cgt tac ttt ctg aac cac atc gac cag acc acc acc tgg caa
K T S S G Q R Y F L N H I D Q T T T W Q
gat ccg cgt aag gcg atg gag aat ctg tat ttt caa ggt cat cat cat cat cat cat taa
D P R K A M E N L Y F Q G H H H H H H -
```

```
gga tcc
G   S
```

YAP1_WW2 domain-His$_6$

```
cat atg agc gcg agc ggt ccg ctg ccg gat ggt tgg gag cag gcg atg acc caa gat ggt
H   M   S   A   S   G   P   L   P   D   G   W   E   Q   A   M   T   Q   D   G
gaa atc tac tac atc aac cac aag aac aag acc acc agc tgg ctg gac ccg cgt ctg gac
E   I   Y   Y   I   N   H   K   N   K   T   T   S   W   L   D   P   R   L   D
ccg cgt gag aat ctg tat ttt caa ggt cat cat cat cat cat cat taa
P   R   E   N   L   Y   F   Q   G   H   H   H   H   H   H   -
```

hsYAP1_WW1+WW2 domains-His$_6$

```
cat atg agc agc ttt gag atc ccg gac gac gtg ccg ctg ccg gcg ggt tgg gag atg gcg
H   M   S   S   F   E   I   P   D   D   V   P   L   P   A   G   W   E   M   A
aag acc agc agc ggt cag cgt tac ttt ctg aac cac atc gac cag acc acc acc tgg caa
K   T   S   S   G   Q   R   Y   F   L   N   H   I   D   Q   T   T   T   W   Q
gat ccg cgt aag gcg atg ctg agc cag atg aac gtg acc gcg ccg acc agc ccg ccg gtt
D   P   R   K   A   M   L   S   Q   M   N   V   T   A   P   T   S   P   P   V
cag caa aac atg atg aac agc gcg agc ggt ccg ctg ccg gat ggt tgg gag cag gcg atg
Q   Q   N   M   M   N   S   A   S   G   P   L   P   D   G   W   E   Q   A   M
acc caa gat ggt gaa atc tac tac atc aac cac aag aac aag acc acc agc tgg ctg gac
T   Q   D   G   E   I   Y   Y   I   N   H   K   N   K   T   T   S   W   L   D
ccg cgt ctg gac ccg cgt gag aat ctg tat ttt caa ggt cat cat cat cat cat cat taa
P   R   L   D   P   R   E   N   L   Y   F   Q   G   H   H   H   H   H   H   -
```

7 List of Figures

8 List of Tables

9 Bibliography

1. Cosens, D. J. & Manning, A. Abnormal Electroretinogram from a Drosophila Mutant. *Nature* **224,** 285–287 (**1969**).
2. Thompson, J. D., Higgins, D. G. & Gibson, T. J. CLUSTAL W: improving the sensitivity of progressive multiple sequence alignment through sequence weighting, position-specific gap penalties and weight matrix choice. *Nucleic Acids Research* **22,** 4673–4680 (**1994**).
3. Dereeper, A. *et al.* Phylogeny.fr: robust phylogenetic analysis for the non-specialist. *Nucleic Acids Research* **36,** W465–W469 (**2008**).
4. Dereeper, A., Audic, S., Claverie, J.-M. & Blanc, G. BLAST-EXPLORER helps you building datasets for phylogenetic analysis. *BMC Evolutionary Biology* **10,** 8 (**2010**).
5. Hardie, R. C. & Minke, B. The trp gene is essential for a light-activated Ca2+ channel in Drosophila photoreceptors. *Neuron* **8,** 643–651 (**1992**).
6. Nilius, B. & Flockerzi, V. Mammalian transient receptor potential (TRP) cation channels (Springer, New York, **2014**).
7. Clapham, D. E. TRP channels as cellular sensors. *Nature* **426,** 517–524 (**2003**).
8. Huber, A. *et al.* The transient receptor potential protein (Trp), a putative store-operated Ca2+ channel essential for phosphoinositide-mediated photoreception, forms a signaling complex with NorpA, InaC and InaD. *The EMBO journal* **15,** 7036–7045 (**1996**).
9. Giniatullin, R. Ion Channels of Nociception. *International Journal of Molecular Sciences* **21,** 3553 (**2020**).
10. Mickle, A., Shepherd, A. & Mohapatra, D. Nociceptive TRP Channels: Sensory Detectors and Transducers in Multiple Pain Pathologies. *Pharmaceuticals* **9,** 72 (**2016**).
11. Cui, M., Gosu, V., Basith, S., Hong, S. & Choi, S. in *Advances in Protein Chemistry and Structural Biology* 81–125 (Elsevier, **2016**).
12. Ramsey, I. S., Delling, M. & Clapham, D. E. An introduction to TRP channels. *Annual Review of Physiology* **68,** 619–647 (**2006**).

13. Hoffstaetter, L. J., Bagriantsev, S. N. & Gracheva, E. O. TRPs et al.: a molecular toolkit for thermosensory adaptations. *Pflügers Archiv - European Journal of Physiology* (**2018**).

14. Nilius, B., Owsianik, G., Voets, T. & Peters, J. A. Transient Receptor Potential Cation Channels in Disease. *Physiological Reviews* **87,** 165–217 (**2007**).

15. Nilius, B. TRP channels in disease. *Biochimica Et Biophysica Acta* **1772,** 805–812 (**2007**).

16. Chun, J. N. *et al.* A network perspective on unraveling the role of TRP channels in biology and disease. *Pflugers Archiv: European Journal of Physiology* **466,** 173–182 (**2014**).

17. Echeverry, S., Rodriguez, M. J. & Torres, Y. P. Transient Receptor Potential Channels in Microglia: Roles in Physiology and Disease. *Neurotoxicity Research* **30,** 467–478 (**2016**).

18. Botte, M. *et al.* Cryo-EM structural studies of the agonist complexed human TRPV4 ion-channel reveals novel structural rearrangements resulting in an open-conformation. preprint (Molecular Biology, **2020**).

19. Pumroy, R. A., Fluck, E. C., Ahmed, T. & Moiseenkova-Bell, V. Y. Structural insights into the gating mechanisms of TRPV channels. *Cell Calcium* **87,** 102168 (**2020**).

20. Cao, E. Structural mechanisms of transient receptor potential ion channels. *Journal of General Physiology* **152,** e201811998 (**2020**).

21. Goretzki, B. Towards an understanding of the regulation of TRPV4 by PIP2 and PACSIN3. Master thesis. Johhanes Gutenberg-University Mainz (**2016**).

22. Goretzki, B. *et al.* Structural Basis of TRPV4 N Terminus Interaction with Syndapin/PACSIN1-3 and PIP2. *Structure* **26,** 1583–1593.e5 (**2018**).

23. Goretzki, B. Interactions of the ion channel TRPV4 with regulatory lipids and proteins. PhD thesis (Johannes-Gutenberg University, Mainz, **2020**).

24. Hellmich, U. A. & Gaudet, R. in *Mammalian Transient Receptor Potential (TRP) Cation Channels* (eds Nilius, B. & Flockerzi, V.) 963–990 (Springer International Publishing, Cham, **2014**).

25. Liao, M., Cao, E., Julius, D. & Cheng, Y. Structure of the TRPV1 ion channel determined by electron cryo-microscopy. *Nature* **504,** 107–112 (**2013**).

26. Li, J., Mahajan, A. & Tsai, M.-D. Ankyrin Repeat: A Unique Motif Mediating Protein−Protein Interactions. *Biochemistry* **45,** 15168–15178 (**2006**).

27. Inada, H., Procko, E., Sotomayor, M. & Gaudet, R. Structural and Biochemical Consequences of Disease-Causing Mutations in the Ankyrin Repeat Domain of the Human TRPV4 Channel. *Biochemistry* **51,** 6195–6206 (**2012**).

28. Gorina, S. & Pavletich, N. P. Structure of the p53 tumor suppressor bound to the ankyrin and SH3 domains of 53BP2. *Science (New York, N.Y.)* **274,** 1001–1005 (**1996**).

29. Shin, Y.-C., Shin, S.-Y., So, I., Kwon, D. & Jeon, J.-H. TRIP Database: a manually curated database of protein-protein interactions for mammalian TRP channels. *Nucleic Acids Research* **39,** D356–361 (Database issue **2011**).

30. Shin, Y.-C. *et al.* TRIP database 2.0: a manually curated information hub for accessing TRP channel interaction network. *PloS One* **7,** e47165 (**2012**).

31. Nilius, B. & Voets, T. The puzzle of TRPV4 channelopathies. *EMBO reports* **14,** 152–163 (**2013**).

32. Liedtke, W. *et al.* Vanilloid Receptor–Related Osmotically Activated Channel (VR-OAC), a Candidate Vertebrate Osmoreceptor. *Cell* **103,** 525–535 (**2000**).

33. Liedtke, W. & Friedman, J. M. Abnormal osmotic regulation in trpv4-/- mice. *Proceedings of the National Academy of Sciences of the United States of America* **100,** 13698–13703 (**2003**).

34. Mizuno, A., Matsumoto, N., Imai, M. & Suzuki, M. Impaired osmotic sensation in mice lacking TRPV4. *American Journal of Physiology. Cell Physiology* **285,** C96–101 (**2003**).

35. Watanabe, H. *et al.* Activation of TRPV4 Channels (hVRL-2/mTRP12) by Phorbol Derivatives. *Journal of Biological Chemistry* **277,** 13569–13577 (**2002**).

36. Watanabe, H. *et al.* Anandamide and arachidonic acid use epoxyeicosatrienoic acids to activate TRPV4 channels. *Nature* **424,** 434–438 (**2003**).

37. Watanabe, H. *et al.* Heat-evoked activation of TRPV4 channels in a HEK293 cell expression system and in native mouse aorta endothelial cells. *The Journal of Biological Chemistry* **277,** 47044–47051 (**2002**).

38. Gueler, A. D. *et al.* Heat-evoked activation of the ion channel, TRPV4. *The Journal of Neuroscience: The Official Journal of the Society for Neuroscience* **22,** 6408–6414 (**2002**).

39. Garcia-Elias, A. *et al.* Phosphatidylinositol-4,5-biphosphate-dependent rearrangement of TRPV4 cytosolic tails enables channel activation by physiological stimuli. *Proceedings of the National Academy of Sciences* **110,** 9553–9558 (**2013**).

40. Masuyama, R. *et al.* TRPV4-mediated calcium influx regulates terminal differentiation of osteoclasts. *Cell Metabolism* **8,** 257–265 (**2008**).

41. Masuyama, R. *et al.* Calcium/calmodulin-signaling supports TRPV4 activation in osteoclasts and regulates bone mass. *Journal of Bone and Mineral Research* **27,** 1708–1721 (**2012**).

42. Marrelli, S. P., O'neil, R. G., Brown, R. C. & Bryan, R. M. PLA2 and TRPV4 channels regulate endothelial calcium in cerebral arteries. *American Journal of Physiology. Heart and Circulatory Physiology* **292,** H1390–1397 (**2007**).

43. Sonkusare, S. K. *et al.* Elementary Ca2+ signals through endothelial TRPV4 channels regulate vascular function. *Science (New York, N.Y.)* **336,** 597–601 (**2012**).

44. Saliez, J. *et al.* Role of caveolar compartmentation in endothelium-derived hyperpolarizing factor-mediated relaxation: Ca2+ signals and gap junction function are regulated by caveolin in endothelial cells. *Circulation* **117,** 1065–1074 (**2008**).

45. Tabuchi, K., Suzuki, M., Mizuno, A. & Hara, A. Hearing impairment in TRPV4 knockout mice. *Neuroscience Letters* **382,** 304–308 (**2005**).

46. Everaerts, W., Nilius, B. & Owsianik, G. The vanilloid transient receptor potential channel TRPV4: From structure to disease. *Progress in Biophysics and Molecular Biology* **103,** 2–17 (**2010**).

47. Lamandé, S. R. *et al.* Mutations in TRPV4 cause an inherited arthropathy of hands and feet. *Nature Genetics* **43,** 1142–1146 (**2011**).

48. Unger, S. *et al.* Fetal akinesia in metatropic dysplasia: The combined phenotype of chondrodysplasia and neuropathy? *American Journal of Medical Genetics Part A* **155,** 2860–2864 (**2011**).

49. Camacho, N. *et al.* Dominant *TRPV4* mutations in nonlethal and lethal metatropic dysplasia. *American Journal of Medical Genetics Part A* **152A,** 1169–1177 (**2010**).

50. Rock, M. J. *et al.* Gain-of-function mutations in TRPV4 cause autosomal dominant brachyolmia. *Nature Genetics* **40,** 999–1003 (**2008**).

51. Krakow, D. *et al.* Mutations in the Gene Encoding the Calcium-Permeable Ion Channel TRPV4 Produce Spondylometaphyseal Dysplasia, Kozlowski Type and Metatropic Dysplasia. *The American Journal of Human Genetics* **84,** 307–315 (**2009**).

52. Loukin, S., Su, Z. & Kung, C. Increased Basal Activity Is a Key Determinant in the Severity of Human Skeletal Dysplasia Caused by TRPV4 Mutations. *PLoS ONE* **6** (ed Callaerts, P.) e19533 (**2011**).

53. Woolums, B. M. *et al.* TRPV4 disrupts mitochondrial transport and causes axonal degeneration via a CaMKII-dependent elevation of intracellular Ca2+. *Nature Communications* **11** (**2020**).

54. Klein, C. J. *et al.* TRPV4 mutations and cytotoxic hypercalcemia in axonal Charcot-Marie-Tooth neuropathies. *Neurology* **76,** 887–894 (**2011**).

55. Spinal muscular atrophy: disease mechanisms and therapy (eds Sumner, C. J., Paushkin, S. & Ko, C.-P.) OCLC: ocn952982964 (Elsevier/Academic Press, Amsterdam, **2017**). 474 pp.

56. Sullivan, J. M. *et al.* Novel mutations highlight the key role of the ankyrin repeat domain in *TRPV4* -mediated neuropathy. *Neurology Genetics* **1,** e29 (**2015**).

57. Suzuki, Y. *et al.* TRPV6 Variants Interfere with Maternal-Fetal Calcium Transport through the Placenta and Cause Transient Neonatal Hyperparathyroidism. *The American Journal of Human Genetics* **102,** 1104–1114 (**2018**).

58. McGoldrick, L. L. *et al.* Opening of the human epithelial calcium channel TRPV6. *Nature* (**2017**).

59. Singh, A. K., McGoldrick, L. L., Twomey, E. C. & Sobolevsky, A. I. Mechanism of calmodulin inactivation of the calcium-selective TRP channel TRPV6. *Science Advances* **4,** eaau6088 (**2018**).

60. Everaerts, W. *et al.* Inhibition of the cation channel TRPV4 improves bladder function in mice and rats with cyclophosphamide-induced cystitis. *Proceedings of the National Academy of Sciences* **107,** 19084–19089 (**2010**).

61. Goyal, N. *et al.* Clinical Pharmacokinetics, Safety, and Tolerability of a Novel, First-in-Class TRPV4 Ion Channel Inhibitor, GSK2798745, in Healthy and Heart Failure Subjects. *American Journal of Cardiovascular Drugs: Drugs, Devices, and Other Interventions* **19,** 335–342 (**2019**).

62. Thorneloe, K. S. *et al.* An orally active TRPV4 channel blocker prevents and resolves pulmonary edema induced by heart failure. *Science Translational Medicine* **4,** 159ra148 (**2012**).

63. Distler, U., Kuharev, J., Navarro, P. & Tenzer, S. Label-free quantification in ion mobility-enhanced data-independent acquisition proteomics. *Nature Protocols* **11,** 795–812 (**2016**).

64. Hein, M. Y., Sharma, K., Cox, J. & Mann, M. in *Handbook of Systems Biology* 3–25 (Elsevier, **2013**).

65. Lee, A., Fakler, B., Kaczmarek, L. K. & Isom, L. L. More Than a Pore: Ion Channel Signaling Complexes. *Journal of Neuroscience* **34,** 15159–15169 (**2014**).

66. Schulte, U., Müller, C. S. & Fakler, B. Ion channels and their molecular environments – Glimpses and insights from functional proteomics. *Seminars in Cell & Developmental Biology* **22,** 132–144 (**2011**).

67. Schwenk, J. *et al.* High-Resolution Proteomics Unravel Architecture and Molecular Diversity of Native AMPA Receptor Complexes. *Neuron* **74,** 621–633 (**2012**).

68. Caceres, M. *et al.* TRPM4 Is a Novel Component of the Adhesome Required for Focal Adhesion Disassembly, Migration and Contractility. *PloS One* **10,** e0130540 (**2015**).

69. McCray, B. A. *et al.* Neuropathy-causing TRPV4 mutations disrupt TRPV4-RhoA interactions and impair neurite extension. *Nature Communications* **12,** 17 (**2021**).

70. Cuajungco, M. P. *et al.* PACSINs bind to the TRPV4 cation channel. PACSIN 3 modulates the subcellular localization of TRPV4. *The Journal of Biological Chemistry* **281,** 18753–18762 (**2006**).

71. D'hoedt, D. *et al.* Stimulus-specific Modulation of the Cation Channel TRPV4 by PACSIN 3. *Journal of Biological Chemistry* **283,** 6272–6280 (**2008**).

72. Distler, U. *et al.* Drift time-specific collision energies enable deep-coverage data-independent acquisition proteomics. *Nature Methods* **11,** 167–170 (**2014**).

73. Distler, U., Kuharev, J. & Tenzer, S. Biomedical applications of ion mobility-enhanced data-independent acquisition-based label-free quantitative proteomics. *Expert Review of Proteomics* **11,** 675–684 (**2014**).

74. Kuharev, J., Navarro, P., Distler, U., Jahn, O. & Tenzer, S. In-depth evaluation of software tools for data-independent acquisition based label-free quantification. *PROTEOMICS* **15,** 3140–3151 (**2015**).

75. McCray, B. A., Schindler, A., Hoover-Fong, J. E. & Sumner, C. J. in *GeneReviews®* (eds Adam, M. P. *et al.*) (University of Washington, Seattle, Seattle (WA), **1993**).

76. Diehl, E. Investigating the interactome of the TRPV4 N-terminus. PhD thesis (Johannes-Gutenberg University, Mainz, **2017**).

77. Schmitt, P. Biochemische Studien an Ankyrin repeat Domänen von TRP Ionenkanälen. PhD thesis (Johannes-Gutenberg University, **2018**).

78. Doerr, C. Investigating the Interactome of the Human Ion Channel TRPV4 and Associated Channelopathies. PhD thesis (Johannes-Gutenberg University, Mainz, **2019**).

79. Gibson, D. G. *et al.* Enzymatic assembly of DNA molecules up to several hundred kilobases. *Nature Methods* **6,** 343–345 (**2009**).

80. Gibson, D. G. in *Methods in Enzymology* 349–361 (Elsevier, **2011**).

81. Schindelin, J. *et al.* Fiji: an open-source platform for biological-image analysis. *Nature Methods* **9,** 676–682 (**2012**).

82. Kay, B. K., Thai, S. & Volgina, V. V. in *High Throughput Protein Expression and Purification* (eds Walker, J. M. & Doyle, S. A.) 185–198 (Humana Press, Totowa, NJ, **2009**).

83. Holden, P. & Horton, W. A. Crude subcellular fractionation of cultured mammalian cell lines. *BMC Research Notes* **2,** 243 (**2009**).

84. Sehgal, P., Olesen, C. & Møller, J. V. in *P-Type ATPases* (ed Bublitz, M.) Series Title: Methods in Molecular Biology, 105–109 (Springer New York, New York, NY, **2016**).

85. Swamy, M., Siegers, G. M., Minguet, S., Wollscheid, B. & Schamel, W. W. A. Blue Native Polyacrylamide Gel Electrophoresis (BN-PAGE) for the Identification and Analysis of Multiprotein Complexes. *Science Signaling* **2006,** pl4–pl4 (**2006**).

86. Sattler, M. Heteronuclear multidimensional NMR experiments for the structure determination of proteins in solution employing pulsed field gradients. *Progress in Nuclear Magnetic Resonance Spectroscopy* **34,** 93–158 (**1999**).

87. Fürsch, J., Kammer, K.-M., Kreft, S. G., Beck, M. & Stengel, F. Proteome-Wide Structural Probing of Low-Abundant Protein Interactions by Cross-Linking Mass Spectrometry. *Analytical Chemistry* **92,** 4016–4022 (**2020**).

88. Distler, U., Kuharev, J., Navarro, P. & Tenzer, S. Label-free quantification in ion mobility-enhanced data-independent acquisition proteomics. *Nature Protocols* **11,** 795–812 (**2016**).

89. Landoure, G. *et al.* Exome sequencing identifies a novel TRPV4 mutation in a CMT2C family. *Neurology* **79,** 192–194 (**2012**).

90. Landouré, G. *et al.* Mutations in TRPV4 cause Charcot-Marie-Tooth disease type 2C. *Nature Genetics* **42,** 170–174 (**2010**).

91. Kay, B. K., Thai, S. & Volgina, V. V. in *High Throughput Protein Expression and Purification* (ed Doyle, S. A.)red. by Walker, J. M., 185–198 (Humana Press, Totowa, NJ, **2009**).

92. Nishimura, G. *et al.* TRPV4-associated skeletal dysplasias. *American Journal of Medical Genetics Part C: Seminars in Medical Genetics* **160C,** 190–204 (**2012**).

93. Wiedemann, C., Bellstedt, P. & Gorlach, M. CAPITO–a web server-based analysis and plotting tool for circular dichroism data. *Bioinformatics* **29,** 1750–1757 (**2013**).

94. Le Sage, V., Cinti, A. & Mouland, A. J. in *Current Protocols in Cell Biology* (eds Bonifacino, J. S., Dasso, M., Harford, J. B., Lippincott-Schwartz, J. & Yamada, K. M.) 17.19.1–17.19.12 (John Wiley & Sons, Inc., Hoboken, NJ, USA, **2016**).

95. Bar, D. Z. *et al.* Biotinylation by antibody recognition—a method for proximity labeling. *Nature Methods* **15,** 127–133 (**2017**).

96. Cronan, J. E. Biotin and Lipoic Acid: Synthesis, Attachment, and Regulation. *EcoSal Plus* **1** (**2013**).

97. Gene Ontology Consortium. The Gene Ontology project in 2008. *Nucleic Acids Research* **36,** D440–444 (Database issue **2008**).

98. Szklarczyk, D. *et al.* STRING v10: protein–protein interaction networks, integrated over the tree of life. *Nucleic Acids Research* **43,** D447–D452 (D1 **2015**).

99. Gama-Carvalho, M. & Carmo-Fonseca, M. The rules and roles of nucleocytoplasmic shuttling proteins. *FEBS Letters* **498,** 157–163 (**2001**).

100. Lin, Y., Protter, D. S., Rosen, M. K. & Parker, R. Formation and Maturation of Phase-Separated Liquid Droplets by RNA-Binding Proteins. *Molecular Cell* **60,** 208–219 (**2015**).

101. Protter, D. S. *et al.* Intrinsically Disordered Regions Can Contribute Promiscuous Interactions to RNP Granule Assembly. *Cell Reports* **22,** 1401–1412 (**2018**).

102. Kedersha, N. *et al.* Dynamic Shuttling of Tia-1 Accompanies the Recruitment of mRNA to Mammalian Stress Granules. *Journal of Cell Biology* **151,** 1257–1268 (**2000**).

103. Kedersha, N. *et al.* G3BP–Caprin1–USP10 complexes mediate stress granule condensation and associate with 40S subunits. *Journal of Cell Biology* **212** (**2016**).

104. Kedersha, N., Ivanov, P. & Anderson, P. Stress granules and cell signaling: more than just a passing phase? *Trends in Biochemical Sciences* **38,** 494–506 (**2013**).

105. Hofmann, S., Kedersha, N., Anderson, P. & Ivanov, P. Molecular mechanisms of stress granule assembly and disassembly. *Biochimica et Biophysica Acta (BBA) - Molecular Cell Research* **1868,** 118876 (**2021**).

106. Anderson, P. & Kedersha, N. Stress granules: the Tao of RNA triage. *Trends in Biochemical Sciences* **33,** 141–150 (**2008**).

107. Jain, S. *et al.* ATPase-Modulated Stress Granules Contain a Diverse Proteome and Substructure. *Cell* **164,** 487–498 (**2016**).

108. Markmiller, S. *et al.* Context-Dependent and Disease-Specific Diversity in Protein Interactions within Stress Granules. *Cell* **172,** 590–604.e13 (**2018**).

109. Youn, J.-Y. *et al.* High-Density Proximity Mapping Reveals the Subcellular Organization of mRNA-Associated Granules and Bodies. *Molecular Cell* **69,** 517–532.e11 (**2018**).

110. Reineke, L. C. & Neilson, J. R. Differences between acute and chronic stress granules, and how these differences may impact function in human disease. *Biochemical Pharmacology* **162,** 123–131 (**2019**).

111. Luo, Y., Na, Z. & Slavoff, S. A. P-Bodies: Composition, Properties, and Functions. *Biochemistry* **57,** 2424–2431 (**2018**).

112. Krichevsky, A. M. & Kosik, K. S. Neuronal RNA Granules. *Neuron* **32,** 683–696 (**2001**).

113. Kimball, S. R., Horetsky, R. L., Ron, D., Jefferson, L. S. & Harding, H. P. Mammalian stress granules represent sites of accumulation of stalled translation initiation complexes. *American Journal of Physiology-Cell Physiology* **284,** C273–C284 (**2003**).

114. Amen, T. & Kaganovich, D. Stress granules sense metabolic stress at the plasma membrane and potentiate recovery by storing active Pkc1. *Science Signaling* **13,** eaaz6339 (**2020**).

115. Liu-Yesucevitz, L. *et al.* Local RNA Translation at the Synapse and in Disease. *Journal of Neuroscience* **31,** 16086–16093 (**2011**).

116. Onishi, H. *et al.* MBNL1 associates with YB-1 in cytoplasmic stress granules. *Journal of Neuroscience Research* **86,** 1994–2002 (**2008**).

117. Celia Cui, B. *et al.* Pharmacological inhibition of DEAD-Box RNA Helicase 3 attenuates stress granule assembly. *Biochemical Pharmacology,* 114280 (**2020**).

118. Shih, J.-W. *et al.* Critical roles of RNA helicase DDX3 and its interactions with eIF4E/PABP1 in stress granule assembly and stress response. *Biochemical Journal* **441,** 119–129 (**2012**).

119. Valentin-Vega, Y. A. *et al.* Cancer-associated DDX3X mutations drive stress granule assembly and impair global translation. *Scientific Reports* **6** (**2016**).

120. Weidensdorfer, D. *et al.* Control of c-myc mRNA stability by IGF2BP1-associated cytoplasmic RNPs. *RNA (New York, N.Y.)* **15,** 104–115 (**2009**).

121. Fang, M. Y. *et al.* Modulation of RNA-dependent interactions in stress granules prevents persistent TDP-43 accumulation in ALS/FTD. preprint (Neuroscience, **2018**).

122. Fang, M. Y. *et al.* Small-Molecule Modulation of TDP-43 Recruitment to Stress Granules Prevents Persistent TDP-43 Accumulation in ALS/FTD. *Neuron* **103,** 802–819.e11 (**2019**).

123. Guillén-Boixet, J. *et al.* RNA-Induced Conformational Switching and Clustering of G3BP Drive Stress Granule Assembly by Condensation. *Cell* **181,** 346–361.e17 (**2020**).

124. Henao-Mejia, J. & He, J. J. Sam68 relocalization into stress granules in response to oxidative stress through complexing with TIA-1. *Experimental Cell Research* **315,** 3381–3395 (**2009**).

125. Mitsumori, K., Takei, Y. & Hirokawa, N. Components of RNA granules affect their localization and dynamics in neuronal dendrites. *Molecular Biology of the Cell* **28** (ed Forscher, P.) 1412–1417 (**2017**).

126. McDonald, K. K. *et al.* TAR DNA-binding protein 43 (TDP-43) regulates stress granule dynamics via differential regulation of G3BP and TIA-1. *Human Molecular Genetics* **20,** 1400–1410 (**2011**).

127. Shih, J.-W. *et al.* Critical roles of RNA helicase DDX3 and its interactions with eIF4E/PABP1 in stress granule assembly and stress response. *Biochemical Journal* **441,** 119–129 (**2012**).

128. Smith, B. N. *et al.* Exome-wide Rare Variant Analysis Identifies TUBA4A Mutations Associated with Familial ALS. *Neuron* **84,** 324–331 (**2014**).

129. Chernov, K. G. *et al.* Role of Microtubules in Stress Granule Assembly: MICROTUBULE DYNAMICAL INSTABILITY FAVORS THE FORMATION OF MICROMETRIC STRESS GRANULES IN CELLS. *Journal of Biological Chemistry* **284,** 36569–36580 (**2009**).

130. Nadezhdina, E. S., Lomakin, A. J., Shpilman, A. A., Chudinova, E. M. & Ivanov, P. A. Microtubules govern stress granule mobility and dynamics. *Biochimica et Biophysica Acta (BBA) - Molecular Cell Research* **1803,** 361–371 (**2010**).

131. Gentile, F. *et al.* The Peripheral Nervous System in Amyotrophic Lateral Sclerosis: Opportunities for Translational Research. *Frontiers in Neuroscience* **13** (**2019**).

132. Murakami, T. *et al.* ALS/FTD Mutation-Induced Phase Transition of FUS Liquid Droplets and Reversible Hydrogels into Irreversible Hydrogels Impairs RNP Granule Function. *Neuron* **88,** 678–690 (**2015**).

133. Dormann, D. *et al.* ALS-associated fused in sarcoma (FUS) mutations disrupt Transportin-mediated nuclear import. *The EMBO Journal* **29,** 2841–2857 (**2010**).

134. Ash, P. E., Vanderweyde, T. E., Youmans, K. L., Apicco, D. J. & Wolozin, B. Pathological stress granules in Alzheimer's disease. *Brain Research* **1584,** 52–58 (**2014**).

135. Vanderweyde, T. *et al.* Contrasting Pathology of the Stress Granule Proteins TIA-1 and G3BP in Tauopathies. *Journal of Neuroscience* **32,** 8270–8283 (**2012**).

136. Doñate-Macián, P. *et al.* The TRPV4 channel links calcium influx to DDX3X activity and viral infectivity. *Nature Communications* **9** (**2018**).

137. Lennox, A. L. *et al.* Pathogenic DDX3X Mutations Impair RNA Metabolism and Neurogenesis during Fetal Cortical Development. *Neuron* **106,** 404–420.e8 (**2020**).

138. Samir, P. *et al.* DDX3X acts as a live-or-die checkpoint in stressed cells by regulating NLRP3 inflammasome. *Nature* **573,** 590–594 (**2019**).

139. Snijders Blok, L. *et al.* Mutations in DDX3X Are a Common Cause of Unexplained Intellectual Disability with Gender-Specific Effects on Wnt Signaling. *The American Journal of Human Genetics* **97,** 343–352 (**2015**).

140. Oughtred, R. *et al.* The BioGRID database: A comprehensive biomedical resource of curated protein, genetic, and chemical interactions. *Protein Science: A Publication of the Protein Society* **30,** 187–200 (**2021**).

141. Bader, G. D. & Hogue, C. W. Analyzing yeast protein–protein interaction data obtained from different sources. *Nature Biotechnology* **20,** 991–997 (**2002**).

142. Epling, L. B., Grace, C. R., Lowe, B. R., Partridge, J. F. & Enemark, E. J. Cancer-Associated Mutants of RNA Helicase DDX3X Are Defective in RNA-Stimulated ATP Hydrolysis. *Journal of Molecular Biology* **427,** 1779–1796 (**2015**).

143. Mitrovic, S.-A. Structural investigations of the TRPV4 intrinsically disordered N-terminus and structural studies of MIP-inhibitor interactions. PhD thesis (Johannes-Gutenberg University, Mainz, **2019**).

144. Song, H. & Ji, X. The mechanism of RNA duplex recognition and unwinding by DEAD-box helicase DDX3X. *Nature Communications* **10** (**2019**).

145. Hellmann, N. & Schneider, D. in *Protein Supersecondary Structures* (ed Kister, A. E.) Series Title: Methods in Molecular Biology, 379–401 (Springer New York, New York, NY, **2019**).

146. Mascotti, D. P. & Lohman, T. M. Thermodynamics of single-stranded RNA binding to oligolysines containing tryptophan. *Biochemistry* **31,** 8932–8946 (**1992**).

147. Robinson, K. E., Orans, J., Kovach, A. R., Link, T. M. & Brennan, R. G. Mapping Hfq-RNA interaction surfaces using tryptophan fluorescence quenching. *Nucleic Acids Research* **42,** 2736–2749 (**2014**).

148. Floor, S. N., Condon, K. J., Sharma, D., Jankowsky, E. & Doudna, J. A. Autoinhibitory Interdomain Interactions and Subfamily-specific Extensions Redefine the Catalytic Core of the Human DEAD-box Protein DDX3. *Journal of Biological Chemistry* **291,** 2412–2421 (**2016**).

149. Wheeler, J. R., Matheny, T., Jain, S., Abrisch, R. & Parker, R. Distinct stages in stress granule assembly and disassembly. *eLife* **5** (**2016**).

150. Protter, D. S. & Parker, R. Principles and Properties of Stress Granules. *Trends in Cell Biology* **26,** 668–679 (**2016**).

151. Wolozin, B. & Ivanov, P. Stress granules and neurodegeneration. *Nature Reviews Neuroscience* **20,** 649–666 (**2019**).

152. Thorneloe, K. S. *et al.* N-((1S)-1- -3-hydroxypropanoyl)-1-piperazinyl]carbonyl)-3-methylbutyl)-1-benzothiophene-2-carboxamide (GSK1016790A), a Novel and Potent Transient Receptor Potential Vanilloid 4 Channel Agonist Induces Urinary Bladder Contraction and Hyperactivity: Part I. *Journal of Pharmacology and Experimental Therapeutics* **326,** 432–442 (**2008**).

153. Willette, R. N. *et al.* Systemic Activation of the Transient Receptor Potential Vanilloid Subtype 4 Channel Causes Endothelial Failure and Circulatory Collapse: Part 2. *Journal of Pharmacology and Experimental Therapeutics* **326,** 443–452 (**2008**).

154. Modregger, J., Ritter, B., Witter, B., Paulsson, M. & Plomann, M. All three PACSIN isoforms bind to endocytic proteins and inhibit endocytosis. *Journal of Cell Science* **113 Pt 24,** 4511–4521 (**2000**).

155. Toescu, E. C. & Verkhratsky, A. The importance of being subtle: small changes in calcium homeostasis control cognitive decline in normal aging. *Aging Cell* **6,** 267–273 (**2007**).

156. Wang, Q. *et al.* Molecular mechanism of membrane constriction and tubulation mediated by the F-BAR protein Pacsin/Syndapin. *Proceedings of the National Academy of Sciences* **106,** 12700–12705 (**2009**).

157. Rao, Y. *et al.* Molecular basis for SH3 domain regulation of F-BAR-mediated membrane deformation. *Proceedings of the National Academy of Sciences* **107,** 8213–8218 (**2010**).

158. Caires, R. *et al.* Omega-3 Fatty Acids Modulate TRPV4 Function through Plasma Membrane Remodeling. *Cell Reports* **21,** 246–258 (**2017**).

159. Bai, X., Meng, G., Luo, M. & Zheng, X. Rigidity of Wedge Loop in PACSIN 3 Protein Is a Key Factor in Dictating Diameters of Tubules. *Journal of Biological Chemistry* **287,** 22387–22396 (**2012**).

160. Goh, S. L., Wang, Q., Byrnes, L. J. & Sondermann, H. Versatile Membrane Deformation Potential of Activated Pacsin. *PLoS ONE* **7** (ed Johannes, L.) e51628 (**2012**).

161. Ryskamp, D. A. *et al.* TRPV4 regulates calcium homeostasis, cytoskeletal remodeling, conventional outflow and intraocular pressure in the mammalian eye. *Scientific Reports* **6,** 30583 (**2016**).

162. Lee, W. H. *et al.* TRPV4 Regulates Breast Cancer Cell Extravasation, Stiffness and Actin Cortex. *Scientific Reports* **6** (**2016**).

163. Shin, S. H. *et al.* Phosphorylation on the Ser 824 residue of TRPV4 prefers to bind with F-actin than with microtubules to expand the cell surface area. *Cellular Signalling* **24,** 641–651 (**2012**).

164. Becker, D., Müller, M., Leuner, K. & Jendrach, M. The C-terminal domain of TRPV4 is essential for plasma membrane localization. *Molecular Membrane Biology* **25,** 139–151 (**2008**).

165. Becker, D., Bereiter-Hahn, J. & Jendrach, M. Functional interaction of the cation channel transient receptor potential vanilloid 4 (TRPV4) and actin in volume regulation. *European Journal of Cell Biology* **88,** 141–152 (**2009**).

166. Spiering, D. & Hodgson, L. Dynamics of the Rho-family small GTPases in actin regulation and motility. *Cell Adhesion & Migration* **5,** 170–180 (**2011**).

167. Dupraz, S. *et al.* RhoA Controls Axon Extension Independent of Specification in the Developing Brain. *Current biology: CB* **29,** 3874–3886.e9 (**2019**).

168. Luo, L. Rho GTPases in neuronal morphogenesis. *Nature Reviews. Neuroscience* **1,** 173–180 (**2000**).

169. Schaefer, A., Reinhard, N. R. & Hordijk, P. L. Toward understanding RhoGTPase specificity: structure, function and local activation. *Small GTPases* **5,** 6 (**2014**).

170. Gasmi-Seabrook, G. M. C. *et al.* Real-time NMR Study of Guanine Nucleotide Exchange and Activation of RhoA by PDZ-RhoGEF. *Journal of Biological Chemistry* **285,** 5137–5145 (**2010**).

171. Wei, Y. *et al.* Crystal structure of RhoA–GDP and its functional implications. *Nature Structural Biology* **4,** 699–703 (**1997**).

172. Wegierski, T., Hill, K., Schaefer, M. & Walz, G. The HECT ubiquitin ligase AIP4 regulates the cell surface expression of select TRP channels. *The EMBO Journal* **25,** 5659–5669 (**2006**).

173. Shukla, A. K. *et al.* Arresting a Transient Receptor Potential (TRP) Channel: beta-ARRESTIN 1 MEDIATES UBIQUITINATION AND FUNCTIONAL DOWN-REGULATION OF TRPV4. *Journal of Biological Chemistry* **285,** 30115–30125 (**2010**).

174. Zhang, D. & Aravind, L. Identification of novel families and classification of the C2 domain superfamily elucidate the origin and evolution of membrane targeting activities in eukaryotes. *Gene* **469,** 18–30 (**2010**).

175. Zhu, K. *et al.* Allosteric auto-inhibition and activation of the Nedd4 family E3 ligase Itch. *EMBO reports* **18,** 1618–1630 (**2017**).

176. Shaw, A. Z. *et al.* Phosphorylation of either Ser16 or Thr30 does not disrupt the structure of the Itch E3 ubiquitin ligase third WW domain. *Proteins* **60,** 558–560 (**2005**).

177. Chen, Z. *et al.* A Tunable Brake for HECT Ubiquitin Ligases. *Molecular Cell* **66,** 345–357.e6 (**2017**).

178. Melino, G. *et al.* Itch: a HECT-type E3 ligase regulating immunity, skin and cancer. *Cell Death & Differentiation* **15,** 1103–1112 (**2008**).

179. Riling, C. *et al.* Itch WW Domains Inhibit Its E3 Ubiquitin Ligase Activity by Blocking E2-E3 Ligase Trans-thiolation. *Journal of Biological Chemistry* **290,** 23875–23887 (**2015**).

180. Polo, S. *et al.* A single motif responsible for ubiquitin recognition and monoubiquitination in endocytic proteins. *Nature* **416,** 451–455 (**2002**).

181. Shih, S. C., Sloper-Mould, K. E. & Hicke, L. Monoubiquitin carries a novel internalization signal that is appended to activated receptors. *The EMBO Journal* **19,** 187–198 (**2000**).

182. Lorenz, S., Cantor, A. J., Rape, M. & Kuriyan, J. Macromolecular juggling by ubiquitylation enzymes. *BMC biology* **11,** 65 (**2013**).

183. Takahashi, N. *et al.* TRPV4 channel activity is modulated by direct interaction of the ankyrin domain to PI(4,5)P2. *Nature Communications* **5,** 4994 (**2014**).

184. Harraz, O. F., Longden, T. A., Hill-Eubanks, D. & Nelson, M. T. PIP2 depletion promotes TRPV4 channel activity in mouse brain capillary endothelial cells. *eLife* **7,** e38689 (**2018**).

185. Goswami, C., Kuhn, J., Heppenstall, P. A. & Hucho, T. Importance of Non-Selective Cation Channel TRPV4 Interaction with Cytoskeleton and Their Reciprocal Regulations in Cultured Cells. *PLoS ONE* **5** (ed Matsunami, H.) e11654 (**2010**).

186. Martin, E. *et al.* Involvement of TRPV1 and TRPV4 channels in migration of rat pulmonary arterial smooth muscle cells. *Pflügers Archiv - European Journal of Physiology* **464,** 261–272 (**2012**).

187. Fiorio Pla, A. *et al.* TRPV4 mediates tumor-derived endothelial cell migration via arachidonic acid-activated actin remodeling. *Oncogene* **31,** 200–212 (**2012**).

188. Dunn, K. W., Kamocka, M. M. & McDonald, J. H. A practical guide to evaluating colocalization in biological microscopy. *American Journal of Physiology-Cell Physiology* **300,** C723–C742 (**2011**).

189. Costes, S. V. *et al.* Automatic and quantitative measurement of protein-protein colocalization in live cells. *Biophysical Journal* **86,** 3993–4003 (**2004**).

190. Ujfalusi-Pozsonyi, K. *et al.* The effects of detergents on the polymerization properties of actin. *Cytometry Part A* (**2010**).

191. Pugh, T. J. *et al.* Medulloblastoma exome sequencing uncovers subtype-specific somatic mutations. *Nature* **488,** 106–110 (**2012**).

192. Kellaris, G. *et al.* A hypomorphic inherited pathogenic variant in DDX3X causes male intellectual disability with additional neurodevelopmental and neurodegenerative features. *Human Genomics* **12,** 11 (**2018**).

193. Wang, X. *et al.* Phenotypic expansion in DDX3X - a common cause of intellectual disability in females. *Annals of Clinical and Translational Neurology* **5,** 1277–1285 (**2018**).

194. Nicola, P. *et al.* De novo DDX3X missense variants in males appear viable and contribute to syndromic intellectual disability. *American Journal of Medical Genetics. Part A* **179,** 570–578 (**2019**).

195. Jones, D. T. W. *et al.* Dissecting the genomic complexity underlying medulloblastoma. *Nature* **488,** 100–105 (**2012**).

196. Perfetto, M., Xu, X., Yousaf, N., Li, J. & Wei, S. The RNA helicase DDX3 induces neural crest by promoting AKT activity. preprint (Developmental Biology, **2019**).

197. Lennox, A. L. *et al.* Pathogenic mutations impair RNA metabolism and neurogenesis during fetal cortical development. *bioRxiv* (**2018**).

198. Yang, S. N. Y. *et al.* RK-33 Is a Broad-Spectrum Antiviral Agent That Targets DEAD-Box RNA Helicase DDX3X. *Cells* **9** (**2020**).

199. Phung, B. *et al.* The X-Linked DDX3X RNA Helicase Dictates Translation Reprogramming and Metastasis in Melanoma. *Cell Reports* **27,** 3573–3586.e7 (**2019**).

200. Saito, M. *et al.* Acetylation of intrinsically disordered regions regulates phase separation. *Nature Chemical Biology* **15,** 51–61 (**2019**).

201. Lai, M.-C., Lee, Y.-H. W. & Tarn, W.-Y. The DEAD-box RNA helicase DDX3 associates with export messenger ribonucleoproteins as well as tip-associated protein and participates in translational control. *Molecular Biology of the Cell* **19,** 3847–3858 (**2008**).

202. Soto-Rifo, R. *et al.* DEAD-box protein DDX3 associates with eIF4F to promote translation of selected mRNAs. *The EMBO journal* **31,** 3745–3756 (**2012**).

203. Choi, Y.-J. & Lee, S.-G. The DEAD-box RNA helicase DDX3 interacts with DDX5, co-localizes with it in the cytoplasm during the G2/M phase of the cycle, and affects its shuttling during mRNP export. *Journal of Cellular Biochemistry* **113,** 985–996 (**2012**).

204. Lee, A. K. *et al.* Translational Repression of G3BP in Cancer and Germ Cells Suppresses Stress Granules and Enhances Stress Tolerance. *Molecular Cell* **79,** 645–659.e9 (**2020**).

205. Marmor-Kollet, H. *et al.* Spatiotemporal Proteomic Analysis of Stress Granule Disassembly Using APEX Reveals Regulation by SUMOylation and Links to ALS Pathogenesis. *Molecular Cell* **80,** 876–891.e6 (**2020**).

206. Jønson, L. *et al.* Molecular Composition of IMP1 Ribonucleoprotein Granules. *Molecular & Cellular Proteomics* **6,** 798–811 (**2007**).

207. Thomas, M. G., Tosar, L. J. M., Desbats, M. A., Leishman, C. C. & Boccaccio, G. L. Mammalian Staufen 1 is recruited to stress granules and impairs their assembly. *Journal of Cell Science* **122,** 563–573 (**2009**).

208. Burgess, H. M. *et al.* Nuclear relocalisation of cytoplasmic poly(A)-binding proteins PABP1 and PABP4 in response to UV irradiation reveals mRNA-dependent export of metazoan PABPs. *Journal of Cell Science* **124,** 3344–3355 (**2011**).

209. Mazroui, R. Trapping of messenger RNA by Fragile X Mental Retardation protein into cytoplasmic granules induces translation repression. *Human Molecular Genetics* **11,** 3007–3017 (**2002**).

210. Villace, P. The composition of Staufen-containing RNA granules from human cells indicates their role in the regulated transport and translation of messenger RNAs. *Nucleic Acids Research* **32,** 2411–2420 (**2004**).

211. Yang, P. *et al.* G3BP1 Is a Tunable Switch that Triggers Phase Separation to Assemble Stress Granules. *Cell* **181,** 325–345.e28 (**2020**).

212. Sfakianos, A. P. *et al.* The mTOR-S6 kinase pathway promotes stress granule assembly. *Cell Death & Differentiation* **25,** 1766–1780 (**2018**).

213. Somasekharan, S. P. *et al.* YB-1 regulates stress granule formation and tumor progression by translationally activating G3BP1. *Journal of Cell Biology* **208,** 913–929 (**2015**).

214. Vascotto, C. *et al.* APE1/Ref-1 Interacts with NPM1 within Nucleoli and Plays a Role in the rRNA Quality Control Process. *Molecular and Cellular Biology* **29,** 1834–1854 (**2009**).

215. Hubstenberger, A. *et al.* P-Body Purification Reveals the Condensation of Repressed mRNA Regulons. *Molecular Cell* **68,** 144–157.e5 (**2017**).

216. Dammer, E. B. *et al.* Coaggregation of RNA-Binding Proteins in a Model of TDP-43 Proteinopathy with Selective RGG Motif Methylation and a Role for RRM1 Ubiquitination. *PLoS ONE* **7** (ed Iijima, K. M.) e38658 (**2012**).

217. Furukawa, M. T., Sakamoto, H. & Inoue, K. Interaction and colocalization of HERMES/RBPMS with NonO, PSF, and G3BP1 in neuronal cytoplasmic RNP granules in mouse retinal line cells. *Genes to Cells* **20,** 257–266 (**2015**).

218. Tsai, N.-P., Tsui, Y.-C. & Wei, L.-N. Dynein motor contributes to stress granule dynamics in primary neurons. *Neuroscience* **159,** 647–656 (**2009**).

219. Guil, S., Long, J. C. & Cáceres, J. F. hnRNP A1 Relocalization to the Stress Granules Reflects a Role in the Stress Response. *Molecular and Cellular Biology* **26,** 5744–5758 (**2006**).

220. Mackenzie, I. R. *et al.* TIA1 Mutations in Amyotrophic Lateral Sclerosis and Frontotemporal Dementia Promote Phase Separation and Alter Stress Granule Dynamics. *Neuron* **95,** 808–816.e9 (**2017**).

221. Huang, C. *et al.* UBAP2L arginine methylation by PRMT1 modulates stress granule assembly. *Cell Death & Differentiation* **27,** 227–241 (**2020**).

222. Fu, Y. & Zhuang, X. m6A-binding YTHDF proteins promote stress granule formation. *Nature Chemical Biology* **16,** 955–963 (**2020**).

223. Matsuki, H. *et al.* Both G3BP1 and G3BP2 contribute to stress granule formation. *Genes to Cells: Devoted to Molecular & Cellular Mechanisms* **18,** 135–146 (**2013**).

224. Kobayashi, T., Winslow, S., Sunesson, L., Hellman, U. & Larsson, C. PKCalpha Binds G3BP2 and Regulates Stress Granule Formation Following Cellular Stress. *PLoS ONE* **7** (ed Kahle, P. J.) e35820 (**2012**).

225. Li, C. H., Ohn, T., Ivanov, P., Tisdale, S. & Anderson, P. eIF5A promotes translation elongation, polysome disassembly and stress granule assembly. *PloS One* **5,** e9942 (**2010**).

226. Thomas, M. G. *et al.* Staufen Recruitment into Stress Granules Does Not Affect Early mRNA Transport in Oligodendrocytes. *Molecular Biology of the Cell* **16,** 405–420 (**2005**).

227. Goodier, J. L., Zhang, L., Vetter, M. R. & Kazazian, H. H. LINE-1 ORF1 Protein Localizes in Stress Granules with Other RNA-Binding Proteins, Including Components of RNA Interference RNA-Induced Silencing Complex. *Molecular and Cellular Biology* **27,** 6469–6483 (**2007**).

228. Hamada, T. *et al.* Stress granule formation is induced by a threshold temperature rather than a temperature difference in *Arabidopsis*. *Journal of Cell Science* **131,** jcs216051 (**2018**).

229. Wang, W., Zhang, X., Gao, Q. & Xu, H. TRPML1: an ion channel in the lysosome. *Handbook of Experimental Pharmacology* **222,** 631–645 (**2014**)**.**

230. Desrochers, G. *et al.* Molecular basis of interactions between SH3 domain-containing proteins and the proline-rich region of the ubiquitin ligase Itch. *Journal of Biological Chemistry* **292,** 6325–6338 (**2017**)**.**

Curriculum Vitae

Education and Research Experience

Jan 2019 – Jun 2019	Visiting researcher at the research group of Prof. [redacted], Johns Hopkins University, USA (Fulbright Fellowship). "The impact of selected TRPV4 interactors upon TRPV4 mediated Ca^{2+}-influx activity" *Live Ca^{2+}-influx imaging in cellulo. Immunostaining and subsequent confocal microscopy. Mouse studies on peripheral neuropathies.*
Since Apr 2017	PhD candidate in chemistry (TransMED as well as Sybille Kalkhof Rose-Fellowship), Johannes Gutenberg-University (JGU) Mainz "Elucidating molecular details in the interactome of the human ion channel TRPV4" *Investigation of direct protein-protein interactions (PPI) via $UDMS^E$, NMR and analytical FPLC. Indirect PPI studies via co-IPs and microscopical co-localization studies. Developing an in-house software for microscopical co-localization analysis.*
Jun 2016 – Apr 2017	Master-Thesis, "Investigating the interactome of the TRPV4 N-terminus", JGU Mainz *Recombinant expression of human proteins in E. coli, P. pastoris and HEK293T cells. Purification via several chromatographic methods, including preparative FPLC. Confirming structural protein integrity via CD spectroscopy and 2D-NMR.*
Apr 2015 – Jun 2015	Research internship, "AOM-induced colorectal carcinogenesis in PARP-1 k.o. mice", JGU Mainz *Inducing colorectal cancer in PARP-1 k.o. mice. Evaluation of carcinogenesis in vivo via colonoscopy. Immunohistostaining of colorectal tissues and subsequent confocal microscopy. ELISAs for TNFα level determination.*
Oct 2014 – Apr 2017	Studies in Biomedical Chemistry (M.Sc.), JGU Mainz Elective subjects: Pharmacology, Oncology
Apr 2014 – Mar 2016	Student staff member at the IMG Innovations-Management GmbH *Novelty assessment of inventions with focus on industrial property rights in life science and chemistry. Composition of technological summaries of approved patents in English and German. Acquisition of technology licensees.*
Apr 2014 – Sep 2014	Bachelor-Thesis, "Influence of disulfide compounds on the tumor-supressor protein p53", JGU Mainz *Cell culture with colorectal cancer cell lines. ELISAs, EMSAs with subsequent Western- and Southern blotting. Recombinant expression of human proteins in Sf9 insect cells via baculoviruses*
Oct 2013 – Apr 2014	Interdisciplinary advanced seminar "Tumor biology, oncological dia-gnostics and novel therapies", JGU Mainz
July 2012	Extracurricular research internship, "Expression level of CD91 in leukemic stem cells", JGU Mainz *Cell culture with suspension cells, FACS*
Oct 2010 – Sep 2014	Studies in Biomedical Chemistry (B.Sc.), JGU Mainz Elective subject: Genotoxicology
Mar 2010	Higher education entrance qualification, "Abitur" Gymnasium Kusel

Awards

Nov 2019	Sybille Kalkhof Rose-Stiftung Fellowship
Sep 2019	Best Talk Award of a young researcher by the association *frei für forschung – Neue Wege in der Medizin e.V.* at the 6th TransMED ScienceDay, JGU Mainz
Sep 2018	Science Award by the association *frei für forschung – Neue Wege in der Medizin e.V.* at the CRISPR Genome Editing Workshop, JGU Mainz
Aug 2018	Fulbright Fellowship
Mar 2018	Best Presentation Award at the 3rd Interdisciplinary symposium JGU Mainz
Oct 2017	TransMED – Mainz Research School of Translational Biomedicine Fellowship

Organizing and Teaching Experience

Oct 2017+ Apr 2018	Conference conception and organization of 2nd BioChem Symposium and 3rd Life Science Meeting, JGU Mainz
since Apr 2017	Supervision of 9 undergraduate students during their Bachelor and Master theses in (biomedical) chemistry. Conception and lecturing of undergraduate literature seminars and practical courses in “Biochemistry 2”
Oct 2011 – Oct 2012	Undergraduate research assistant, JGU Mainz Conception, supervision and correction of exams in the subject “Allgemeine und anorganische Chemie I”.

List of publications

- McCray BA, Diehl E, Sullivan JM, Aisenberg WH, Zaccor NW, Lau AR, Goretzki B, Hellmich UA, Llyod TE, Sumner CJ. „*Neuropathy-causing TRPV4 mutations disrupt TRPV4-RhoA interactions and impair actin cytoskeleton regulation*“ (*Nature Communications* **12,** 1444 (2021)
- Wesenberg LJ, Diehl E, Zähringer TJB, Schollmeyer D, Shimizu A, Yoshida J, Hellmich UA, Waldvogel SR. „*Twofold Electrochemical C,H-Amination of Activated Benzene Derivatives“* (Accepted, Chemistry – A European Journal)
- Neitzel, C., Seiwert, N., Göder, A., Diehl, E, Weber, C., Nagel, G., Stroh, S., Rasenberger, B., Christmann, M., and Fahrer, J. (2019). *Lipoic Acid Synergizes with Antineoplastic Drugs in Colorectal Cancer by Targeting p53 for Proteasomal Degradation*. Cells *8*, 794 (2019)
- Wagner A, Le TA, Brennich M, Klein P, Bader N, Diehl E, Paszek D, Weickhmann AK, Dirdjaja N, Krauth-Siegel RL. *Inhibitor-Induced Dimerization of an Essential Oxidoreductase from African Trypanosomes*. Angewandte der Chemie International Edition 58, 3640–3644. (2019)
- Goretzki B, Glogowski NA, Diehl E, Durchardt-Ferner E, Hacker C, Gaudet R, Hellmich UA. *Structural Basis of TRPV4 N-Terminus Interaction with Syndapin/PACSIN1-3 and PIP2.* Structure 26, 1583-1593.e5 (2018).
- Dörsam B, Seiwerth S, Foersch S, Stroh S, Nagel G, Begaliew D, Diehl E, Kraus A, McKeague M, Minneker V, Roukos V, Reißig S, Waisman A, Moehler M, Stier A, Mangerich A, Dantzer F, Kaina B and Fahrer, J. *PARP-1 protects against colorectal tumor induction, but promotes inflammation-driven colorectal tumor progression.* Proc. Nat. Acad. Sci. 115, E4061–E4070 (2018).
- Wagner A, Diehl E, Krauth-Siegel RL, Hellmich UA. *Backbone NMR assignment of tryparedoxin, the central protein in the hydroperoxide detoxification cascade of African trypanosomes, in the oxidized and reduced form.* Biomol NMR Assign. Volume 11, Issue 2, pp 193-196 (2017)

Supervised theses

Jul 2020 – Oct 2020	[redacted] – Bachelor thesis “A biochemical study of selected TRPV4 interaction partners”
Jun2018 – Mar 2019	[redacted] Diploma thesis “Investigating the Interactome of the Human Ion Channel TRPV4 and Associated Channelopathies”
Oct 2017 – Jan 2018	[redacted] – Bachelor thesis “Biochemische Studien an Ankyrin Repeat Domains von TRPV-Ionenkanälen”

Conference contributions (Selection)

Sep 2019	6th TransMed Science Day, JGU Mainz “Towards elucidating the channelopathy interactome of the human ion channel TRPV4” (talk)
Sep 2018	Laureate lecture at the CRISPR Genome Editing Workshop, JGU Mainz “Why CRISPR? A TR(i)P through the interactome world of the Transient Receptor Potential channel 4”
Mar 2018	3rd Interdisciplinary Symposium, JGU Mainz “Transient receptor potential channels – Building a bridge between Aristotle and chili” (talk)